



Università degli Studi di Cagliari

Ph.D. DEGREE

Life, Environmental and Drug Sciences

Cycle XXXIV

**EXPLORING THE CHEMICAL SYNTHESIS AND
UNDERLYING THE PHARMACOLOGICAL
APPLICATION OF BENZOPYRONE DERIVATIVES AS
ANTICANCER AGENTS**

Scientific Disciplinary Sector

CHIM08

Ph.D. Student:

Ana Lisa Sousa Sequeira

Supervisor:

Prof. Elias Maccioni

Final exam. Academic Year 2020/2021

Thesis defence: April 2022 Session

Eu não sei o que o amanhã trará.

Fernando Pessoa

Publications

The data contained in the following publications are contained in this Thesis.

Manuscripts in International Peer-Review Journals

1. Rita Meleddu, Angela Corona, Simona Distinto, Filippo Cottiglia, Serenella Deplano, **Lisa Sequeira**, Daniela Secci, Alessia Onali, Erica Sanna, Francesca Esposito, Italo Cirone, Francesco Ortuso, Stefano Alcaro, Enzo Tramontano, Peter Matyus and Elias Maccioni. Exploring new scaffolds for the dual inhibition of HIV-1 RT polymerase and ribonuclease associated functions. *Molecules*. 2021; 26: 3821.
2. Simona Distinto, Rita Meleddu, Francesco Ortuso, Filippo Cottiglia, Serenella Deplano, **Lisa Sequeira**, Claudia Melis, Benedetta Fois, Andrea Angeli, Clemente Capasso, Rossella Angius, Stefano Alcaro, Claudiu T. Supuran and Elias Maccioni. Exploring new structural features of the 4-[(3-methyl-4-aryl-2,3-dihydro-1,3-thiazol-2-ylidene)amino]benzenesulphonamide scaffold for the inhibition of human carbonic anhydrases. *J Enzyme Inhib Med Chem*. 2019; 34 (1): 1526–1533.

Poster Communications in Scientific Meetings

1. **Lisa Sequeira**, Rita Meleddu, Elias Maccioni, Fernanda Borges, Claudiu T. Supuran, Eugenio Uriarte. Synthesis of Furobenzopyrone Derivatives with Potential Anticancer Activity. *4th WG meeting – final status of WG activities within the MuTaLig COST Action*. 2020, 5-6 March, Izmir, Turkey.
2. **Lisa Sequeira**, Rita Meleddu, Elias Maccioni. Synthesis of furochromone derivatives with potential anticancer activity. *4th annual meeting MuTaLig COST ACTION and IX Meeting of the Paul Ehrlich Euro-PhD Network*. 2019, 13-15, Catanzaro, Italy.
3. **Lisa Sequeira**, Rita Meleddu, Elias Maccioni. Synthesis of 2-(7-hydroxy-4,8-dimethyl-2-oxo-2H-chromen-3-yl)acetate derivatives with potential anticancer activity. *MuTaLig COST ACTION CA15135 3rd WG Meeting*. 2019, 23-24 February, Paris, France.
4. **Lisa Sequeira**, Tiago Silva, Elias Maccioni, Fernanda Borges. Development of Dual COMT Inhibitors and Iron Chelators. *26th Young Research Fellows Meeting*. 2019, 20-22 February, Paris, France.
5. **Lisa Sequeira**, Tiago Silva, Fernanda Borges. Development of Dual COMT Inhibitors and Iron Chelators: Studies on Synthetic Routes Optimization. *MuTaLig COST Action CA15135, Annual Meeting*. 2018, 18-19 October, Valletta, Malta.

Oral Communications in Scientific Meetings

1. **Lisa Sequeira**, Elias Maccioni, Fernanda Borges, Claudiu T. Supuran, and Eugenio Uriarte. Development of Tumour-Associated Carbonic Anhydrases Inhibitors Based on Benzopyrone Scaffold. *Paul Ehrlich Euro-PhD Network virtual meeting (#PEVM2021)*. 2021, 26-28 July.
2. **Lisa Sequeira**, Rita Meleddu, and Elias Maccioni. Development of tumour-associated enzymes inhibitors. *SardiniaChem*. 2019, 21 June, Sassari, Sardinia.

Acknowledgments

Institutional acknowledgements are addressed to the Italian Ministry of Education, University and Research for the financial support.

First of all, I would like to express my gratitude to my supervisor **Prof. Elias Maccioni** for the continuous support, patience, constant motivation, transmitted knowledge, and good mood, that made the work beyond challenging, appealing. My thanks go also to all the people with whom I worked in this new home, and which welcomed me since the first day, **Prof. Filippo, Benedetta, Serenella, Daniela, Alessia, Erica**, and specially **Simona** and **Rita**.

To my supervisor abroad, **Prof. Eugenio Uriarte**, a big thank you for accepting me in your group and guide my work. For your eternal patience, interest, and joy. My thanks go also to all the team in Santiago de Compostela, especially **Maria João**.

To **Prof. Claudiu Supuran** for the valuable help in the carbonic anhydrase inhibition assays.

A big thanks to **Prof. Fernanda Borges** and her team, at the Faculty of Sciences of University of Porto. Despite the distance you were always present. Thank you, **Tiago, Fernando, Catarina, Carlos, Daniel M., Pedro, Cátia, Miguel**, and **Brandon. Alexandra** and **Francesco** thank you for all the help regarding synthesis doubts and, in the case of Francesco, Italian doubts as well. To **Daniel C.** and **Sofia**, a special thanks also for carried out supplementary assays on my compounds.

My gratitude goes also to **Dr. Mariana Sardo, Dr. Luís Mafra, Sérgio, Ricardo, Leandro, Joana Carrola** and **Sónia** from University of Aveiro and **João** from Faculty of Engineering of University of Porto. You were part of my academic path, and your support and friendship were much appreciated.

And because there are people without whom our life loses some of its meaning, I must thank those who, being part of what I am, are part of all this.

To my friends, that helped me in the bad days, with laugh and distraction, and in the good days with constant encouragement and support. Friends are, after all, the family that we choose. Thank you **Joaninha, Joana, Marta** and **Tânia**.

And speaking of family, I must thank mine, because without them none of this would be possible. To my **parents**, without whom I will not be here. And that even if not happy with the distance, always supported me. To **Sissi**, for the many questions and the explicit

ACKNOWLEDGMENTS

interest. To **Jacinta, Paulo, Laura,** and **Su** for all the moments shared and for the effort you always made to try to understand me. To **Tati**, I thank you for all the support in the years that I was a student (there were many), for the help in everything, for the discussions at the table and for the great interest that you have always had in my work. Thank you for putting up with me in the morning and for the good times we share. Thank you for making me, for the most part, who I am.

Last but not least, thank you **Bruno** for being with me at all times, even from far away, and with my bad mood. Your constant support made me achieve the goals I set myself. Without you, everything would have made less sense. Thank you for never let me get out of the way.

Abstract

Cancer is characterized by the uncontrolled growth of abnormal cells with malignant potential, that begins when a cell breaks free from the normal restraints on cell division and begins to follow its own schedule for proliferation. As the second leading cause of death in most of the countries after cardiovascular diseases, cancer is a major public health problem in all populations, unrelated with wealth and social status. This disease is a financial and psychologic burden on both economy and families of patients. Failures in the treatment of metastatic disease and development of drug resistance are the main reasons for the high mortality rate. Hence, is of global interest to reduce this burden through early detection of cancer and appropriate treatment and care of patients.

Tumor-associated carbonic anhydrase (CA) IX and XII have been consistently validated as markers of disease progression in many solid tumors. Their overexpression in cancer and contribution to tumor physiology shows their great potential as biomarkers and therapeutic targets, leading the research community to undoubtedly focus on these isoforms in the last two decades. The two main strategies to target the tumor associated CAs for cancer therapy include the development of monoclonal antibodies and the design and synthesis of small molecules that selectively inhibit CA IX and XII. Many carbonic anhydrase inhibitors (CAIs) which selectively inhibit these two isoforms, belong to sulfonamide, coumarin and sulfocoumarin classes.

Coumarins and chromones are two groups of naturally occurring heterocycle compounds widely distributed in nature. Their chemical and biological aspects have been studied in detail. Molecules containing the coumarin and chromone skeleton have a wide variety of biological activities. The potential of coumarin and chromone scaffolds together with the research results, regarding their pharmaceutical use and potential, are the background for the work of this thesis. In addition, the previous work of the group regarding coumarins and furocoumarins showed the potential of these scaffolds as selective inhibitors of the tumor associated CAs.

Hence, the work herein present follows the study of coumarins and chromones as promising scaffolds for the development of CA IX and XII selective inhibitors. Accordingly, the first aim involved the development of possible potent, selective, and reversible CA IX and XII inhibitors by the synthesis of compounds based in the coumarin (furanocoumarins included) and chromone scaffolds.

Coumarin and chromone based libraries were successfully synthesized and characterized. The predicted properties of the compounds were calculated, and the theoretical

ABSTRACT

parameters were encouraging. Compound EMAC10163b proved to be the most potent and isozyme selective compound, within the EMAC10163 series. EMAC10163b selectively inhibit *hCA* IX and XII ($K_i = 0.53 \mu\text{M}$ and $0.47 \mu\text{M}$, respectively) over the isozymes *hCA* I and II. Compound EMAC10164d proved to be the most potent and isozyme selective compound, within the EMAC10164 series. EMAC10164d acted as selective inhibitor toward *hCA* IX and XII ($K_i = 0.46 \mu\text{M}$ and $0.80 \mu\text{M}$, respectively). Compound EMAC10169m proved to be the most potent and isozyme selective compound, within the EMAC10169 series. EMAC10169m acted as selective inhibitor toward *hCA* IX and XII ($K_i = 0.31 \mu\text{M}$ and $0.24 \mu\text{M}$, respectively).

The docking experiments that consider the IX isoform, highlighted that the rigidity of the EMAC10164 and EMAC10169 series helps to orientate the compounds in the binding pocket with the chromene portion toward the Zn^{2+} . This lead also to a general better activity of these series. The influence of the substituents in the phenyl ring is not clear among the different series.

In the hydrolyzed compounds (EMAC10163-open and EMAC10164-open) what seems important is the Zn^{2+} chelation and the interactions between the newly formed carboxylate moiety in the catalytic site.

The docking solutions, considering the XII isoform, are often characterized by the interaction with common residues such as Lys69, His117, Thr198 or Thr199. Also, the open compounds are stabilized by an array of hydrogen bonds involving the residues in the catalytic cavity.

Overall, the coumarin and chromone scaffolds were validated as a suitable framework for the development of selective carbonic anhydrase IX and XII inhibitors. The investigation performed in the course of this project provided understanding of the bioactivity of the developed compounds and paved the way for further studies of this scaffolds and derivatives towards other targets associated with cancer.

Keywords: Cancer-associated carbonic anhydrases; Carbonic anhydrases inhibitors; Coumarins; Furocoumarins; Chromones; Docking studies.

Thesis outline

This Thesis is organized in six main chapters:

Chapter 1. Introduction

Chapter 1 includes a brief literature review on pathophysiological and pharmacological aspects of cancer and carbonic anhydrases and their inhibitors to contextualize the research aims, which are included in the final part of the chapter.

Chapter 2. Experimental section

Chapter 2 is composed by the description of the experimental procedures.

Chapter 3. Results and discussion

Chapter 3 encompasses the obtained results and their discussion within the scope of this Thesis.

Chapter 4. Conclusions

Chapter 4 comprises the main conclusions of the Thesis, highlighting the most relevant findings and open questions for future endeavors.

Chapter 5. Other projects

Chapter 5 cover all the work performed within side projects during this period.

Chapter 6. Bibliography

Chapter 6 lists all the references used in the previous chapters.

Table of contents

Publications.....	v
Acknowledgments	vii
Abstract.....	ix
Thesis outline	xi
Table of contents.....	xiii
List of figures.....	xix
List of tables.....	xxvii
List of abbreviations	xxxii
CHAPTER 1. Introduction	1
1.1. Cancer: an overview	3
1.1.1. Etiology and pathogenesis	4
1.1.2. Pharmacotherapy.....	5
1.1.3. Future directions	7
1.2. Carbonic anhydrases	9
1.2.1. CAs physiological and pathological roles	11
1.2.2. CAs structural features.....	12
1.2.2.1. α -CAs structure.....	14
1.2.3. CAs catalytic features	15
1.2.4. Activators and Inhibitors.....	16
1.2.4.1. CAs inhibition mechanisms	17
1.2.5. CAs as targets for medicinal chemistry	20
1.2.5.1. Tumor-associated CA IX and XII.....	21
1.2.6. CAIs.....	23
1.2.6.1. CAIs as diuretics.....	23
1.2.6.2. CAIs as anti-glaucoma drugs	25
1.2.6.3. CAIs in osteoporosis treatment	26

TABLE OF CONTENTS

1.2.6.4.	CAIs as anticonvulsants.....	26
1.2.6.5.	CAIs as novel anti-obesity drugs.....	27
1.2.6.6.	CAIs as antitumor agents.....	28
1.3.	Coumarin and chromone scaffolds.....	31
1.4.	Thesis research objectives.....	40
CHAPTER 2. Experimental Section.....		41
2.1.	Material and methods.....	43
2.2.	Synthesis of furocoumarins.....	45
2.2.1.	Synthetic pathway.....	45
2.2.2.	Synthesis of methyl 2-(7-hydroxy-4,8-dimethyl-2-oxo-2 <i>H</i> -chromen-3-yl)acetate (EMAC10163).....	45
2.2.3.	Synthesis of the 2 <i>H</i> -chromen compounds (EMAC10163 series).....	46
2.2.3.1.	Synthesis of methyl 2-(4,8-dimethyl-2-oxo-7-(2-oxo-2-(<i>p</i> -tolyl)ethoxy)-2 <i>H</i> -chromen-3-yl)acetate (EMAC10163a).....	46
2.2.3.2.	Synthesis of methyl 2-(7-(2-(4-methoxyphenyl)-2-oxoethoxy)-4,8-dimethyl-2-oxo-2 <i>H</i> -chromen-3-yl)acetate (EMAC10163b).....	47
2.2.3.3.	Synthesis of methyl 2-(7-(2-(4-bromophenyl)-2-oxoethoxy)-4,8-dimethyl-2-oxo-2 <i>H</i> -chromen-3-yl)acetate (EMAC10163c).....	48
2.2.3.4.	Synthesis of methyl 2-(7-(2-(4-fluorophenyl)-2-oxoethoxy)-4,8-dimethyl-2-oxo-2 <i>H</i> -chromen-3-yl)acetate (EMAC10163d).....	49
2.2.3.5.	Synthesis of methyl 2-(4,8-dimethyl-7-(2-(4-nitrophenyl)-2-oxoethoxy)-2-oxo-2 <i>H</i> -chromen-3-yl)acetate (EMAC10163e).....	50
2.2.3.6.	Synthesis of methyl 2-(4,8-dimethyl-7-(2-(3-nitrophenyl)-2-oxoethoxy)-2-oxo-2 <i>H</i> -chromen-3-yl)acetate (EMAC10163f).....	51
2.2.3.7.	Synthesis of methyl 2-(7-(2-([1,1'-biphenyl]-4-yl)-2-oxoethoxy)-4,8-dimethyl-2-oxo-2 <i>H</i> -chromen-3-yl)acetate (EMAC10163g).....	52
2.2.3.8.	Synthesis of methyl 2-(7-(2-(2,4-difluorophenyl)-2-oxoethoxy)-4,8-dimethyl-2-oxo-2 <i>H</i> -chromen-3-yl)acetate (EMAC10163h).....	53
2.2.3.9.	Synthesis of methyl 2-(4,8-dimethyl-2-oxo-7-(2-oxo-2-phenylethoxy)-2 <i>H</i> -chromen-3-yl)acetate (EMAC10163j).....	54

2.2.3.10. Synthesis of methyl 2-(7-(2-(4-chlorophenyl)-2-oxoethoxy)-4,8-dimethyl-2-oxo-2 <i>H</i> -chromen-3-yl)acetate (EMAC10163k).....	55
2.2.3.11. Synthesis of methyl 2-(7-(2-(3-methoxyphenyl)-2-oxoethoxy)-4,8-dimethyl-2-oxo-2 <i>H</i> -chromen-3-yl)acetate (EMAC10163m).....	56
2.2.4. Synthesis of the 7 <i>H</i> -furo-chromen compounds (EMAC10164 series).....	57
2.2.4.1. Synthesis of 2-(5,9-dimethyl-7-oxo-3-(<i>p</i> -tolyl)-7 <i>H</i> -furo[3,2- <i>g</i>]chromen-6-yl)acetic acid (EMAC10164a)	57
2.2.4.2. Synthesis of 2-(3-(4-methoxyphenyl)-5,9-dimethyl-7-oxo-7 <i>H</i> -furo[3,2- <i>g</i>]chromen-6-yl)acetic acid (EMAC10164b)	58
2.2.4.3. Synthesis of 2-(3-(4-bromophenyl)-5,9-dimethyl-7-oxo-7 <i>H</i> -furo[3,2- <i>g</i>]chromen-6-yl)acetic acid (EMAC10164c).....	58
2.2.4.4. Synthesis of 2-(3-(4-fluorophenyl)-5,9-dimethyl-7-oxo-7 <i>H</i> -furo[3,2- <i>g</i>]chromen-6-yl)acetic acid (EMAC10164d)	59
2.2.4.5. Synthesis of 2-(3-([1,1'-biphenyl]-4-yl)-5,9-dimethyl-7-oxo-7 <i>H</i> -furo[3,2- <i>g</i>]chromen-6-yl)acetic acid (EMAC10164g)	60
2.2.4.6. Synthesis of 2-(3-(2,4-difluorophenyl)-5,9-dimethyl-7-oxo-7 <i>H</i> -furo[3,2- <i>g</i>]chromen-6-yl)acetic acid (EMAC10164h)	61
2.2.4.7. Synthesis of 2-(5,9-dimethyl-7-oxo-3-phenyl-7 <i>H</i> -furo[3,2- <i>g</i>]chromen-6-yl)acetic acid (EMAC10164j).....	62
2.2.4.8. Synthesis of 2-(3-(4-chlorophenyl)-5,9-dimethyl-7-oxo-7 <i>H</i> -furo[3,2- <i>g</i>]chromen-6-yl)acetic acid (EMAC10164k).....	62
2.2.4.9. Synthesis of 2-(3-(3-methoxyphenyl)-5,9-dimethyl-7-oxo-7 <i>H</i> -furo[3,2- <i>g</i>]chromen-6-yl)acetic acid (EMAC10164m)	63
2.3. Synthesis of chromones.....	65
2.3.1. Synthetic pathway	65
2.3.2. Synthesis of the phenylethanone compounds (EMAC10168 series)	65
2.3.2.1. Synthesis of 2-(4-acetyl-3-hydroxyphenoxy)-1-(<i>p</i> -tolyl)ethan-1-one (EMAC10168a).....	66
2.3.2.2. Synthesis of 2-(4-acetyl-3-hydroxyphenoxy)-1-(4-methoxyphenyl)ethan-1-one (EMAC10168b).....	66

TABLE OF CONTENTS

2.3.2.3. Synthesis of 2-(4-acetyl-3-hydroxyphenoxy)-1-(4-bromophenyl)ethan-1-one (EMAC10168c)	67
2.3.2.4. Synthesis of 2-(4-acetyl-3-hydroxyphenoxy)-1-(4-fluorophenyl)ethan-1-one (EMAC10168d)	68
2.3.2.5. Synthesis of 1-([1,1'-biphenyl]-4-yl)-2-(4-acetyl-3-hydroxyphenoxy)ethan-1-one (EMAC10168g)	69
2.3.2.6. Synthesis of 2-(4-acetyl-3-hydroxyphenoxy)-1-(4-chlorophenyl)ethan-1-one (EMAC10168k)	70
2.3.2.7. Synthesis of 2-(4-acetyl-3-hydroxyphenoxy)-1-(3-methoxyphenyl)ethan-1-one (EMAC10168m)	70
2.3.3. Synthesis of the 4 <i>H</i> -chromene compounds (EMAC10169 series)	71
2.3.3.1. Synthesis of 4-oxo-7-(2-oxo-2-(<i>p</i> -tolyl)ethoxy)-4 <i>H</i> -chromene-3-carbaldehyde (EMAC10169a)	72
2.3.3.2. Synthesis of 7-(2-(4-methoxyphenyl)-2-oxoethoxy)-4-oxo-4 <i>H</i> -chromene-3-carbaldehyde (EMAC10169b)	73
2.3.3.3. Synthesis of 7-(2-(4-bromophenyl)-2-oxoethoxy)-4-oxo-4 <i>H</i> -chromene-3-carbaldehyde (EMAC10169c)	74
2.3.3.4. Synthesis of 7-(2-(4-fluorophenyl)-2-oxoethoxy)-4-oxo-4 <i>H</i> -chromene-3-carbaldehyde (EMAC10169d)	75
2.3.3.5. Synthesis of 7-(2-([1,1'-biphenyl]-4-yl)-2-oxoethoxy)-4-oxo-4 <i>H</i> -chromene-3-carbaldehyde (EMAC10169g)	76
2.3.3.6. Synthesis of 7-(2-(4-chlorophenyl)-2-oxoethoxy)-4-oxo-4 <i>H</i> -chromene-3-carbaldehyde (EMAC10169k)	77
2.3.3.7. Synthesis of 7-(2-(3-methoxyphenyl)-2-oxoethoxy)-4-oxo-4 <i>H</i> -chromene-3-carbaldehyde (EMAC10169m)	78
2.4. Carbonic anhydrase inhibition assay	79
2.5. Binding DB and Pipeline Pilot as chemoinformatic tools for data search and mining	80
2.6. Theoretical prediction of drug-like properties	84
2.7. Molecular Docking	87
2.7.1. Ligand preparation	90

2.7.2.	Protein preparation.....	90
2.7.3.	Docking experiments.....	90
2.7.4.	Post-docking experiments.....	90
CHAPTER 3. Results and Discussion		93
3.1.	Synthesis of furocoumarins.....	95
3.2.	Synthesis of chromones.....	98
3.3.	Structural elucidation.....	100
3.3.1	Methyl 2-(7-hydroxy-4,8-dimethyl-2-oxo-2 <i>H</i> -chromen-3-yl)acetate (EMAC10163)	100
3.3.2.	2 <i>H</i> -chromen compounds (EMAC10163 series)	101
3.3.3.	<i>H</i> -furo-chromen compounds (EMAC10164 series).....	107
3.3.4.	Phenylethanone compounds (EMAC10168 series)	113
3.3.5.	4 <i>H</i> -chromene compounds (EMAC10169 series)	117
3.4.	Carbonic anhydrases inhibition	122
3.4.2.	2 <i>H</i> -chromen compounds (EMAC10163 series)	122
3.4.3.	7 <i>H</i> -furo-chromen compounds (EMAC10164series).....	123
3.4.4.	4 <i>H</i> -chromene compounds (EMAC10169 series)	124
3.5.	Theoretical prediction of drug-like properties.....	125
3.6.	Molecular docking	131
3.6.1.	CA IX docking	132
3.6.2.	CA XII docking	139
CHAPTER 4. Conclusions.....		145
CHAPTER 5. Other Projects		149
5.1.	Studies on synthetic route optimization	151
5.1.1.	An overview on Parkinson's disease	151
5.1.2.	Parkinson's disease therapy	151
5.1.3.	Project's synthetic strategy.....	153

TABLE OF CONTENTS

5.1.4.	Synthesis of 5-(benzyloxy)-2-(hydroxymethyl)-4 <i>H</i> -pyran-4-one (compound 2)	154
5.1.5.	Synthesis of 5-(benzyloxy)-4-oxo-4 <i>H</i> -pyran-2-carboxylic acid (compound 3)	154
5.1.6.	Synthesis of 3-(benzyloxy)-4 <i>H</i> -pyran-4-one (compound 4).....	155
5.1.7.	Synthesis of 3-(benzyloxy)-4 <i>H</i> -pyran-4-one (compound 5).....	157
5.1.8.	Final remarks	158
5.2.	Investigation on potential anti-HIV multi-target agents.....	159
5.2.1.	HIV – an overview	159
5.2.2.	HIV targets and their inhibitors	159
5.2.2.1.	Nucleoside and nucleotide reverse transcriptase inhibitors (NRTIs)	160
5.2.2.2.	Non-nucleoside reverse transcriptase inhibitors (NNRTIs)	161
5.2.2.3.	Protease inhibitors (PIs)	161
5.2.2.4.	Integrase inhibitors (INIs)	162
5.2.2.5.	Entry inhibitors (EIs).....	163
5.2.3.	Therapy in the management of HIV.....	164
5.2.4.	New approaches for HIV treatment	164
CHAPTER 6.	Bibliography.....	165
Appendix	203

List of figures

Figure 1. Estimated age-standardized incidence and mortality ratio of different types of cancer in 2020 worldwide	4
Figure 2. Schematic illustration of the subcellular localization of α -CAs	9
Figure 3. Protein fold in: (A) Monomeric α -CA, <i>hCA II</i> (PDB file 1CA2); (B) tetrameric β -CA, from <i>porphyridium purpureum</i> (PDB file 1DDZ); (C) homotrimeric γ -CA, from <i>methanosarcina thermophila</i> (PDB file 1THJ); (D) monomeric ζ -CA, from <i>Conticribra weissflogii</i> (PDB file 3BOB)	13
Figure 4. (A) Binding pocket of <i>hCA II</i> (PDB file: 1CA2); (B) Tetrahedral coordination of Zn^{2+} by the three catalytic histidine residues and a water molecule/hydroxide ion, which is involved in a well-defined network of hydrogen bonds.....	14
Figure 5. Catalytic mechanism of α -CAs	15
Figure 6. Binding mode of the CAls belonging to the zinc binders	17
Figure 7. Binding mode of the CAls which anchor to the Zn(II)-coordinated water molecule/hydroxide ion.....	18
Figure 8. Schematic representation of the inhibition active site with entrance-occluding CAls	19
Figure 9. Schematic representation of the inhibitor binding site with “out of the active site” CAls	20
Figure 10. Structures of clinically approved CAls used as diuretics	24
Figure 11. Structures of clinically approved CAls used in the treatment of glaucoma. ..	25
Figure 12. Structures of marketed CAls as anticonvulsants.....	27
Figure 13. Structure of Qnexa/Qsymia components, marketed drug used in the treatment of obesity.....	28
Figure 14. Structure of indisulam	29

LIST OF FIGURES

Figure 15. Structure of SCL-011, compound in Phase II clinical trials for treatment of advanced, metastatic solid tumors	30
Figure 16. Chemical structures of coumarin and chromone	31
Figure 17. Warfarin and novobiocin, two coumarin-based compounds used as pharmaceutical agents	32
Figure 18. Number of cross entries regarding coumarin substructures with biologic activity in CA IX and XII.....	32
Figure 19. Structures of the three series of compounds synthesized by the group and published in [238]	33
Figure 20. Structures of the coumarins isolated and published in [240]	34
Figure 21. Structures of the coumarin derivatives synthesized by the group and published in [239]	36
Figure 22. Examples of chromone-based compounds used as pharmaceutical agents...38	
Figure 23. Number of cross entries regarding chromone substructures with biologic activity in CA IX and XII.....	39
Figure 24. Rational design strategy followed for the development of CAIs based on coumarin and chromone scaffold.....	40
Figure 25. Schematic representation of the synthetic pathway used for the obtention of the furocoumarin family	45
Figure 26. Structure of EMAC10163.....	45
Figure 27. Structure of EMAC10163a.....	46
Figure 28. Structure of EMAC10163b.....	47
Figure 29. Structure of EMAC10163c.....	48
Figure 30. Structure of EMAC10163d.....	49
Figure 31. Structure of EMAC10163e.....	50
Figure 32. Structure of EMAC10163f.....	51

Figure 33. Structure of EMAC10163g.....	52
Figure 34. Structure of EMAC10163h.....	53
Figure 35. Structure of EMAC10163j.....	54
Figure 36. Structure of EMAC10163k.....	55
Figure 37. Structure of EMAC10163m.....	56
Figure 38. Structure of EMAC10164a.....	57
Figure 39. Structure of EMAC10164b.....	58
Figure 40. Structure of EMAC10164c.....	58
Figure 41. Structure of EMAC10164d.....	59
Figure 42. Structure of EMAC10164g.....	60
Figure 43. Structure of EMAC10164h.....	61
Figure 44. Structure of EMAC10164j.....	62
Figure 45. Structure of EMAC10164k.....	62
Figure 46. Structure of EMAC10164m.....	63
Figure 47. Schematic representation of the synthetic pathway used for the obtention of the chromone family.....	65
Figure 48. Structure of EMAC10168a.....	66
Figure 49. Structure of EMAC10168b.....	66
Figure 50. Structure of EMAC10168c.....	67
Figure 51. Structure of EMAC10168d.....	68
Figure 52. Structure of EMAC10168g.....	69
Figure 53. Structure of EMAC10168k.....	70
Figure 54. Structure of EMAC10168m.....	70

LIST OF FIGURES

Figure 55. Structure of EMAC10169a.....	72
Figure 56. Structure of EMAC10169b.....	73
Figure 57. Structure of EMAC10169c.....	74
Figure 58. Structure of EMAC10169d.....	75
Figure 59. Structure of EMAC10169g.....	76
Figure 60. Structure of EMAC10169k.....	77
Figure 61. Structure of EMAC10169m.....	78
Figure 62. Screenshot from Binding DB regarding chemical structure search of coumarin by substructure type and activity filters.....	80
Figure 63. Screenshot showing the results, without filtering, for substructure search in Binding DB: (A) coumarin; (B) chromone.....	80
Figure 64. Screenshot of Binding DB search results, with filtering, for: (A) coumarin; (B) chromone.....	81
Figure 65. Screenshot of the simple search page in Binding DB.....	82
Figure 66. Screenshot of the results table for (A) CA IX and (B) CA XII simple search in Binding DB.....	82
Figure 67. Screenshot of the Pipeline Pilot protocol for substructure search	83
Figure 68. Pechmann condensation proposed mechanism.....	95
Figure 69. Williamson Ether synthesis suggested mechanism.....	96
Figure 70. Intramolecular condensation and ester saponification proposed mechanism occurred in the synthesis of EMAC10164 series	97
Figure 71. Vilsmeier-Haack reagent <i>in situ</i> formation mechanistic proposal	99
Figure 72. Mechanistic proposal for the POCl ₃ -induced cyclisation.....	99
Figure 73. Representation of the putative binding mode of the most potent compounds from EMAC10163 series obtained by docking experiments to <i>hCA IX</i> . (A) 3D depiction of	

EMAC10163a and its respective interactions with CA IX residues; (B) 2D depiction of interactions; (C) 3D depiction of EMAC10163a and its respective interactions with CA IX residues considering a different orientation of the compound; (D) 2D depiction of interactions; (E) 3D depiction of EMAC10163b and its respective interactions with CA IX residues; (F) 2D depiction of interactions; (G) 3D depiction of EMAC10163b and its respective interactions with CA IX residues considering a different orientation of the compound; (H) 2D depiction of interactions. 133

Figure 74. Representation of the putative binding mode of the most potent compounds from EMAC10164 series obtained by docking experiments to *hCA IX*. (A) 3D depiction of EMAC10164d and its respective interactions with CA IX residues; (B) 2D depiction of interactions; (C) 3D depiction of EMAC10164g and its respective interactions with CA IX residues; (D) 2D depiction of interactions. 134

Figure 75. Representation of the putative binding mode of the most potent compounds from EMAC10169 series obtained by docking experiments to *hCA IX*. (A) 3D depiction of EMAC10164k and its respective interactions with CA IX residues; (B) 2D depiction of interactions; (C) 3D depiction of EMAC10164m and its respective interactions with CA IX residues; (D) 2D depiction of interactions. 134

Figure 76. Formation of the open EMAC10163 and EMAC10164 series by the CA-mediated hydrolysis of coumarins. 135

Figure 77. Representation of the putative binding mode of the most potent compounds from EMAC10163-open series obtained by docking experiments to *hCA IX*. (A) 3D depiction of EMAC10163a-open-E and its respective interactions with CA IX residues; (B) 2D depiction of interactions; (C) 3D depiction of EMAC10163a-open-Z and its respective interactions with CA IX residues; (D) 2D depiction of interactions; (E) 3D depiction of EMAC10163b-open-E and its respective interactions with CA IX residues; (F) 2D depiction of interactions; (G) 3D depiction of EMAC10163b-open-Z and its respective interactions with CA IX residues; (H) 2D depiction of interactions..... 137

Figure 78. Representation of the putative binding mode of the most potent compounds from EMAC10164-open series obtained by docking experiments to *hCA IX*. (A) 3D depiction of EMAC10164d-open-E and its respective interactions with CA IX residues; (B) 2D depiction of interactions; (C) 3D depiction of EMAC10164d-open-Z and its respective interactions with CA IX residues; (D) 2D depiction of interactions; (E) 3D depiction of EMAC10164g-open-E and its respective interactions with CA IX residues; (F) 2D depiction

of interactions; (G) 3D depiction of EMAC10164g-open-Z and its respective interactions with CA IX residues; (H) 2D depiction of interactions..... 138

Figure 79. Representation of the putative binding mode of the most potent compounds from EMAC10163 series obtained by docking experiments to *hCA XII*. (A) 3D depiction of EMAC10163a and its respective interactions with CA XII residues; (B) 2D depiction of interactions; (C) 3D depiction of EMAC10163b and its respective interactions with CA XII residues; (D) 2D depiction of interactions; (E) 3D depiction of EMAC10164b and its respective interactions with CA XII residues considering a different orientation of the compound; (F) 2D depiction of interactions 140

Figure 80. Representation of the putative binding mode of the most potent compounds from EMAC10164 series obtained by docking experiments to *hCA XII*. (A) 3D depiction of EMAC10164d and its respective interactions with CA XII residues; (B) 2D depiction of interactions; (C) 3D depiction of EMAC10164g and its respective interactions with CA XII residues; (D) 2D depiction of interactions. 141

Figure 81. Representation of the putative binding mode of the most potent compounds from EMAC10169 series obtained by docking experiments. (A) 3D depiction of EMAC10169k and its respective interactions with CA XII residues; (B) 2D depiction of interactions; (C) 3D depiction of EMAC10169k and its respective interactions with CA XII residues considering a different orientation of the compound; (D) 2D depiction of interactions;(E) 3D depiction of EMAC10169m and its respective interactions with CA XII residues; (F) 2D depiction of interactions; (G) 3D depiction of EMAC10169m and its respective interactions with CA XII residues considering a different orientation of the compound; (H) 2D depiction of interactions..... 142

Figure 82. Representation of the putative binding mode of the most potent compounds from EMAC10163-open series obtained by docking experiments to *hCA XII*. (A) 3D depiction of EMAC10163a-open-E and its respective interactions with CA XII residues; (B) 2D depiction of interactions; (C) 3D depiction of EMAC10163b-open-E and its respective interactions with CA XII residues; (D) 2D depiction of interactions..... 143

Figure 83. Representation of the putative binding mode of the most potent compounds from EMAC10164-open series obtained by docking experiments to *hCA XII*. (A) 3D depiction of EMAC10164d-open-E and its respective interactions with CA XII residues; (B) 2D depiction of interactions; (C) 3D depiction of EMAC10164g-open-E and its respective interactions with CA XII residues; (D) 2D depiction of interactions..... 144

Figure 84. Chemical structures of nitrocatechol-based COMT inhibitors: tolcapone, entacapone and opicapone	152
Figure 85. Schematic representation of the synthetic pathway used for the obtention of the HetCAMs libraries	153
Figure 86. Structure of compound 2	154
Figure 87. Structure of compound 3	154
Figure 88. Structure of compound 4	155
Figure 89. Structure of compound 5	157
Figure 90. Structure of nucleoside reverse transcriptase inhibitors and the nucleotide reverse transcriptase inhibitor	160
Figure 91. Structure of the approved NNRTIs.....	161
Figure 92. Structure of approved PIs	162
Figure 93. Structure of the marketed INIs	163
Figure 94. Structure of the marketed EI, maraviroc.....	163

List of tables

Table 1. Examples of pharmacotherapy used in the management of cancer	6
Table 2. Subcellular localization, organ/tissue distribution and level of catalytic activity of the 16 α -CA isozymes	10
Table 3. Reactions catalyzed by α -Cas.....	12
Table 4. Diseases in which CAs are involved.....	21
Table 5. Inhibition data of <i>hCA</i> I, II, IX and XII for the compounds published by Melis <i>et al.</i> and AAZ.....	33
Table 6. Inhibition data of <i>hCA</i> I, II, IX and XII for the compounds published by Fois <i>et al.</i> and AAZ.....	35
Table 7. Inhibition data of <i>hCA</i> I, II, IX and XII for the compounds published by Meleddu <i>et al.</i> and AAZ	36
Table 8. QikProp properties and descriptors with description and range or recommended values, from the QikPro user manual	84
Table 9. PDB code and ligand structure of the complexes formed with <i>hCA</i> IX.....	87
Table 10. PDB code and ligand structure of the complexes formed with <i>hCA</i> XII.....	88
Table 11. Cross-docking results considering the co-crystallized ligands reported in pdb complexes.....	89
Table 12. Yields of the EMAC10163 series synthesis	96
Table 13. Yields of the EMAC10164 series synthesis	97
Table 14. Yields of the EMAC10168 series synthesis	98
Table 15. Yields of the EMAC10169 series syntheses	99
Table 16. ^1H NMR data from EMAC10163	100
Table 17. ^{13}C NMR data from EMAC10163.....	101

LIST OF TABLES

Table 18. ^1H NMR data from EMAC10163a-e.....	103
Table 19. ^1H NMR data from EMAC10163f-h and j-m.....	104
Table 20. ^{13}C and DEPT NMR data from EMAC10163a-e.....	105
Table 21. ^{13}C and DEPT NMR data from EMAC10163f-h and j-m.....	106
Table 22. ^1H NMR data from EMAC10164a-d.....	108
Table 23. ^1H NMR data from EMAC10164g-h and j-m.....	109
Table 24. ^{13}C and DEPT NMR data from EMAC10164a-d.....	111
Table 25. ^{13}C and DEPT NMR data from EMAC10164g-h and j-m.....	112
Table 26. ^1H NMR data from EMAC 10168a-d.....	114
Table 27. ^1H NMR data from EMAC 10168g, k, and m.....	115
Table 28. ^{13}C and DEPT NMR data from the EMAC10168 series.....	116
Table 29. ^1H NMR data from EMAC10169a-d.....	118
Table 30. ^1H NMR data from EMAC 10169g, k, and m.....	119
Table 31. ^{13}C and DEPT NMR data from the EMAC10169 series.....	120
Table 32. Mass spectrometry data.....	121
Table 33. Inhibition data of <i>hCA</i> I, II, IX and XII for the EMAC10163 series and AAZ..	122
Table 34. Inhibition data of <i>hCA</i> I, II, IX and XII for the EMAC10164 series and AAZ..	123
Table 35. Inhibition data of <i>hCA</i> I, II, IX and XII for the EMAC10169 series and AAZ..	124
Table 36. Predicted properties for the series EMAC10163.....	125
Table 37. Predicted properties for the series EMAC10164.....	126
Table 38. Predicted properties for the series EMAC10169.....	126
Table 39. Ranges of pharmacokinetics properties calculated considering 95% of drugs	127

Table 40. Predicted pharmacokinetics properties for the series EMAC10163	127
Table 41. Predicted pharmacokinetics properties for the series EMAC10164	128
Table 42. Predicted pharmacokinetics properties for the series EMAC10169	128
Table 43. Detailed reaction conditions for optimization purposes	156

List of abbreviations

AAZ	<i>Acetazolamide</i>
AIDS	<i>Acquired immunodeficiency syndrome</i>
ARS	<i>Age-standardized rate</i>
BBB	<i>Blood-brain barrier</i>
CA	<i>Carbonic anhydrase</i>
CAAs	<i>Carbonic anhydrase activators</i>
CACO	<i>Colorectal adenocarcinoma</i>
CAIs	<i>Carbonic anhydrases inhibitors</i>
CARPs	<i>CA-related proteins</i>
COMT	<i>Catechol-O-methyltransferase</i>
DA	<i>Dopamine</i>
DCM	<i>Dichloromethane</i>
DEPT	<i>Distortionless enhancement by polarization transfer</i>
EI	<i>Entry inhibitor</i>
ESI/MS	<i>Electrospray ionization mass spectrometry</i>
EtOAc	<i>Ethyl acetate</i>
GB/SA	<i>generalized Born/surface area</i>
GPI	<i>Glycosylphosphatidylinositol</i>
H	<i>Human</i>
HIV	<i>Human immunodeficiency virus</i>
HPV	<i>Human papillomavirus</i>

LIST OF ABBREVIATIONS

INI	<i>Integrase inhibitor</i>
MDCK	<i>Madin-Darby Canine Kidney</i>
MMFF	<i>Merck Molecular Force Field</i>
NMP	<i>1-Methyl-2-pyrrolidinone</i>
NNRTI	<i>Non-nucleoside reverse transcriptase inhibitor</i>
NRTI	<i>Nucleoside and nucleotide reverse transcriptase inhibitor</i>
PD	<i>Parkinson's disease</i>
PI	<i>Protease inhibitor</i>
PRCG	<i>Polak–Ribier Conjugate Gradient</i>
QMPL	<i>Quantum Mechanics-Polarized Ligand</i>
Rf	<i>Retention factor</i>
RMCD	<i>Root Mean Square Deviation</i>
TLC	<i>Thin layer chromatography</i>
TMS	<i>Tetramethylsilane</i>
ZBG	<i>Zinc-binding group</i>

CHAPTER 1. Introduction

1.1. Cancer: an overview

Cancer is a hypernym that describes more than two hundred different diseases characterized by the uncontrolled growth of abnormal cells with malignant potential. Even though cancer can develop in virtually any tissue, and each type of cancer has its unique characteristics, the basic processes that produce cancer are quite similar in all forms of the disease [1, 2]. Cancer begins when a cell breaks free from the normal restraints on cell division and begins to follow its own schedule for proliferation. All the cells produced by division of this first cell also display inappropriate proliferation. A tumor, or mass of cells, formed of these abnormal cells may remain within the tissue in which its originated or it may begin to invade nearby tissues. Tumors threaten an individual's life when their growth disrupts the tissues and organs needed for survival [3-5].

As the second leading cause of death in most of the countries after cardiovascular diseases, cancer is a major public health problem in all populations, unrelated with wealth and social status [6, 7]. Cancer is already responsible for 1 in 6 deaths in the world. In 2018, 18.1 million people around the world had cancer, and 9.6 million died from the disease. By 2040 cancer rates are projected to rise by at least 60 %, with the greatest increase in lower-middle-income countries, where two thirds of the world cancers will occur [8, 9]. The most common types are lung, colorectal, breast, prostate, skin, stomach and liver cancer. Regarding incidence, the most frequently diagnosed cancer is breast cancer followed by prostate and lung cancer, and concerning mortality, lung cancer leads, followed by breast and colorectum cancer (Figure 1). On men, the most diagnosed is lung cancer followed by prostate cancer, which is the major cancer-related cause of death in men, followed by liver cancer. Breast cancers have the higher incidence rate in women, followed by colorectal and lung cancer. Not surprisingly, breast cancer is the leading cancer-related cause of death in women followed by lung cancer [8, 10-12].

Significant progress has been made in recent years regarding prevention and treatment options, for certain cancers. However, despite this progress, as life-expectancy and global population rises, cancer burden will continue incrising [13-17]. Hence, is of global interest to reduce this burden through early detection of cancer and appropriate treatment and care of patients who develop cancer.

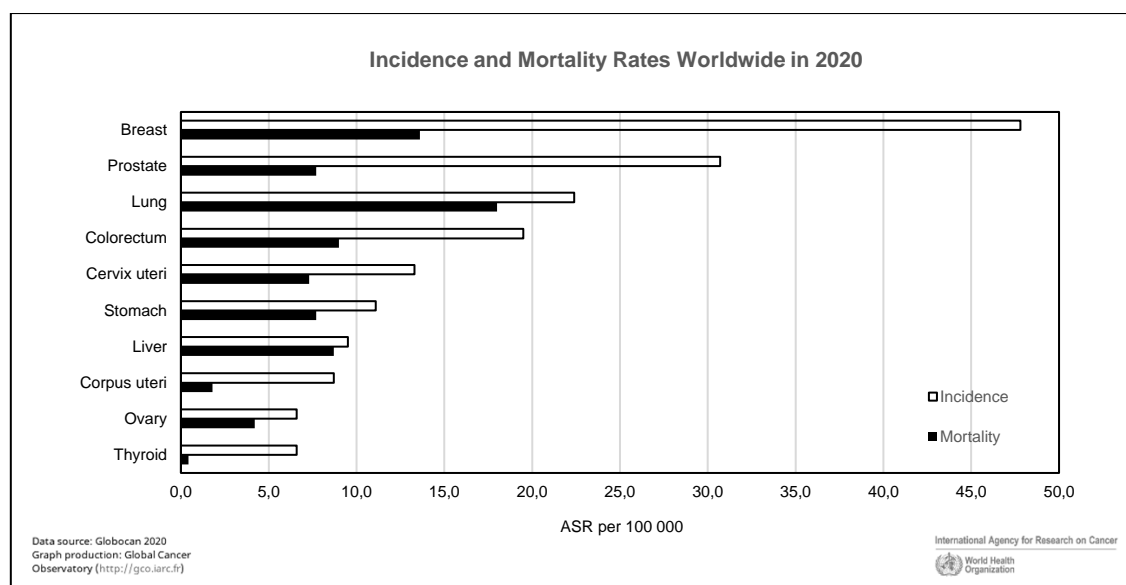


Figure 1. Estimated age-standardized incidence and mortality ratio of different types of cancer in 2020 worldwide (both sexes combined, all ages).

1.1.1. Etiology and pathogenesis

It is consensual in the academic community that genetic factors play a small role in cancer susceptibility (around 5 – 10%) and that the bigger contribution is due to environmental and lifestyle factors, such as cigarette smoking, diet, alcohol, sun exposure, stress, pollutants, and infections (90 – 95 %) [18-21]. Except for certain types of familial cancer at a few sites (such as prostate, colorectal, bladder and breast), familial predisposition for cancer may be due to the effects of several fewer penetrant genes interacting with environmental factors and only a small percentage of common cancers will be due to a strong inherited susceptibility [21-28]. Although all cancers are a result of multiple mutations, these mutations are a result of a multi-stage interaction of genetic and environmental factors [29].

Cancer is classified into four types according with nature of cells or tissues involved: carcinoma (neoplastic cells in the skin and tissues in the linings of internal organs); sarcoma (connective tissues like bone, cartilage, blood vessels, and muscles); leukemia (bone marrow, leading to formation of abnormal blood cells); lymphoma (immune cells) [30]. Evidence indicates that of all cancer-related deaths, almost 25-30 % are due to tobacco [31-33], 30-25% are linked to diet [19, 33, 34] and about 15-20% are attributable to infections (such as *Helicobacter pylori*, human papillomavirus (HPV), hepatitis B virus, and hepatitis C virus) [18, 35]. The remaining percentage are a consequence for other factors like radiation, stress, environmental pollutants, etc. [34, 36-38]. The importance of

lifestyle factors in the development of cancer was also shown in studies of monozygotic twins [18, 21, 39, 40].

The hallmarks of cancer were originally outlined in 2000 and reviewed in 2011 by Hanahan and Weinberg [2, 41] to cover key biological capabilities that are acquired and essential for development, growth, and dissemination of all human cancers. Eight hallmarks of cancer (sustaining proliferative signaling, evading growth suppressors, resisting cell death, enabling replicative immortality, inducing angiogenesis, activating invasion and metastasis, reprogramming energy metabolism, and evading immune destruction) and two characteristics that facilitate the acquisition of hallmark capabilities (genome instability and mutation, and tumor promoting inflammation) were described by them and referred in the years that followed [42-45]. More recently, Welch and Hurst proposed four hallmarks of metastasis: mobility and invasion, modulate microenvironment, plasticity, and colonization in an attempt to make available the means for directing efforts on the aspects of metastasis, that will improve patient outcomes [46].

1.1.2. Pharmacotherapy

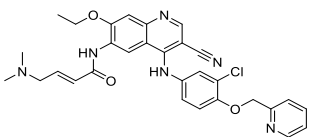
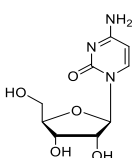
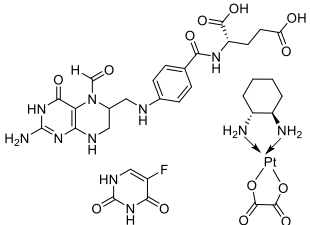
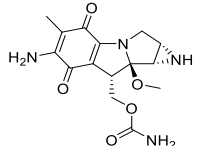
Cancer management has evolved drastically in the last years with the improved understanding of cancer biology, and a range of treatments are used, primarily depending on the location, type, and extent of the cancer to treat. The main approaches are surgery, radiation, and pharmacotherapy, that may be used either alone or in combination [47]. Cancer pharmacotherapy can be divided in four different groups, accordingly with the medication impact mechanism: chemotherapy, hormonal therapies, targeted and immunologic drugs [48, 49]. Pharmacotherapy may be used for primary treatment of cancer where the goal is to completely remove the cancer; as adjuvant pharmacotherapy, used after surgery, in which the goal is to target any remaining cancer cells following primary treatment; as neoadjuvant pharmacotherapy, in which the goal is to shrink tumors and reduce cancer, before surgery; and for palliative care where the goal is the symptom management through tumor reduction to give the patient the best quality of life [49].

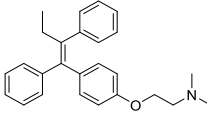
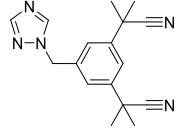
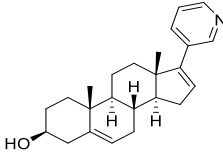
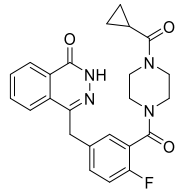
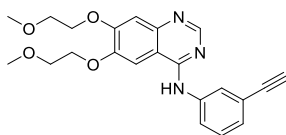
Cancer pharmacotherapy, surgery and radiation carry different risks and benefits, with potential antagonist and synergistic interactions between them [48]. The choice of treatment is primarily dependent on location, type and extent of the cancer being treated. On the case of early-stage lung cancer, surgery remains the treatment of choice, with radiotherapy as second option for patients not suitable for surgical lobectomy. In locally advanced disease, the recommendation is surgery with adjuvant chemotherapy or combination chemotherapy and radiotherapy, whereas for metastatic disease

pharmacotherapy guided by tumor type, including the presence of genetic mutation, is used [49-51]. Management of breast cancer is dependent on factors such as health, tumor location, involvement of nodes, tumor stage and molecular target. Pharmacotherapy can be used as neoadjuvant or adjuvant therapy as chemotherapy, HER-targeted treatments, and endocrine therapy [49, 52]. Regarding localized prostate cancer, radiotherapy or prostatectomy remain first-line treatment with adjuvant and neoadjuvant androgen deprivation pharmacotherapy [49, 53]. Surgery is the primary option to treat colon cancer with pharmacotherapy reserved for later stages, for example chemotherapy is used for tumors classified as stage III or above [49, 54]. On Table 1 are some examples of pharmacotherapeutic drugs used in the management of cancer.

Even though many of the pharmacotherapies used nowadays show effectiveness, the side effects associated with them can be severe, often limiting their use and consequently, their effectiveness. Hence, the development of effective pharmacotherapies, more targeted, better tolerated, and with less adverse impacts on the patients has receive major attention.

Table 1. Examples of pharmacotherapy used in the management of cancer.

Type of therapy	Drug	Structure	Cancer	Reference
Chemotherapy	Neratinib		Breast cancer	[52]
	Cytarabine		Acute myeloid leukemia	[55]
	FOLFOX (leucovorin/ 5-fluorouracil/ oxaliplatin)		Colon cancer	[54]
	Mytomicin		Lung cancer	[50]

Hormonal therapies	Tamoxifen		Breast cancer	[56]
	Anastrozole		Breast cancer	[48]
	Abiraterone		Prostate cancer	[53]
Targeted drugs	Olaparib		Ovarian and breast cancer, pancreatic adenocarcinoma, prostate cancer	[57, 58]
	Erlotinib		Lung cancer	[51]
Immunologic drugs	Bevacizumab	Antibody	Lung cancer	[59]
	Trastuzumab Lapatinib	Monoclonal antibodies	Metastatic breast cancer	[52, 59]
	Nivolumab	Monoclonal antibody	Melanoma, renal cell carcinoma, lung cancer	[60]

1.1.3. Future directions

In parallel with the observations made regarding the psychological and economic burden caused by cancer (see section 1.1), which have a significant impact on patients, caregivers and healthcare systems, there is an emergent clinical need of therapies that overcome the drawbacks of conventional cancer therapies (e.g., drug resistance, lack of specificity and selectivity, cytotoxicity, accumulation of drugs on non-target tissues, and adverse events).

Major attention is being given to the development of advanced drug delivery systems as a strategy on cancer treatment, which can overcome the drawbacks of conventional therapies and improve the efficacy of drugs [61, 62]. Targeted nanocarriers have been

evaluated for their better efficacy in animal models, but their clinical success is limited. Hence, more data are needed for better understanding the pros and cons of these vehicles [63]. Hydrogels are also being studied as a platform for localized therapy, but few are available in the market for tumor therapy. Despite their great potential more studies and research regarding the combination with other therapies are needed to overcome some of their limitations [64]. Recently, immune system of patients and its activation via biological therapies, for instance immunotherapy and oncolytic virus therapy, are also receiving a great deal of attention, for being usually more physiological and well tolerated. These therapies aim to specifically activate the immune system against cancer and have lower side effects due to immune tolerance mechanisms, when compared with chemotherapy [65].

In addition, the pharmacotherapy used in the conventional treatments is continuously being studied and adjusted accordingly [66-69].

1.2. Carbonic anhydrases

Carbonic anhydrases (CAs) are a class of metalloenzymes, more precisely, zinc enzymes, widely distributed in all living organisms that catalyse the reversible hydration reaction of carbon dioxide into bicarbonate and a proton ($\text{CO}_2 + \text{H}_2\text{O} \leftrightarrow \text{HCO}_3^- + \text{H}^+$) [70, 71]. These enzymes are encoded, up until now, by eight different, evolutionarily unrelated gene families or classes: the α -CAs (present in vertebrates, plants, Bacteria, Archaea, cyanobacteria marine diatoms, protozoa, and some filamentous ascomycetes), the β -CAs (predominantly in Bacteria, Archaea, cyanobacteria, protozoa and filamentous ascomycetes), the γ -CAs (mainly in Bacteria, Archaea and cyanobacteria), the δ -CAs (recognized in some marine diatoms and in the fungal kingdom), the ζ -CAs (encoded by marine diatoms), the η -CAs (detected in protozoa), the θ -CAs (contained in marine diatoms), and the ι -CAs (present in Bacteria, Archaea, cyanobacteria and marine diatoms) [72-78]. These families or classes can be classified as non-homologous isofunctional enzymes that catalyse the same reaction considering they are phylogenetically unrelated [74].

Mammals encode only for α -CAs class that have 16 known isoforms with different subcellular localization (Figure 2), and catalytic activity (see Table 2). Accordingly, CA I, II, III, VII, VIII, X, XI and XIII are expressed in the cytoplasm; CA IX, XII, and XIV are membrane bound forms; CA IV and XV (this one not expressed in humans [79]) are glycosylphosphatidylinositol (GPI)-anchored membrane forms; CA VA and VB are mitochondrial forms and CA VI is a saliva-secreted form. Three of the cytosolic isoforms (VIII, X, and XI), called CA-related proteins (CARPs) are catalytically inactive as they lack one or more histidine residues coordinating the zinc ion in the active site. On the other hand, transmembrane isoforms are highly active enzymes and glycoproteins [71, 80, 81].

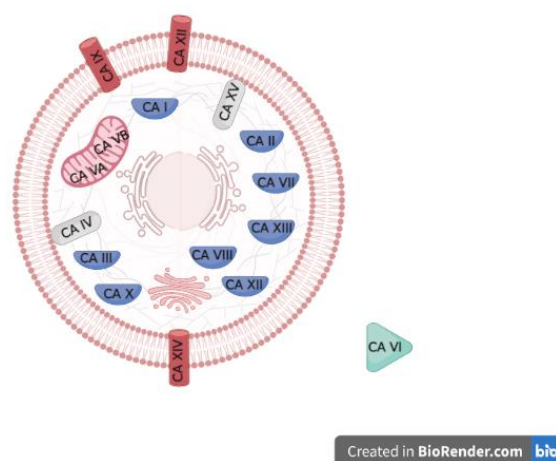


Figure 2. Schematic illustration of the subcellular localization of α -CAs.

Table 2. Subcellular localization, organ/tissue distribution and level of catalytic activity of the 16 α -CA isozymes.

Isozyme	Subcellular Localization	Organ/Tissue Distribution	CO ₂ Hydration Activity	References
<i>hCA I</i>	Cytosol	Erythrocytes, kidneys, gastrointestinal tract, lungs, brain, eyes	Low	[82]
<i>hCA II</i>	Cytosol	Erythrocytes, eye, gastrointestinal tract, kidney, brain	High	[83]
<i>hCA III</i>	Cytosol	Skeletal muscle, liver, adipocytes	Low	[84]
<i>hCA IV</i>	(GPI)-anchored	Kidney, lung, pancreas, brain capillaries, colon, heart muscle, eye	High	[85]
<i>hCA VA</i>	Mitochondria	Liver, skeletal muscle, kidneys, brain	Moderate	
<i>hCA VB</i>	Mitochondria	Heart, skeletal muscle, pancreas, kidney, spinal cord, salivary glands	High	[86]
<i>hCA VI</i>	Secreted	Salivary and mammary glands	Moderate	[87]
<i>hCA VII</i>	Cytosol	Brain, colon, liver, skeletal muscle, stomach, duodenum, colon, liver	Very high	[88]
<i>hCA VIII</i>	Cytosol	Brain, liver, lung, heart, gut, kidney, tumors	-	
<i>hCA IX</i>	Membrane-bound	Tumors, gastrointestinal tract	High	[89]
<i>hCA X</i>	Cytosol	Brain	-	[90]
<i>hCA XI</i>	Cytosol	Brain, tumors	-	
<i>hCA XII</i>	Membrane-bound	Kidney, colon, prostate, brain, pancreas, ovary, eye, tumors	High	[89]
<i>hCA XIII</i>	Cytosol	Kidney, brain, prostate, gastrointestinal tract, reproductive tract	Low	[91]
<i>hCA XIV</i>	Membrane-bound	Brain, heart, skeletal muscle, kidney, liver	Medium	[90]
<i>mCA XV</i>	(GPI)-anchored	Kidney, brain, testis	Low	[79]

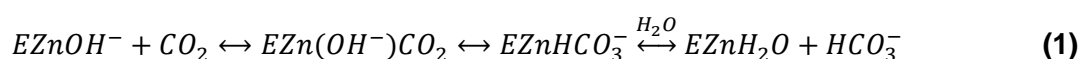
h = human; *m* = mouse enzyme. *hCA VIII*, *X* and *XI* are catalytically inactive.

1.2.1. CAs physiological and pathological roles

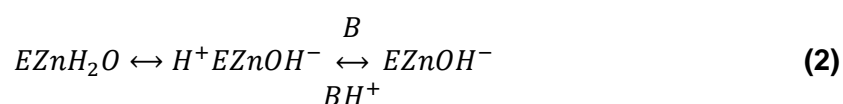
As referred before (see section 1.2), these metalloenzymes catalyse a very simple physiological reaction, the reversible hydration of CO₂ (reaction 3, Table 3), which allows them to regulate intra- and extra-cellular concentrations of CO₂, H⁺, and HCO₃⁻. Decades of research have implicated CA in a broad range of crucial physiological processes connected with respiration and transport of CO₂/bicarbonate across membranes, pH and CO₂ homeostasis, electrolyte secretion in a variety of tissues/organs, biosynthetic reactions in metabolically active tissue (such as gluconeogenesis, lipogenesis and ureagenesis), bone resorption, calcification, acid–base balance, tumorigenicity, signal transduction, proliferation and many other physiologic or pathologic processes [72, 81].

It's important to refer that the chemical kinetics of CO₂ hydration and HCO₃⁻ dehydration are too slow for CO₂ elimination making carbonic anhydrases of great importance for the CO₂ transport and elimination [92, 93]. This catalytic mechanism has been fully described [81, 94], and nevertheless most of the work done to understand it concerns the cytosolic high-activity isozyme, *hCA II*, available evidence indicates that all α-CAs share the same general mechanism, usually called the zinc-hydroxide mechanism since they possess within their active sites a highly nucleophilic metal hydroxide ion [95].

Briefly, the first step in the hydration direction of the reaction is the nucleophilic attack by the zinc-bound hydroxide to a substrate molecule (CO₂) that is brought into the active site pocket of the CA. This directly forms a bicarbonate ion, which is then displaced from the active site by a water molecule [94, 95]. This process can be described by the following equation:



Then the second step takes place with the regeneration of the catalytically active zinc-bound hydroxide ion consisting in a proton transfer reaction from the zinc-bound water molecule to an exogenous proton acceptor or to an active site residue (B) [94, 95], as described by the following equation:



In addition to the hydration of CO₂, α-CAs are also involved in a range of other hydrolytic processes, such as: the hydration of cyanate to carbamic acid, or of cyanamide to urea (reactions 4 and 5, Table 3); the aldehyde hydration to gem-diols (reaction 6, Table 3); the

hydrolysis of carboxylic, or sulfonic (reactions 7 and 8, Table 3), as well as other less investigated hydrolytic processes, such as those described by reactions 9–11 in Table 3. It should be mentioned that it is unclear at this moment whether α -CA catalyzed reactions other than the CO_2 hydration have physiological significance [72, 96].

Table 3. Reactions catalyzed by α -Cas.

(3) $\text{CO}_2 + \text{H}_2\text{O} \rightleftharpoons \text{HCO}_3^- + \text{H}^+$
(4) $\text{CONH} + \text{H}_2\text{O} \rightleftharpoons \text{H}_2\text{NCOOH}$
(5) $\text{C}(\text{NH})_2 + \text{H}_2\text{O} \rightleftharpoons \text{H}_2\text{NCONH}_2$
(6) $\text{RCHO} + \text{H}_2\text{O} \rightleftharpoons \text{RCH}(\text{OH})_2$
(7) $\text{RCOOAr} + \text{H}_2\text{O} \rightleftharpoons \text{RCOOH} + \text{ArOH}$
(8) $\text{RSO}_3\text{Ar} + \text{H}_2\text{O} \rightleftharpoons \text{RSO}_3\text{H} + \text{ArOH}$
(9) $\text{ArF} + \text{H}_2\text{O} \rightleftharpoons \text{HF} + \text{ArOH}$ (Ar = 2,4 – dinitrophenyl)
(10) $\text{PhCH}_2\text{OCOCl} + \text{H}_2\text{O} \rightleftharpoons \text{PhCH}_2\text{OH} + \text{CO}_2 + \text{HCl}$
(11) $\text{RSO}_2\text{Cl} + \text{H}_2\text{O} \rightleftharpoons \text{RSO}_3\text{H} + \text{HCl}$ (R = Me; Ph)

Not surprisingly, dysregulated expression and/or abnormal activity of *h*CAs can result in severe pathological conditions as they are involved in a wealth of essential physiological processes [92, 93].

1.2.2. CAs structural features

All life kingdoms present CAs, which are grouped into eight genetically distinct families reported so far: α -, β -, γ -, δ -, ζ -, η -, θ - and ι -classes [97, 98]. Though the eight different CA-classes originated from a common ancestor, they are phylogenetically distinct. The representative amino acid sequences of each CA-class show little sequence similarity, diverse folds, and structures when compared with the polypeptide chain of other CAs belonging to a different class. In contrast, the mechanism involved in the reversible hydration of the CO_2 is strictly conserved among all the CA-classes, demonstrating the prevalent convergent evolution of the CA superfamily. [98]. All CAs are metalloenzymes,

most of them zinc containing enzymes in a tetrahedral geometry, nevertheless Fe (II) is present within the active site of the γ -CAs (although they can coordinate Zn (II) or Co (II), too), whereas Cd (II) or Zn(II) ions are equally effective for promoting catalysis in the ζ -CAs and Mn (II) is preferred as ion cofactor by ι -CAs. The metal ion from the enzyme active site is coordinated by three amino acid residues from the protein backbone: His residues (in the α -, γ - δ -, η - and θ -class enzymes), one His, and two Cys residues (in the β - and ζ -CAs) or two His and one Gln residues (in η -class enzymes). Probably, in the diatom ι -CAs the residues involved in the coordination of Mn^{2+} are two His, one Asp and one Glu, even though their nature was not yet undoubtedly identified. The fourth ion ligand is a water molecule/ hydroxide ion acting as the nucleophile in the catalytic cycle of the enzyme [97-99].

Regarding the structural point of view, as mentioned above, the representatives belonging to a certain CA-class show a diverse folding and structure compared to those belonging to other CA-classes, as can be seen in Figure 3. α -CAs are usually active as monomers or dimers; β -CAs are active only as dimers, tetramers, or octamers. The γ -CAs must be trimers for accomplishing their catalytic function [98, 100-103]. The X-ray structure of the θ -CAs resulted to be very similar to the β -CAs [104]. The crystal structure of ζ -CA showed three slightly different active sites on the same polypeptide chain [105]. At this moment, no information is available on the structures of δ -, η -, and ι -CAs.

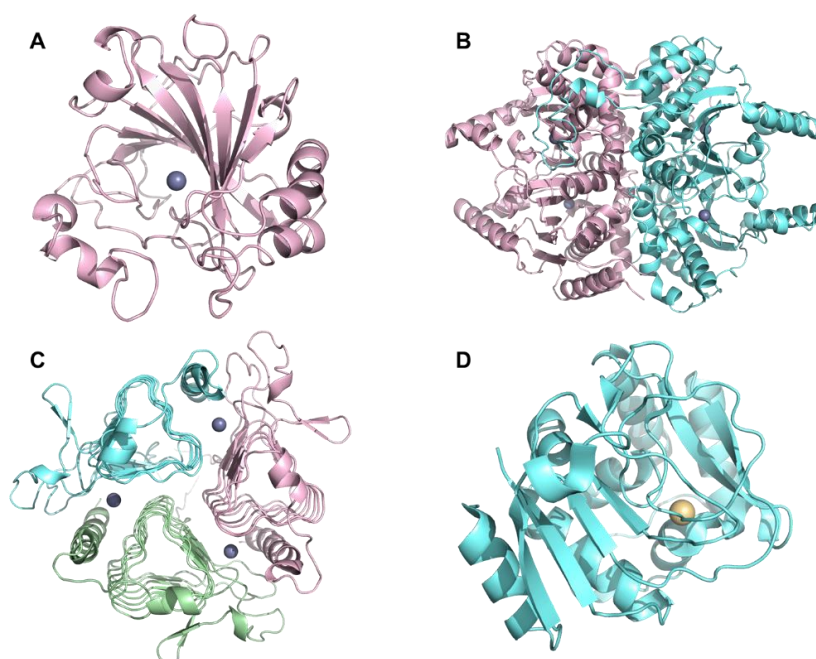


Figure 3. Protein fold in: (A) Monomeric α -CA, *hCA II* (PDB file 1CA2); (B) tetrameric β -CA, from *porphyridium purpureum* (PDB file 1DDZ); (C) homotrimeric γ -CA, from *methanosarcina thermophila* (PDB file 1THJ); (D) monomeric ζ -CA, from *Conticribra weissflogii* (PDB file 3BOB).

1.2.2.1. α -CAs structure

Up to the present, all human catalytically active α -CAs have been determined by X-ray crystallography [106-110], excluding the mitochondrial isoforms CAs VA and VB, for which only the corresponding murine enzyme mCA V has been characterized [111]. Analyzing such structures revealed that, as expected on the basis of their high degree of sequence identity [112] and independently on their subcellular localization, all these enzymes present a typical three-dimensional fold consisting of a central twisted β -sheet surrounded by several helical connections and additional β -strands (Figure 3). Moreover, all isoforms are monomeric [111], except the two membrane-associated CA IX [108] and CA XII [113] and the secreted CA VI [114], which, on the contrary, are dimeric proteins [83]. Although the best-studied isozyme characterized CA isoform is CA II, an accurate structural comparison of all *h*CAs crystallized so far can highlight that only a small number of local structural differences exist [99, 115, 116].

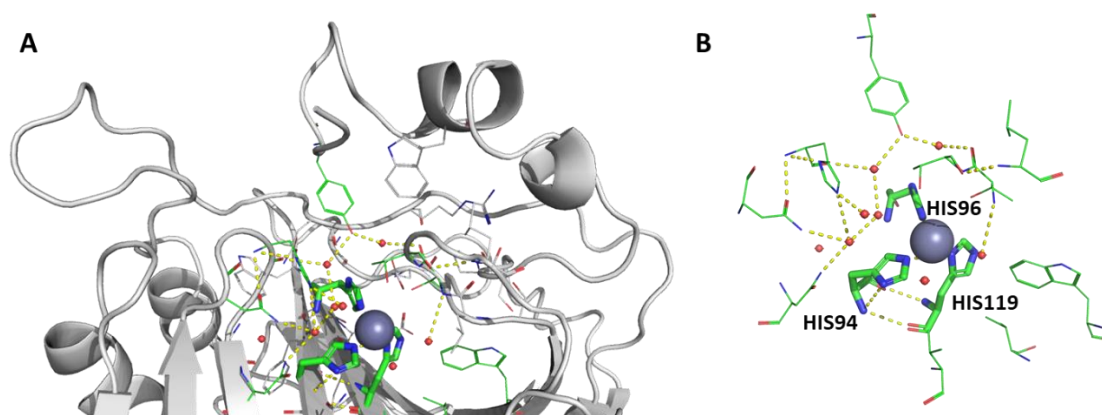


Figure 4. (A) Binding pocket of *h*CA II (PDB file: 1CA2); (B) Tetrahedral coordination of Zn²⁺ by the three catalytic histidine residues and a water molecule/hydroxide ion, which is involved in a well-defined network of hydrogen bonds. Water molecules are indicated as red spheres.

X-ray crystallographic data showed that the active site is located in a large conical cavity, which crosses the protein from the center to its surface. In all isoforms, the active site cavity contains two very different regions: the first one bound by a cluster of hydrophobic amino acids, and the second one formed by hydrophilic residues. As suggested by several studies the hydrophobic region is necessary to sequester the CO₂ substrate and conveniently orient the carbon atom for the catalytic reaction, whereas the hydrophilic region is involved in the release of the polar components generated from the CO₂ hydration reaction (bicarbonate and protons) from the cavity toward the solvent. The catalytic metal ion, which is Zn (II) in all α -CA investigated until now, is situated at the bottom of this active site cleft, approximately wide 12 Å and deep 15 Å, and is tetrahedrally coordinated by

three histidine residues (His94, His96 and His119, residue number is referred to hCA II) and a water molecule/ hydroxide ion. Figure 4, chosen as a representative *hCA* isoform shows the Zn^{2+} active site. [72, 75, 117, 118].

1.2.3. CAs catalytic features

The reaction catalyzed by the α -CAs follows a well-understood two-step catalytic mechanism (see section 1.2.1), with the zinc-bound hydroxide acting as the catalytically active specie in the active site [83]. In the first step, the nucleophilic attack of this hydroxide ion on a CO_2 molecule (Figure 5-B), bound in a hydrophobic pocket in its neighborhood [119], leads to the formation of a zinc-bound bicarbonate (Figure 5-C). The binding mode of the bicarbonate to the zinc is rather unstable, and thus the intermediate C is readily transformed to D by reaction with water, liberating bicarbonate into solution [120, 121] and generating the acidic form of the enzyme, catalytically ineffective (Figure 5-D). For many CA classes (including α -CA) the rate-limiting step of the catalytic mechanism is the second step, where the catalytically active form of the enzyme is regenerated through a proton transfer reaction from the zinc-coordinated water molecule to the environment [122].

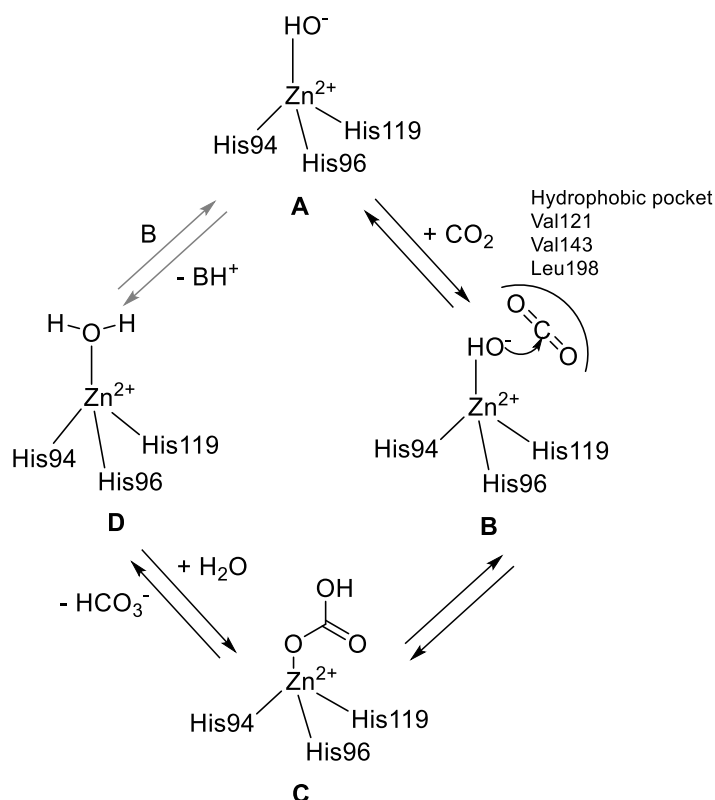
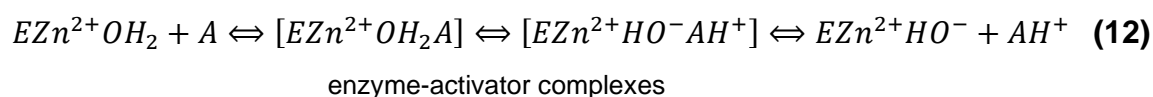


Figure 5. Catalytic mechanism of α -Cas. Black arrows correspond to the step reactions and grey arrow to the second step reaction of the catalytic mechanism. Adapted from [120].

This mechanism has been deeply studied [83, 94, 121] and although this physiological pathway is simple, there are some relevant features which characterize it, which have important consequences for the catalysis and inhibition of this superfamily of enzymes. First, CO₂ substrate is a gas and a quite hydrophobic molecule, and the product obtained by its hydration, bicarbonate, is a polar, highly water-soluble ion. Both of them are particularly small and it would be expected that the CAs are enzymes with small active sites. Apart from this, an even more striking feature of these active sites is that half of the cavity is aligned only with hydrophobic amino acid residues (comprising residues Val121, Val143 and Leu198 in the case of the *hCA II*), while the opposite half with hydrophilic ones, leading to a 'bipolar' active site architecture exclusive for this enzyme superfamily [117, 119, 123]. The most probable explanation for this particular active site architecture is that the hydrophobic part is used to entrap the CO₂ molecule, whereas the hydrophilic half may be involved in the release of the ions generated from the CO₂ hydration reaction (bicarbonate and protons) from the cavity to the environment. This fact is well demonstrated for the proton release pathway, in which a relay of water molecules and several histidines (acting as proton shuttling residues) were shown to be involved. Last but not least, these particular active sites also have important consequences for the binding of CA inhibitors (CAIs) and activators to the enzymes [119, 123-125].

1.2.4. Activators and Inhibitors

CA activators (CAAs) bind at the entrance of the active site cavity and form an enzyme-activator complex, hence participating on the rate-determining step of the catalytic cycle [126]. CAAs were a controversial issue for a long time until work with highly purified enzymes and very precise techniques unquestionably demonstrated that they exist and interfere directly in the proton-transfer step of the catalytic cycle, facilitating the intramolecular process by means of transient enzyme-activator complexes. As intramolecular reactions are faster than the intermolecular ones this results in a significantly catalytic rate increase [126, 127]. A general mechanism of action was proposed [127], based in the following equation:



It has been reported that some CAAs administered to animals improve memory deficits, cognitive performance, and learning [128, 129], proving that this class of enzyme modulators may have important applications in conditions such as aging or Alzheimer's disease, where learning and memory are implicated. However, no clinical trials for the use

of CAAs on these health conditions were done and, hence there are not clinically approved CAAs for the moment [129-131]. Contrarily, inhibition of the CAs has pharmacological applications for decades to treat various conditions [127, 130, 132]. CA inhibitors (CAIs) can be used as diuretics and anticonvulsants [133, 134], in the management of glaucoma [135], edema [136], epilepsy [137], obesity [138], and hypoxic tumors [139], neuropathic pain [140], cerebral ischemia [141], and arthritis [142].

1.2.4.1. CAIs inhibition mechanisms

The activation and inhibition of CAs are well-understood mechanisms: activators bind at the entrance of the active site cavity, while most types of classical inhibitors bind to the metal center [143]. The most general CA inhibition mechanism, with zinc binders, including sulfonamides, sulfamates, and sulfamides, is shown in Figure 6 [144]. In this mechanism the CAIs bind as anions (deprotonated form) to the Zn(II) ion from the enzyme active site, with the zinc-binding group (ZBG) that interact directly with the metal ion. In the case of sulfonamides, sulfamates, and sulfamides SO_2 moieties act as ZBG [111]. In addition, the ZBG also interact with two other conserved residues, acting as “gate keepers”, (Thr199 and Glu106) as evidenced in Figure 6 [123, 144].

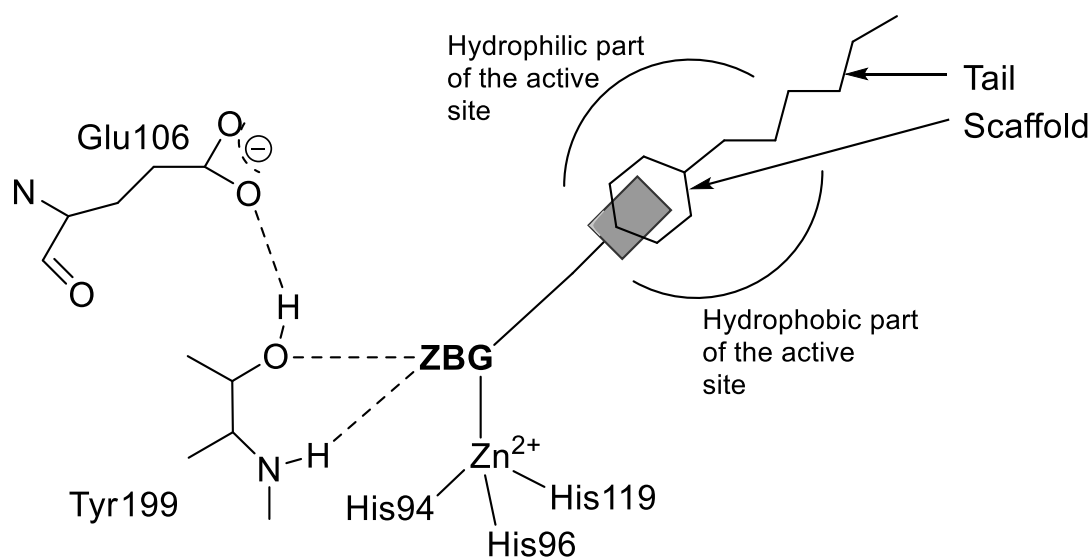


Figure 6. Binding mode of the CAIs belonging to the zinc binders. The ZBG is coordinated to the metal ion and participate in strong interactions with the residues Thr199 and Glu106. The scaffold may occupy either the hydrophilic or the hydrophobic (or both) halves of the active site, while the tails usually are orientated toward the exit of the cavity [119, 145].

Another mechanism of inhibition is described when CAIs anchor to the zinc-coordinated water/hydroxide ion [144, 146]. In this mechanism (Figure 7), CAIs are characterized by the presence of an anchoring group (AG) which is attached to a scaffold, this one with the

possibility to have a tail which can interact with the two halves of the active site (in the same way as zinc binders). The key difference between the previous mechanism and this one is the fact that anchoring inhibitors are not in direct contact with the metal ion [123, 144]. Several AGs were reported in the last years, belonging to different chemical functionalities, such as phenolic [147], amine [146], carboxylic acid [148], and sulfur moieties [149], whereas the scaffolds of these inhibitors can be aromatic, aliphatic, heterocyclic, or sugar type [149-151].

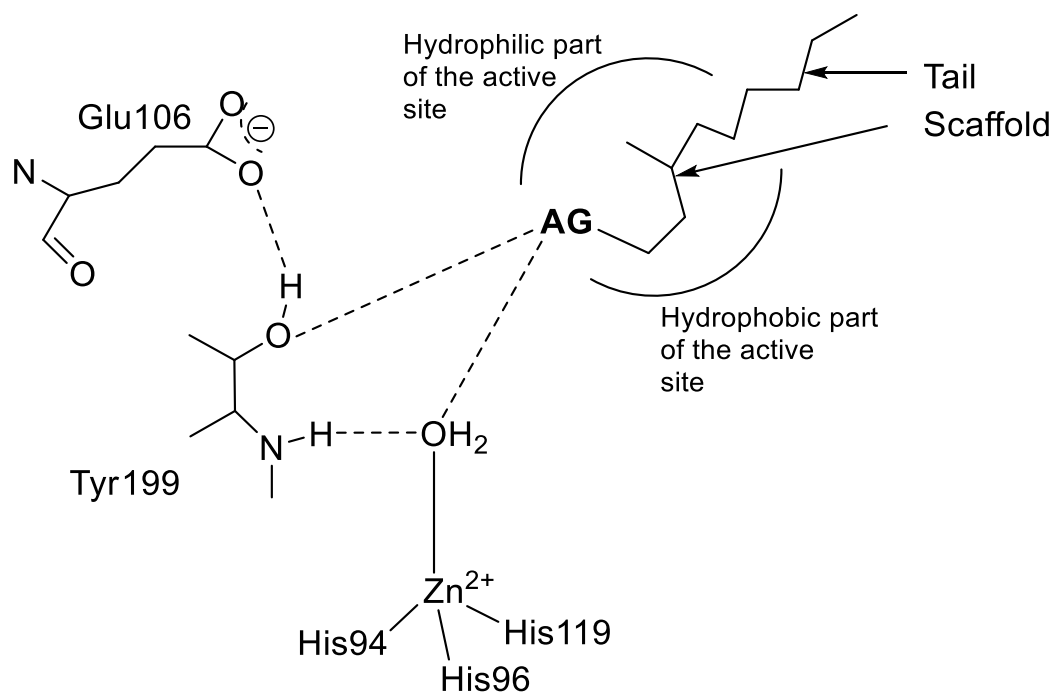


Figure 7. Binding mode of the CAIs which anchor to the Zn(II)-coordinated water molecule/hydroxide ion [144].

A third mechanism was evidenced for the first time for coumarins [152, 153]. This mechanism consists of the active site entrance occlusion and is schematically represented in Figure 8. These inhibitors bind even further away from the metal ion compared to the zinc binders or the compounds anchoring to the zinc coordinated water molecule, essentially, at the entrance of the active site cavity (which is the most variable region between the 16 different human isoforms, otherwise relatively homologous with each other) [123, 144]. CAIs acting by this mechanism of inhibition possess a sticky group (SG) attached to a scaffold which can be aromatic, heterocyclic, or aliphatic, and may also incorporate a tail, which can extend away from the active site, since, as mentioned above, these compounds bind in a rather external region of the cavity [144].

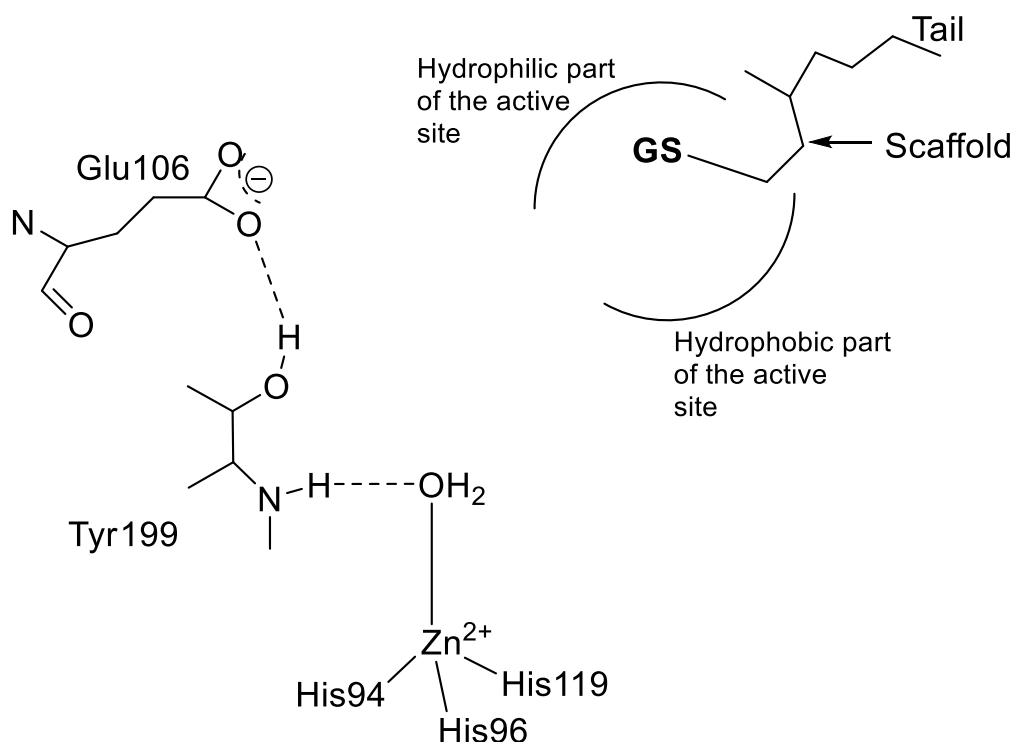


Figure 8. Schematic representation of the inhibition active site with entrance-occluding CAIs [144].

The last mechanism to be discovered is shown in Figure 9, and possess the particularity to have an “out of the active site” binding [154]. This type of compounds binds in an adjacent binding pocket to the active site [123]. From a crystallographic study it was showed that compounds that inhibit by this mechanism block the proton shuttle of the enzyme, His64, in its out conformation, interfering thus with the rate determining step of the entire catalytic cycle, which is indeed the transfer of a proton from the zinc-coordinated water molecule to the environment, with generation of the zinc hydroxide species of the enzyme. This amino acid residue (His64) has a high flexibility with two main conformations, the in one (closer to the metal ion) and the out one, toward the exit of the active site cavity. By accepting a proton from the zinc-coordinated water, the imidazole moiety of this residue becomes protonated (in its in conformation) whereas when it is in the out one, the same proton may be transferred to the environment. Interfering with this process may block the entire catalytic cycle [144, 154].

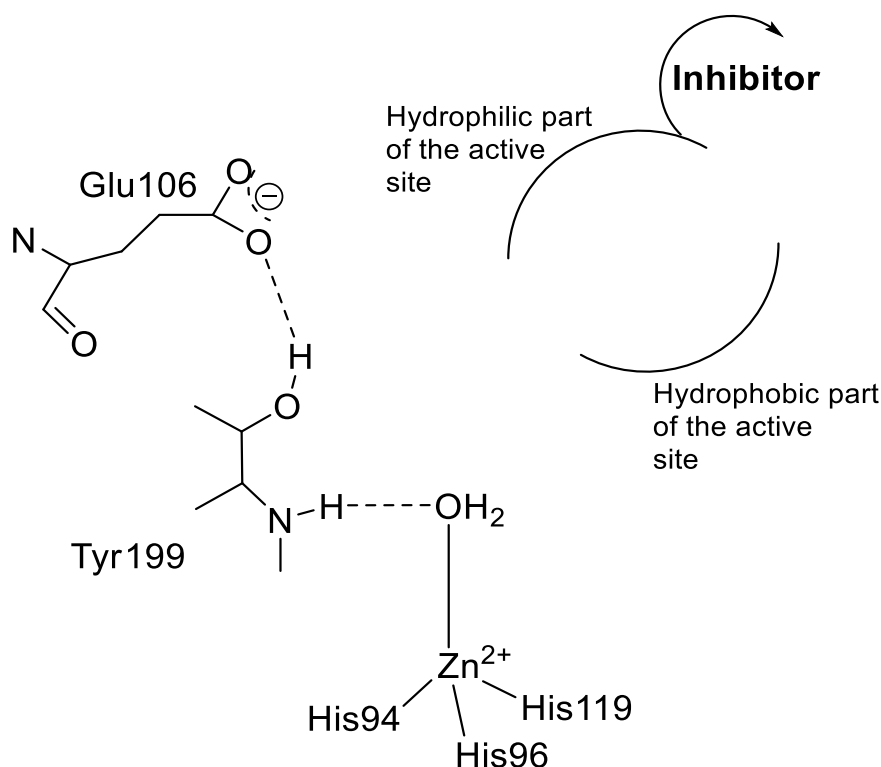


Figure 9. Schematic representation of the inhibitor binding site with "out of the active site" CAIs [154].

The four inhibition mechanisms discussed above are well understood as they were thoroughly documented by means of kinetic and more importantly, X-ray crystallographic studies. Nevertheless, in the last years relevant evidence accumulated on other classes of compounds, which show various levels of CA inhibitory properties, but for which the precise mechanism of action is not known due to the fact that they were not yet crystallized in adducts with the enzyme, suggests that there are other inhibition mechanisms. The difficulty to obtain crystallographic data is most of the time due to solubility problems for some of these compounds, but it should be also point out that many classes of CAIs only recently started to be investigated [144, 155-158].

A different mechanism, not considered for small molecules, is the one described for monoclonal antibodies which binds to the proteoglycan-like domain of CA IX [159, 160].

1.2.5. CAs as targets for medicinal chemistry

Considering their function and diverse localization in the human body, CAs can be considered as important targets for the design of inhibitors for several diseases. Table 4 lists different diseases in which CAs are involved [83]. Unfortunately, as they are present in several organs and tissues, CAs can be both targets and off-targets in some diseases,

which is related with the side-effects observed in CAIs and the interest in develop selective CAIs [161].

Table 4. Diseases in which CAs are involved.

Isozyme	Diseases in which is involved
<i>hCA I</i>	Retinal and cerebral edema [162]
<i>hCA II</i>	Glaucoma [163], epilepsy [164], and altitude sickness [165]
<i>hCA III</i>	Oxidative stress [166]
<i>hCA IV</i>	Glaucoma [135], retinitis pigmentosa [167], and stroke [168]
<i>hCA VA</i> <i>hCA VB</i>	Obesity [138, 169]
<i>hCA VI</i>	Cariogenesis [170]
<i>hCA VII</i>	Epilepsy [171]
<i>hCA IX</i>	Cancer [172-174]
<i>hCA XII</i>	Cancer [174, 175], and glaucoma [176]
<i>hCA XIII</i>	Sterility [177]
<i>hCA XIV</i>	Epilepsy [164], and retinopathies [178]

The role of CA I in some types of retinal and cerebral edema [162] has been demonstrated, making it a valuable target for the treatment of these conditions. The deregulation of CA II has important pathological consequences in glaucoma [163], and epilepsy [164], and is also implicated in pathologies such as altitude sickness [165]. CA III is involved in inflammatory conditions due to its implication in the oxidative stress [179] and CA IV is considered a drug target for several diseases such as glaucoma [135], retinitis pigmentosa [167] and stroke [180]. The involvement of the mitochondrial isoforms CA VA and VB in significant weight loss in obese patients validate them as drug targets for obesity [86]. The speculation of the caries inducing effect of CA VI implicate it in cariogenesis [170]. CA VII has been studied for the treatment of epilepsy [88]. CA XIII was implicated in sterility [177] and CA XIV was reported to be involved in epilepsy [164] and retinopathies [178].

1.2.5.1. Tumor-associated CA IX and XII

Tumor-associated CA IX and XII have been consistently validated as markers of disease progression in many solid tumors. Experimental evidence has indicated an important

relationship between pH regulation and tumor cell proliferation and survival [181]. These two isoforms are actively involved in carbon dioxide metabolism, and consequently play a role in pH control and tumor progression. Their overexpression in cancer and contribution to tumor physiology set in evidence a great potential as biomarkers and therapeutic targets [182], leading the research community to undoubtedly focus the most efforts on these isoforms in the last two decades [182-184], and put aside several other isoforms [93].

The membrane-bound CA isoforms CA IX and CA XII, as well as intracellular CAs such as CA I and CA II, are the primarily CAs isoforms expressed in cancer [185]. Among these cancer related CAs, CA IX gained most attention, since its distribution in tissues is quite peculiar [182]. Particularly, CA IX is almost exclusively expressed in a broad range of tumors representing a more reliable indicator of malignant lesions [89, 93, 182]. CA IX, a tumor-associated and hypoxia induced isozyme [186], was first identified in 1994 by Pastorek *et al.*, successively demonstrated to be abundantly expressed in a vast array of solid tumors [187], and associated to hypoxic cancer phenotypes and chemotherapy resistance [188]. CA IX appears implicated in cell adhesion and disturbances in pH balance caused by tumor metabolism, thus there is a great potential to use it as a surrogate marker of hypoxia and a prognostic indicator. [182]. This protein contains 459 amino acids, and its structure consists in a N-terminal single peptide extracellular region, a transmembrane region, and an intracellular C-terminal region [172, 189-191]. CA IX contributes to acidify the extracellular microenvironment while shuttling bicarbonate into the cytoplasm. The expression of CA IX is under control of the hypoxia inducible factor HIF-1 α , predominantly located in chronically hypoxic tumor regions. As maintaining a slightly alkaline intracellular pH has been shown to favor tumor cell growth, the inhibition of CA IX results in a decreased of the intracellular pH, which as a negative influence in tumor cell survival. CA IX also appears to contribute to cellular adhesion and migration, both of which are important for metastatic cancer, which makes this isozyme a good target for anticancer drugs [185, 189].

CA XII role in tumor biology is much less addressed in published papers, when compared with CA IX, mostly because nevertheless this isoform is overexpressed in several tumor types, its present also in many normal tissues [192, 193]. In 1998, two independent research groups identified and characterized CA XII as a second tumor-related CA isoform [192]. This isoform, also induced by hypoxia [194], has been detected in a certain number of tumor types, including breast tumors, brain, renal tissues [195], ovarian, pancreatic colorectal and gastrointestinal carcinoma, and is generally associated with less-aggressive, well-differentiated tumor phenotypes compared with the CA IX-expressing tumors [93, 193, 196]. CA XII, like CA IX is a transmembrane protein that contains an N-

terminal extracellular domain, a transmembrane domain, and an intracellular C-terminal domain [113, 191].

Hypoxia leads to the stabilization and transcriptional activation of HIF-1, which binds to hypoxia-response elements in the promoter of the *ca9* and *ca12* genes. Since tumor expression of HIF-1 and CA IX correlates with poor patient survival, it is essential to examine the physiological role of CAs IX and XII at the cellular level and the implication of these two membrane-bound CAs in tumor growth and invasion [197, 198]. Their potential as therapeutic or diagnostic targets, mainly for the management of hypoxic tumors and metastasis are the main reason why they are increasingly becoming a focus of attention in research.

1.2.6. CAIs

The different CA isoforms are involved in several physiological roles, reason why their inhibitors have found clinical applications for the treatment of various diseases, including glaucoma [78], epilepsy [164], obesity [80,81], and cancer [83][199]. However, the existing clinically used CAIs (acetazolamide, brinzolamide, dorzolamide, etc.) lack selectivity, which leads to a range of side effects [125, 176, 199]. The main scope of the drug design campaigns in the last years was to obtain isoform selective CAIs for the different pathologies. However, this is not an easy task, considering that the catalytically active isoforms present in primates have an active site architecture quite similar with each other. In the last decades the efforts of several researchers all over the world involve the design and synthesis of effective and selective novel CAIs against these pathologies in which the activity of CAs is dysregulated [200]. Part of these strategy involve the search for compounds from different structural classes, such as pyrimidine, pyrazoline, isatin, indole, among others [199].

Becomes important to clarify that up to now none of the clinically used CAIs appears to be a selective inhibitor for a specific isozyme, meaning that they inhibit not only the target but also other off-target isoforms [200].

1.2.6.1. CAIs as diuretics

Acetazolamide (AAZ), one of the marketed CAIs, which structure can be seen in Figure 10, was the first non-mercurial diuretic to be used clinically, already in 1956. It increases the urine volume and changes the normal acidic pH of urine into alkaline [134, 200]. For

this outcome an increased amount of bicarbonate is eliminated into the urine, together with Na^+ , and K^+ , whereas the amount of chloride excreted is diminished. The increased alkalinity of the urine is accompanied by a decrease in the excretion of titratable acid and ammonia, and in consequence by metabolic acidosis. This sequence of events is the consequence of the inhibition of various CA isozymes. Inhibition of both cytosolic (CA II) as well as membrane-bound (CA IV and CA XIV) enzymes seems to be involved in the diuretic effects of the sulfonamides [134, 201, 202]. AAZ and structurally related sulfonamides, such as methazolamide, and ethoxzolamide (Figure 10), were and still are used as diuretics in patients with edema due to congestive heart failure [203]. However, their use as diuretic is limited due to side effects and availability of better solutions [134, 203]. Starting from AAZ as a lead, other groups of relatively successful sulfonamide diuretics were developed in the 1960s and 1970s (Figure 10), and currently are amongst the most commonly used diuretics alone or in combination with other drugs [203].

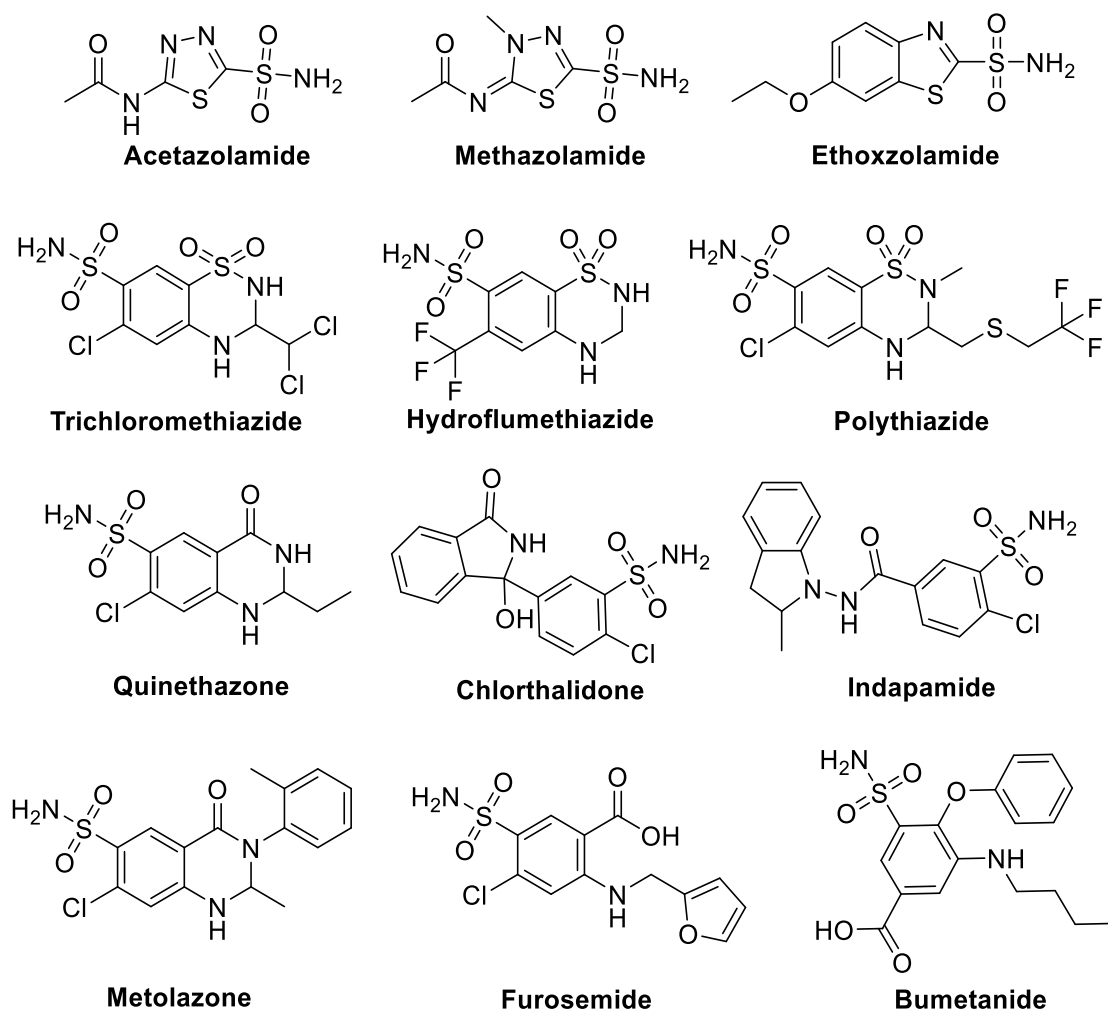


Figure 10. Structures of clinically approved CAIs used as diuretics.

1.2.6.2. CAIs as anti-glaucoma drugs

Glaucoma, a chronic and degenerative eye disease, is characterized by high intraocular pressure (IOP) that causes distinctive alteration of the optic nerve head leading to progressive loss of visual function and eventually blindness [204]. Research in the past decades recognized CAs as an appropriate and effective target to treat glaucoma by lowering IOP. Studies identified sodium bicarbonate as the main constituent of aqueous humor and several CA isoforms are involved in its secretion. In addition, isoforms CA I, CA II, and CA IV are most widely diffused in the human eye [176, 200]. Nowadays, CAIs represent the leading physiological treatment of glaucoma with the systemic administration of sulphonamides such as acetazolamide, methazolamide, ethoxzolamide or dichlorophenamide (Figure 11). The best-studied drug is acetazolamide, which is frequently administered long-term owing to its efficient reduction of IOP, minimal toxicity and ideal pharmacokinetic properties. Though this type of administration leads to nonspecific CA inhibition and is associated with undesired side effects, including numbness, and tingling of extremities; metallic taste; depression; fatigue; malaise; weight loss; decreased libido; gastrointestinal irritation; metabolic acidosis; renal calculi; and transient myopia [205]. To overcome this problem the development of water-soluble sulphonamide CAIs to be used as eye drops began in the 1990s. Dorzolamide and brinzolamide (Figure 11) were launched for the topical treatment of glaucoma [163]. Dorzolamide and brinzolamide are potent water-soluble CAIs that are sufficiently liposoluble to penetrate the cornea and may be administered topically, directly into the eye, several times a day. The two drugs are effective in reducing IOP and show fewer systemic side effects when compared with systemically applied drugs, but they show many ocular side effects [205-207].

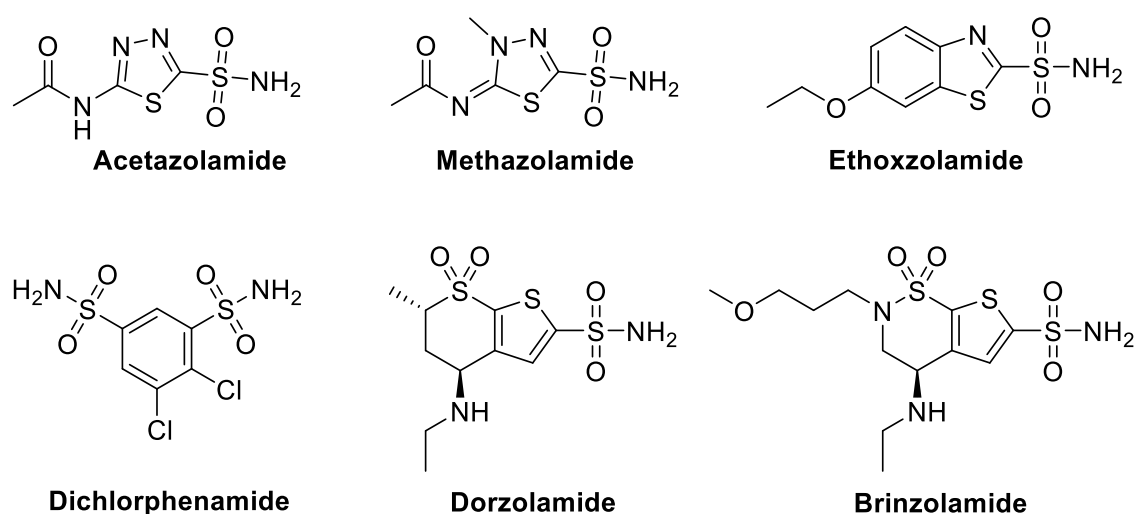


Figure 11. Structures of clinically approved CAIs used in the treatment of glaucoma.

1.2.6.3. CAIs in osteoporosis treatment

CAIs have also been studied for the treatment of osteoporosis [200], a skeletal disease characterized by microarchitectural deterioration of bone tissue and low bone mass, leading to bone fragility and an enhanced risk of fractures [208]. CA II, the highly active CA isoform, is abundantly expressed in the bone and its involved in the provision of hydrogen ions for mobilization of calcium from the bone by an ATP-dependent proton pump [200]. The inorganic component of bone, tricalcium diphosphate is solubilized in the presence of H⁺ ions furnished by the CA-catalyzed reaction, being transformed in calcium hydrogen phosphates [125]. The inhibition of CA II suppresses the acid formation by osteoclasts. Thus, it appeared of interest to use CAIs in the treatment of osteoporosis, a condition characterized by excessive loss of bone calcium [209]. Acetazolamide is capable of inhibit CA II, but as mentioned earlier it leads to undesired and sometimes serious side effects due to inhibition of other isoforms. Studies show the attempt of producing selective inhibitors based in acetazolamide. Unfortunately, no detailed clinical studies with such CAIs or even acetazolamide in the management of osteoporosis are available to date [170, 206, 210]. More recent studies showed that membrane-bound isoenzymes CA IV and CA XIV are expressed in osteoclasts *in vivo* and *in vitro* and these expressions were observed at both mRNA as well as protein levels [200, 209]. Thus, taking into account these evidences the potential role of CAs as a drug target for the management of osteoporosis is clearly seen.

1.2.6.4. CAIs as anticonvulsants

In the last years, research in the field of epilepsy has turned the spotlight on the role of CAs in this disease and they emerged as an attractive target for designing new anticonvulsant drugs [211]. The physiological role of cerebral CAs (i.e., isoforms II, VII, and XIV) as pH regulators and their involvement in neuropathological processes associated with seizure generation ensured that their inhibition may effectively act in modulating the uncontrolled electric activities [164, 211]. Sulphonamides such as acetazolamide, methazolamide, zonisamide, topiramate, and sulthiame, showed in Figure 12, were (and still are) used as anti-epileptics [200, 206, 211]. Nowadays, clinical use of acetazolamide and methazolamide is rare [212]. Since these drugs are administered systemically, their usual side effects, related with the unselective inhibition of CAs isoforms, constitute serious drawbacks for their extensive use [206, 211]. AAZ is used in cases of partial and generalized seizures uncontrolled by other classical antiepileptic drugs [212], and methazolamide is very effective in the treatment of generalized epilepsy [137].

Zonisamide and topiramate seems to be an effective anti-epileptic and are currently used for epilepsy treatment [206, 211]. Zonisamide, a benzisoxazole derivative, is used for adjunctive treatment of partial seizures as well for monotherapy of simple and complex partial seizures. Topiramate, unlike other antiepileptic drugs, is a sulfamate substituted monosaccharide that has a broad spectrum of clinical use. It has been found to be effective mainly against partial epilepsy in adults [212]. Sulthiame started as an antiepileptic in Europe in early 1960s. Later in 1960s and 1970s doubts on its antiepileptic activity were raised, and the drug made a return in 1988, after it was found to be effective in partial epilepsy cases among children. Currently, the drug is prescribed fairly regularly in Germany, Ireland, Australia, and Israel, but is not well marketed in the United States. However, recent studies performed on six children with benign epilepsy have shown deterioration of cognitive ability during the treatment with sulthiame. The drug showed improvement in epileptic seizures, but it also affected the reading ability, general memory, attention, and mathematical skills of all the children [137, 213]. Figure 12 shows some examples of the marketed CAIs used as anticonvulsants.

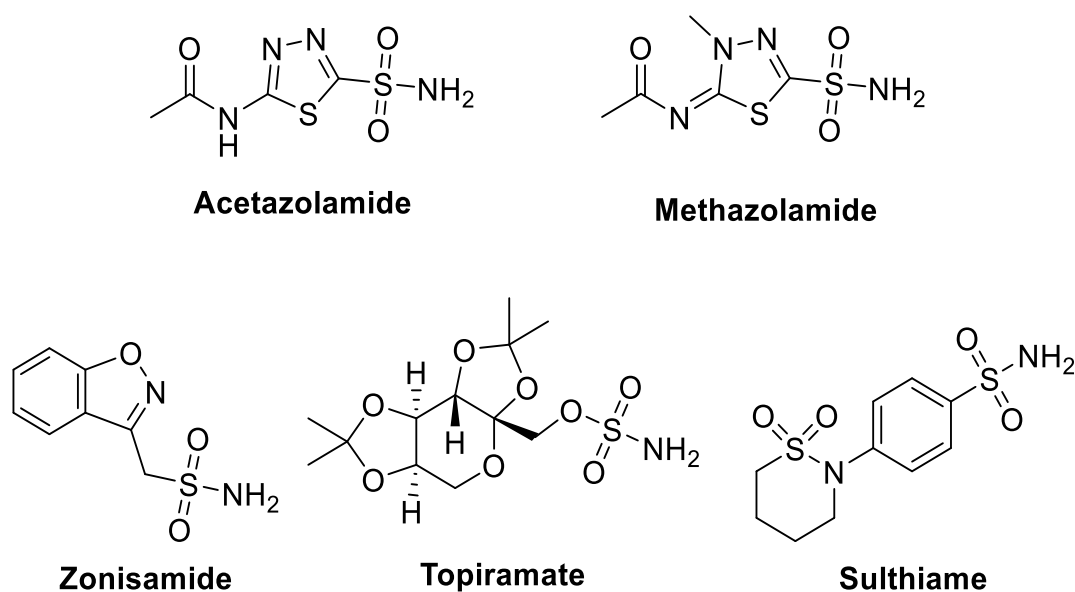


Figure 12. Structures of marketed CAIs as anticonvulsants.

1.2.6.5. CAIs as novel anti-obesity drugs

The starting point for the validation of CAIs as obesity targets came from the observation that topiramate led to a marked body weight reduction [211, 214]. The anti-epileptic drug had this side effect in obese epileptic patients that were receiving the treatment for epilepsy

[214-216]. All clinical cases commonly revealed body weight loss only when topiramate was administered, whereas no significant weight alterations were observed in patients under treatment with alternative antiepileptic pharmacologic treatments [211]. Later, and similar to topiramate, Zonisamide, another anti-epileptic, demonstrated additional potential for obesity [125, 216]. Zonisamide is an aliphatic sulphonamide, which also potently inhibits cytosolic (CA II) and mitochondrial CAs (CA VA and VB) involved in lipogenesis [216]. Furthermore, zonisamide in conjunction with a reduced-calorie diet, resulted in weight loss compared with diet alone in obese female patients [125, 200, 217]. In 2012, with the approval from the FDA, a combination containing topiramate and phentermine under the tradename Qnexa/Qsymia (Figure 13), was released for the treatment of obesity [138, 211, 218]. The combination of these two drugs in lower doses resulted in high efficacy with mild side effects compared with single administrations at the usual doses. Moreover, no significant differences in the risk of cardiovascular death, nonfatal myocardial infarction, and nonfatal stroke between phentermine-topiramate and placebo were determined [211, 218]. Following the same combination therapy approach, a bupropione-zonisamide slow-release compound, Empatic, is undergoing FDA phase III clinical development [211].

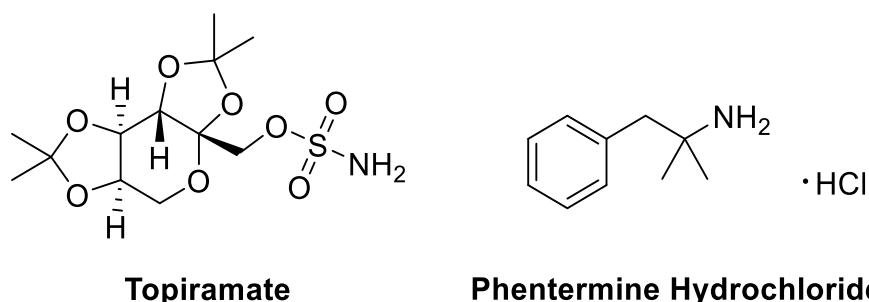


Figure 13. Structure of Qnexa/Qsymia components, marketed drug used in the treatment of obesity.

1.2.6.6. CAIs as antitumor agents

CA IX and XII are two isozymes reasonably designated cancer-associated, as CA IX is predominantly found in tumor cells and have restricted expression in normal tissues, and both are overexpressed in many tumor types [200, 219]. Their overexpression in many tumors, in response to the hypoxia inducible factor pathway, led the research on the involvement of these isozymes in cancer to progress significantly in recent years [132]. Studies have indicated that CA XII is less strongly regulated by hypoxia when compared with CA IX [200], but the two of them are associated with tumor hypoxia, tumor propagation, malignant progression, and resistance to chemotherapy and radiotherapy

[125]. The two main strategies to target the tumor associated CAs for cancer therapy include the development of monoclonal antibodies and the design and synthesis of small molecules that selectively inhibit CA IX and XII [184].

Indisulam (Figure 14), a benzenesulphonamide derivative (originally called E7070) with powerful anticancer activity, was shown to act as a nanomolar inhibitor of CA IX. Indisulam presented *in vivo* efficacy against human tumor xenografts in nude mice, exhibiting a significant antitumor effect and progressed to Phase II clinical trials for the treatment of solid tumors [125, 161]. However, indisulam is no longer being developed as an anticancer agent, probably due to the lack of significant effects in Phase II trials [161].

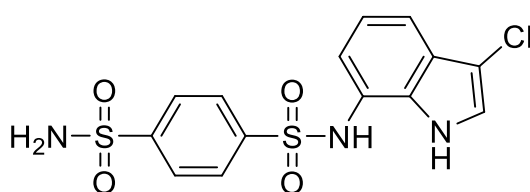


Figure 14. Structure of indisulam.

Nevertheless, in the last decade, isoform CA IX and XII were validated as antitumor/antimetastatic drug targets as well as for imaging hypoxic tumors. Many CAIs which selectively inhibit these two isoforms, belong to sulfonamide, coumarin and sulfocoumarin classes of CAIs [132, 161, 220]. Another advance was a fluorescent sulphonamide derivative that binds only to CA IX under hypoxic conditions *in vivo* and may therefore be used as a fluorescent probe in hypoxic tumor imaging [125, 221]. Alone or in combination with other agents, CA IX and XII inhibitors inhibit the growth of the primary tumors, the formation of metastases and deplete the cancer stem cell population, three beneficial antitumor mechanisms, making them unique among all anticancer drugs available to date. But the real breakthrough was the compound SLC-0111 (Figure 15) which progressed to Phase II clinical trials late in 2016 for the treatment of advanced, metastatic solid tumors with high isoform selectivity for the tumor associated CA IX and XII isoforms [219]. It showed good bioavailability and effectiveness alone or in combination with other anticancer drugs in both animal models and preliminary clinical trials [139, 161]. Undeniably, the extensive preclinical models carried out by numerous independent groups with the lead CA IX and XII inhibitors, including SLC-0111, have demonstrated that the use of such inhibitors in combination with chemotherapy agents, immunotherapy, and radiotherapy is highly important and desirable for sustained therapeutic response [93, 222]. Being the first in-class CAI, SLC-0111 has been used as a lead molecule for designing other compounds with isoform-selective inhibitory activity. Many of these

analogs were also obtained and investigated in detail as well as CAIs incorporating positron emitting isotopes for possible theragnostic applications, for the treatment and imaging of hypoxic tumors [161].

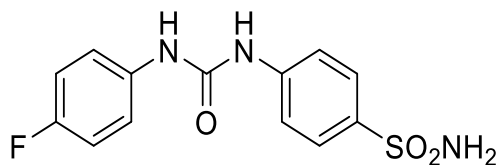


Figure 15. Structure of SCL-011, compound in Phase II clinical trials for treatment of advanced, metastatic solid tumors.

1.3. Coumarin and chromone scaffolds

Coumarins and chromones, represented in Figure 16, are two groups of naturally occurring heterocycle compounds widely distributed in nature. Their chemical and biological aspects have been studied in detail. Molecules containing the coumarin and chromone skeleton have a wide variety of biological activities [223].

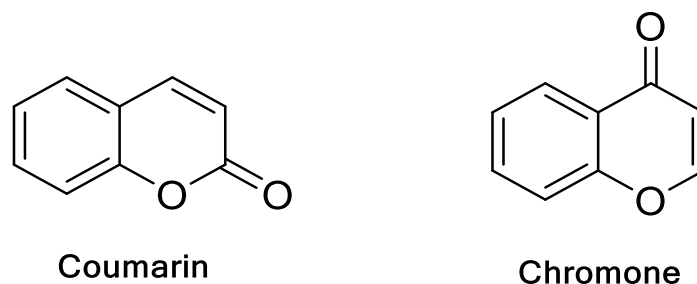


Figure 16. Chemical structures of coumarin and chromone.

Coumarins (2H-chromen-2-one, 2H-1-benzopyran-2-one) are organic heterocycles, and their nucleus is constructed from an α -pyrone ring fused with benzene ring [224]. They belong to a wide family of secondary metabolites found in various species of plants, fungi, and microorganisms. Based on their chemical diversity, can be subdivided in different classes: simple coumarins, isocoumarins, furanocoumarins, pyranocoumarins and biscoumarins [225, 226]. The different substituents in the coumarin nucleus strongly influence the biological activity of the resulting derivatives [226]. Coumarins have several attractive features, such as low molecular weight, simple structure, high bioavailability, high solubility in most of the organic solvents and low toxicity, which, together with their multifaceted biological activities, as well as their simple structural architecture and chemical stability, ensure them a prominent role as lead compounds in drug research and development [225, 226]. Coumarins exhibit several pharmacological activities including anticoagulant [227], anti-inflammatory [228], neuroprotective [229], antioxidant [230], anticoagulant [231], antibacterial [232], anti-fungal [233], antiviral [234], and anticancer [224, 235, 236]. Over the last 50 years coumarin compounds have been widely used as pharmaceuticals [226]. Two examples can be seen in Figure 17. Their structural and physicochemical characteristics attracted much attention by medicinal chemists and made them a privileged scaffold in medicinal chemistry [224, 237]. Moreover, the ability of coumarin derivatives to inhibit human CAs IX and XII has also been reported, inclusively by our research group [238-240].

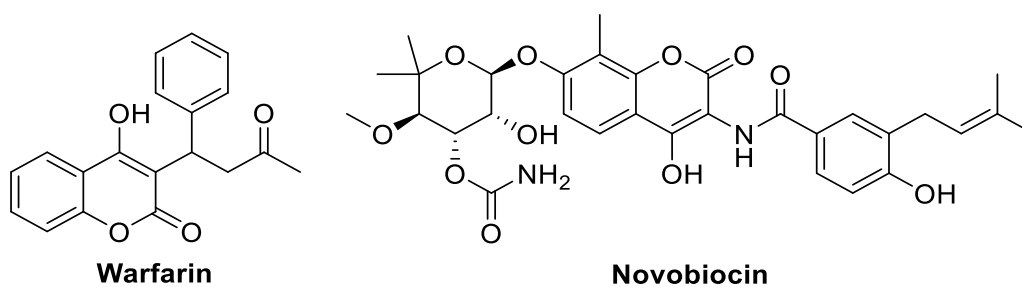


Figure 17. Warfarin and novobiocin, two coumarin-based compounds used as pharmaceutical agents.

A refined search for coumarin scaffold in Binding DB [241], reporting biologic activity, results in almost 800 entries. Moreover, crossing a search of carbonic anhydrase IX in Binding DB, that give us the data regarding this isoform, with a protocol in Pipeline Pilot software that select coumarin substructures within this database, we obtain 245 entries, 126 of which regarding compounds with less than 100 nM of inhibitory activity [142, 153, 238, 242-250], as can be seen in Figure 18. The same procedure was made for CA XII with coumarin substructures, and 214 entries were obtained, 115 of which for compounds with less than 100 nM of inhibitory activity (Figure 18) [238, 242-249, 251-254].

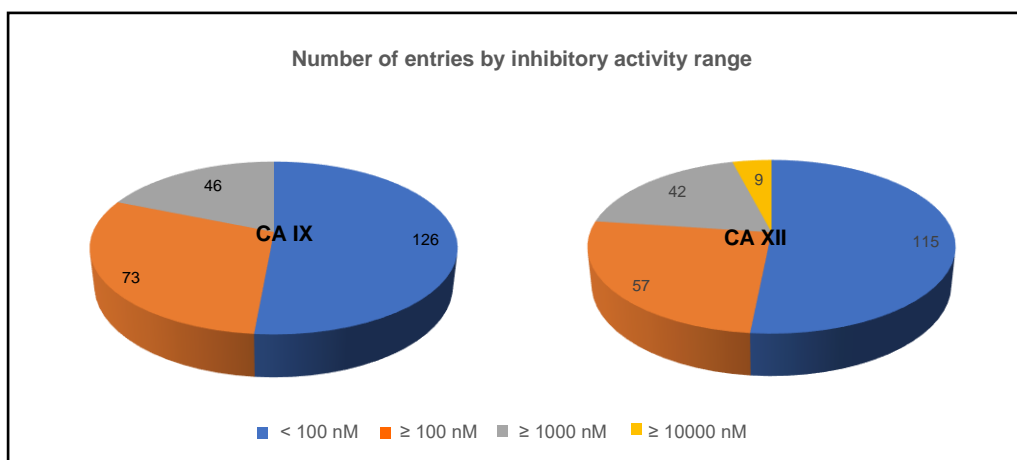


Figure 18. Number of cross entries regarding coumarin substructures with biologic activity in CA IX and XII.

Regarding the group research, Melis *et al.* reported in 2018 the synthesis of coumarin derivatives, which structure can be seen in Figure 19 and their activity and selectivity towards CAs IX and XII over CAs I and II was evaluated and compared with the reference AAZ. As observed in Table 5, the compounds selectively inhibit the tumor-associated CA isoforms IX and XII over the cytosolic ones I and II. Also, when compared with AAZ, some compounds are more potent [238].

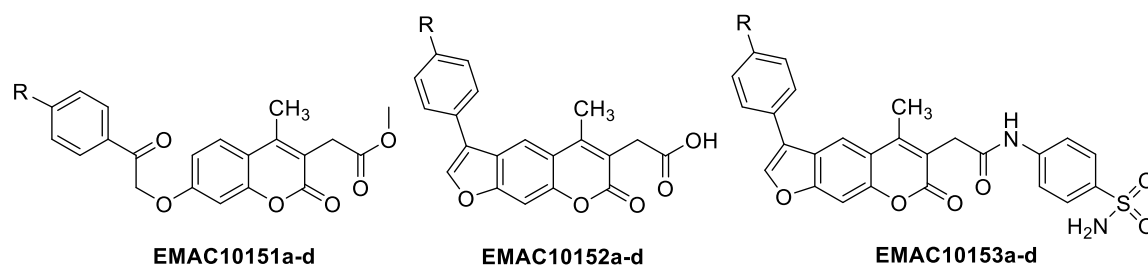


Figure 19. Structures of the three series of compounds synthesized by the group and published in [238].

Table 5. Inhibition data of *hCA* I, II, IX and XII for the compounds published by Melis *et al.* and AAZ (used as reference).

Compound	R	Ki (μM)			
		<i>hCA</i> I	<i>hCA</i> II	<i>hCA</i> IX	<i>hCA</i> XII
EMAC10151a	4'-Cl	> 100	> 100	0.0236	0.447
EMAC10151b	4'-CH ₃	> 100	> 100	0.123	0.0566
EMAC10151c	-	> 100	> 100	0.0897	0.0725
EMAC10151d	4'-F	> 100	> 100	0.0847	0.250
EMAC10152a	4'-Cl	> 100	> 100	0.0947	0.00930
EMAC10152b	4'-CH ₃	> 100	> 100	0.0230	0.00910
EMAC10152c	-	> 100	> 100	0.0175	0.00940
EMAC10152d	4'-F	> 100	> 100	0.0177	0.00740
EMAC10153a	4'-Cl	> 100	> 100	0.0178	0.00240
EMAC10153b	4'-CH ₃	> 100	> 100	0.0916	0.00340
EMAC10153c	-	> 100	> 100	0.0165	0.00360
EMAC10153d	4'-F	> 100	> 100	0.0108	0.0499
AAZ	-	0.250	0.0125	0.0258	0.00570

In another paper, Fois *et al.* reported in 2020 the isolation of coumarins, which structures are in Figure 20.

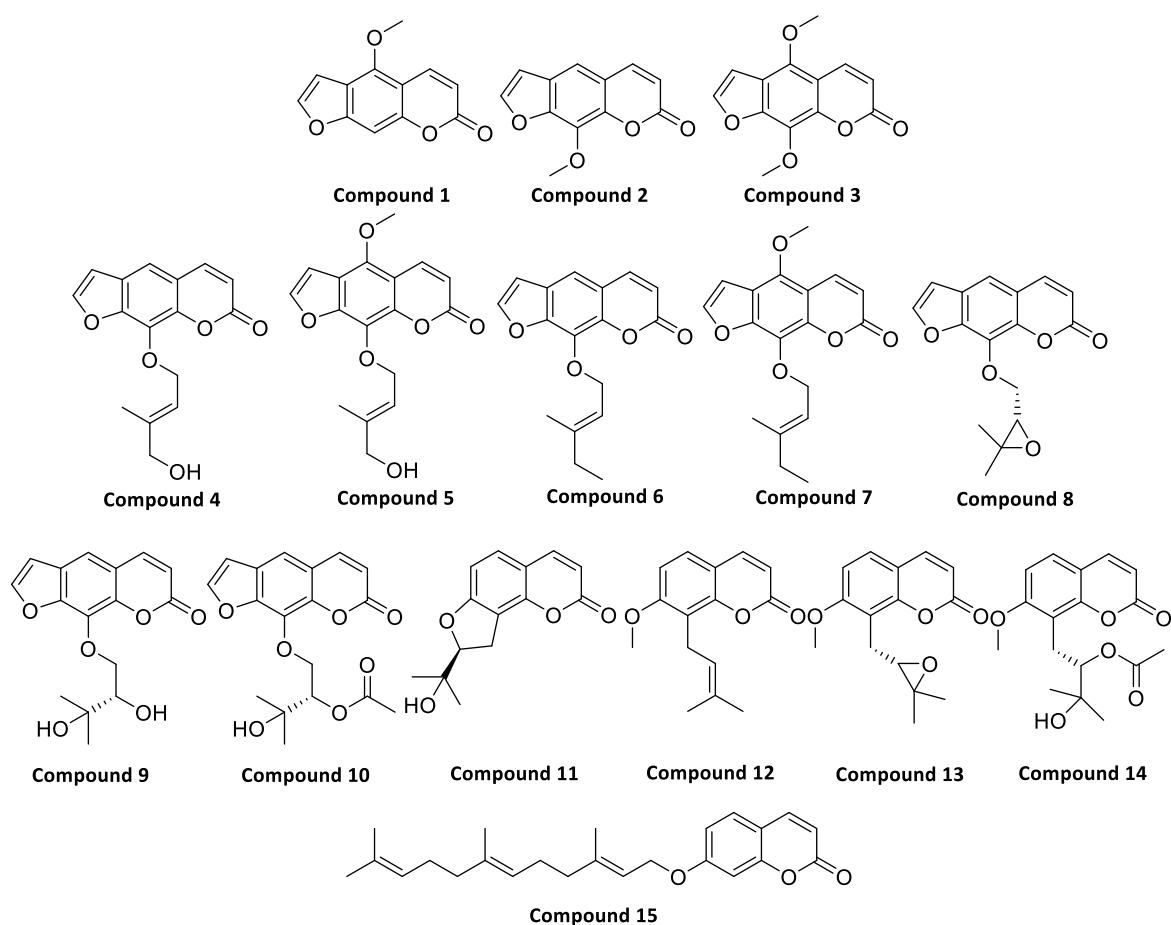


Figure 20. Structures of the coumarins isolated and published in [240].

As observed in the following table, the majority of the compounds are selective inhibitors towards CAs IX and XII, with only three exceptions. Compounds 10 and 13 are selective only towards CA IX and compound 14 shows selectivity only towards CA XII. All the isolated compounds were inactive towards the cytosolic isoforms *hCA* I and II and significantly active towards the trans-membrane isoforms *hCA* IX and XII [240].

Table 6. Inhibition data of *hCA* I, II, IX and XII for the compounds published by Fois *et al.* and AAZ (used as reference).

Compound	Ki (μM)			
	<i>hCA</i> I	<i>hCA</i> II	<i>hCA</i> IX	<i>hCA</i> XII
1	> 100	> 100	1.95	0.855
2	> 100	> 100	0.195	0.876
3	> 100	> 100	0.160	0.590
4	> 100	> 100	2.34	0.550
5	> 100	> 100	1.50	0.0635
6	> 100	> 100	0.221	0.833
7	> 100	> 100	0.202	0.787
8	> 100	> 100	0.162	0.836
9	> 100	> 100	0.0275	0.814
10	> 100	> 100	0.192	>100
11	> 100	> 100	0.151	0.623
12	> 100	> 100	2.47	0.0745
13	> 100	> 100	1.89	>100
14	> 100	> 100	>100	0.291
15	> 100	> 100	0.266	0.0058
AAZ	0.250	0.00121	0.0258	0.0057

In a more recent paper, Meleddu *et al.* reported the synthesis of two coumarin derivatives series (Figure 21) and the activity and selectivity towards the isoforms *hCA* I, II, IX and XII was evaluated (Table 7) [239].

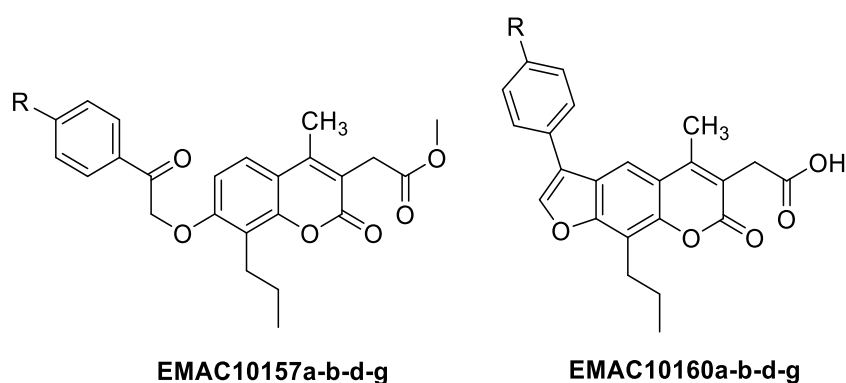


Figure 21. Structures of the coumarin derivatives synthesized by the group and published in [239].

The data presented in the following table shows the selectivity of all the compounds towards the tumor-associated isoforms *hCA IX* and *hCA XII* over the cytosolic isoforms *hCA I* and *hCA II* [239].

Table 7. Inhibition data of *hCA I, II, IX* and *hCA XII* for the compounds published by Meleddu *et al.* and AAZ (used as reference).

Compound	R	Ki (μM)			
		<i>hCA I</i>	<i>hCA II</i>	<i>hCA IX</i>	<i>hCA XII</i>
EMAC10157a	4'-CH ₃	> 100	> 100	0.248	0.350
EMAC10157b	4'-OCH ₃	> 100	> 100	0.353	0.324
EMAC10157d	4-F	> 100	> 100	0.240	0.257
EMAC10157g	4-C ₆ H ₅	> 100	> 100	0.135	0.283
EMAC10160a	4'-CH ₃	> 100	> 100	0.467	0.758
EMAC10160b	4'-OCH ₃	> 100	> 100	0.489	0.859
EMAC10160d	4-F	> 100	> 100	0.380	0.460
EMAC10160g	4-C ₆ H ₅	> 100	> 100	0.398	0.550
AAZ	-	0.250	0.00120	0.0250	0.0057

The research on coumarin derivatives by the group contributed to validate these scaffolds as CAIs and justify further evaluation of these scaffold derivatives. Overall, this scaffold is an important class of CAIs for mainly three reasons: (i) coumarin derivatives show high selectivity for inhibiting tumor-associated isoforms CA IX and XII; (ii) the possibility to generate a large number of structurally diverse coumarin derivatives due to the chemical simplicity of the scaffold; (iii) the studies already showed the promising results of the coumarin derivatives as selective CAIs with an interesting inhibition mechanism.

Chromone (4H-chromen-4-one, 4H-1-benzopyran-4-one) belongs to an important class of oxygen-containing heterocyclic compounds with a benzoannulated γ -pyrone ring, and they are part of the flavonoid family [255-257]. The structural diversity found in their family led to the roughly division into simple chromones and fused chromones (pyrano and furanochromones) [257, 258]. Chromone derivatives are abundant in nature, especially in the plant kingdom, and have been extensively studied [257]. Several pharmacological activities have been attributed to simple chromones and their analogues. Among them, antibacterial, antifungal [259], anticancer [258, 260], antioxidant [261], anti-HIV [262], immune-stimulators [263], wound healing [264], analgesic and anti-inflammatory [265]. These compounds also possess low mammalian toxicity and are present in large amounts in the diet of humans, due to their presence in edible plants. An effective strategy for the generation of innovative hits/leads and successful optimization processes is the use of privileged structures in drug design. Chromone is undoubtedly recognized as a privileged structure and a suitable scaffold for the design of new compounds with potential pharmacological interest and have featured in several clinically used drugs [256-258]. Modifications of their structure allows the synthesis of a wide range of compounds with different properties and diverse pharmacological profiles, which is useful for the search of new therapeutic agents. A great volume of research has been carried out on this scaffold and their derivatives [255, 256]. Due to the synthetic accessibility and potential structural diversity, and the multitude of receptors in which might bind, chromone is recognized as a privileged scaffold for the design of novel compounds and drug discovery [256]. Some examples of chromone derivatives used as therapeutic agents today are represented in Figure 22 [255]. The study of chromones as a useful scaffold for drug discovery in cancer has been largely focused on the discovery of novel kinase inhibitors [266, 267]. Nevertheless, other targets have been studied, including CAs [147, 268, 269].

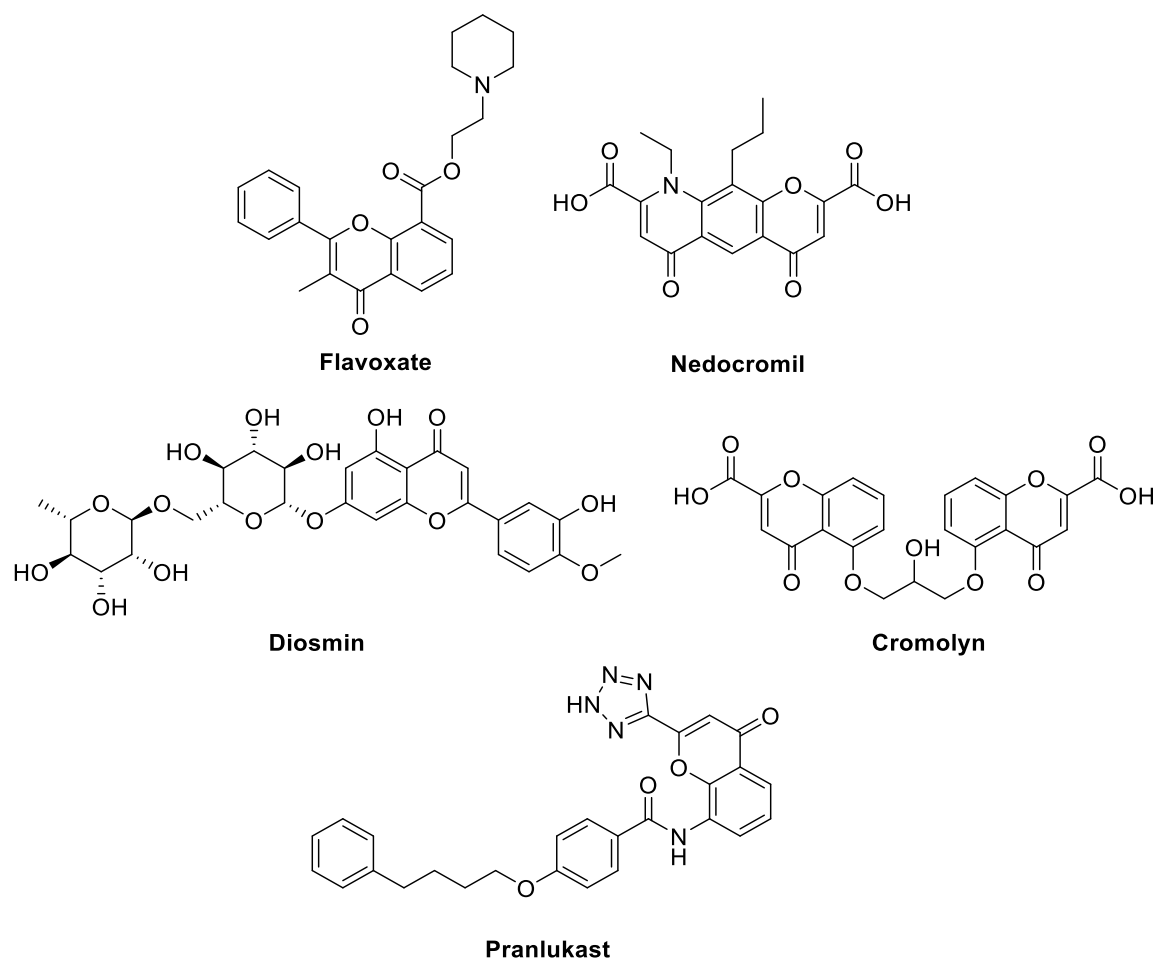


Figure 22. Examples of chromone-based compounds used as pharmaceutical agents.

A refined search for chromone scaffold in Binding DB, reporting biologic activity, results in more than 1000 entries, more than 200 of which identifying compounds with less than 100 nM of inhibitory activity [269-284]. Moreover, crossing a search of carbonic anhydrase IX in Binding DB, that give us the data regarding this isoform, with a protocol in Pipeline Pilot software that select chromone substructures within this database, we obtain 29 entries, 18 of which regarding compounds with less than 100 nM of inhibitory activity [285, 286] as can be seen in Figure 23. The same procedure was made for CA XII with chromones substructures, and 41 entries were obtained, 24 of which for compounds with less than 100 nM of inhibitory activity (Figure 23) [269, 285, 286].

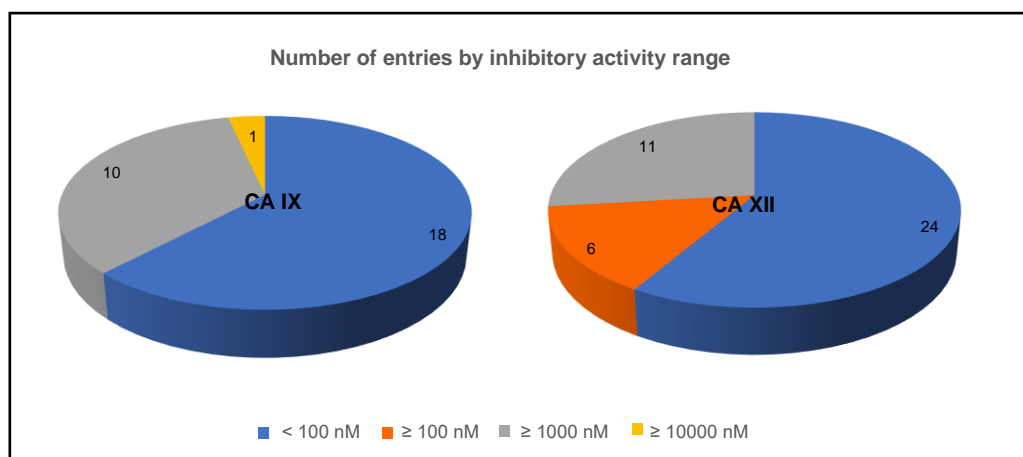


Figure 23. Number of cross entries regarding chromone substructures with biologic activity in CA IX and XII.

1.4. Thesis research objectives

The potential of coumarin and chromone scaffolds, together with the research results regarding their pharmaceutical use and potential, showed in section 1.3 are the background for the work of this Thesis. In addition, the previous work of the group regarding coumarins and furocoumarins [238-240], also summarized in 1.3, showed the potential of these scaffolds as selective inhibitors of the tumor-associated CAs.

Hence, the work herein presented follows the study of coumarins and chromones as promising scaffolds for the development of CA IX and XII selective inhibitors. Accordingly, the first aim of this work is to develop possible potent, selective, and reversible CA IX and XII inhibitors by the synthesis of compounds based in the coumarin (furanocoumarins included) and chromone scaffolds according to the general strategy depicted in Figure 24.

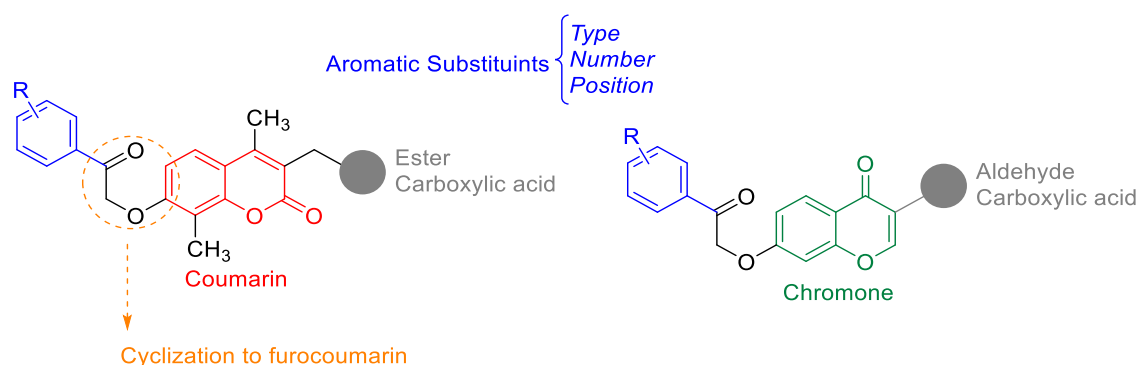


Figure 24. Rational design strategy followed for the development of CAs based on coumarin and chromone scaffold.

The specific aims set for the present project are listed as followed:

- **Design** and **synthesis** of two small libraries of coumarin and chromone scaffolds derivatives.
- **NMR** and **MS** analysis of coumarin- and chromone-based derivatives.
- **In vitro** screening of coumarin- and chromone-based derivatives on *hCA* I, II, IX and XII.
- **Theoretical prediction of drug-like properties** of coumarin- and chromone-based derivatives.
- **Docking studies** on selected coumarin- and chromone-based derivatives.

CHAPTER 2. Experimental Section

2.1. Material and methods

Unless otherwise noted, starting materials, reagents and solvents were obtained from commercial suppliers and were used without any further purification.

All the reactions were controlled by thin layer chromatography (TLC) using precoated silica gel 60 F254 (Merck) with layer thickness of 0.2 mm. For analytical control the following systems were used: dichloromethane, ethyl acetate and dichloromethane/ ethyl acetate in several proportions. The spots were visualized under UV detection (254 and 366 nm). Flash column chromatography was performed using silica gel 60 0.040-0.063 mm (Carlo Erba Reagents). Following the workup and after extraction, the organic phases were dried over Na_2SO_4 . Solvents were evaporated in a Rotavapor.

All melting points were determined by the capillary method on a *Stuart Scientific* melting point apparatus and are uncorrected.

Nuclear magnetic resonance (NMR) was recorded on a Bruker AMX 400 NMR spectrometer. ^1H and ^{13}C NMR spectra of samples were recorded at room temperature in 5 mm outside diameter (o.d.) tubes. Tetramethylsilane (TMS) was used as internal standard, chemical shifts (δ) are expressed in parts per million (ppm) and the coupling constant (J) in Hz. For the DEPT (Distortionless Enhancement by Polarization Transfer) sequence, the width of the 90° pulse for ^{13}C was 4 μs , and that of the 90° pulse for ^1H was 9.5 μs ; the delay $2J_{\text{C,H}}^{-1}$ was set to 3.5 ms (underlined values). All samples were measured in DMSO- and chloroform- d_6 as a solvent.

Electrospray ionization mass spectrometry (ESI/MS) were acquired on an Orbitrap Exploris mass spectrometer (Thermo Fisher Scientific, Germany). Compounds were initially dissolved in dimethylsulfoxide (DMSO) at 5 mg/mL concentration. Stock solutions were then diluted 50-fold in acetonitrile and diluted further 10-fold in 70% acetonitrile containing 0.1% of formic acid. Solutions were directly infused in the mass spectrometer at 5 $\mu\text{L}/\text{min}$. Mass spectra were acquired in positive ion mode (3200 V). Ion transfer tube temperature was 320 $^\circ\text{C}$, whereas S-lens value was 20 units. Full MS spectra were acquired at a resolution of 240,000, in the m/z range 180-1000. The data are reported as m/z (percentage of relative intensity of the most important fragments).

The CA catalyzed CO_2 hydration/inhibition was measured by using a stopped-flow instrument (Applied Photophysics, Oxford, U.K.).

The refined searches for coumarin and chromone scaffolds with biologic activity were made using the online database Binding DB (<http://www.bindingdb.org>). Database Binding DB and Pipeline Pilot were used for the crossed search between CAs IX and XII and coumarin and chromone scaffolds.

Drug-like properties of compounds were theoretical predicted using QikProp software.

The ligands, for ligand preparation, were built using the Maestro GUI. The most stable conformation has been determined by molecular mechanics conformational analysis performed by Macromodel software version 9.2.

The coordinates for *hCA* isoforms enzymes were taken from the RCSB Protein Data Bank. The proteins were prepared by using the Maestro Protein Preparation Wizard. Original water molecules were removed.

Molecular docking studies were performed using QM-Polarized Ligand workflow protocol.

2.2. Synthesis of furocoumarins

2.2.1. Synthetic pathway

Figure 25 reproduces the synthetic strategy in which methylresorcinol (compound 1) and dimethyl 2-acetylsuccinate (compound 2) were mixed in acidic conditions at room temperature to perform a Pechman condensation (reactional step A) and the correspondent coumarin (compound EMAC10163) was obtained. This step was followed by a Williamson reaction (reaction step B) between EMAC10163 and an α -haloketone with the desired substitution (compound 3) originating the compounds EMAC10163a-m. These compounds were submitted to an intramolecular condensation and ester saponification (reactional step C) to obtain the correspondents furocoumarins (compounds EMAC10164a-m).

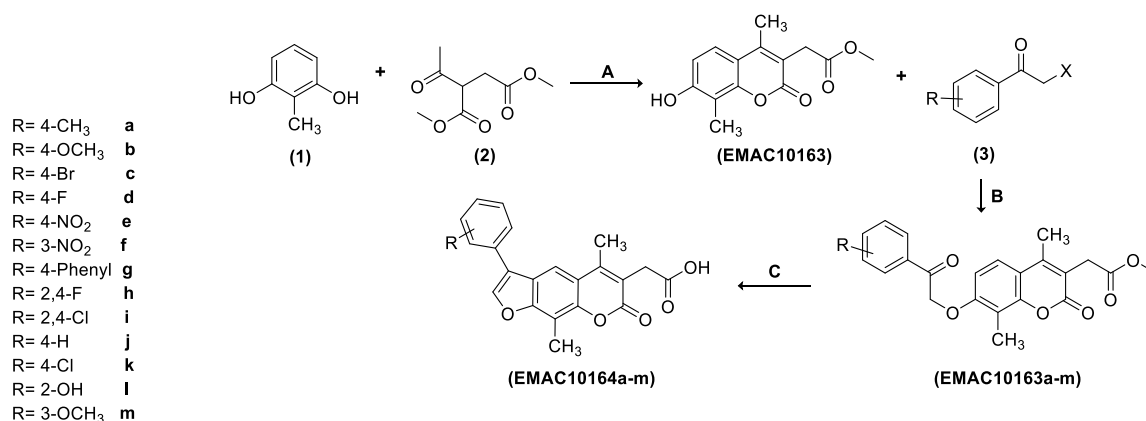


Figure 25. Schematic representation of the synthetic pathway used for the obtention of the furocoumarin family. Reaction conditions: (A) sulfuric acid, room temperature, 8 h; (B) acetone, K₂CO₃, α -haloketone, reflux, 6 – 24 h; (C) propan-2-ol, NaOH, reflux 2 – 5 h.

2.2.2. Synthesis of methyl 2-(7-hydroxy-4,8-dimethyl-2-oxo-2H-chromen-3-yl)acetate (EMAC10163)

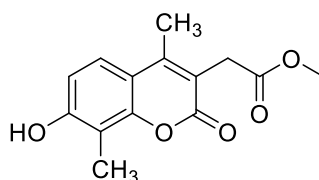


Figure 26. Structure of EMAC10163.

To a mixture of 2-methylresorcinol (0.5 g, 4.03 mmol) and dimethylsuccinate (650 μ L, 4.03 mmol) was added 3 mL of H₂SO₄ 98%. The mixture was vigorously stirred at room

temperature for 8 hours. The homogeneous mixture was poured into iced water and stirred until the melting of the ice. The precipitate was kept in the fridge overnight and filtrated in the next day. The desired compound (Figure 26) was obtained as a white solid after drying in a vacuum oven.

Yield: 62.6 %

^1H NMR (400 MHz, DMSO): δ = 2.16 (s, 3H, CH_3), 2.34 (s, 3H, CH_3), 3.62 (s, 3H, CH_3), 3.65 (s, 2H, CH_2), 6.88 (d, J = 8.8 Hz, 1H, H(Ar)), 7.51 (d, J = 8.8, 1H, H(Ar)), 10.38 (s, 1H, OH).

^{13}C NMR (100 MHz, DMSO): δ = 8.41 (CH_3), 15.51 (CH_3), 32.80 (CH_2), 52.27 (CH_3), 110.92 (C(Ar)), 112.40 (C(Ar)), 112.62 (C(Ar)), 115.07 (C(Ar)), 123.92 (C(Ar)), 150.33 (C(Ar)), 151.94 (C(Ar)), 158.94 (C7), 161.57 (C2), 171.22 (COOCH_3).

Melting point: [179 – 180] °C.

Molecular weight: 262.26 g/mol.

Rf (DCM/EtOAc 8:2): 0.58.

2.2.3. Synthesis of the 2H-chromen compounds (EMAC10163 series)

General procedure: A hot solution of EMAC10163 (1 mmol) in acetone was treated with K_2CO_3 (2.5 mmol), stirred vigorously, heated and the appropriate α -haloketone (1.1 mmol) was added. The reaction mixture was heated to reflux and stirred. The mixture was poured into a solution of H_2SO_4 0.5 M. The resulting precipitate was filtered. The solid was purified by chromatographic column. The resulting fractions were evaporated and recrystallized to obtain the desired compound.

2.2.3.1. Synthesis of methyl 2-(4,8-dimethyl-2-oxo-7-(2-oxo-2-(p-tolyl)ethoxy)-2H-chromen-3-yl)acetate (EMAC10163a)

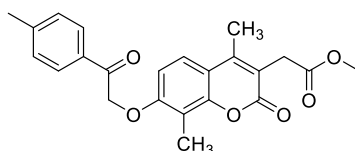


Figure 27. Structure of EMAC10163a.

The compound EMAC10163a (Figure 27) was obtained through the general procedure referred on the section 2.2.3. on the following conditions: EMAC 10163 (1.00 g, 3.81

mmol), acetone (20 mL) and K_2CO_3 (1.31 g, 9.5 mmol) were mixed and 2-bromo-4'-methylacetophenone (0.89 g, 4.18 mmol) was added. After 6 h the mixture was poured into 100 mL of H_2SO_4 0.5 M. For the purification by chromatographic column, DCM/EtOAc 88:12 to 100% of EtOAc were used as eluents. The white solid was obtained by recrystallization with DCM/*n*-hexane.

Yield: 86.1 %

1H NMR (400 MHz, $CDCl_3$): δ = 2.35 (s, 3H, CH_3), 2.38 (s, 3H, CH_3), 2.43 (s, 3H, CH_3), 3.70 (s, 3H, OCH_3), 3.72 (s, 2H, CH_2), 5.36 (s, 2H, CH_2), 6.71 (d, J = 8.9 Hz, 1H, H(Ar)), 7.28 – 7.34 (m, 2H, 2 x H(Ar')), 7.39 (d, J = 9.0 Hz, 1H, H(Ar)), 7.85 – 7.94 (m, 2H, 2 x H(Ar')).

^{13}C NMR (100 MHz, $CDCl_3$): δ = 8.42 (CH_3), 15.38 (CH_3), 21.80 (CH_3), 32.75 (CH_2), 52.21 (CH_3), 71.17 (CH_2), 107.90 (C(Ar)), 114.68 (C(Ar)), 114.73 (C(Ar)), 116.62 (C(Ar)), 122.64 (C(Ar)), 128.26 (2 x C(Ar')), 129.59 (2 x C(Ar')), 131.86 (C(Ar)), 145.16 (C(Ar)), 149.04 (C(Ar)), 151.68 (C(Ar)), 158.36 (C(Ar)), 161.84 (C(Ar)), 170.88 ($COOCH_3$) 193.71 (CO).

ESI/MS m/z (%): 395 ($[M+H]^+$, 100).

Melting point: [178 – 181] °C.

Molecular weight: 394.42 g/mol.

Rf (DCM/EtOAc 5:5): 0.86

2.2.3.2. Synthesis of methyl 2-(7-(2-(4-methoxyphenyl)-2-oxoethoxy)-4,8-dimethyl-2-oxo-2H-chromen-3-yl)acetate (EMAC10163b)

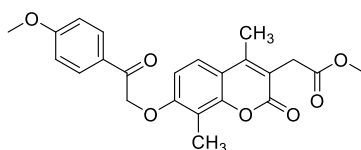


Figure 28. Structure of EMAC10163b.

The compound EMAC10163b (Figure 28) was obtained through the general procedure referred on the section 2.2.3. on the following conditions: EMAC10163 (0.50 g, 1.91 mmol), acetone (10 mL) and K_2CO_3 (0.66 g, 4.8 mmol) were mixed and 2-bromo-4'-methoxyacetophenone (0.48 g, 2.10 mmol) was added. After 6 h the mixture was poured into 50 mL of H_2SO_4 0.5 M. For the purification by chromatographic column, DCM/EtOAc 88:12 to 100% of EtOAc were used as eluents. The white solid was obtained by recrystallization with DCM/*n*-hexane.

Yield: 27.8 %

^1H NMR (400 MHz, CDCl_3): δ = 2.35 (s, 3H, CH_3), 2.38 (s, 3H, CH_3), 3.70 (s, 3H, CH_3), 3.72 (s, 2H, CH_2), 3.89 (s, 3H, CH_3), 5.33 (s, 2H, CH_2), 6.73 (d, J = 8.9 Hz, 1H, H(Ar)), 6.94 – 7.00 (m, 2H, 2 x H(Ar')), 7.39 (d, J = 8.7 Hz, 1H, H(Ar)), 7.96 – 8.02 (m, 2H, 2 x H(Ar')).

^{13}C NMR (100 MHz, CDCl_3): δ = 8.43 (CH_3), 15.38 (CH_3), 32.75 (CH_2), 52.21 (CH_3), 55.57 (CH_3), 71.15 (CH_2), 107.91 (C(Ar)), 114.10 (2 x C(Ar')), 114.67 (C(Ar)), 114.68 (C(Ar)), 116.60 (C(Ar)), 122.65 (C(Ar)), 127.37 (C(Ar)), 130.57 (2 x C(Ar')), 149.04 (C(Ar)), 151.68 (C(Ar)), 158.40 (C(Ar)), 161.84 (C(Ar)), 164.25 (C(Ar)), 170.88 (COOCH_3) 192.64 (CO).

ESI/MS m/z (%): 411 ($[\text{M}+\text{H}]^+$, 100).

Melting point: [173 – 175] °C.

Molecular weight: 410.42 g/mol.

Rf (DCM/EtOAc 5:5): 0.80.

2.2.3.3. Synthesis of methyl 2-(7-(2-(4-bromophenyl)-2-oxoethoxy)-4,8-dimethyl-2-oxo-2H-chromen-3-yl)acetate (EMAC10163c)

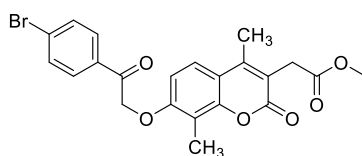


Figure 29. Structure of EMAC10163c.

The compound EMAC10163c (Figure 29) was obtained through the general procedure referred on the section 2.2.3. on the following conditions: EMAC10163 (1.00 g, 3.81 mmol), acetone (20 mL) and K_2CO_3 (1.31 g, 9.51 mmol) were mixed and, 2,4'-dibromoacetophenone (1.17 g, 4.21 mmol) was added. After 24 h, the mixture was poured into 100 mL of H_2SO_4 . For the purification by chromatographic column, DCM/EtOAc 88:12 to 100% of EtOAc were used as eluents. The white solid was obtained by recrystallization with DCM/*n*-hexane.

Yield: 46.1 %.

^1H NMR (400 MHz, CDCl_3): δ = 2.35 (s, 3H, CH_3), 2.37 (s, 3H, CH_3), 3.70 (s, 3H, CH_3), 3.72 (s, 2H, CH_2), 5.33 (s, 2H, CH_2), 6.71 (d, J = 8.9 Hz, 1H, H(Ar)), 7.40 (d, J = 8.7 Hz, 1H, H(Ar)), 7.63 – 7.68 (m, 2H, 2 x H(Ar')), 7.85 – 7.89 (m, 2H, 2 x H(Ar')).

^{13}C NMR (100 MHz, CDCl_3): $\delta = 8.43$ (CH_3), 15.40 (CH_3), 32.75 (CH_2), 52.24 (OCH_3), 71.23 (CH_2), 107.76 (C(Ar)), 114.79 (C(Ar)), 114.88 (C(Ar)), 116.83 (C(Ar)), 122.70 (C(Ar)), 129.45 (C(Ar)), 129.71 (2 x C(Ar')), 132.28 (2 x C(Ar')), 133.05 (C(Ar)), 148.96 (C(Ar)), 151.71 (C(Ar)), 158.07 (C(Ar)), 161.75 (C(Ar)), 170.85 (COOCH_3), 193.43 (CO).

ESI/MS m/z (%): 459 ($[\text{M}+\text{H}]^+$, 44).

Melting point: [199 – 201] $^\circ\text{C}$.

Molecular weight: 459.29 g/mol.

R_f (DCM/EtOAc 5:5): 0.89.

2.2.3.4. Synthesis of methyl 2-(7-(2-(4-fluorophenyl)-2-oxoethoxy)-4,8-dimethyl-2-oxo-2H-chromen-3-yl)acetate (EMAC10163d)

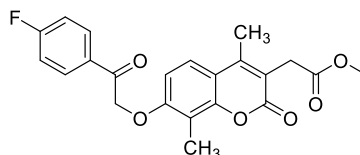


Figure 30. Structure of EMAC10163d.

The compound EMAC10163d (Figure 30) was obtained through the general procedure referred on the section 2.2.3. on the following conditions: EMAC10163 (1.00 g, 3.82 mmol), acetone (20 mL) and K_2CO_3 (1.32 g, 9.59 mmol) were mixed and, 2-bromo-4-fluoroacetophenone (0.91 g, 4.22 mmol) was added. After 6 h, the mixture was poured into 100 mL of H_2SO_4 . For the purification by chromatographic column, DCM/MeOH 98:2 to 20% of MeOH were used as eluents. The very light-yellow solid was obtained by recrystallization with DCM/*n*-hexane.

Yield: 63.0 %

^1H NMR (400 MHz, CDCl_3): $\delta = 2.35$ (s, 3H, CH_3), 2.37 (s, 3H, CH_3), 3.70 (s, 3H, OCH_3), 3.72 (s, 2H, CH_2), 5.34 (s, 2H, CH_2), 6.72 (d, $J = 8.9$ Hz, 1H, H(Ar)), $7.13 - 7.22$ (m, 2H, 2 x H(Ar')), 7.40 (d, $J = 8.9$ Hz, 1H, H(Ar)), $8.02 - 8.08$ (m, 2H, 2 x H(Ar')).

^{13}C NMR (100 MHz, CDCl_3): $\delta = 8.42$ (CH_3), 15.39 (CH_3), 32.75 (CH_2), 52.23 (OCH_3), 71.22 (CH_2), 107.81 (C(Ar)), 114.76 (C(Ar)), 114.84 (C(Ar)), 116.17 (d, $J_{\text{CF}} = 22.0$ Hz, C3', C5'), 116.78 (C(Ar)), 122.70 (C(Ar)), 130.81 (d, $J_{\text{CF}} = 3.1$ Hz, C1'), 131.00 (d, $J_{\text{CF}} = 9.5$ Hz, C2', C6'), 148.99 (C(Ar)), 151.70 (C(Ar)), 158.15 (C(Ar)), 161.77 (C(Ar)), 166.26 (d, $J_{\text{CF}} = 256.7$ Hz, C4'), 170.86 (COOCH_3), 192.75 (CO).

ESI/MS m/z (%): 399 ($[M+H]^+$, 100).

Melting point: [155 – 157] °C.

Molecular weight: 398.39 g/mol.

Rf (DCM/EtOAc 5:5): 0.89.

2.2.3.5. Synthesis of methyl 2-(4,8-dimethyl-7-(2-(4-nitrophenyl)-2-oxoethoxy)-2-oxo-2H-chromen-3-yl)acetate (EMAC10163e)

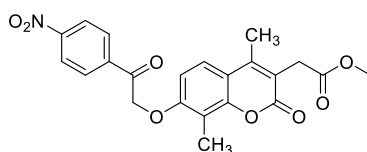


Figure 31. Structure of EMAC10163e.

The compound EMAC10163e (Figure 31) was obtained through the general procedure referred on the section 2.2.3. on the following conditions: EMAC10163 (0.50 g, 1.91 mmol), acetone (10 mL) and K_2CO_3 (0.66 g, 4.80 mmol) were mixed and, 2-bromo-4-nitroacetophenone (0.51 g, 2.10 mmol) was added. After 8 h, the mixture was poured into 50 mL of H_2SO_4 . For the purification by chromatographic column, DCM/EtOAc 88:12 to 100% of EtOAc were used as eluents. The light brown solid was obtained by recrystallization with DCM/*n*-hexane.

Yield: 37.9 %

1H NMR (400 MHz, $CDCl_3$): δ = 2.27 (s, 3H, CH_3), 2.29 (s, 3H, CH_3), 3.64 (s, 3H, CH_3), 3.65 (s, 2H, CH_2), 5.31 (s, 2H, CH_2), 6.67 (d, J = 8.9 Hz, 1H, H(Ar)), 7.35 (d, J = 8.7 Hz, 1H, H(Ar)), 8.09 – 8.12 (m, 2H, 2 x H(Ar')), 8.27 – 8.29 (m, 2H, 2 x H(Ar')).

^{13}C NMR (100 MHz, $CDCl_3$): δ = 8.43 (CH_3), 15.41 (CH_3), 32.73 (CH_2), 52.26 (CH_3), 71.53 (CH_2), 107.64 (C(Ar)), 114.83 (C(Ar)), 115.10 (C(Ar)), 117.05 (C(Ar)), 122.79 (C(Ar)), 124.08 (2 x C(Ar')), 129.44 (2 x C(Ar')), 138.77 (C(Ar)), 148.90 (C(Ar)), 150.82 (C(Ar)), 151.71 (C(Ar)), 157.74 (C(Ar)), 161.65 (C(Ar)), 170.82 ($COOCH_3$), 193.36 ($C=O$).

ESI/MS m/z (%): 426 ($[M+H]^+$, 100).

Melting point: [180 – 183] °C.

Molecular weight: 425.39 g/mol.

Rf (DCM/EtOAc 5:5): 0.80.

2.2.3.6. Synthesis of methyl 2-(4,8-dimethyl-7-(2-(3-nitrophenyl)-2-oxoethoxy)-2-oxo-2H-chromen-3-yl)acetate (EMAC10163f)

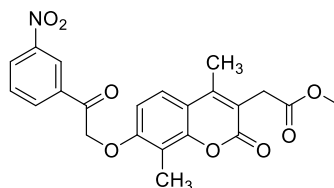


Figure 32. Structure of EMAC10163f.

The compound EMAC10163f (Figure 32) was obtained through the general procedure referred on the section 2.2.3. on the following conditions: EMAC10163 (1.00 g, 3.82 mmol), acetone (20 mL) and K_2CO_3 (1.31 g, 9.49 mmol) were mixed and, 3-nitrophenacyl bromide (1.02 g, 4.18 mmol) was added. After 7 h, the mixture was poured into 100 mL of H_2SO_4 . For the purification by chromatographic column, DCM/EtOAc 88:12 to 100% of EtOAc were used as eluents. The yellow solid was obtained by recrystallization with DCM/*n*-hexane.

Yield: 19.6 %

1H NMR (400 MHz, $CDCl_3$): δ = 2.35 (s, 3H, CH_3), 2.36 (s, 3H, CH_3), 3.71 (s, 3H, CH_3), 3.72 (s, 2H, CH_2), 5.40 (s, 2H, CH_2), 6.76 (d, J = 8.9 Hz, 1H, H(Ar)), 7.42 (d, J = 8.6 Hz, 1H, H(Ar)), 7.74 (t, J = 8.6 Hz, 1H, H5'), 8.34 – 8.36 (m, 1H, H(Ar')), 8.47 – 8.49 (m, 1H, H(Ar')), 8.85 – 8.86 (m, 1H, H(Ar')).

^{13}C NMR (100 MHz, $CDCl_3$): δ = 8.40 (CH_3), 15.41 (CH_3), 32.74 (CH_2), 52.25 (CH_3), 71.53 (CH_2), 107.67 (C(Ar)), 114.84 (C(Ar)), 115.10 (C(Ar)), 117.03 (C(Ar)), 122.82 (C(Ar)), 123.30 (C(Ar)), 128.27 (C(Ar)), 130.24 (C(Ar)), 133.91 (C(Ar)), 135.54 (C(Ar)), 148.49 (C(Ar)), 148.92 (C(Ar)), 151.71 (C(Ar)), 157.74 (C(Ar)), 161.65 (C(Ar)), 170.82 ($COOCH_3$), 192.82 (CO).

ESI/MS m/z (%): 426 ($[M+H]^+$, 51).

Melting point: [165 – 167] °C.

Molecular weight: 425.39 g/mol.

R_f (DCM/EtOAc 5:5): 0.78.

2.2.3.7. Synthesis of methyl 2-(7-(2-([1,1'-biphenyl]-4-yl)-2-oxoethoxy)-4,8-dimethyl-2-oxo-2H-chromen-3-yl)acetate (EMAC10163g)

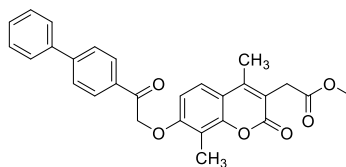


Figure 33. Structure of EMAC10163g.

The compound EMAC10163g (Figure 33) was obtained through the general procedure referred on the section 2.2.3. on the following conditions: EMAC10163 (1.00 g, 3.83 mmol), acetone (20 mL) and K_2CO_3 (1.31 g, 9.49 mmol) were mixed and, 2-bromo-1-(4-phenylphenyl)ethan-1-one (1.15 g, 4.18 mmol) was added. After 6 h, the mixture was poured into 100 mL of H_2SO_4 . For the purification by chromatographic column, DCM/EtOAc 88:12 to 100% of EtOAc were used as solvents. The white solid was obtained by recrystallization with DCM/*n*-hexane.

Yield: 73.9 %

1H NMR (400 MHz, $CDCl_3$): δ = 2.35 (s, 3H, CH_3), 2.40 (s, 3H, CH_3), 3.70 (s, 3H, CH_3), 3.72 (s, 2H, CH_2), 5.41 (s, 2H, CH_2), 6.74 (d, J = 8.9 Hz, 1H, H(Ar)), 7.39 – 7.44 (m, 2H, 2 x H(Ar)), 7.46 – 7.50 (m, 2H, 2 x H(Ar)), 7.61 – 7.64 (m, 2H, 2 x H(Ar)); 7.71 – 7.74 (m, 2H, 2 x H(Ar)), 8.06 – 8.09 (m, 2H, 2 x H(Ar)).

^{13}C NMR (100 MHz, $CDCl_3$): δ = 8.45 (CH_3), 15.39 (CH_3), 32.75 (CH_2), 52.22 (OCH_3), 71.28 (CH_2), 107.90 (C(Ar)), 114.75 (C(Ar)), 114.77 (C(Ar)), 116.68 (C(Ar)), 122.68 (C(Ar)), 127.29 (2 x C(Ar)), 127.50 (2 x C(Ar)), 128.54 (C(Ar)), 128.77 (2 x C(Ar)), 129.05 (2 x C(Ar)), 132.99 (C(Ar)), 139.53 (C(Ar)), 146.81 (C(Ar)), 149.03 (C(Ar)), 151.70 (C(Ar)), 158.32 (C(Ar)), 161.82 (C(Ar)), 170.87 ($COOCH_3$), 193.70 (CO).

ESI/MS m/z (%): 457 ($[M+H]^+$, 88).

Melting point: [168 – 169] °C.

Molecular weight: 456.49 g/mol.

R_f (DCM/EtOAc 5:5): 0.94.

2.2.3.8. Synthesis of methyl 2-(7-(2-(2,4-difluorophenyl)-2-oxoethoxy)-4,8-dimethyl-2-oxo-2H-chromen-3-yl)acetate (EMAC10163h)

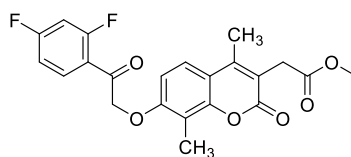


Figure 34. Structure of EMAC10163h.

The compound EMAC10163h (Figure 34) was obtained through the general procedure referred on the section 2.2.3. on the following conditions: EMAC10163 (0.50 g, 1.91 mmol), acetone (10 mL) and K_2CO_3 (0.66 g, 4.80 mmol) were mixed and, 2-chloro-1-(2,4-difluorophenyl)ethanone (0.41 g, 2.13 mmol) was added. The mixture was kept reacting overnight, and then poured into 50 mL of H_2SO_4 . The resulting precipitate was recrystallized with DCM/*n*-hexane giving a light-yellow solid.

Yield: 49.0 %

1H NMR (400 MHz, $CDCl_3$): δ = 2.36 (s, 3H, CH_3), 2.38 (s, 3H, CH_3), 3.71 (s, 3H, CH_3), 3.73 (s, 2H, CH_2), 5.30 (m, 2H, CH_2), 6.68 (d, J = 8.9 Hz, 1H, H(Ar)), 6.92 – 6.98 (m, 1H, H(Ar)), 7.02 – 7.07 (m, 1H, H(Ar)), 7.40 (d, J = 8.9 Hz, 1H, H(Ar)), 8.00 – 8.06 (m, 1H, H(Ar)).

^{13}C NMR (100 MHz, $CDCl_3$): δ = 8.35 (CH_3), 15.40 (CH_3), 32.76 ($C3CH_2$), 52.23 (CH_3), 73.71 (d, J = 12.3 Hz, CH_2), 104.82 (dd, J_{CF} = 27.5, 25.7 Hz, C3'), 107.84 (C(Ar)), 113.00 (dd, J_{CF} = 21.6, 3.2 Hz, C5'), 114.78 (C(Ar)), 114.88 (C(Ar)), 116.73 (C(Ar)), 119.41 (dd, J_{CF} = 15.3, 3.6 Hz, C1'), 122.59 (C(Ar)), 132.91 (dd, J_{CF} = 10.8, 4.9 Hz, C6'), 149.00 (C(Ar)), 151.75 (C(Ar)), 158.28 (C(Ar)), 163.03 (dd, J_{CF} = 256.1, 12.8 Hz, C2'), 166.54 (dd, J_{CF} = 259.1, 12.5 Hz, C4'), 170.88 ($COOCH_3$), 190.86 (d, J_{CF} = 5.6 Hz, CO).

ESI/MS m/z (%): 417 ($[M+H]^+$, 100).

Melting point: [188 – 190] °C.

Molecular weight: 416.38 g/mol.

R_f (DCM/EtOAc 5:5): 0.87.

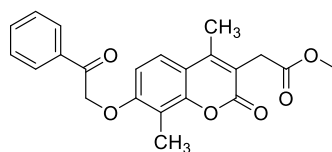
2.2.3.9. Synthesis of methyl 2-(4,8-dimethyl-2-oxo-7-(2-oxo-2-phenylethoxy)-2H-chromen-3-yl)acetate (EMAC10163j)

Figure 35. Structure of EMAC10163j.

The compound EMAC10163j (Figure 35) was obtained through the general procedure referred on the section 2.2.3. on the following conditions: EMAC10163 (1.00 g, 3.82 mmol), acetone (20 mL) and K_2CO_3 (1.32 g, 9.56 mmol) were mixed and, 2-bromoacetophenone (0.8344 g, 4.19 mmol) was added. After 7 h, the mixture was poured into 100 mL of H_2SO_4 0.5 M. The light-yellow solid was obtained by recrystallization with DCM/*n*-hexane.

Yield: 88.6 %

1H NMR (400 MHz, $CDCl_3$): δ = 2.35 (s, 3H, CH_3), 2.38 (s, 3H, CH_3), 3.70 (s, 3H, CH_3), 3.72 (s, 2H, CH_2), 5.39 (s, 2H, CH_2), 6.72 (d, J = 8.9 Hz, 1H, H(6)), 7.38 – 7.40 (m, 1H, H(Ar)), 7.49 – 7.53 (m, 2H, 2 x H(Ar')), 7.61 – 7.65 (m, 1H, H(Ar')); 7.99 – 8.01 (m, 2H, 2 x H(Ar')).

^{13}C NMR (100 MHz, $CDCl_3$): δ = 8.42 (CH_3), 15.39 (CH_3), 32.76 (CH_2), 52.22 (CH_3), 71.20 (CH_2), 107.88 (C(Ar)), 114.75 (C(Ar)), 114.80 (C(Ar)), 116.69 (C(Ar)), 122.65 (C(Ar)), 128.14 (2 x C(Ar')), 128.93 (2 x C(Ar')), 134.11 (C(Ar)), 134.36 (C(Ar)), 149.01 (C(Ar)), 151.71 (C(Ar)), 158.30 (C(Ar)), 161.81 (C(Ar)), 170.87 ($COOCH_3$), 194.08 (CO).

ESI/MS m/z (%): 381 ($[M+H]^+$, 100).

Melting point: [157 – 159] °C.

Molecular weight: 380.40 g/mol.

R_f (DCM/EtOAc 5:5): 0.84.

2.2.3.10. Synthesis of methyl 2-(7-(2-(4-chlorophenyl)-2-oxoethoxy)-4,8-dimethyl-2-oxo-2H-chromen-3-yl)acetate (EMAC10163k)

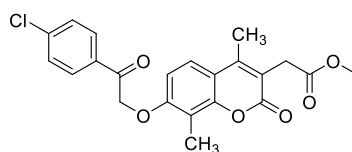


Figure 36. Structure of EMAC10163k.

The compound EMAC10163k (Figure 36) was obtained through the general procedure referred on the section 2.2.3. on the following conditions: EMAC10163 (0.50 g, 1.91 mmol), acetone (10 mL) and K_2CO_3 (0.66 g, 4.80 mmol) were mixed and, 2-bromo-4'-chloroacetophenone (0.49 g, 2.12 mmol) was added. After 6 h, the mixture was poured into 50 mL of H_2SO_4 0.5 M. For the purification by chromatographic column, DCM/EtOAc 80:20 to 30% of EtOAc were used as eluents. The white solid was obtained by recrystallization with DCM/*n*-hexane.

Yield: 46.0 %

1H NMR (400 MHz, $CDCl_3$): δ = 2.37 (s, 3H, CH_3), 2.38 (s, 3H, CH_3), 3.72 (s, 3H, OCH_3), 3.74 (s, 2H, CH_2), 5.35 (s, 2H, CH_2), 6.73 (d, J = 8.6 Hz, 1H, H(Ar)), 7.41 (d, J = 8.9 Hz, 1H, H(Ar)), 7.48 – 7.52 (m, 2H, 2 x H(Ar')), 7.95 – 7.98 (m, 2H, 2 x H(Ar')).

^{13}C NMR (100 MHz, $CDCl_3$): δ = 8.42 (CH_3), 15.39 (CH_3), 32.74 (CH_2), 52.23 (OCH_3), 71.24 (CH_2), 107.77 (C(Ar)), 114.76 (C(Ar)), 114.86 (C(Ar)), 116.80 (C(Ar)), 122.70 (C(Ar)), 129.28 (2 x C(Ar')), 129.64 (2 x C(Ar')), 132.64 (C(Ar)), 140.67 (C(Ar)), 148.97 (C(Ar)), 151.69 (C(Ar)), 158.08 (C(Ar)), 161.75 (C(Ar)), 170.85 ($COOCH_3$) 193.20 (CO).

ESI/MS m/z (%): 415 ($[M+H]^+$, 96).

Melting point: [182 – 184] °C.

Molecular weight: 414.84 g/mol.

R_f (DCM/EtOAc 5:5): 0.80.

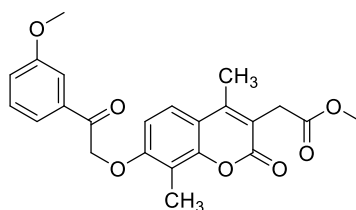
2.2.3.11. Synthesis of methyl 2-(7-(2-(3-methoxyphenyl)-2-oxoethoxy)-4,8-dimethyl-2-oxo-2H-chromen-3-yl)acetate (EMAC10163m)

Figure 37. Structure of EMAC10163m.

The compound EMAC10163m (Figure 37) was obtained through the general procedure referred on the section 2.2.3. on the following conditions: EMAC10163 (1.00 g, 3.82 mmol), acetone (20 mL) and K₂CO₃ (1.32 g, 9.57 mmol) were mixed and, 2-bromo-3'-methoxyacetophenone (0.96 g, 4.19 mmol) was added. After 6 h, the mixture was poured into 100 mL of H₂SO₄ 0.5 M. For the purification by chromatographic column, DCM/EtOAc 88:12 to 100% of EtOAc were used as eluents. The white solid was obtained by recrystallization with DCM/*n*-hexane.

Yield: 55.3 %

¹H NMR (400 MHz, CDCl₃): δ = 2.35 (s, 3H, CH₃), 2.39 (s, 3H, CH₃), 3.70 (s, 3H, CH₃), 3.72 (s, 2H, CH₂), 3.86 (s, 3H, OCH₃), 5.38 (s, 2H, CH₂), 6.71 (d, *J* = 8.9 Hz, 1H, H(Ar)), 7.16 – 7.19 (m, 1H, H(Ar)), 7.38 – 7.44 (m, 2H, 2 x H(Ar')), 7.51 – 7.52 (m, 1H, H(Ar)), 7.56 – 7.58 (m, 1H, H(Ar)).

¹³C NMR (100 MHz, CDCl₃): δ = 8.43 (CH₃), 15.39 (CH₃), 32.76 (CH₂), 52.22 (CH₃), 52.52 (OCH₃), 71.22 (CH₂), 107.89 (C(Ar)), 112.51 (C(Ar)), 114.75 (C(Ar)), 114.82 (C(Ar)), 116.69 (C(Ar)), 120.52 (2 x C(Ar')), 122.64 (C(Ar)), 129.93 (C(Ar)), 135.59 (C(Ar)), 149.02 (C(Ar)), 151.70 (C(Ar)), 158.31 (C(Ar)), 160.05 (C(Ar)), 161.82 (C(Ar)), 170.88 (COOCH₃), 193.86 (CO).

ESI/MS *m/z* (%): 411 ([M+H]⁺, 98).

Melting point: [157 – 160] °C.

Molecular weight: 410.42 g/mol.

R_f (DCM/EtOAc 5:5): 0.80.

2.2.4. Synthesis of the 7H-furo-chromen compounds (EMAC10164 series)

General procedure: To a suspension of EMAC10163a - m (1 mmol) in propan-2-ol was added an aqueous solution of NaOH or KOH 1M (4 mmol). The reaction mixture was heated to reflux and stirred. After the completion of the reaction, the mixture was poured into iced water and acidify with a solution of HCl 6M. The resulting precipitate was filtered to obtain the desired compound.

2.2.4.1. Synthesis of 2-(5,9-dimethyl-7-oxo-3-(p-tolyl)-7H-furo[3,2-g]chromen-6-yl)acetic acid (EMAC10164a)

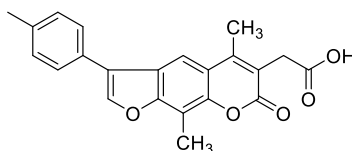


Figure 38. Structure of EMAC10164a.

The compound EMAC10164a (Figure 38) was obtained through the general procedure referred on the section 2.2.4. on the following conditions: EMAC10163a (0.50 g, 1.27 mmol), 5 mL of propan-2-ol and an aqueous solution of NaOH 1M (5.1 mL) were mixed and stirred for 4 h. After filtration a light brown solid was obtained.

Yield: 96.0 %

^1H NMR (400 MHz, DMSO): δ = 2.38 (s, 3H, CH_3), 2.48 (s, 3H, CH_3), 2.50 (s, 3H, CH_3), 3.64 (s, 2H, CH_2), 7.33 – 7.35 (m, 2H, 2 x H(Ar')), 7.65 – 7.67 (m, 2H, 2 x H(Ar')), 7.96 (s, 1H, H5), 8.39 (s, 1H, H7).

^{13}C NMR (100 MHz, DMSO): δ = 8.66 (CH_3), 16.07 (CH_3), 21.29 (CH_3), 33.44 (CH_2), 108.96 (C(Ar)), 114.18 (C(Ar)), 117.05 (C(Ar)), 118.33 (C(Ar)), 121.94 (C(Ar)), 122.47 (C(Ar)), 127.52 (2 x C(Ar')), 128.34 (C(Ar)), 130.19 (2 x C(Ar')), 137.56 (C(Ar)), 144.07 (C(Ar)), 148.01 (C(Ar)), 149.92 (C(Ar)), 155.44 (C(Ar)), 161.21 (C(Ar)), 171.99 (COOH).

ESI/MS m/z (%): 363 ($[\text{M}+\text{H}]^+$, 100).

Melting point: [228 – 231] °C.

Molecular weight: 362.38 g/mol.

Rf (DCM/EtOAc 5:5): 0.15.

2.2.4.2. Synthesis of 2-(3-(4-methoxyphenyl)-5,9-dimethyl-7-oxo-7H-furo[3,2-g]chromen-6-yl)acetic acid (EMAC10164b)

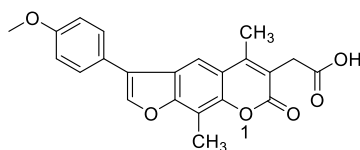


Figure 39. Structure of EMAC10164b.

The compound EMAC10164b (Figure 39) was obtained through the general procedure referred on the section 2.2.4. on the following conditions: EMAC10163b (0.35 g, 0.86 mmol), 3 mL of propan-2-ol and an aqueous solution of NaOH 1M (3.5 mL) were mixed and stirred for 4 h. After filtration a light brown solid was obtained.

Yield: 67.3 %

^1H NMR (400 MHz, DMSO): δ = 2.52 (s, 3H, CH_3), 2.54 (s, 3H, CH_3), 3.66 (s, 2H, CH_2), 3.83 (s, 3H, $\text{C4}'\text{OCH}_3$), 7.10 – 7.12 (m, 2 x H(Ar')), 7.73 – 7.75 (m, 2 x H(Ar')), 8.01 (s, 1H, H5), 8.39 (s, 1H, H7), 12.50 (s, 1H, COOH).

^{13}C NMR (100 MHz, DMSO): δ = 8.71 (CH_3), 16.13 (CH_3), 33.42 (CH_2), 55.70 ($\text{C4}'\text{OCH}_3$), 108.99 (C(Ar)), 114.28 (C(Ar)), 115.13 (2 x C(Ar')), 117.07 (C(Ar)), 118.31 (C(Ar)), 121.75 (C(Ar)), 122.65 (C(Ar)), 123.54 (C(Ar)), 128.95 (2 x C(Ar')), 143.70 (C(Ar)), 148.06 (C(Ar)), 150.04 (C(Ar)), 155.46 (C(Ar)), 159.44 (C(Ar)), 161.25 (C(Ar)), 171.98 (COOH).

ESI/MS m/z (%): 379 ($[\text{M}+\text{H}]^+$, 100).

Melting point: [226 – 227] °C.

Molecular weight: 378.38 g/mol.

R_f (DCM/EtOAc 5:5): 0.35.

2.2.4.3. Synthesis of 2-(3-(4-bromophenyl)-5,9-dimethyl-7-oxo-7H-furo[3,2-g]chromen-6-yl)acetic acid (EMAC10164c)

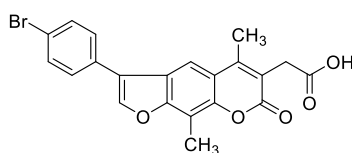


Figure 40. Structure of EMAC10164c.

The compound EMAC10164c (Figure 40) was obtained through the general procedure referred on the section 2.2.4. on the following conditions: EMAC10163c (0.50 g, 1.10 mmol), 5 mL of propan-2-ol and an aqueous solution of NaOH 1M (4.4 mL) were mixed and stirred for 3 h. After filtration a light brown solid was obtained.

Yield: 90.5 %

^1H NMR (400 MHz, DMSO): δ = 2.49 (s, 3H, CH_3), 2.50 (s, 3H, CH_3), 3.64 (s, 2H, CH_2), 7.69 – 7.76 (m, 4H, 4 x H(Ar')), 7.96 (s, 1H, H5), 8.50 (s, 1H, H7), 12.49 (s, 1H, COOH).

^{13}C NMR (100 MHz, DMSO): δ = 8.68 (CH_3), 16.13 (CH_3), 33.40 (CH_2), 109.11 (C(Ar)), 114.25 (C(Ar)), 117.23 (C(Ar)), 118.42 (C(Ar)), 120.99 (C(Ar)), 121.28 (C(Ar)), 121.98 (C(Ar)), 129.66 (2 x C(Ar')), 130.56 (C(Ar)), 132.53 (2 x C(Ar')), 144.93 (C(Ar)), 148.13 (C(Ar)), 150.00 (C(Ar)), 155.46 (C(Ar)), 161.16 (C(Ar)), 171.95 (COOH).

ESI/MS m/z (%): 427 ($[\text{M}+\text{H}]^+$, 28).

Melting point: [263 – 267] °C

Molecular weight: 427.25 g/mol.

Rf (DCM/EtOAc 5:5): 0.26.

2.2.4.4. Synthesis of 2-(3-(4-fluorophenyl)-5,9-dimethyl-7-oxo-7H-furo[3,2-g]chromen-6-yl)acetic acid (EMAC10164d)

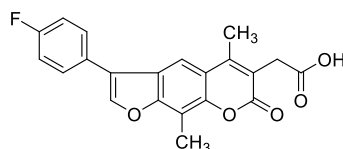


Figure 41. Structure of EMAC10164d.

The compound EMAC10164d (Figure 41) was obtained through the general procedure referred on the section 2.2.4. on the following conditions: EMAC10163d (0.50 g, 1.26 mmol), 5 mL of propan-2-ol and an aqueous solution of NaOH 1M (5.0 mL) were mixed and stirred for 4 h. After the filtration a light brown solid was obtained.

Yield: 89.7 %

^1H NMR (400 MHz, DMSO): δ = 2.50 (s, 3H, CH_3), 2.50 (s, 3H, CH_3), 3.64 (s, 2H, CH_2), 7.34 – 7.38 (m, 2H, 2 x H(Ar')), 7.82 – 7.85 (m, 2H, 2 x H(Ar')), 7.97 (s, 1H, H5), 8.44 (s, 1H, H7), 12.55 (s, 1H, COOH).

^{13}C NMR (100 MHz, DMSO): $\delta = 8.66$ ($\underline{\text{C}}\text{H}_3$), 16.11 ($\underline{\text{C}}\text{H}_3$), 33.39 ($\underline{\text{C}}\text{H}_2$), 109.04 (C(Ar)), 114.17 (C(Ar)), 116.52 (*d*, $J_{\text{CF}} = 21.5$ Hz, C3', C5'), 117.15 (C(Ar)), 118.36 (C(Ar)), 121.09 (C(Ar)), 122.24 (C(Ar)), 127.71 (*d*, $J_{\text{CF}} = 3.1$ Hz, C1'), 129.67 (*d*, $J_{\text{CF}} = 8.1$ Hz, C2', C6'), 144.51 (C(Ar)), 148.08 (C(Ar)), 150.00 (C(Ar)), 155.41 (C(Ar)), 160.99 (C(Ar)), 162.30 (*d*, $J_{\text{CF}} = 225$ Hz, C4'), 171.97 ($\underline{\text{C}}\text{OOH}$).

ESI/MS *m/z* (%): 367 ([M+H]⁺, 88).

Melting point: [277 – 279] °C.

Molecular weight: 366.34 g/mol.

R_f (DCM/EtOAc 5:5): 0.28.

2.2.4.5. Synthesis of 2-(3-([1,1'-biphenyl]-4-yl)-5,9-dimethyl-7-oxo-7H-furo[3,2-g]chromen-6-yl)acetic acid (EMAC10164g)

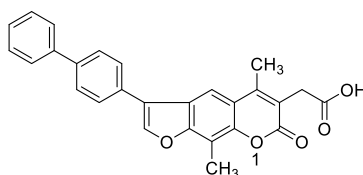


Figure 42. Structure of EMAC10164g.

The compound EMAC10164g (Figure 42) was obtained through the general procedure referred on the section 2.2.4. on the following conditions: EMAC10163g (0.50 g, 1.20 mmol), 5 mL of propan-2-ol and an aqueous solution of KOH 1M (5.0 mL) were mixed and stirred for 4 h. After the filtration a light brown solid was obtained.

Yield: 50.1 %

^1H NMR (400 MHz, DMSO): $\delta = 2.48$ (s, 3H, $\underline{\text{C}}\text{H}_3$), 2.51 (s, 3H, $\underline{\text{C}}\text{H}_3$), 3.59 (s, 2H, $\underline{\text{C}}\text{H}_2$), 7.38 – 7.41 (*m*, 1H, H(Ar)), 7.47 – 7.51 (*m*, 2H, 2 x H(Ar)), 7.72 – 7.74 (*m*, 2H, 2 x H(Ar)), 7.79 – 7.81 (*m*, 2H, 2 x H(Ar)), 7.86 – 7.88 (*m*, 2H, 2 x H(Ar)), 8.01 (s, 1H, H5), 8.49 (s, 1H, H7).

^{13}C NMR (100 MHz, DMSO): $\delta = 8.69$ ($\underline{\text{C}}\text{H}_3$), 16.10 ($\underline{\text{C}}\text{H}_3$), 34.03 ($\underline{\text{C}}\text{H}_2$), 108.99 (C(Ar)), 114.17 (C5), 117.30 (C(Ar)), 119.11 (C(Ar)), 121.60 (C(Ar)), 122.23 (C(Ar)), 127.01 (2 x C(Ar)), 127.81 (2 x C(Ar)), 128.06 (C(Ar)), 128.11 (2 x C(Ar)), 129.49 (2 x C(Ar)), 130.47 (C(Ar)), 139.83 (C(Ar)), 140.04 (C(Ar)), 144.60 (C7), 148.07 (C(Ar)), 149.43 (C(Ar)), 155.44 (C(Ar)), 161.27 ($\underline{\text{C}}\text{O}$), 172.01 ($\underline{\text{C}}\text{OOH}$).

ESI/MS *m/z* (%): 425 ([M+H]⁺, 57).

Melting point: [248 – 250] °C.

Molecular weight: 424.45 g/mol.

Rf (DCM/EtOAc 5:5): 0.15.

2.2.4.6. Synthesis of 2-(3-(2,4-difluorophenyl)-5,9-dimethyl-7-oxo-7H-furo[3,2-g]chromen-6-yl)acetic acid (EMAC10164h)

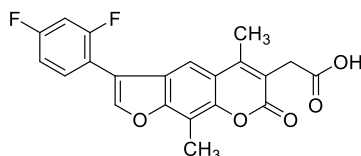


Figure 43. Structure of EMAC10164h.

The compound EMAC10164h (Figure 43) was obtained through the general procedure referred on the section 2.2.4. on the following conditions: EMAC10163h (0.50 g, 1.20 mmol), 5 mL of propan-2-ol and an aqueous solution of NaOH 1M (4.8 mL) were mixed and stirred for 2 h. After the filtration a brown solid was obtained.

Yield: 93.2 %

¹H NMR (400 MHz, DMSO): δ = 2.47 (s, 3H, CH₃), 2.54 (s, 3H, CH₃), 3.65 (s, 2H, CH₂), 7.25 – 7.30 (m, 1H, H(Ar)), 7.45 – 7.51 (m, 1H, H(Ar)), 7.85 – 7.91 (m, 2H, 2 x H(Ar)), 8.41 (s, 1H, H7).

¹³C NMR (100 MHz, DMSO): δ = 8.68 (CH₃), 16.07 (CH₃), 33.42 (CH₂), 105.30 (t, J_{CF} = 26.2 Hz, C3'), 109.08 (C(Ar)), 112.74 (dd, J_{CF} = 21.3, 3.5 Hz, C5'), 114.48 (d, J_{CF} = 3.1 Hz, C5), 115.36 (dd, J_{CF} = 14.6, 3.2 Hz, C1'), 117.23 (C(Ar)), 118.55 (C(Ar)), 122.44 (C(Ar)), 131.96 (dd, J_{CF} = 9.8, 5.3 Hz, C6'), 146.16 (d, J_{CF} = 5.5 Hz, C7), 148.15 (C(Ar)), 149.85 (C(Ar)), 154.91 (C(Ar)), 158.60 (C2), 159.91 (d, J_{CF} = 237.2 Hz, C2'), 161.16 (C(Ar)), 162.38 (d, J_{CF} = 235.7 Hz, C4'), 171.93 (COOH).

ESI/MS m/z (%): 385 ([M+H]⁺, 100).

Melting point: [227 – 230] °C.

Molecular weight: 384.33 g/mol.

Rf (DCM/EtOAc 5:5): 0.14.

2.2.4.7. Synthesis of 2-(5,9-dimethyl-7-oxo-3-phenyl-7H-furo[3,2-g]chromen-6-yl)acetic acid (EMAC10164j)

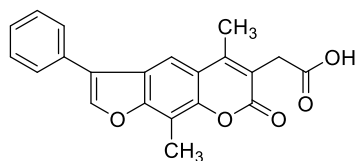


Figure 44. Structure of EMAC10164j.

The compound EMAC10164j (Figure 44) was obtained through the general procedure referred on the section 2.2.4. on the following conditions: EMAC10163j (0.50 g, 1.32 mmol), 5 mL of propan-2-ol and an aqueous solution of NaOH 1M (5.3 mL) were mixed and stirred for 5 h. After filtration a light brown solid was obtained.

Yield: 87.1 %

^1H NMR (400 MHz, DMSO): δ = 2.49 (s, 3H, CH_3), 2.50 (s, 3H, CH_3), 3.63 (s, 2H, CH_2), 7.41 – 7.45 (m, 1H, H4'), 7.52 – 7.56 (m, 2H, 2 x H(Ar')), 7.77 – 7.80 (m, 2H, 2 x H(Ar')), 7.99 (s, 1H, H5), 8.45 (s, 1H, H7).

^{13}C NMR (100 MHz, DMSO): δ = 8.66 (CH_3), 16.08 (CH_3), 33.47 (CH_2), 109.01 (C(Ar)), 114.19 (C(Ar)), 117.12 (C(Ar)), 118.41 (C(Ar)), 122.01 (C(Ar)), 122.30 (C(Ar)), 127.61 (2 x C(Ar')), 128.22 (C(Ar)), 129.65 (2 x C(Ar)), 131.29 (C(Ar)), 144.50 (C(Ar)), 148.04 (C(Ar)), 149.90 (C(Ar)), 155.47 (C(Ar)), 161.20 (C(Ar)), 172.00 (COOH).

ESI/MS m/z (%): 349 ($[\text{M}+\text{H}]^+$, 100).

Melting point: [242 – 245] °C.

Molecular weight: 348.35 g/mol.

Rf (DCM/EtOAc 5:5): 0.39.

2.2.4.8. Synthesis of 2-(3-(4-chlorophenyl)-5,9-dimethyl-7-oxo-7H-furo[3,2-g]chromen-6-yl)acetic acid (EMAC10164k)

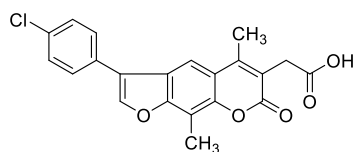


Figure 45. Structure of EMAC10164k.

The compound EMAC10164k (Figure 45) was obtained through the general procedure referred on the section 2.2.4. on the following conditions: EMAC10163k (0.35 g, 0.84 mmol), 4 mL of propan-2-ol and an aqueous solution of NaOH 1M (3.4 mL) were mixed and stirred for 4 h. After the filtration a light brown solid was obtained.

Yield: 67.9 %

^1H NMR (400 MHz, DMSO): δ = 2.51 (s, 3H, CH_3), 2.51 (s, 3H, CH_3), 3.65 (s, 2H, CH_2), 7.56 – 7.60 m, 2H, 2 x H(Ar), 7.81 – 7.84 (m, 2H, 2 x H(Ar')), 7.99 (s, 1H, H5), 8.51 (s, 1H, H7), 12.55 (s, 1H, COOH).

^{13}C NMR (100 MHz, DMSO): δ = 8.68 (CH_3), 16.12 (CH_3), 33.41 (CH_2), 109.10 (C(Ar)), 114.24 (C(Ar)), 117.22 (C(Ar)), 118.43 (C(Ar)), 120.94 (C(Ar)), 122.02 (C(Ar)), 129.36 (2 x C(Ar')), 129.61 (2 x C(Ar')), 130.20 (C(Ar)), 132.77 (C(Ar)), 144.95 (C(Ar)), 148.12 (C(Ar)), 149.99 (C(Ar)), 155.46 (C(Ar)), 161.16 (C(Ar)), 171.95 (COOH).

ESI/MS m/z (%): 383 ($[\text{M}+\text{H}]^+$, 32).

Melting point: [266 – 269] °C.

Molecular weight: 382.80 g/mol.

Rf (DCM/EtOAc 5:5): 0.11.

2.2.4.9. Synthesis of 2-(3-(3-methoxyphenyl)-5,9-dimethyl-7-oxo-7H-furo[3,2-g]chromen-6-yl)acetic acid (EMAC10164m)

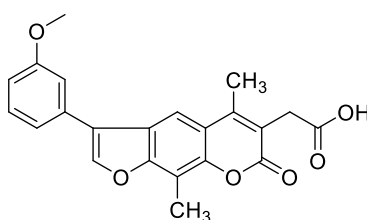


Figure 46. Structure of EMAC10164m.

The compound EMAC10164m (Figure 46) was obtained through the general procedure referred on the section 2.2.4. on the following conditions: EMAC 10163 m (0.50 g, 1.22 mmol), 5 mL of propan-2-ol and an aqueous solution of NaOH 1M (4.9 mL) were mixed and stirred for 4 h. After the filtration a light brown solid was obtained.

Yield: 91.7 %

^1H NMR (400 MHz, DMSO): δ = 2.51 (s, 3H, CH_3), 2.53 (s, 3H, CH_3), 3.65 (s, 2H, CH_2), 3.86 (s, 3H, OCH_3), 6.99 – 7.02 (m, 1H, H(Ar)), 7.30 (m, 1H, H6'), 7.37 – 7.39 (m, 1H, H(Ar)), 7.44 – 7.49 (m, 1H, H(Ar)), 8.01 (s, 1H, H5), 8.48 (s, 1H, H7).

^{13}C NMR (100 MHz, DMSO): δ = 8.69 (CH_3), 16.08 (CH_3), 33.42 (CH_2), 55.67 (OCH_3), 109.06 (C(Ar)), 112.99 (C(Ar)), 113.99 (C(Ar)), 114.29 (C(Ar)), 117.15 (C(Ar)), 118.39 (C(Ar)), 119.94 (C(Ar)), 121.99 (C(Ar)), 122.35 (C(Ar)), 130.79 (C(Ar)), 132.59 (C(Ar)), 144.77 (C(Ar)), 148.08 (C(Ar)), 149.96 (C(Ar)), 155.48 (C(Ar)), 160.28 (C(Ar)), 161.21 (C(Ar)), 171.97 (COOH).

ESI/MS m/z (%): 379 ($[\text{M}+\text{H}]^+$, 100).

Melting point: [220 – 224] °C.

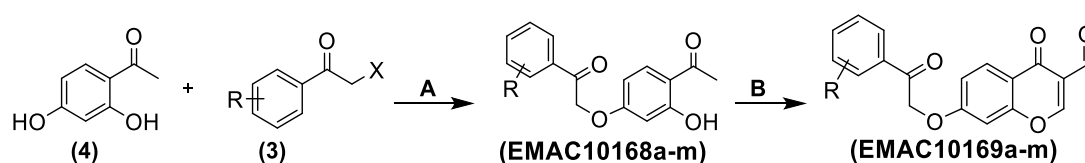
Molecular weight: 378.38 g/mol.

Rf (DCM/EtOAc 5:5): 0.41.

2.3. Synthesis of chromones

2.3.1. Synthetic pathway

Figure 47 represents the synthetic strategy in which 2,4-dihydroxyphenylethan-1-one (compound 4) and an α -haloketone with the desired substitution (compound 3) originate the compounds EMAC10168a-m through a Williamson reaction (reactional step A). These compounds were submitted to a POCl_3 -induced cyclization (reactional step B) to obtain the correspondent chromone (compounds EMAC10169a-m).



R= 4- CH_3 (a), 4- OCH_3 (b), 4-Br (c), 4-F (d), 4- NO_2 (e), 3- NO_2 (f), 4-Phenyl (g), 2,4-F (h), 2,4-Cl (i), 4-H (j), 4-Cl (k), 2-OH (l), 3- OCH_3 (m)

Figure 47. Schematic representation of the synthetic pathway used for the obtention of the chromone family. Reaction conditions: (A) acetone, K_2CO_3 , α -haloketone, reflux, 3 – 6 h; (B) POCl_3 , DMF, $-10\text{ }^\circ\text{C}$ (1 h), room temperature (3 – 6 days).

2.3.2. Synthesis of the phenylethanone compounds (EMAC10168 series)

General procedure: To a mixture of 2',4'-dihydroxyacetophenone (1 mmol) and acetone was added K_2CO_3 (2.5 mmol), this mixture was kept stirring at $40\text{ }^\circ\text{C}$ for 30 min. The appropriate α -haloketone (1.1 mmol) was added. The reaction mixture was heated to reflux and stirred. After the completion of the reaction, followed by TLC, the mixture was poured into a solution of H_2SO_4 0.5M and the resulting precipitate was filtered. The solid was purified by chromatographic column and the resulting fractions were evaporated and recrystallized to obtain the desired compound.

2.3.2.1. Synthesis of 2-(4-acetyl-3-hydroxyphenoxy)-1-(p-tolyl)ethan-1-one (EMAC10168a)

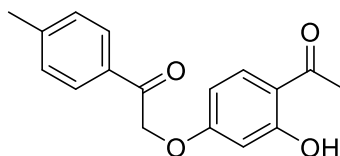


Figure 48. Structure of EMAC10168a.

The compound EMAC10168a (Figure 48) was obtained through the general procedure referred on the section 2.3.2. on the following conditions: 2',4'-dihydroxyacetophenone (1.01 g, 6.64 mmol), acetone (20 mL) and K_2CO_3 (2.27 g, 16.4 mmol) were mixed and 2-bromo-4'-methylacetophenone (1.55 g, 7.27 mmol) was added. The reaction was stirred for 4 h. Afterward, the mixture was poured into 100 mL of H_2SO_4 0.5M. For the purification by chromatographic column DCM was used as eluent. The resulting fractions were recrystallized from DCM/*n*-hexane giving a white solid.

Yield: 72.6 %

1H NMR (400 MHz, $CDCl_3$): δ = 2.44 (s, 3H, CH_3), 2.55 (s, 3H, $COCH_3$), 5.30 (s, 2H, CH_2), 6.39 (d, J = 2.5 Hz, 1H, H3), 6.54 (dd, J = 8.9, 2.6 Hz, 1H, H5), 7.29 – 7.32 (m, 2H, 2 x H(Ar)), 7.65 (d, J = 8.9 Hz, 1H, H6), 7.86 – 7.88 (m, 2H, 2 x H(Ar')), 12.68 (s, 1H, OH).

^{13}C NMR (100 MHz, $CDCl_3$): δ = : 21.80 (CH_3), 26.27 ($COCH_3$), 70.27 (CH_2), 101.84 (C(Ar)), 107.92 (C(Ar)), 114.54 (C(Ar)), 128.12 (2 x C(Ar')), 129.65 (2 x C(Ar')), 131.75 (C(Ar)), 132.52 (C(Ar)), 145.22 (C(Ar)), 164.37 (C(Ar)), 165.05 (C(Ar)), 192.58 (CO), 202.70 ($COCH_3$).

Melting point: [147 – 149] °C.

Molecular weight: 284.31 g/mol.

R_f (DCM/EtOAc 5:5): 0.39.

2.3.2.2. Synthesis of 2-(4-acetyl-3-hydroxyphenoxy)-1-(4-methoxyphenyl)ethan-1-one (EMAC10168b)

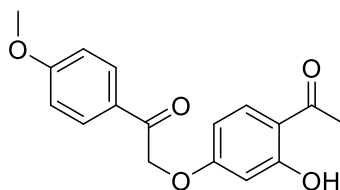


Figure 49. Structure of EMAC10168b.

The compound EMAC10168b (Figure 49) was obtained through the general procedure referred on the section 2.3.2. on the following conditions: 2',4'-dihydroxyacetophenone (0.52 g, 3.40 mmol), acetone (10 mL) and K₂CO₃ (1.14 g, 8.22 mmol) were mixed, and 2-bromo-4'-methoxyacetophenone (0.82 g, 3.61 mmol) was added. The reaction mixture was stirred for 5 h. Afterward, the mixture was poured into 50 mL of H₂SO₄ 0. The precipitate was purified by recrystallization from DCM/*n*-hexane giving a dark white solid.

Yield: 97.1 %

¹H NMR (400 MHz, CDCl₃): δ = 2.55 (s, 3H, CH₃), 3.89 (s, 3H, OCH₃), 5.27 (s, 2H, CH₂), 6.39 (d, *J* = 2.5 Hz, 1H, H3), 6.53 (dd, *J* = 8.9, 2.6 Hz, 1H, H5), 6.96 – 6.99 (m, 2H, 2 x H(Ar')), 7.65 (d, *J* = 8.9 Hz, 1H, H6), 7.94 – 7.98 (m, 2H, 2 x H(Ar')), 12.68 (s, 1H, OH).

¹³C NMR (100 MHz, CDCl₃): δ = : 26.27 (CH₃), 55.58 (OCH₃), 70.22 (CH₂), 101.87 (C(Ar)), 107.89 (C(Ar)), 114.17 (2 x C(Ar')), 114.53 (C(Ar)), 127.27 (C(Ar)), 130.42 (2 x C(Ar')), 132.52 (C(Ar)), 164.28 (C(Ar)), 164.42 (C(Ar)), 165.05 (C(Ar)), 191.49 (C=O), 202.69 (C=OCH₃).

Melting point: [127 – 129] °C.

Molecular weight: 300.31 g/mol.

R_f (DCM/EtOAc 5:5): 0.55.

2.3.2.3. Synthesis of 2-(4-acetyl-3-hydroxyphenoxy)-1-(4-bromophenyl)ethan-1-one (EMAC10168c)

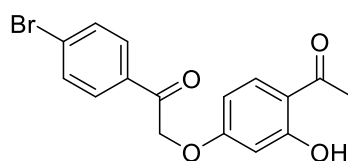


Figure 50. Structure of EMAC10168c.

The compound EMAC10168c (Figure 50) was obtained through the general procedure referred on the section 2.3.2. on the following conditions: 2',4'-dihydroxyacetophenone (1.00 g, 6.58 mmol), acetone (20 mL) and K₂CO₃ (2.27 g, 16.4 mmol) were mixed, and 2,4'-dibromoacetophenone (2.01 g, 7.24 mmol) was added. The reaction mixture was stirred for 4 h. Afterward, the mixture was poured into 100 mL of H₂SO₄ 0.5M. For the solid chromatographic column DCM was used as eluent. The resulting fractions were recrystallized from DCM/*n*-hexane giving a light-yellow solid.

Yield: 78.9 %

^1H NMR (400 MHz, CDCl_3): δ = 2.58 (s, 3H, COCH_3), 5.29 (s, 2H, CH_2), 6.40 (d, J = 2.5 Hz, 1H, H3), 6.54 (dd, J = 8.9, 2.6 Hz, 1H, H5), 7.66 – 7.69 (m, 3H, 3 x H(Ar)), 7.85 – 7.88 (m, 2H, 2 x H(Ar')), 12.70 (s, 1H, OH).

^{13}C NMR (100 MHz, CDCl_3): δ = : 26.30 (COCH_3), 70.35 (CH_2), 101.81 (C(Ar)), 107.81 (C(Ar)), 114.68 (C(Ar)), 129.50 (C(Ar)), 129.59 (2 x C(Ar')), 132.34 (2 x C(Ar')), 132.60 (C(Ar)), 132.92 (C(Ar)), 164.04 (C(Ar)), 165.03 (C(Ar)), 192.39 (CO), 202.74 (COCH_3).

Melting point: [124 – 125] °C.

Molecular weight: 349.18 g/mol.

Rf (DCM/EtOAc 5:5): 0.50.

2.3.2.4. Synthesis of 2-(4-acetyl-3-hydroxyphenoxy)-1-(4-fluorophenyl)ethan-1-one (EMAC10168d)

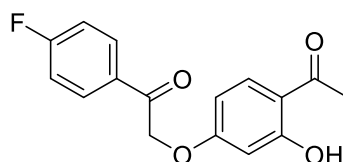


Figure 51. Structure of EMAC10168d.

The compound EMAC10168d (Figure 51) was obtained through the general procedure referred on the section 2.3.2. on the following conditions: 2',4'-dihydroxyacetophenone (1.00 g, 6.58 mmol), acetone (20 mL) and K_2CO_3 (2.28 g, 16.5 mmol) were mixed, and 2-bromo-4'-fluoroacetophenone (1.57 g, 7.24 mmol) was added. The reaction mixture was stirred for 5 h. Afterward, the mixture was poured into 100 mL of H_2SO_4 . For the chromatographic column DCM was used as eluent. The resulting fractions were recrystallized from DCM/*n*-hexane giving a white solid.

Yield 85.1 %

^1H NMR (400 MHz, CDCl_3): δ = 2.58 (s, 3H, COCH_3), 5.30 (s, 2H, CH_2), 6.40 (d, J = 2.6 Hz, 1H, H3), 6.55 (dd, J = 8.9, 2.6 Hz, 1H, H5), 7.18 – 7.24 (m, 2H, 2 x H(Ar')), 7.68 (d, J = 8.9 Hz, 1H, H6), 8.01 – 8.06 (m, 2H, 2 x H(Ar')), 12.70 (s, 1H, OH).

^{13}C NMR (100 MHz, CDCl_3): δ = : 26.28 (COCH_3), 70.33 (CH_2), 101.81 (C(Ar)), 107.83 (C(Ar)), 114.65 (C(Ar)), 116.23 (d, J_{CF} = 22.0 Hz, C3', C5'), 130.68 (d, J_{CF} = 3.1 Hz, C1'), 130.88 (d, J_{CF} = 9.5 Hz, C2', C6'), 132.58 (C(Ar)), 164.12 (C(Ar)), 165.01 (C(Ar)), 166.30 (d, J_{CF} = 254.0 Hz, C4'), 191.69 (CO), 202.73 (COCH_3).

Melting point: [124 – 126] °C.

Molecular weight: 288.27 g/mol.

R_f (DCM/EtOAc 5:5): 0.51.

2.3.2.5. Synthesis of 1-([1,1'-biphenyl]-4-yl)-2-(4-acetyl-3-hydroxyphenoxy)ethan-1-one (EMAC10168g)

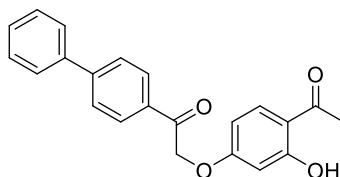


Figure 52. Structure of EMAC10168g.

The compound EMAC10168g (Figure 52) was obtained through the general procedure referred on the section 2.3.2. on the following conditions: 2',4'-dihydroxyacetophenone (0.50 g, 3.29 mmol), acetone (10 mL) and K₂CO₃ (1.14 g, 8.25 mmol) were mixed, and 2-bromo-1-(4-phenylphenyl)ethan-1-one (0.99 g, 3.60 mmol) was added. The reaction mixture was stirred for 6 h. Afterward, the mixture was poured into 50 mL of H₂SO₄ 0.5M. For the chromatographic column DCM was used as eluent. The resulting fractions were recrystallized from DCM/*n*-hexane giving a light orange solid.

Yield: 50.0 %

¹H NMR (400 MHz, CDCl₃): δ = 2.56 (s, 3H, OCH₃), 5.35 (s, 2H, CH₂), 6.42 (d, *J* = 2.5 Hz, 1H, H₃), 6.56 (dd, *J* = 8.9, 2.6 Hz, 1H, H₅), 7.40 – 7.45 (m, 1H, H(Ar)), 7.45 – 7.51 (m, 2H, 2 x H(Ar)), 7.61 – 7.66 (m, 3H, 3 x H(Ar)), 7.71 – 7.76 (m, 1H, H(Ar)), 8.02 – 8.08 (m, 2H, 2 x H(Ar)), 12.69 (s, 1H, OH).

¹³C NMR (100 MHz, CDCl₃): δ = : 26.28 (COCH₃), 70.41 (CH₂), 101.87 (C(Ar)), 107.91 (C(Ar)), 114.60 (C(Ar)), 127.31 (2 x (C(Ar))), 127.57 (2 x (C(Ar))), 128.54 (C(Ar)), 128.65 (2 x (C(Ar))), 129.05 (2 x (C(Ar))), 132.56 (C(Ar)), 132.88 (C(Ar)), 139.56 (C(Ar)), 146.89 (C(Ar)), 164.31 (C(Ar)), 165.07 (C(Ar)), 192.63 (C=O), 202.71 (C=OCH₃).

Melting point: [142 – 145] °C.

Molecular weight: 346.38 g/mol.

R_f (DCM/EtOAc 5:5): 0.55.

2.3.2.6. Synthesis of 2-(4-acetyl-3-hydroxyphenoxy)-1-(4-chlorophenyl)ethan-1-one (EMAC10168k)

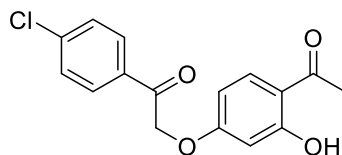


Figure 53. Structure of EMAC10168k.

The compound EMAC10168k (Figure 53) was obtained through the general procedure referred on the section 2.3.2. on the following conditions: 2',4'-dihydroxyacetophenone (0.50 g, 3.30 mmol), acetone (10 mL) and K_2CO_3 (1.14 g, 8.28 mmol) were mixed, and 2-bromo-4'-chloroacetophenone (0.84 g, 3.61 mmol) was added. The reaction mixture was stirred for 3 h. Afterward, the mixture was poured into 50 mL of H_2SO_4 0.5M. For the chromatographic column DCM was used as eluent. The resulting fractions were recrystallized from DCM/*n*-hexane giving a light-yellow solid.

Yield: 65.3 %

1H NMR (400 MHz, $CDCl_3$): δ = 2.58 (s, 3H, $COCH_3$), 5.29 (s, 2H, CH_2), 6.40 (d, J = 2.6 Hz, 1H, H3), 6.54 (dd, J = 8.9, 2.6 Hz, 1H, H5), 7.49 – 7.53 (m, 2H, 2 x H(Ar')), 7.68 (d, J = 8.9 Hz, 1H, H6), 8.93 – 8.96 (m, 2H, 2 x H(Ar')), 12.70 (s, 1H, OH).

^{13}C NMR (100 MHz, $CDCl_3$): δ = : 26.29 ($COCH_3$), 70.37 (CH_2), 101.81 (C(Ar)), 107.81 (C(Ar)), 114.67 (C(Ar)), 129.34 (2 x (C(Ar'))), 129.53 (2 x (C(Ar'))), 132.59 (C(Ar)), 132.59 (C(Ar)), 140.73 (C(Ar)), 164.06 (C(Ar)), 165.04 (C(Ar)), 192.16 (CO), 202.73 ($COCH_3$).

Melting point: [112 – 114] °C.

Molecular weight: 304.73 g/mol.

R_f (DCM/EtOAc 5:5): 0.57.

2.3.2.7. Synthesis of 2-(4-acetyl-3-hydroxyphenoxy)-1-(3-methoxyphenyl)ethan-1-one (EMAC10168m)

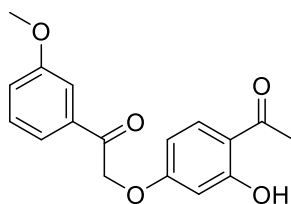


Figure 54. Structure of EMAC10168m.

The compound EMAC10168m (Figure 54) was obtained through the general procedure referred on the section 2.3.2. on the following conditions: 2',4'-dihydroxyacetophenone (1.00 g, 6.60 mmol), acetone (20 mL) and K₂CO₃ (2.28 g, 16.5 mmol) were mixed, and 2-bromo-3'-methoxyacetophenone (1.66 g, 7.27 mmol) was added. The reaction mixture was stirred for 5 h. Afterward, the mixture was poured into 100 mL of H₂SO₄ 0.5M. For the chromatographic column DCM was used as eluent. The resulting fractions were recrystallized from DCM/*n*-hexane giving a white solid.

Yield: 82.4 %

¹H NMR (400 MHz, CDCl₃): δ = 2.55 (s, 3H, CH₃), 3.87 (s, 3H, CH₃), 5.32 (s, 2H, CH₂), 6.38 (d, *J* = 2.5 Hz, 1H, H₃), 6.54 (dd, *J* = 8.9, 2.6 Hz, 1H, H₅), 7.16 – 7.19 (m, 1H, H(Ar')), 7.40 – 7.44 (m, 1H, H(Ar')), 7.49 – 7.50 (m, 1H, H(Ar')), 7.52 – 7.55 (m, 1H, H(Ar')), 7.65 (d, *J* = 8.9 Hz, 1H, H₆), 12.69 (s, 1H, OH).

¹³C NMR (100 MHz, CDCl₃): δ = : 26.28 (CH₃), 55.54 (CH₃), 70.35 (CH₂), 101.81 (C(Ar)), 107.90 (C(Ar)), 112.35 (C(Ar)), 114.58 (C(Ar)), 120.38 (C(Ar)), 120.66 (C(Ar)), 129.98 (C(Ar)), 132.54 (C(Ar)), 135.48 (C(Ar)), 160.09 (C(Ar)), 164.29 (C(Ar)), 165.04 (C(Ar)), 192.80 (C=O), 202.71 (C=OCH₃).

Melting point: [100 – 101] °C.

Molecular weight: 300.31 g/mol.

R_f (DCM/EtOAc 5:5): 0.42.

2.3.3. Synthesis of the 4H-chromene compounds (EMAC10169 series)

General procedure: In a vial, DMF was added to POCl₃ (2 mmol) at -10 °C and the mixture stayed with stirring for 10 min. EMAC10168a-m (1 mmol) dissolved in DMF was added to the previous mixture at -10 °C and kept stirring for 1 hour. After that time the reaction was kept at room temperature and controlled with TLC until completion. After finishing, the mixture was extracted with ethyl acetate. The combined organic layers were dried with anhydrous sodium sulphate, filtered and the solvent evaporated. The compound was purified by chromatographic column and the fractions with the desired compound were collected, evaporated, and recrystallized.

2.3.3.1. Synthesis of 4-oxo-7-(2-oxo-2-(*p*-tolyl)ethoxy)-4*H*-chromene-3-carbaldehyde (EMAC10169a)

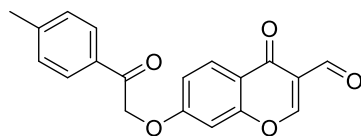


Figure 55. Structure of EMAC10169a.

The compound EMAC10169a (Figure 55) was obtained through the general procedure referred on the section 2.3.3. on the following conditions: 6 mL of DMF were added to POCl₃ (650 μL, 6.97 mmol). EMAC10168a (1.00 g, 3.51 mmol) dissolved in another 6 mL of DMF was added to the previous mixture. The reaction finished 6 days later, and the eluent used on the chromatographic column was DCM/EtOAc 88:12 to 100% of EtOAc. The fractions collected were recrystallized from DCM/*n*-hexane giving a light-yellow solid.

Yield: 22.3 %

¹H NMR (400 MHz, CDCl₃): δ = 2.45 (s, 3H, CH₃), 5.42 (s, 2H, CH₂), 6.91 (*d*, *J* = 2.4 Hz, 1H, H₈), 7.10 (*dd*, *J* = 8.9, 2.4 Hz, 1H, H₆), 7.32 – 7.34 (*m*, 2H, 2 x H(Ar')), 7.88 – 7.91 (*m*, 2H, 2 x H(Ar')), 8.21 (*d*, *J* = 8.9 Hz, 1H, H₅), 8.45 (s, 1H, H₂), 10.36 (s, 1H, CHO).

¹³C NMR (100 MHz, CDCl₃): δ = 21.84 (CH₃), 70.65 (CH₂), 102.50 (C(Ar)), 115.55 (C(Ar)), 119.51 (C(Ar)), 120.30 (C(Ar)), 127.83 (C(Ar)), 128.15 (2 x (C(Ar'))), 129.77 (2 x (C(Ar'))), 131.53 (C(Ar)), 145.57 (C(Ar)), 157.73 (C(Ar)), 160.27 (C(Ar)), 175.20 (C(Ar)), 188.78 (CHO), 192.24 (CO).

ESI/MS *m/z* (%): 323 ([M+H]⁺, 100).

Melting point: [159 – 161] °C.

Molecular weight: 322.32 g/mol.

R_f (DCM/EtOAc 5:5): 0.82.

2.3.3.2. Synthesis of 7-(2-(4-methoxyphenyl)-2-oxoethoxy)-4-oxo-4H-chromene-3-carbaldehyde (EMAC10169b)

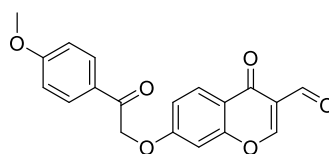


Figure 56. Structure of EMAC10169b.

The compound EMAC10169b (Figure 56) was obtained through the general procedure referred on the section 2.3.3. on the following conditions: 3 mL of DMF were added to POCl₃ (310 μL, 3.33 mmol). EMAC10168b (0.50 g, 1.66 mmol) dissolved in another 3 mL of DMF was added to the previous mixture. The reaction finished 72 h later and the eluent used on the chromatographic column was DCM/EtOAc 88:12 to 100% of EtOAc. The fractions collected were recrystallized from DCM/*n*-hexane giving a light-yellow solid.

Yield: 34.5 %

¹H NMR (400 MHz, CDCl₃): δ = 3.90 (s, 3H, OCH₃), 5.39 (s, 2H, CH₂), 6.91 (d, *J* = 2.4 Hz, 1H, H8), 6.97 – 7.01 (m, 2H, 2 x H(Ar')), 7.10 (dd, *J* = 8.9, 2.4 Hz, 1H, H6), 7.96 – 8.00 (m, 2H, 2 x H(Ar')), 8.20 (d, *J* = 8.9 Hz, 1H, H5), 8.44 (s, 1H, H2), 10.36 (s, 1H, CHO).

¹³C NMR (100 MHz, CDCl₃): δ = 55.63 (OCH₃), 70.58 (CH₂), 102.49 (C(Ar)), 114.29 (2 x C(Ar')), 115.58 (C(Ar')), 119.47 (C(Ar)), 120.28 (C(Ar)), 127.00 (C(Ar)), 127.79 (C(Ar)), 130.46 (2 x C(Ar')), 157.73 (C(Ar)), 160.28 (C(Ar)), 163.32 (C(Ar)), 164.49 (C(Ar)), 175.19 (C(Ar)), 188.78 (CHO), 191.14 (CO).

ESI/MS *m/z* (%): 379 ([M+H]⁺, 100).

Melting point: [160 – 162] °C.

Molecular weight: 338.32 g/mol.

R_f (DCM/EtOAc 5:5): 0.65.

2.3.3.3. Synthesis of 7-(2-(4-bromophenyl)-2-oxoethoxy)-4-oxo-4H-chromene-3-carbaldehyde (EMAC10169c)

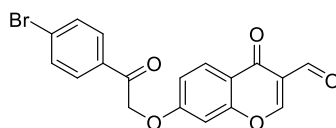


Figure 57. Structure of EMAC10169c.

The compound EMAC10169c (Figure 57) was obtained through the general procedure referred on the section 2.3.3. on the following conditions: 3 mL of DMF were added to POCl₃ (270 μ L, 2.90 mmol). EMAC10168c (0.50 g, 1.43 mmol) dissolved in another 3 mL of DMF was added to the previous mixture. The reaction finished 6 days later, and the eluent used on the chromatographic column was DCM/EtOAc 88:12 to 100% of EtOAc. The fractions collected were recrystallized from DCM/*n*-hexane giving a yellow solid.

Yield: 36.1 %

¹H NMR (400 MHz, DMSO): δ = 5.81 (s, 2H, CH₂), 7.24 (dd, *J* = 8.9, 2.4 Hz, 1H, H₆), 7.39 (d, *J* = 2.4 Hz, 1H, H₈), 7.81 – 7.83 (m, 2H, 2 x H(Ar')), 7.96 – 7.98 (m, 2H, 2 x H(Ar')), 8.06 (d, *J* = 8.9 Hz, 1H, H₅), 8.85 (s, 1H, H₂), 10.11 (s, 1H, CHO).

¹³C NMR (100 MHz, DMSO): δ = 71.30 (CH₂), 103.16 (C(Ar)), 116.32 (C(Ar)), 118.94 (C(Ar)), 120.34 (C(Ar)), 127.23 (C(Ar)), 128.53 (C(Ar)), 130.42 (2 x C(Ar')), 132.37 (2 x C(Ar')), 133.62 (C(Ar)), 157.79 (C(Ar)), 163.60 (C(Ar)), 163.65 (C(Ar)), 174.59 (C(Ar)), 189.01 (CHO), 193.24 (CO).

ESI/MS *m/z* (%): 386 ([M+H]⁺, 100).

Melting point: [191 – 194] °C.

Molecular weight: 387.19 g/mol.

R_f (DCM/EtOAc 5:5): 0.80.

2.3.3.4. Synthesis of 7-(2-(4-fluorophenyl)-2-oxoethoxy)-4-oxo-4H-chromene-3-carbaldehyde (EMAC10169d)

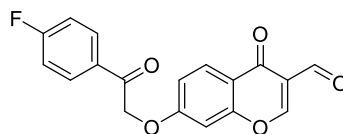


Figure 58. Structure of EMAC10169d.

The compound EMAC10169d (Figure 58) was obtained through the general procedure referred on the section 2.3.3. on the following conditions: 6 mL of DMF were added to POCl₃ (650 μ L, 6.97 mmol). EMAC10168d (1.00 g, 3.48 mmol) dissolved in another 6 mL of DMF was added to the previous mixture. The reaction finished 4 days later, and the eluent used on the chromatographic column was DCM/EtOAc 88:12 to 100% of EtOAc. The fractions collected were recrystallized from DCM/*n*-hexane giving a light-orange solid.

Yield: 25.3 %

¹H NMR (400 MHz, DMSO): δ = 5.82 (s, 2H, CH₂), 7.24 (dd, *J* = 8.9, 2.4 Hz, 1H, H₆), 7.38 (d, *J* = 2.4 Hz, 1H, H₈), 7.41 – 7.46 (m, 2H, 2 x H(Ar')), 8.06 (d, *J* = 8.9 Hz, 1H, H₅), 8.11 – 8.15 (m, 2H, 2 x H(Ar')), 8.85 (s, 1H, H₂), 10.12 (s, 1H, CHO).

¹³C NMR (100 MHz, DMSO): δ = 71.25 (CH₂), 103.15 (C(Ar)), 116.29 (C(Ar)), 116.41 (d, *J*_{CF} = 18.7 Hz, C3', C5'), 118.92 (C(Ar)), 120.34 (C(Ar)), 127.22 (C(Ar)), 131.40 (d, *J*_{CF} = 2.8 Hz, C1'), 131.51 (d, *J*_{CF} = 9.6 Hz, C2', C6'), 157.80 (C(Ar)), 163.59 (C(Ar)), 163.70 (C(Ar)), 165.90 (d, *J*_{CF} = 252.6 Hz, C4'), 189.02 (CHO), 192.56 (CO).

ESI/MS *m/z* (%): 327 ([M+H]⁺, 100).

Melting point: [199 – 202] °C.

Molecular weight: 326.28 g/mol.

R_f (DCM/EtOAc 5:5): 0.77.

2.3.3.5. Synthesis of 7-(2-([1,1'-biphenyl]-4-yl)-2-oxoethoxy)-4-oxo-4H-chromene-3-carbaldehyde (EMAC10169g)

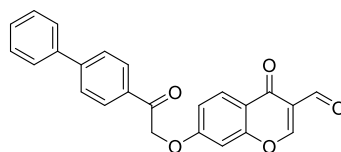


Figure 59. Structure of EMAC10169g.

The compound EMAC10169g (Figure 59) was obtained through the general procedure referred on the section 2.3.3. on the following conditions: 3 mL of DMF were added to POCl₃ (270 μ L, 2.89 mmol). EMAC10168g (0.50 g, 1.45 mmol) dissolved in another 3 mL of DMF was added to the previous mixture. The reaction finished 4 days later, and the eluent used for the chromatographic column was DCM/EtOAc 88:12 to 100% of EtOAc. The fractions collected were recrystallized from DCM/*n*-hexane giving a light-yellow solid.

Yield: 17.4 %

¹H NMR (400 MHz, CDCl₃): δ = 5.47 (s, 2H, CH₂), 6.94 (d, *J* = 2.4 Hz, 1H, H₈), 7.13 (dd, *J* = 8.9, 2.4 Hz, 1H, H₆), 7.42 – 7.46 (m, 1H, H(Ar)), 7.47 – 7.52 (m, 2H, 2 x H(Ar)), 7.63 – 7.66 (m, 2H, 2 x H(Ar)), 7.74 – 7.77 (m, 2H, 2 x H(Ar)), 8.06 – 8.09 (m, 2H, 2 x H(Ar)), 8.23 (d, *J* = 8.9 Hz, 1H, H₅), 8.46 (s, 1H, H₂), 10.37 (s, 1H, CHO).

¹³C NMR (100 MHz, CDCl₃): δ = 70.79 (CH₂), 102.55 (C(Ar)), 115.54 (C(Ar)), 119.61 (C(Ar)), 120.33 (C(Ar)), 127.31 (2 x C(Ar)), 127.69 (2 x C(Ar)), 127.91 (C(Ar)), 128.68 (C(Ar)), 128.68 (2 x C(Ar)), 129.11 (2 x C(Ar)), 132.64 (C(Ar)), 139.45 (C(Ar)), 147.20 (C(Ar)), 157.75 (C(Ar)), 160.27 (C(Ar)), 163.21 (C(Ar)), 175.21 (C(Ar)), 188.77 (CHO), 192.28 (CO).

ESI/MS *m/z* (%): 385 ([M+H]⁺, 100).

Melting point: [189 – 192] °C.

Molecular weight: 384.39 g/mol.

R_f (DCM/EtOAc 5:5): 0.94.

2.3.3.6. Synthesis of 7-(2-(4-chlorophenyl)-2-oxoethoxy)-4-oxo-4H-chromene-3-carbaldehyde (EMAC10169k)

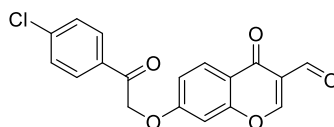


Figure 60. Structure of EMAC10169k.

The compound EMAC10169k (Figure 60) was obtained through the general procedure referred on the section 2.3.3. on the following conditions: 3 mL of DMF were added to POCl₃ (310 μL, 3.31 mmol). EMAC10168k (0.50 g, 1.64 mmol) dissolved in another 3 mL of DMF was added to the previous mixture. The reaction finished 6 days later, and the eluent used for the chromatographic column was DCM/AcOEt 88:12 to 100% of AcOEt. The fractions collected were recrystallized from DCM/*n*-hexane giving a light-yellow solid.

Yield: 23.0 %

¹H NMR (400 MHz, CDCl₃): δ = 5.39 (s, 2H, CH₂), 6.92 (d, *J* = 2.4 Hz, 1H, H8), 7.09 (dd, *J* = 8.9, 2.4 Hz, 1H, H6), 7.50 – 7.53 (m, 2H, 2 x H(Ar)), 7.93 – 7.96 (m, 2H, 2 x H(Ar)), 8.22 (d, *J* = 8.9 Hz, 1H, H5), 8.45 (s, 1H, H2), 10.36 (s, 1H, CHO).

¹³C NMR (100 MHz, CDCl₃): δ = 70.72 (CH₂), 102.54 (C8), 115.43 (C6), 119.70 (C(Ar)), 120.34 (C(Ar)), 127.96 (C5), 129.48 (2 x C(Ar)), 129.53 (2 x C(Ar)), 132.30 (C(Ar)), 141.06 (C(Ar)), 157.71 (C(Ar)), 160.30 (C2), 162.98 (C(Ar)), 175.15 (C(Ar)), 188.71 (CHO), 191.76 (CO).

ESI/MS *m/z* (%): 343 ([M+H]⁺, 100).

Melting point: [171 – 173] °C.

Molecular weight: 342.73 g/mol.

R_f (DCM/EtOAc 5:5): 0.83.

2.3.3.7. Synthesis of 7-(2-(3-methoxyphenyl)-2-oxoethoxy)-4-oxo-4H-chromene-3-carbaldehyde (EMAC10169m)

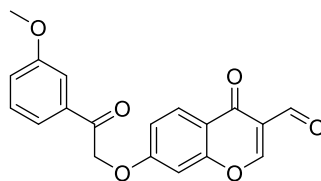


Figure 61. Structure of EMAC10169m.

The compound EMAC10169m (Figure 61) was obtained through the general procedure referred on the section 2.3.3. on the following conditions: 3 mL of DMF were added to POCl₃ (310 μ L, 3.32 mmol). EMAC10168m (0.50 g, 1.66 mmol) dissolved in another 3 mL of DMF was added to the previous mixture. The reaction finished 4 days later, and the eluent used for the chromatographic column was DCM/AcOEt 88:12 to 100% of AcOEt. The fractions were collected and recrystallized from DCM/*n*-hexane giving a light-yellow solid.

Yield: 26.0 %

¹H NMR (400 MHz, CDCl₃): δ = 3.88 (s, 3H, OCH₃), 5.43 (s, 2H, CH₂), 6.91 (d, *J* = 2.4 Hz, 1H, H8), 7.10 (dd, *J* = 8.9, 2.4 Hz, 1H, H6), 7.19 – 7.22 (*m*, 1H, H(Ar')), 7.42 – 7.46 (*m*, 1H, H(Ar')), 7.51 – 7.52 (*m*, 1H, H(Ar')), 7.55 – 7.57 (*m*, 1H, H(Ar')), 8.22 (d, *J* = 8.9 Hz, 1H, H5), 8.45 (s, 1H, H2), 10.37 (s, 1H, CHO).

¹³C NMR (100 MHz, CDCl₃): δ = 55.57 (OCH₃), 70.73 (CH₂), 102.52 (C(Ar)), 112.48 (C(Ar)), 115.52 (C(Ar)), 119.58 (C(Ar)), 120.32 (C(Ar)), 120.36 (C(Ar)), 120.80 (C(Ar)), 127.88 (C(Ar)), 130.10 (C(Ar)), 135.25 (C(Ar)), 157.73 (C(Ar)), 160.19 (C(Ar)), 160.28 (C(Ar)), 163.19 (C(Ar)), 175.20 (C(Ar)), 188.77 (CHO), 192.47 (CO).

ESI/MS *m/z* (%): 339 ([M+H]⁺, 100).

Melting point: [156 – 157] °C.

Molecular weight: 338.32 g/mol.

R_f (DCM/EtOAc 5:5): 0.82.

2.4. Carbonic anhydrase inhibition assay

The CA catalyzed CO₂ hydration/inhibition was measured by using a stopped-flow instrument as the method previously described [287]. Initial rates of the CA-catalyzed CO₂ hydration reaction were followed for 10 – 100 s. The CO₂ concentrations were ranged from 1.7 to 17 mM for the determination of the inhibition constants. For each inhibitor, at least six traces of the initial 5 – 10 % of the reaction were used for assessing the initial velocity. The uncatalyzed rates were subtracted from the total observed rates. Stock solutions of inhibitors (10 mM) and dilutions up to 0.01 nM were prepared in distilled-deionized water. Inhibitor and enzyme solutions were preincubated together for 15 min at room temperature prior to assay, in order to allow for the formation of the E – I complex. The inhibition constants were obtained by non-linear least-squares methods using PRISM 3 as reported earlier and represent the mean from at least three different determinations. *hCA I*, *hCA II*, *hCA IX*, and *hCA XII* (catalytic domain) were recombinant proteins produced inhouse using our standardized protocol and their concentration in the assay system was in the range of 3 – 10 nM. AAZ was used as reference CAI [251, 252, 288].

2.5. Binding DB and Pipeline Pilot as chemoinformatic tools for data search and mining

Data search, which results were included in section 1.3, was performed as follows.

Using Binding DB platform (www.bindingdb.org) [241], a chemical structure search was made with the coumarin structure, substructure search type and activity filter as shown in Figure 62. The same was made with the chromone structure.

The screenshot shows the Binding Database interface. The search type is 'Substructure' with a similarity filter of 0.85. The activity filter is set to 'none' for ΔG° (kcal/mol). The molecular weight filter is also set to 'none'. The search button is visible.

Figure 62. Screenshot from Binding DB regarding chemical structure search of coumarin by substructure type and activity filters.

The search gave 5707 entries for coumarin and 5051 for chromone, without filtering (Figure 63).

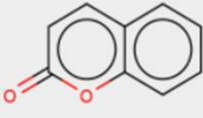
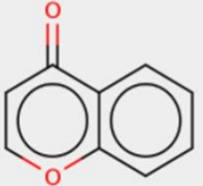
A Results of multiple-compound chemical search		B Results of multiple-compound chemical search	
Query Compound	Compounds Found	Query Compound	Compounds Found
All queried compounds (Merged results)	5707	All queried compounds (Merged results)	5051
	5707(without filtering)		5051(without filtering)
<chem>O=C1OC2=C(C=CC=C2)C=C1</chem>		<chem>O=C1C=COC2=C1C=CC=C2</chem>	

Figure 63. Screenshot showing the results, without filtering, for substructure search in Binding DB: (A) coumarin; (B) chromone.

Accessing these results, we were able to see the entries with filtering, in table format, as shown in Figure 64.

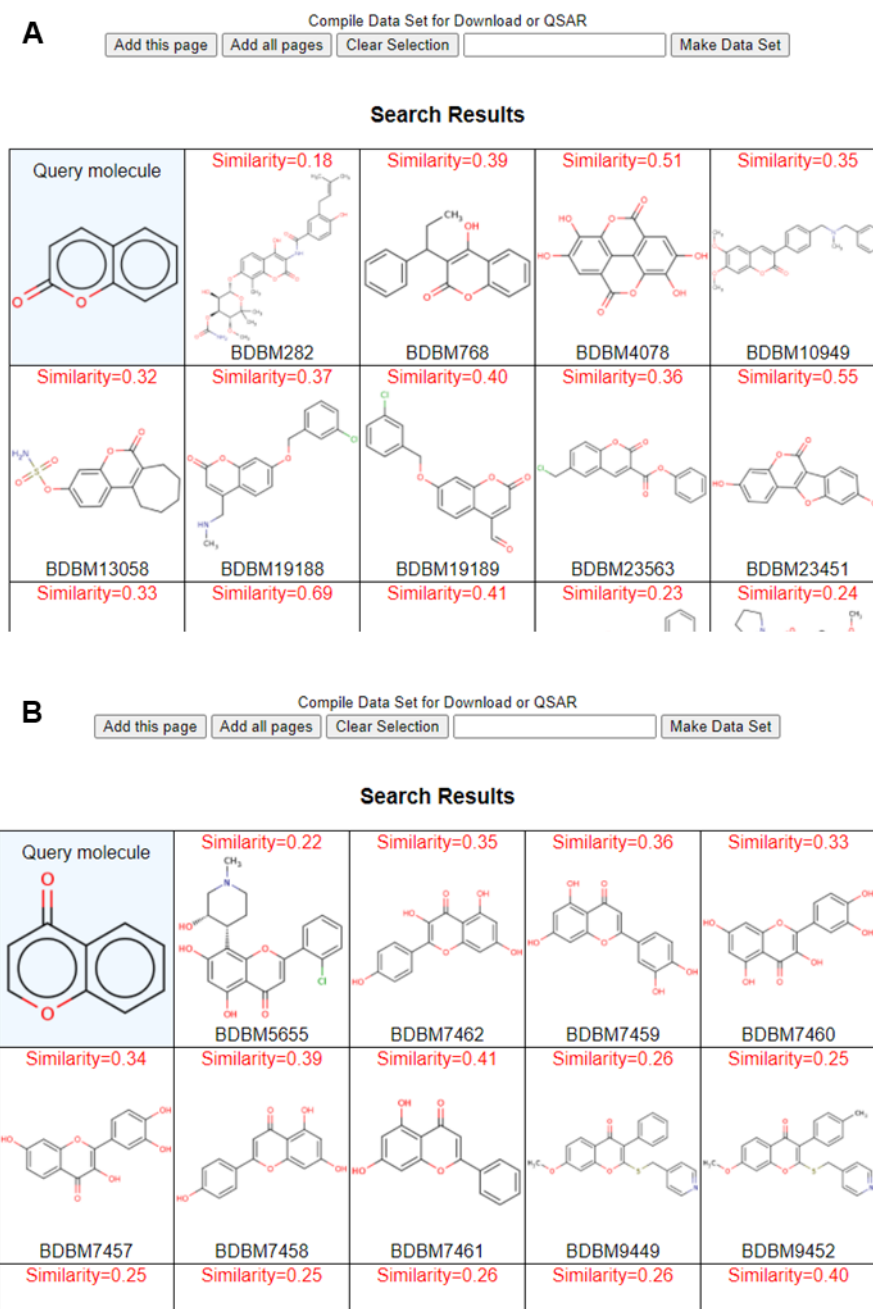
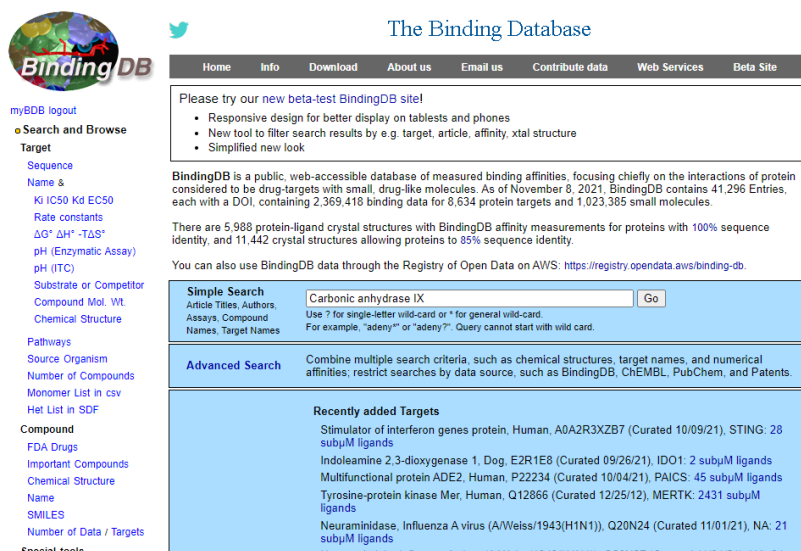


Figure 64. Screenshot of Binding DB search results, with filtering, for: (A) coumarin; (B) chromone.

Afterwards all pages were added, and a Data Set was made, opened in Maestro, seen in table and this table was exported in text format, in order to be opened in excel. In excel the data was organized by activity and also by target and a bibliographic research was made based on these search entries from Binding DB.

Another data search was performed using Binding DB and Pipeline Pilot [289]. Firstly, a simple search was made in Binding DB (Figure 65). This search was made for carbonic

anhydrase IX and carbonic anhydrase XII, separately and without substructure restriction. For CA IX we obtained 6248 hits and for CA XII 4758 hits, as shown in Figure 66. All the pages were added, and a data set was made for each isoform.



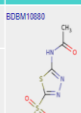


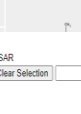
The screenshot shows the BindingDB website interface. At the top, there is a navigation bar with links: Home, Info, Download, About us, Email us, Contribute data, Web Services, and Beta Site. Below this is a search bar with the text 'Carbonic anhydrase IX' and a 'Go' button. To the left of the search bar is a sidebar with various search options: Target, Sequence, Name & Ki, IC50, Kd, EC50, Rate constants, ΔG° , ΔH° , $-\Delta S^\circ$, pH (Enzymatic Assay), pH (ITC), Substrate or Competitor, Compound Mol. Wt., Chemical Structure, Pathways, Source Organism, Number of Compounds, Monomer List in csv, Hat List in SDF, Compound, FDA Drugs, Important Compounds, Chemical Structure, Name, SMILES, Number of Data / Targets, and Special tools. Below the search bar, there is a 'Simple Search' section with a text input field containing 'Carbonic anhydrase IX' and a 'Go' button. Below that is an 'Advanced Search' section with a text input field and a 'Go' button. At the bottom, there is a 'Recently added Targets' section listing several targets with their respective ligands and assay descriptions.

Figure 65. Screenshot of the simple search page in Binding DB.

Compile Data Set for Download or QSAR

Add this page | Add all pages | Clear Selection | Make Data Set

Found 6248 hits

Target/Host (Institution)	Ligand	Target/Host Links	Ligand Links	Trig + Lig Links	Ki off	ΔG° kcal/mol	IC50 off	Kd off	EC50 off	K_{cat} s ⁻¹	K_m μ M	pH	Temp °C
Carbonic anhydrases, II & IX (Homo sapiens (Human))	 EDBM10800	PDB MMDB NCI pathway Reactome pathway KEGG	Purchase CHEBI ChEMBL DrugBank KEGG		0.0600	n/a	n/a	n/a	n/a	n/a	n/a	n/a	n/a
Universitè degli Studi di Firenze Curated by ChEMBL	 NCA1A241 (AZ1) acetazolamide / Acetazolamide, AZ1	DrugBank antibodypedia GoogleScholar	Patents Similar										
Carbonic anhydrases, II & IX (Homo sapiens (Human))	 EDBM50515336	PDB MMDB NCI pathway Reactome pathway KEGG	PC cid PC icd PC sid UniProtKB/SwissProt UniProtKB/EMBL UniChem	Article PubMed	0.0600	n/a	n/a	n/a	n/a	n/a	n/a	n/a	n/a
Saint Petersburg State University Curated by ChEMBL	 CHEMBL450220	DrugBank antibodypedia GoogleScholar	Patents Similar										
Carbonic anhydrase 9 (Homo sapiens (Human))	EDBM50153970	PDB MMDB NCI pathway			0.120	n/a	n/a	n/a	n/a	n/a	n/a	n/a	n/a

Compile Data Set for Download or QSAR

Add this page | Add all pages | Clear Selection | Make Data Set

Found 4758 hits

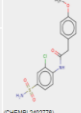
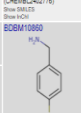
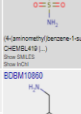
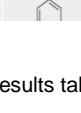

Target/Host (Institution)	Ligand	Target/Host Links	Ligand Links	Trig + Lig Links	Ki off	ΔG° kcal/mol	IC50 off	Kd off	EC50 off	K_{cat} s ⁻¹	K_m μ M	pH	Temp °C
Carbonic anhydrase (Homo sapiens (Human))	 EDBM50402450	PDB MMDB Reactome pathway KEGG	PC cid PC icd PC sid UniProtKB/SwissProt UniChem	Article PubMed	0.240	n/a	n/a	n/a	n/a	n/a	n/a	n/a	n/a
Bezmalek Valid University Curated by ChEMBL	 CHEMBL242776	DrugBank antibodypedia GoogleScholar	Patents Similar										
Carbonic anhydrase 12 (Homo sapiens (Human))	 EDBM10880	PDB MMDB Reactome pathway KEGG	Purchase CHEBI ChEMBL DrugBank KEGG		0.300	n/a	n/a	n/a	n/a	n/a	n/a	n/a	n/a
Griffith University Curated by ChEMBL	 CHEMBL419 (1)	DrugBank antibodypedia GoogleScholar	Patents Similar										
Carbonic anhydrase 12 (Homo sapiens (Human))	 EDBM10880	PDB MMDB Reactome pathway	Purchase CHEBI ChEMBL DrugBank KEGG		0.300	n/a	n/a	n/a	n/a	n/a	n/a	n/a	n/a

Figure 66. Screenshot of the results table for (A) CA IX and (B) CA XII simple search in Binding DB.

The database saved was used in a Pipeline Pilot protocol, represented in Figure 67, in order to search coumarin and chromone substructures in these two databases.

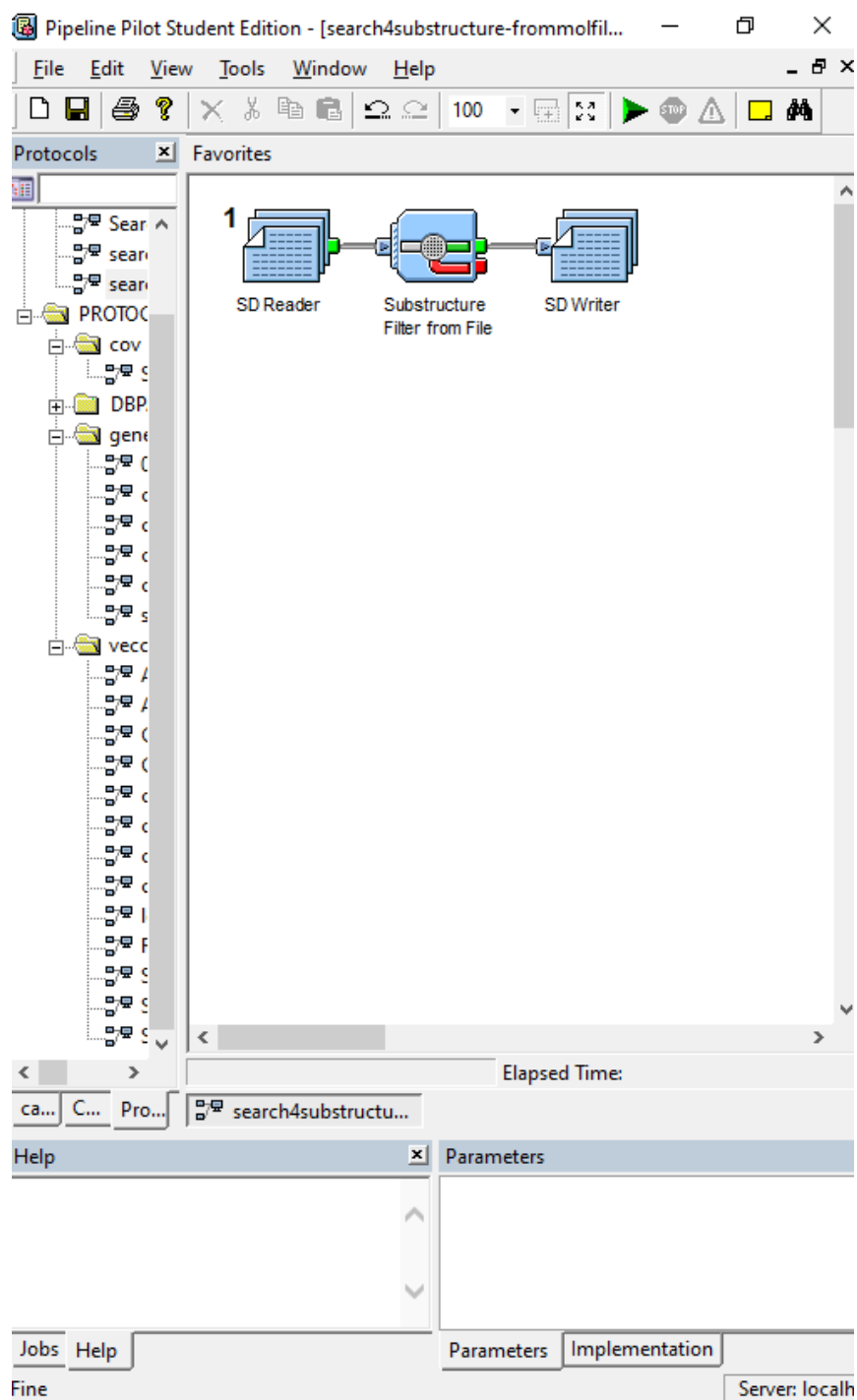


Figure 67. Screenshot of the Pipeline Pilot protocol for substructure search.

2.6. Theoretical prediction of drug-like properties

Rules such as the ones first introduced by Lipinski [290, 291], and then further upgraded by Veber et al. [292] influence decision making before the synthesis of drug candidates and are also important in the selection of molecules from screening large compounds libraries obtained from commercial providers. The software QikProp 2.1, developed by Jorgensen and coworkers, has the capacity of calculating 36 molecular and biological properties [293, 294]. Ioakimidis et al. investigated the reliability of the program by comparing its physical-chemical property predictions with known measured values and, in the case of the ADME properties, marketed drug compounds with an established therapeutic effect [295]. Good correlation with experimental results was found in most of the properties confirming the conclusions of QikProp developers. Their results led them to recommend this software in the context of drug discovery projects [295]. Table 8 lists the properties and descriptors, relevant for this work, given by QikProp.

Table 8. QikProp properties and descriptors with description and range or recommended values, from the QikProp user manual.

Property or Descriptor	Description	Range or Recommended Values
Stars	Number of property or descriptor values that fall outside the 95% range of similar values for known drugs. A large number of stars suggests that a molecule is less drug-like than molecules with few stars. The following properties and descriptors are included in the determination of stars: MW, dipole, IP, EA, SASA, FOSA, FISA, PISA, WPSA, PSA, volume, rotor, donorHB, accptHB, glob, QPpolrz, QPlogPC16, QPlogPoct, QPlogPw, QPlogPo/w, logS, QPLogKhsa, QPlogBB, metabol.	0 – 5
Rotor	Number of non-trivial (not CX3), non-hindered (not alkene, amide, small ring) rotatable bonds.	0 – 15
rtvFG	Number of reactive functional groups; the specific groups are listed in the jobname .out file. The presence of these groups can lead to false positives in HTS assays and to decomposition, reactivity, or toxicity problems in vivo.	0 - 2
CNS	Predicted central nervous system activity on a -2 (inactive) to +2 (active) scale.	-2 – +2
mol_MW	Molecular weight of the molecule.	130.0 – 725.0
dipole	Computed dipole moment of the molecule.	1.0 – 12.5
SASA	Total solvent accessible surface area (SASA) in square angstroms using a probe with a 1.4 Å radius.	300.0 – 1000.0
FOSA	Hydrophobic component of the SASA (saturated carbon and attached hydrogen).	0.0 – 750.0
FISA	Hydrophilic component of the SASA (SASA on N, O, and H on heteroatoms).	7.0 – 330.0
PISA	π (carbon and attached hydrogen) component of the SASA.	0.0 – 450.0

WPSA	Weakly polar component of the SASA (halogens, P, and S).	0.0 – 175.0
volume	Total solvent-accessible volume in cubic angstroms using a probe with a 1.4 Å radius.	500.0 – 2000.0
donorHB	Estimated number of hydrogen bonds that would be donated by the solute to water molecules in an aqueous solution. Values are averages taken over a number of configurations, so they can be non-integer.	0.0 – 6.0
accptHB	Estimated number of hydrogen bonds that would be accepted by the solute from water molecules in an aqueous solution. Values are averages taken over a number of configurations, so they can be non-integer.	2.0 – 20.0
dip ² /V	Square of the dipole moment divided by the molecular volume. This is the key term in the Kirkwood-Onsager equation for the free energy of solvation of a dipole with volume V.	0.0 – 0.13
ACxDN ^{0.5} /SA	Index of cohesive interaction in solids. This term represents the relationship $(accptHB(\sqrt{donorHB}))/SA$ [296].	0.0 – 0.05
Glob	Globularity descriptor, $(4\pi r^2)/(SASA)$, where r is the radius of a sphere with a volume equal to the molecular volume. Globularity is 1.0 for a spherical molecule.	0.75 – 0.95
QPpolrz	Predicted polarizability in cubic angstroms.	13.0 – 70.0
QPlogPC16	Predicted hexadecane/gas partition coefficient.	4.0 – 18.0
QPlogPoct	Predicted octanol/gas partition coefficient.	8.0 – 35.0
QPlogPw	Predicted water/gas partition coefficient.	4.0 – 45.0
QPlogPo/w	Predicted octanol/water partition coefficient.	-2.0 – +6.5
QPlogS	Predicted aqueous solubility, log S. S in mol dm ⁻³ is the concentration of the solute in a saturated solution that is in equilibrium with the crystalline solid.	-6.5 – +0.5
CIQPlogS	Conformation-independent predicted aqueous solubility, log S. S in mol dm ⁻³ is the concentration of the solute in a saturated solution that is in equilibrium with the crystalline solid.	-6.5 – +0.5
QPlogHERG	Predicted IC ₅₀ value for blockage of HERG K ⁺ channels.	Concern below -5
QPPCaco	Predicted apparent Caco-2 (colorectal adenocarcinoma) cell permeability in nm/sec. Caco-2 cells are a model for the gut-blood barrier. QikProp predictions are for non-active transport.	< 25: poor > 500: great
QPlogBB	Predicted brain/blood partition coefficient. Note: QikProp predictions are for orally delivered drugs so, for example, dopamine and serotonin are CNS negative because they are too polar to cross the blood-brain barrier	-3 – +1.2
QPPMDCK	Predicted apparent MDCK (Madin-Darby Canine Kidney) cell permeability in nm/sec. MDCK cells are considered to be a good mimic for the blood-brain barrier. QikProp predictions are for non-active transport.	< 25: poor > 500: great
QPlogKp	Predicted skin permeability, log K _p .	-8.0 – -1.0
IP(ev)	PM3 calculated ionization potential.	7.9 – 10.5
EA(ev)	PM3 calculated electron affinity.	-0.9 – +1.7
metab	Number of likely metabolic reactions.	1 – 8
QPlogKhsa	Prediction of binding to human serum albumin.	-1.5 – +1.5

CHAPTER 2

HumanOralAbsorption	Predicted qualitative human oral absorption. The text version is reported in the output. The assessment uses a knowledge-based set of rules, including checking for suitable values of PercentHumanOralAbsorption, number of metabolites, number of rotatable bonds, logP, solubility and cell permeability.	1: low 2: medium 3: high
PercentHumanOralAbsorption	Predicted human oral absorption on 0 to 100% scale. The prediction is based on a quantitative multiple linear regression model. This property usually correlates well with HumanOralAbsorption, as both measure the same property.	> 80%: high < 25%: poor
SAFluorine	Solvent-accessible surface area of fluorine atoms.	0.0 – 100.0
PSA	Van der Waals surface area of polar nitrogen and oxygen atoms.	7.0 – 200.0
NandO	Number of nitrogen and oxygen atoms.	2 – 15
RuleOfFive	Number of violations of Lipinski's rule of five. The rules are: mol_MW < 500, QPlogPo/w < 5, donorHB ≤ 5, accptHB ≤ 10. Compounds that satisfy these rules are considered drug-like. (The "five" refers to the limits, which are multiples of 5.)	Maximum is 4
RuleOfThree	Number of violations of Jorgensen's rule of three. The three rules are: QPlogS > -5.7, QP PCaco > 22 nm/s, Primary Metabolites < 7. Compounds with fewer (and preferably no) violations of these rules are more likely to be orally available.	Maximum is 3
ringatoms	Number of atoms in rings.	-
in56	Number of atoms in 5- or 6-membered rings.	-
nonHatm	Number of heavy atoms (nonhydrogen atoms).	-
Jm	Predicted maximum transdermal transport rate, $K_p \times MW \times S$ ($\mu\text{g cm}^{-2}\text{hr}^{-1}$). K_p and S are obtained from the aqueous solubility and skin permeability, QPlogKp and QPlogS. This property is only written to the output file: it is not used in any other calculations.	

All the compounds subjected to carbonic anhydrase inhibition assay were sent to QikProp and their theoretical properties were calculated.

2.7. Molecular Docking

Before docking a molecule into the target structure, it is important to validate the procedure. For that purpose, the complexes with CA IX and known inhibitors were found in Uniprot DB (www.uniprot.org) and BLASTP [297]. The list of the different complexes is shown in Table 9. The complexes without ligand or equal ligands were not considered. Afterwards we proceed to the validation through re- and cross-docking, considering the co-crystallized ligands reported in pdb complexes. This validation method consists in docking the series of ligands into the same conformation of the protein, in this case CA IX. The comparison of docked pose and experimental was made through the calculation of the Root Mean Square Deviation (RMSD) in order to understand if the protocol was able to reproduce the experimental data. The validation is an update of the previous published one [298].

Table 9. PDB code and ligand structure of the complexes formed with *hCA IX*.

PDB	Ligand Structure	PDB	Ligand Structure
5FL4		6G9U	
3IAI		6QN2	
5FL5		6QN5	
5FL6		6QN6	
6FE0		6TL5	
6FE1		6TL6	
6G98			

The same procedure was made for CA XII, and the complexes pdb codes and respective ligand structures can be seen in Table 10.

Table 10. PDB code and ligand structure of the complexes formed with *h*CA XII.

PDB	Ligand Structure	PDB	Ligand Structure
5MSA		5MSB	
4KP5		4KP8	
6T5P		4HT2	
1JD0		4WW8	
5LLP		5LLO	
6G5L		6QNG	
6QN0		6G7A	
4Q0L		4QJ0	
4QJO		6QNL	
4QJW		6R6Y	
5LL9		5LL5	
6R71		5T5Q	

The RMSD calculation results are listed in Table 11. These results allowed us to validate the protocol used for the docking experiments of the synthesized compounds.

Table 11. Cross-docking results considering the co-crystallized ligands reported in pdb complexes. Receptor coordinates were obtained considering *hCA IX* pdb 5FL4, and *hCA XII* pdb 5MSA.

<i>hCA IX</i>			<i>hCA IX</i>		
PDB	PDB Resolution (Å)	RMSD	PDB	PDB Resolution (Å)	RMSD
5FL4	1.82	1.73	5MSA	1.20	1.26
3IAI	2.20	2.00	4KP5	1.45	1.69
5FL5	2.05	1.84	6T5P	1.50	1.62
5FL6	1.95	1.84	1JD0	1.50	1.66
6FE0	1.91	1.97	5LLP	1.48	1.68
6FE1	1.95	1.93	6G5L	1.21	1.10
6G98	2.47	8.62	6QN0	1.89	2.43
6G9U	1.75	8.50	4Q0L	2.00	2.23
6QN2	1.95	1.93	4QJO	1.80	2.12
6QN6	2.25	1.01	4QJW	1.55	4.75
6TL5	2.21	5.92	5LL9	1.45	1.57
6TL6	2.15	1.72	6R71	2.00	0.85
			5MSB	1.30	1.12
			4KP8	1.80	4.60
			4HT2	1.45	1.79
			4WW8	1.42	2.03
			5LLO	1.60	1.28
			6QNG	1.67	1.54
			6G7A	1.42	2.13
			4QJ0	1.55	1.79
			6R6Y	1.38	1.73
			5LL5	1.42	2.52
			5T5Q	1.95	1.55

2.7.1. *Ligand preparation*

Theoretical 3D models of the compounds were built using Maestro GUI software. In the cases of EMAC10163 and EMAC10164 series the opening of the coumarin was also considered, and the compounds were built in both E and Z configurations, considering the same mechanism proposed by Maresca et al. [152, 153]. The ligands most stable conformation has been determined by molecular mechanics conformational analysis performed by Macromodel software version 9.2 [299], considering Merck Molecular Force Fields (MMFFs) [300] as force field and solvent effects by adopting the generalized Born/surface area (GB/SA) water implicit solvation model [301]. The simulations were performed allowing 5000 steps Monte Carlo analysis with Polak–Ribier Conjugate Gradient (PRCG) method and a convergence criterion of 0.05 kcal/ (mol Å) was used. All the other parameters were left as default.

2.7.2. *Protein preparation*

The coordinates for *hCA* isoforms enzymes were taken from the RCSB Protein Data Bank [302] (PDB codes 5FL4 [303], for isoform IX and 5MSA [304], for isoform XII). These 3D structures are high resolutions X-ray models and the alignment with the other 3D structure did not highlight significative difference to justify the use of an ensemble docking approach. Maestro Protein Preparation Wizard was used to prepare the proteins. The original water molecules and ligands were removed. The Gln and Asn residues were analyzed and orientated with the best terminal amide position. Likewise, the best His tautomer was chosen according to the best orientation.

2.7.3. *Docking experiments*

Quantum Mechanics-Polarized Ligand (QMPL) Docking was used for the molecular docking studies [239, 298, 305]. Grids were defined around the refined structure by centering on crystallized ligands. The other settings were left as default.

2.7.4. *Post-docking experiments*

The best pose complexes were then minimized to consider the induced fit phenomena and used to analyze the ligand binding mode. 10.000 steps of the Polak-Ribier conjugate

gradient (PRCG) minimization method were conducted on the top ranked theoretical complexes using OPLS_2005 force field.

The optimization process was performed up to the derivative convergence criterion equal to 0.1 kcal/(mol*Å).

CHAPTER 3. Results and Discussion

3.1. Synthesis of furocoumarins

As described on section 2.2.1 the furocoumarins were synthesized by a three steps pathway (see Figure 25).

Detailed Pechmann condensation proposed mechanism is represented on Figure 68 which starts with the methyl resorcinol and the ester containing a β -carbonyl group [306]. In this step H_2SO_4 act as a condensing agent and solvent.

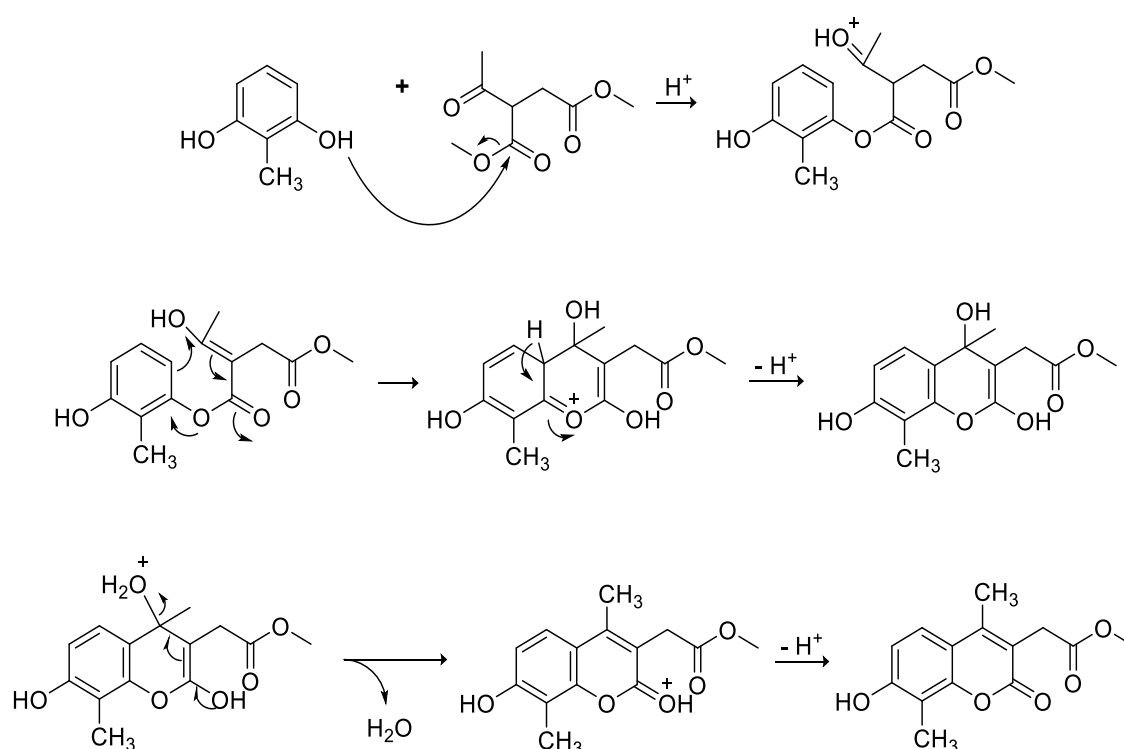


Figure 68. Pechmann condensation proposed mechanism.

This reaction was performed with success and a high yield of 62.6%.

Pechmann condensation was followed by a Williamson reaction [307], which suggested mechanism can be seen on Figure 69. This synthesis involves a deprotonation followed by a $\text{S}_{\text{N}}2$ reaction. On this case, potassium carbonate was used as the base.

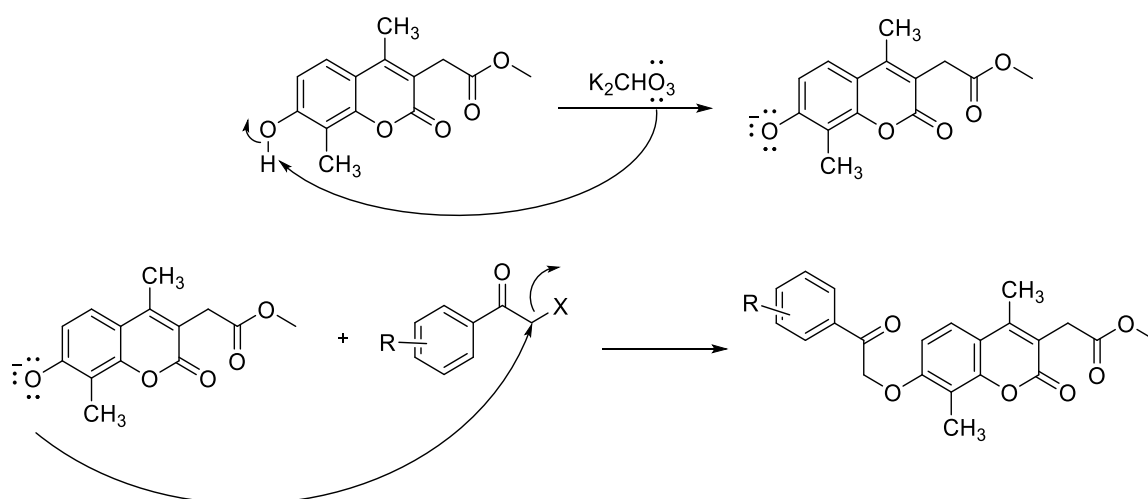


Figure 69. Williamson Ether synthesis suggested mechanism.

These reactions were successfully completed with yields from moderate to high, as seen on Table 12. The exceptions were compound EMAC10163i and EMAC10163l, which synthesis were not accomplished. EMAC10163i has two chlorine groups in positions 2' and 4', while EMAC10163l has a hydroxyl group in position 2'. The high electronegativity of this group may be responsible for the unsuccessful results in this synthesis.

Table 12. Yields of the EMAC10163 series synthesis.

Compound	Yield (%)
EMAC10163a	86.1
EMAC10163b	27.8
EMAC10163c	46.1
EMAC10163d	63.0
EMAC10163e	37.9
EMAC10163f	19.6
EMAC10163g	73.9
EMAC10163h	49.0
EMAC10163j	88.6
EMAC10163k	46.0
EMAC10163m	55.3

On the third and last step of this synthetic pathway, an intramolecular condensation, which is an electrophilic substitution based catalyzed, and ester saponification [308] was performed to obtain the correspondents furocoumarins with a methylcarboxylic acid in C3 position, which proposed mechanism can be seen, with detail, on Figure 70.

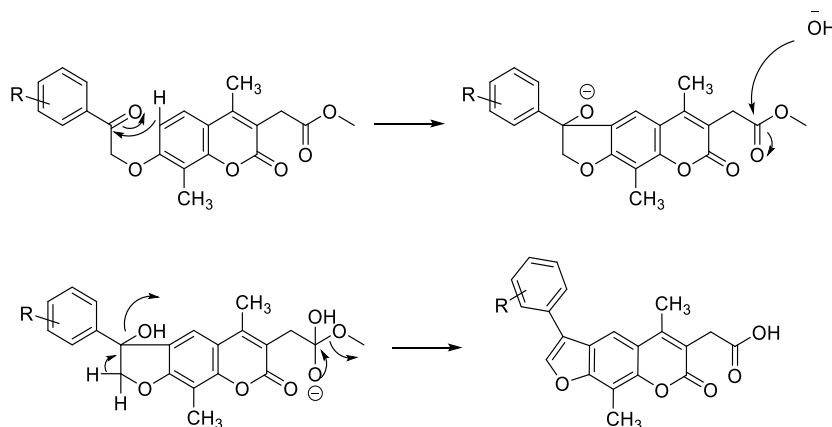


Figure 70. Intramolecular condensation and ester saponification proposed mechanism occurred in the synthesis of EMAC10164 series.

These syntheses were successfully accomplished with high yields, as seen on Table 13. The only exceptions were the compounds EMAC10164e and EMAC10164f, which isolation was not possible. This two compounds have the nitro compound in positions 4' and 3', respectively. The number of side products and solubility problems made so far impossible the isolation of one compound.

Table 13. Yields of the EMAC10164 series synthesis.

Compound	Yield (%)
EMAC10164a	96.0
EMAC10164b	67.3
EMAC10164c	90.5
EMAC10164d	89.7
EMAC10164g	50.1
EMAC10164h	93.2
EMAC10164j	87.1
EMAC10164k	67.9
EMAC10164m	91.7

3.2. Synthesis of chromones

As described on section 2.3.1 the chromones were synthesized on a two steps pathway (see Figure 47). The original synthetic pathway consisted of a POCl_3 -induced cyclization followed by a Williamson condensation, but this strategy showed to be unproductive, since the yields of the POCl_3 -induced cyclization as first step were very low (around 10 %). Therefore, after some attempts to rise the yield of the reaction, the pathway was inverted, which revealed to be effective, as can be confirmed by the high yields of this step (Table 14). Unfortunately, the synthesis of compounds EMAC10168e, f, h, i, j, and l remained unsuccessful. The different electronegativity of the substituents may interfere with the success of this synthesis. However, this doesn't explain the case of EMAC10168j that has no substituent in the aromatic ring. According to our experience a blend of electron density and solubility may play a role in the reaction and in these cases, different conditions should be tested, including different bases, solvents, temperatures, and times of reaction.

Detailed Williamson suggested reaction mechanism is already represented on Figure 69 for the synthesis of furocoumarins and is equal to chromones.

Table 14. Yields of the EMAC10168 series synthesis.

Compound	Yield (%)
EMAC10168a	72.6
EMAC10168b	97.1
EMAC10168c	78.9
EMAC10168d	85.1
EMAC10168g	50.0
EMAC10168k	65.3
EMAC10168m	82.4

The second and last step was the POCl_3 -induced cyclization. In this reaction Vilsmeier-Haack reagent is formed *in situ* (mechanistic proposal is shown on Figure 71) [309]. The reaction of an acetophenone with this reagent allows the cyclisation to form a chromone, as suggested by the mechanism seen in Figure 72 [310, 311].

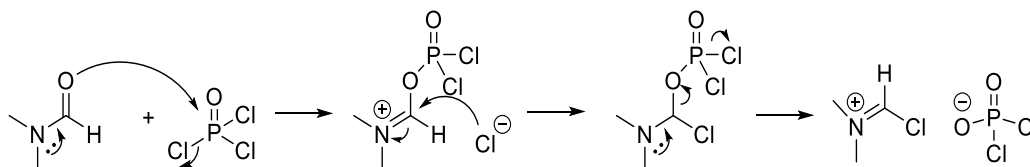


Figure 71. Vilsmeier-Haack reagent *in situ* formation mechanistic proposal.

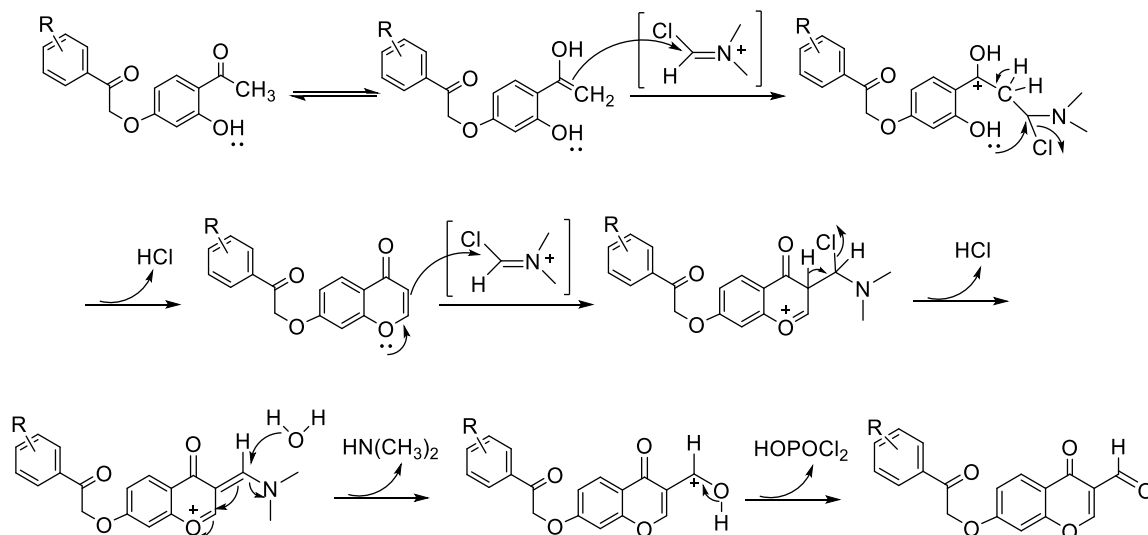


Figure 72. Mechanistic proposal for the POCl₃-induced cyclisation.

These syntheses were successful, with low yields, as seen on Table 15, but nevertheless higher than the 10 % yield obtained with the first synthetic approach, and accordingly with the typical yields of this synthesis [257].

Table 15. Yields of the EMAC10169 series syntheses.

Compound	Yield (%)
EMAC10169a	22.3
EMAC10169b	34.5
EMAC10169c	36.1
EMAC10169d	25.3
EMAC10169g	17.4
EMAC10169k	23.0
EMAC10169m	26.3

3.3. Structural elucidation

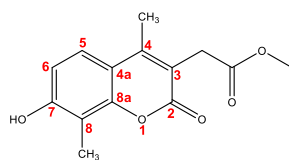
3.3.1 Methyl 2-(7-hydroxy-4,8-dimethyl-2-oxo-2H-chromen-3-yl)acetate (EMAC10163)

This intermediate was characterized by ^1H , ^{13}C and DEPT NMR spectrometry (spectra on Appendix).

On Table 16 are highlighted the ^1H NMR chemical shifts of the compound EMAC10163, indicating chemical shifts (δ), in ppm, the number of protons (I), the signal multiplicity (M) and the coupling constants (J) in Hz. From the obtained ^1H NMR spectrum was possible to identify characteristic signals of some protons.

The protons H (5) and H (6) showed doublet multiplicity with coupling constants of 8.8 Hz, which proves that both couple to each other in ortho position [312]. The protons from the CH_3 and CH_2 groups showed as singlets at chemical shifts between δ 2.16 and δ 3.65 ppm that integrate for 3 H and 2 H, respectively, thus confirming the identity of these groups. The presence of the group OH was confirmed by the singlet at δ 10.38 ppm, that integrates to 1 H.

Table 16. ^1H NMR data from EMAC10163 (solvent: DMSO).



Protons	<u>CH₃</u>	<u>CH₃</u>	<u>CH₃</u>	<u>CH₂</u>	H(Ar)	H(Ar)	<u>OH</u>
δ	2.16	2.34	3.62	3.65	6.88	7.51	10.38
I	3	3	3	2	1	1	1
M	s	s	s	s	d	d	s
J	-	-	-	-	8.8	8.8	-

Table 17 contains the ^{13}C and DEPT (underlined values) NMR data of the compound EMAC10163, indicating the chemical shifts (δ) in ppm. From the ^{13}C and DEPT spectra it was possible to identify some signals.

Carbon C (2) and C (7) were identified with chemical shifts δ 161.06 and δ 158.43 ppm, respectively.

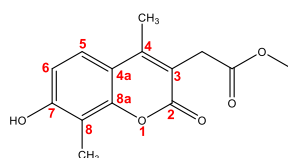
It was possible to identify the C (5) and C (6) carbons, present in the ^{13}C and DEPT NMR spectrum, with chemical shifts δ 123.42 and δ 111.89 ppm, respectively.

The carbons from the CH_3 and CH_2 , present in the ^{13}C and DEPT NMR spectrum, were identified with chemical shifts between δ 7.91 and δ 51.76 ppm.

The carbon of the ester group was identified with chemical shift δ 170.71.

For carbons to which it was not possible to assign a signal it is necessary to obtain two-dimensional NMR spectra. However, the number of signals present agrees with the number of carbon atoms in the molecule and the set of analyzes performed confirms the identity of the compounds.

Table 17. ^{13}C NMR data from EMAC10163 (solvent: DMSO).



Carbons	δ
<u>CH</u> ₃	<u>8.41</u>
C(4) <u>CH</u> ₃	<u>15.51</u>
<u>CH</u> ₂	<u>32.80</u>
C(8) <u>CH</u> ₃	<u>51.27</u>
C(3), C(4), C(4a), C(8), C(8a)	n.d.
C(6)	<u>112.40</u>
C(5)	<u>123.92</u>
C(7)	158.94
C(2)	161.57
<u>COOCH</u> ₃	171.22

n.d. – non defined

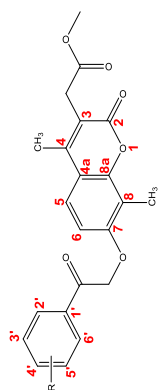
3.3.2. 2H-chromen compounds (EMAC10163 series)

This series was characterized by ^1H , ^{13}C , DEPT NMR (spectra on Appendix) and ESI/MS spectrometry.

On Table 18 and Table 19 are highlighted the ^1H NMR chemical shifts of the EMAC10163 series, indicating chemical shifts (δ), in ppm, the number of protons (I), the signal multiplicity (M) and the coupling constants (J) in Hz. From the obtained ^1H NMR spectrum was possible to identify characteristic signals of some protons.

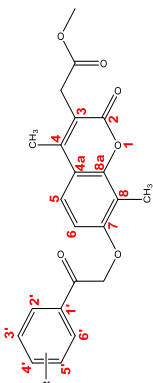
The protons H (5) and H (6) showed doublet multiplicity with chemical shifts between δ 6.67 and δ 7.42 and coupling constants between 8.6 and 9.0 Hz, in all compounds, which proves that both couple to each other in ortho position [312]. The proton H (5) is an exception on compounds EMAC10163g, EMAC10163j and EMAC10163m since the signals showed as multiplets. The benzenic ring protons were identified as multiplets, for all compounds except EMAC10163f where H (5') showed triplet multiplicity.

The protons from the CH₃ and CH₂ groups were identified as singlets, for all compounds, at chemical shifts between δ 2.27 and δ 5.40 ppm, integrating for 3 H and 2 H, respectively, thus confirming the identity of these groups. EMAC10163h is an exception because one of the CH₂ groups showed as multiplet.

Table 18. ¹H NMR data from EMAC10163a-e (solvent: CDCl₃).

Compound	C(8)CH ₃	C(4)CH ₃	C(4')XCH ₃	OCH ₃	C3CH ₂	CH ₂	H(6)	H(2'), H(3'), H(5'), H(6')	H(5)
EMAC10163a	δ	2.35	2.38	2.43	3.70	3.72	6.71	n.d.	7.39
	I	3	3	3	3	2	1	-	1
	M	s	s	s	s	s	d'	-	d'
	J	-	-	-	-	-	8.9	-	9.0
EMAC10163b	δ	2.35	2.38	3.89	3.70	3.72	6.73	n.d.	7.39
	I	3	3	3	3	2	1	-	1
	M	s	s	s	s	s	d'	-	d'
	J	-	-	-	-	-	8.9	-	8.7
EMAC10163c	δ	2.35	2.37	-	3.70	3.72	6.71	n.d.	7.40
	I	3	3	-	3	2	1	-	1
	M	s	s	-	s	s	d'	-	d'
	J	-	-	-	-	-	8.9	-	8.7
EMAC10163d	δ	2.35	2.37	-	3.70	3.72	6.72	n.d.	7.40
	I	3	3	-	3	2	1	-	1
	M	s	s	-	s	s	d'	-	d'
	J	-	-	-	-	-	8.9	-	8.9
EMAC10163e	δ	2.27	2.29	-	3.64	3.65	6.67	n.d.	7.35
	I	3	3	-	3	2	1	-	1
	M	s	s	-	s	s	d'	-	d'
	J	-	-	-	-	-	8.9	-	8.7

n.d. – non defined

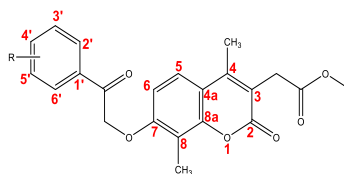
Table 19. ¹H NMR data from EMAC10163f-h and j-m (solvent: CDCl₃).


Compound	δ	C(8)/CH ₃	C(4)CH	C(3')/OCCH ₃	OCCH ₃	C3CH ₂	CH ₂	H(6)	H(2'), H(3'), H(4'), H(5'), H(6')	H(5)
EMAC10163f	δ	2.35	2.36	-	3.71	3.72	5.40	6.76	n.d.	7.42
	I	3	3	-	3	2	2	1	-	1
	M	s	s	-	s	s	s	d	-	d
	J	-	-	-	-	-	-	8.9	-	8.6
EMAC10163g	δ	2.35	2.40	-	3.70	3.72	5.41	6.74	n.d.	n.d.
	I	3	3	-	3	2	2	1	-	-
	M	s	s	-	s	s	s	d	-	-
	J	-	-	-	-	-	-	8.9	-	-
EMAC10163h	δ	2.36	2.38	-	3.71	3.73	5.30	6.68	n.d.	7.40
	I	3	3	-	3	2	2	1	-	1
	M	s	s	-	s	s	m	d	-	d
	J	-	-	-	-	-	-	8.9	-	8.9
EMAC10163j	δ	2.35	2.38	-	3.70	3.72	5.39	6.72	n.d.	n.d.
	I	3	3	-	3	2	2	1	-	-
	M	s	s	-	s	s	s	d	-	-
	J	-	-	-	-	-	-	8.9	-	-
EMAC10163k	δ	2.37	2.38	-	3.72	3.74	5.35	6.73	n.d.	7.41
	I	3	3	-	3	2	2	1	-	1
	M	s	s	-	s	s	s	d	-	d
	J	-	-	-	-	-	-	8.9	-	8.9
EMAC10163m	δ	2.35	2.39	3.86	3.70	3.72	5.38	6.71	n.d.	n.d.
	I	3	3	3	3	2	2	1	-	-
	M	s	s	s	s	s	s	d	-	-
	J	-	-	-	-	-	-	8.9	-	-

n.d. – non defined

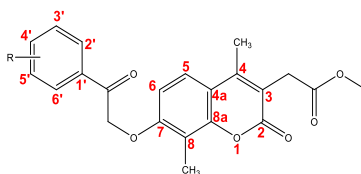
On Table 20 and Table 21 are highlighted the ^{13}C and DEPT NMR data (underlined values) of the EMAC10163 series, indicating the chemical shifts (δ) in ppm. From the ^{13}C and DEPT spectra it was possible to identify some signals.

Table 20. ^{13}C and DEPT NMR data from EMAC10163a-e (solvent: CDCl_3).



Compound	EMAC 10163a	EMAC 10163b	EMAC 10163c	EMAC 10163d	EMAC 10163e
C(8)CH₃	<u>8.42</u>	<u>8.43</u>	<u>8.43</u>	<u>8.42</u>	<u>8.43</u>
C(4)CH₃	<u>15.38</u>	<u>15.38</u>	<u>15.40</u>	<u>15.39</u>	<u>15.41</u>
C(4')XCH₃	<u>21.80</u>	<u>55.57</u>	-	-	-
C(3)CH₂	<u>32.75</u>	<u>32.75</u>	<u>32.75</u>	<u>32.75</u>	<u>32.73</u>
OCH₃	<u>52.21</u>	<u>52.21</u>	<u>52.24</u>	<u>52.23</u>	<u>52.26</u>
CH₂	<u>71.17</u>	<u>71.15</u>	<u>71.23</u>	<u>71.22</u>	<u>71.53</u>
C(2), C(3), C(4), C(4a), C(7), C(8), C(8a)	n.d.	n.d.	n.d.	n.d.	n.d.
C(1')	n.d.	n.d.	n.d.	130.81 (<i>d</i> , <i>J</i> = 3.1 Hz)	n.d.
C(2'), C(6')	<u>n.d.</u>	<u>n.d.</u>	<u>n.d.</u>	<u>131.00</u> (<i>d</i> , <i>J</i> = 9.5 Hz)	<u>n.d.</u>
C(3'), C(5')	<u>n.d.</u>	<u>n.d.</u>	<u>n.d.</u>	<u>116.17</u> (<i>d</i> , <i>J</i> = 22.0 Hz)	<u>n.d.</u>
C(4')	n.d.	n.d.	n.d.	166.26 (<i>d</i> , <i>J</i> = 256.7 Hz)	n.d.
C(5), (6)	<u>n.d.</u>	<u>n.d.</u>	<u>n.d.</u>	<u>n.d.</u>	<u>n.d.</u>
COOCH₃	170.88	170.88	170.85	170.86	170.82
CO	193.71	192.64	193.43	192.75	193.36

n.d. – non defined

Table 21. ^{13}C and DEPT NMR data from EMAC10163f-h and j-m (solvent: CDCl_3).

Compound	EMAC 10163f	EMAC 10163g	EMAC 10163h	EMAC 10163j	EMAC 10163k	EMAC 10163m
$\text{C}(8)\underline{\text{C}}\text{H}_3$	<u>8.40</u>	<u>8.45</u>	<u>8.35</u>	<u>8.42</u>	<u>8.42</u>	<u>8.43</u>
$\text{C}(4)\underline{\text{C}}\text{H}_3$	<u>15.41</u>	<u>15.40</u>	<u>15.40</u>	<u>15.39</u>	<u>15.39</u>	<u>15.39</u>
$\text{C}(3)\underline{\text{C}}\text{H}_2$	<u>32.74</u>	<u>32.75</u>	<u>32.76</u>	<u>32.76</u>	<u>32.74</u>	<u>32.76</u>
$\text{O}\underline{\text{C}}\text{H}_3$	<u>52.25</u>	<u>52.22</u>	<u>52.23</u>	<u>52.22</u>	<u>52.23</u>	<u>52.22</u>
$\text{C}(3')\text{O}\underline{\text{C}}\text{H}_3$	-	-	-	-	-	<u>52.52</u>
$\underline{\text{C}}\text{H}_2$	<u>71.53</u>	<u>71.28</u>	<u>73.71</u> (<i>d</i> , <i>J</i> = 12.3 Hz)	<u>71.20</u>	<u>71.24</u>	<u>71.22</u>
$\text{C}(2), \text{C}(3), \text{C}(4), \text{C}(4\text{a}),$ $\text{C}(7), \text{C}(8), \text{C}(8\text{a})$	n.d.	n.d.	n.d.	n.d.	n.d.	n.d.
$\text{C}(3')$	n.d.	<u>n.d.</u>	<u>104.82</u> (<i>dd</i> , <i>J</i> = 27.5, 25.7 Hz)	<u>n.d.</u>	<u>n.d.</u>	n.d.
$\text{C}(5')$	<u>n.d.</u>	<u>n.d.</u>	<u>113.00</u> (<i>dd</i> , <i>J</i> = 21.6, 3.2 Hz)	<u>n.d.</u>	<u>n.d.</u>	<u>n.d.</u>
$\text{C}(1')$	n.d.	n.d.	119.41 (<i>dd</i> , <i>J</i> = 15.3, 3.6 Hz)	<u>n.d.</u>	n.d.	n.d.
$\text{C}(6')$	<u>n.d.</u>	<u>n.d.</u>	<u>132.91</u> (<i>dd</i> , <i>J</i> = 10.8, 4.9 Hz)	<u>n.d.</u>	<u>n.d.</u>	<u>n.d.</u>
$\text{C}(2')$	n.d.	<u>n.d.</u>	163.03 (<i>dd</i> , <i>J</i> = 256.1, 12.8 Hz)	<u>n.d.</u>	<u>n.d.</u>	<u>n.d.</u>
$\text{C}(4')$	n.d.	n.d.	166.54 (<i>dd</i> , <i>J</i> = 259.1, 12.5 Hz)	<u>n.d.</u>	n.d.	<u>n.d.</u>
$\text{C}(6), \text{C}(5)$	<u>n.d.</u>	<u>n.d.</u>	<u>n.d.</u>	<u>n.d.</u>	<u>n.d.</u>	<u>n.d.</u>
$\underline{\text{C}}\text{OOCH}_3$	170.82	170.87	170.88	170.87	170.85	170.88
$\underline{\text{C}}\text{O}$	192.82	193.70	190.86 (<i>d</i> , <i>J</i> = 5.6 Hz)	194.08	193.20	193.86

n.d. – non defined

The carbons from the CH₃ and CH₂, present in the ¹³C and DEPT NMR spectrum, were identified with chemical shifts between δ8.42 and δ71.52 ppm, for all compounds.

For the compound EMAC10163d the carbons of the benzene ring were identified as doublets. C (1') and C (4') are present in the ¹³C NMR spectra with chemical shifts δ130.81 and δ166.26 ppm and coupling constants of 3.1 and 256.7 Hz, respectively. C (2') and C (6'), and C (3') and C (5') are present in the ¹³C and DEPT NMR spectrum with chemical shifts of δ131.00 and δ116.17 ppm and coupling constant of 9.5 and 22.0 Hz, respectively. All these data are in agreement with the literature for fluorinated compounds [312].

For the compound EMAC10163h the carbons of the benzene ring were identified as double doublets and the CH₂ of the open furane ring was identified as a doublet. C (1'), C (2') and C (4') are present in the ¹³C NMR spectra with chemical shifts δ119.41, δ163.03 and δ166.54 ppm and coupling constant of 15.3 and 3.6, 256.1 and 12.8, and 259.1 and 12.5 Hz, respectively. C (3'), C (5') and C (6') are present in the ¹³C and DEPT NMR spectrum with chemical shifts δ104.82, δ113.00 and δ132.91 ppm and coupling constant of 27.5 and 25.7, 21.6 and 3.2, and 10.8 and 4.9 Hz, respectively. All these data are in agreement with the literature for fluorinated compounds [312].

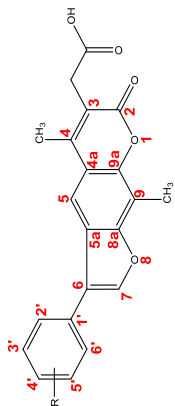
The carbon of the ester group was identified with chemical shifts between δ170.81 and δ170.88 ppm, for all compounds.

For carbons to which it was not possible to assign a signal it is necessary to obtain two-dimensional NMR spectra. However, the number of signals present agrees with the number of carbon atoms in the molecule and the set of analyzes performed confirms the identity of the compounds.

3.3.3. H-furo-chromen compounds (EMAC10164 series)

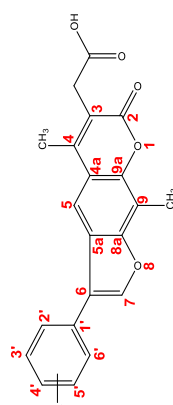
This series was characterized by ¹H, ¹³C, DEPT NMR (spectra on Appendix) and ESI/MS spectrometry.

On Table 22 and Table 23 are highlighted the ¹H NMR chemical shifts of the EMAC10164 series, indicating chemical shifts (δ), in ppm, the number of protons (I), the signal multiplicity (M) and the coupling constants (J) in Hz. From the obtained ¹H NMR spectrum was possible to identify characteristic signals of some protons.

Table 22. ¹H NMR data from EMAC10164a-d (solvent: DMSO).


Compound	C(9)CH ₃	C(4)CH ₃	CH ₂	C(4')XCH ₃	H(5)	H(7)	H(2'), H(3'), H(4'), H(5'), H(6')	COOH
EMAC10164a	δ	2.38	3.64	2.50	7.90	8.39	n.d.	n.d.
	I	3	2	3	1	1	-	-
	M	s	s	s	s	s	-	-
	J	-	-	-	-	-	-	-
EMAC10164b	δ	2.52	3.66	3.83	8.01	8.39	n.d.	12.50
	I	3	2	3	1	1	-	1
	M	s	s	s	s	s	-	s
	J	-	-	-	-	-	-	-
EMAC10164c	δ	2.49	3.64	-	7.96	8.50	n.d.	12.49
	I	3	2	-	1	1	-	1
	M	s	s	-	s	s	-	s
	J	-	-	-	-	-	-	-
EMAC10164d	δ	2.50	3.64	-	7.97	8.44	n.d.	12.55
	I	3	2	-	1	1	-	1
	M	s	s	-	s	s	-	s
	J	-	-	-	-	-	-	-

n.d. – non defined

Table 23. ¹H NMR data from EMAC10164g-h and j-m (solvent: DMSO).


Compound	C(9)CH ₃	C(4)CH ₃	CH ₂	C(3') OCH ₃	H(5)	H(7)	H(2'), H(3'), H(4'), H(5'), H(6')	COOH
EMAC10164g	δ	2.48	2.51	3.59	-	8.01	8.49	n.d.
	I	3	3	2	-	1	1	-
	M	S	S	S	S	S	-	-
	J	-	-	-	-	-	-	-
EMAC10164h	δ	2.47	2.54	3.65	-	n.d.	8.41	n.d.
	I	3	3	2	-	-	1	-
	M	S	S	S	-	-	S	-
	J	-	-	-	-	-	-	-
EMAC 10164	δ	2.49	2.50	3.63	-	7.99	8.45	n.d.
	I	3	3	2	-	1	1	-
	M	S	S	S	S	S	-	-
	J	-	-	-	-	-	-	-
EMAC 10164k	δ	2.51	2.51	3.65	-	7.99	8.51	12.55
	I	3	3	2	-	1	1	1
	M	S	S	S	S	S	-	S
	J	-	-	-	-	-	-	-
EMAC 10164m	δ	2.51	2.53	3.65	3.86	8.01	8.48	n.d.
	I	3	3	2	3	1	1	-
	M	S	S	S	S	S	S	-
	J	-	-	-	-	-	-	-

n.d. – non defined

The protons H (5) and H (7) showed singlet multiplicity with chemical shifts between δ 7.96 and δ 8.51 ppm, in all compounds. The proton H (5) is an exception on compound EMAC10164h since the signal was identified as multiplet.

The benzenic ring protons showed as multiplets, for all compounds.

The protons from the CH₃ and CH₂ groups were identified as singlets, for all compounds, at chemical shifts between δ 2.38 and δ 3.66 ppm, integrating for 3 H and 2 H, respectively, thus confirming the identity of these groups.

The proton of the carboxylic group was identified as broad singlet at chemical shifts between δ 12.49 and δ 12.55 ppm, characteristic zone for this group [312], for four compounds. On the other five compounds this signal was not present, but the group was confirmed by carbon NMR.

On Table 24 and Table 25 are highlighted the ¹³C and DEPT NMR data (underlined values) of the EMAC10164 series, indicating the chemical shifts (δ) in ppm. From the ¹³C and DEPT spectra it was possible to identify some signs.

The carbons from the CH₃ and CH₂, present in the ¹³C and DEPT NMR spectrum, were identified with chemical shifts between δ 8.66 and δ 55.70 ppm, for all compounds.

For the compound EMAC10164d the carbons of the benzene ring were identified as doublets. C (1') and C (4') are present in the ¹³C NMR spectra with chemical shifts δ 127.71 and δ 162.30 ppm and coupling constant of 3.1 and 225 Hz, respectively. C (2') and C (6'), and C (3') and C (5') are present in the ¹³C and DEPT NMR spectrum with chemical shifts of δ 129.67 and δ 116.52 ppm and coupling constant of 8.1 and 21.5 Hz, respectively. All these data are in agreement with the literature for fluorinated compounds [312].

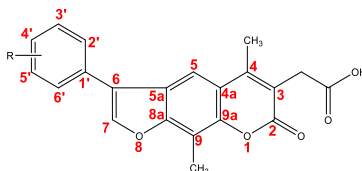
For the compound EMAC10163h the carbons C (5), C (7), C (2') and C (4') showed doublet multiplicity, C (3') triplet multiplicity and C (1'), C (5') and C (6') double doublet multiplicity. C (2') and C (4') are present in the ¹³C NMR spectra with chemical shifts δ 159.91 and δ 162.38 ppm and coupling constants of 237.2 and 235.7 Hz, respectively. C (5), and C (7) are present in the ¹³C NMR and DEPT spectrum with chemical shifts δ 114.48 and δ 146.16 ppm and coupling constants of 3.1 and 5.5, respectively. C (3') is present in the ¹³C NMR and DEPT spectrum with chemical shift δ 105.03 ppm and coupling constant of 26.2Hz. All these data are in agreement with the literature for fluorinated compounds [312].

The carbon of the carboxylic group was identified with chemical shifts between δ 171.93 and δ 172.01 ppm, for all compounds.

For carbons to which it was not possible to assign a signal it is necessary to obtain two-dimensional NMR spectra. However, the number of signals present agrees with the

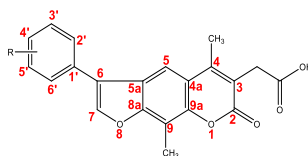
number of carbon atoms in the molecule and the set of analyzes performed confirms the identity of the compounds.

Table 24. ^{13}C and DEPT NMR data from EMAC10164a-d (solvent: DMSO).



Compound	EMAC 10164a	EMAC 10164b	EMAC 10164c	EMAC 10164d
C(9)CH₃	<u>8.66</u>	<u>8.71</u>	<u>8.68</u>	<u>8.66</u>
C(4)CH₃	<u>16.07</u>	<u>16.13</u>	<u>16.13</u>	<u>16.11</u>
CH₂	<u>33.44</u>	<u>33.42</u>	<u>33.40</u>	<u>33.39</u>
C(X')YCH₃	<u>21.29</u>	<u>55.70</u>	-	-
C(3'), C(5')	<u>n.d.</u>	<u>n.d.</u>	<u>n.d.</u>	<u>116.52</u> (<i>d</i> , <i>J</i> = 21.5 Hz)
C(5)	<u>114.18</u>	<u>114.28</u>	<u>114.25</u>	<u>114.17</u>
C(1')	<u>n.d.</u>	<u>n.d.</u>	<u>n.d.</u>	127.71 (<i>d</i> , <i>J</i> = 3.1 Hz)
C(2'), C(6')	<u>n.d.</u>	<u>n.d.</u>	<u>n.d.</u>	<u>129.67</u> (<i>d</i> , <i>J</i> = 8.1 Hz)
C(7)	<u>144.07</u>	<u>143.70</u>	<u>144.93</u>	<u>144.51</u>
C(4')	<u>n.d.</u>	<u>n.d.</u>	<u>n.d.</u>	162.30 (<i>d</i> , <i>J</i> = 225 Hz)
C(4a), C(3), C(9), C(5a), C(4), C(9a), C(8a), C(2), C(6)	<u>n.d.</u>	<u>n.d.</u>	<u>n.d.</u>	<u>n.d.</u>
COOH	<u>171.99</u>	<u>171.98</u>	<u>171.95</u>	<u>171.97</u>

n.d. – non defined

Table 25. ^{13}C and DEPT NMR data from EMAC10164g-h and j-m (solvent: DMSO).

Compound	EMAC 10164g	EMAC 10164h	EMAC 10164j	EMAC 10164k	EMAC 10164m
C(9)CH₃	<u>8.69</u>	<u>8.68</u>	<u>8.66</u>	<u>8.68</u>	<u>8.69</u>
C(4)CH₃	<u>16.10</u>	<u>16.07</u>	<u>16.08</u>	<u>16.12</u>	<u>16.08</u>
CH₂	<u>34.03</u>	<u>33.42</u>	<u>33.47</u>	<u>33.41</u>	<u>33.42</u>
C(X')YCH₃	-	-	-	-	55.67
C(3')	<u>n.d.</u>	<u>105.30</u> (<i>t</i> , <i>J</i> = 26.2 Hz)	<u>n.d.</u>	<u>n.d.</u>	<u>n.d.</u>
C(5')	<u>n.d.</u>	<u>112.74</u> (<i>dd</i> , <i>J</i> = 21.3, 3.5 Hz)	<u>n.d.</u>	<u>n.d.</u>	<u>n.d.</u>
C(5)	<u>114.17</u>	<u>114.48</u> (<i>d</i> , <i>J</i> = 3.1 Hz)	<u>114.19</u>	<u>114.24</u>	<u>n.d.</u>
C(1')	<u>n.d.</u>	<u>115.36</u> (<i>dd</i> , <i>J</i> = 14.6, 3.2 Hz)	<u>n.d.</u>	<u>n.d.</u>	<u>n.d.</u>
C(2')	<u>n.d.</u>	<u>159.91</u> (<i>d</i> , <i>J</i> = 237.2 Hz)	<u>n.d.</u>	<u>n.d.</u>	<u>n.d.</u>
C(6')	<u>n.d.</u>	<u>131.96</u> (<i>dd</i> , <i>J</i> = 9.8, 5.3 Hz)	<u>n.d.</u>	<u>n.d.</u>	<u>n.d.</u>
C(7)	<u>144.60</u>	<u>146.16</u> (<i>d</i> , <i>J</i> = 5.5 Hz)	<u>144.50</u>	<u>144.95</u>	<u>144.77</u>
C(4')	<u>n.d.</u>	<u>162.38</u> (<i>d</i> , <i>J</i> = 235.7 Hz)	<u>n.d.</u>	<u>n.d.</u>	<u>n.d.</u>
C(4a), C(3), C(9), C(5a), C(4), C(9a), C(8a), C(2), C(6)	<u>n.d.</u>	<u>n.d.</u>	<u>n.d.</u>	<u>n.d.</u>	<u>n.d.</u>
COOH	<u>172.01</u>	<u>171.93</u>	<u>172.00</u>	<u>171.95</u>	<u>171.97</u>

n.d. – non defined

3.3.4. Phenylethanone compounds (EMAC10168 series)

This series was characterized by ^1H , ^{13}C and DEPT NMR spectrometry (spectra on Appendix).

On Table 26 and Table 27 are highlighted the ^1H NMR chemical shifts of the EMAC10168 series, indicating chemical shifts (δ), in ppm, the number of protons (I), the signal multiplicity (M) and the coupling constants (J) in Hz. From the obtained ^1H NMR spectrum was possible to identify characteristic signals of some protons.

The protons H (3) and H (6) showed doublet multiplicity with chemical shifts between $\delta 6.38$ and $\delta 7.68$ ppm and coupling constants between 2.5 and 2.6 Hz for H (3) (in -meta position related to H (5)) and 8.9 Hz for H (6) (in -ortho position related to H(5)) [312] , in all compounds. The proton H (6) is an exception on compound EMAC10168c and 10168g since the signs were identified as multiplets.

It was possible to identify the proton H (5) as a double doublet with chemical shifts between $\delta 6.53$ and $\delta 6.56$ ppm and coupling constants of 2.6 and 8.9 Hz, since H (5) is in -ortho position related to H (6) and -meta position related to H (3) [312].

The benzenic ring protons showed as multiplets, for all compounds.

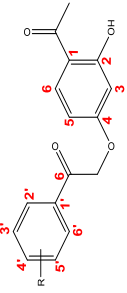
The protons from the CH_3 and CH_2 groups were identified as singlets, for all compounds, at chemical shifts between $\delta 2.55$ and $\delta 5.35$ ppm, integrating for 3 H and 2 H, respectively, thus confirming the identity of these groups.

The proton of the hydroxyl group showed singlet multiplicity at chemical shifts between $\delta 12.68$ and $\delta 12.70$ ppm, characteristic zone for this group [312], in all compounds.

On Table 28 are highlighted the ^{13}C and DEPT NMR data (underlined values) of the EMAC10168 series, indicating the chemical shifts (δ) in ppm. From the ^{13}C and DEPT spectra it was possible to identify some signals.

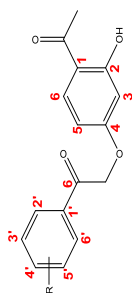
The carbons from the CH_3 and CH_2 , present in the ^{13}C and DEPT NMR spectrum, were identified with chemical shifts between $\delta 21.80$ and $\delta 70.41$ ppm, for all compounds.

For the compound EMAC10164d the carbons of the benzene ring were identified as doublets. C (1') and C (4') are present in the ^{13}C NMR spectra with chemical shifts $\delta 130.68$ and $\delta 166.30$ ppm and coupling constant of 3.1 and 254 Hz, respectively. C (2') and C (6'), and C (3') and C (5') are present in the ^{13}C and DEPT NMR spectrum with chemical shifts of $\delta 130.88$ and $\delta 116.23$ ppm and coupling constant of 9.5 and 22.0 Hz, respectively. All these data are in agreement with the literature for fluorinated compounds [312].

Table 26. ¹H NMR data from EMAC10168a-d (solvent: CDCl₃).


Compound	δ	CH ₃	C(4')XCH ₃	CH ₂	H(3)	H(5)	H(6)	H(2'), H(3'), H(5'), H(6')	OH
EMAC10168a		2.55	2.44	5.30	6.39	6.54	7.65	n.d.	12.68
	I	3	3	2	1	1	1	-	1
	M	s	s	s	d	dd	d	-	s
	J	-	-	-	2.5	8.9, 2.6	8.9	-	-
EMAC10168b		2.55	3.89	5.27	6.39	6.53	7.65	n.d.	12.68
	I	3	3	2	1	1	1	-	1
	M	s	s	s	d	dd	d	-	s
	J	-	-	-	2.5	8.9, 2.6	8.9	-	-
EMAC10168c		2.58	-	5.29	6.40	6.54	n.d.	n.d.	12.70
	I	3	-	2	1	1	-	-	1
	M	s	-	s	d	dd	-	-	s
	J	-	-	-	2.5	8.9, 2.6	-	-	-
EMAC10168d		2.58	-	5.30	6.40	6.55	7.68	n.d.	12.70
	I	3	-	2	1	1	1	-	1
	M	s	-	s	d	dd	d	-	s
	J	-	-	-	2.6	8.9, 2.6	8.9	-	-

n.d. – non defined

Table 27. ^1H NMR data from EMAC10168g, k, and m (solvent: CDCl_3).

Compound	δ	CH_3	$\text{C}(3')\text{OCH}_3$	CH_2	H(3)	H(5)	H(6)	H(2'), H(3'), H(4'), H(5'), H(6')	OH
EMAC10168g		2.56	-	5.35	6.42	6.56	n.d.	n.d.	12.69
	I	3	-	2	1	1	-	-	1
	M	s	-	s	d	dd	-	-	s
	J	-	-	-	2.5	8.9, 2.6	-	-	-
EMAC10168k		2.58	-	5.29	6.40	6.54	7.68	n.d.	12.70
	I	3	-	2	1	1	1	-	1
	M	s	-	s	d	dd	d	-	s
	J	-	-	-	2.6	8.9, 2.6	8.9	-	-
EMAC10168m		2.55	3.87	5.32	6.38	6.54	7.65	n.d.	12.69
	I	3	3	2	1	1	1	-	1
	M	s	s	s	d	dd	d	-	s
	J	-	-	-	2.5	8.9, 2.6	8.9	-	-

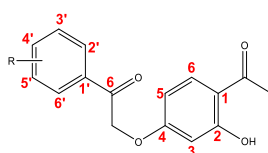
n.d. – non defined

The carbon of the ketone group was identified with chemical shifts between δ 191.49 and δ 192.80 ppm, for all compounds.

The carbon of the acetyl group was identified with chemical shifts between δ 202.69 and δ 202.73 ppm, for all compounds.

For carbons to which it was not possible to assign a signal it is necessary to obtain two-dimensional NMR spectra. However, the number of signals present agrees with the number of carbon atoms in the molecule and the set of analyzes performed confirms the identity of the compounds.

Table 28. ^{13}C and DEPT NMR data from the EMAC10168 series (solvent: CDCl_3).



Compound	EMAC 10168a	EMAC 10168b	EMAC 10168c	EMAC 10168d	EMAC 10168g	EMAC 10168k	EMAC 10168m
C(X)YCH_3	<u>21.80</u>	<u>55.58</u>	-	-	-	-	<u>55.54</u>
C(1)OCH_3	<u>26.27</u>	<u>26.27</u>	<u>26.30</u>	<u>26.28</u>	<u>26.28</u>	<u>26.29</u>	<u>26.28</u>
CH_2	<u>70.27</u>	<u>70.22</u>	<u>70.35</u>	<u>70.33</u>	<u>70.41</u>	<u>70.37</u>	<u>70.35</u>
$\text{C(3')}, \text{C(5')}$	<u>n.d.</u>	<u>n.d.</u>	<u>n.d.</u>	<u>116.23</u> (<i>d</i> , <i>J</i> = 22.0 Hz)	<u>n.d.</u>	<u>n.d.</u>	<u>n.d.</u>
C(1')	<u>n.d.</u>	<u>n.d.</u>	<u>n.d.</u>	130.68 (<i>d</i> , <i>J</i> = 3.1 Hz)	<u>n.d.</u>	<u>n.d.</u>	<u>n.d.</u>
$\text{C(2')}, \text{C(6')}$	<u>n.d.</u>	<u>n.d.</u>	<u>n.d.</u>	<u>130.88</u> (<i>d</i> , <i>J</i> = 9.5 Hz)	<u>n.d.</u>	<u>n.d.</u>	<u>n.d.</u>
C(4')	<u>n.d.</u>	<u>n.d.</u>	<u>n.d.</u>	166.30 (<i>d</i> , <i>J</i> = 254 Hz)	<u>n.d.</u>	<u>n.d.</u>	<u>n.d.</u>
$\text{C(3)}, \text{C(5)}, \text{C(6)}$	<u>n.d.</u>	<u>n.d.</u>	<u>n.d.</u>	<u>n.d.</u>	<u>n.d.</u>	<u>n.d.</u>	<u>n.d.</u>
$\text{C(1)}, \text{C(2)}, \text{C(4)}$	<u>n.d.</u>	<u>n.d.</u>	<u>n.d.</u>	<u>n.d.</u>	<u>n.d.</u>	<u>n.d.</u>	<u>n.d.</u>
CO	192.58	191.49	192.39	191.69	192.63	192.16	192.80
COCH_3	202.70	202.69	202.74	202.73	202.71	202.73	202.71

n.d. – non defined

3.3.5. 4H-chromene compounds (EMAC10169 series)

This series was characterized by ^1H , ^{13}C , DEPT NMR (spectra on Appendix).and ESI/MS spectrometry

On Table 29 and Table 30 are highlighted the ^1H NMR chemical shifts of the EMAC10169 series, indicating chemical shifts (δ), in ppm, the number of protons (I), the signal multiplicity (M) and the coupling constants (J) in Hz. From the obtained ^1H NMR spectrum was possible to identify characteristic signals of some protons.

The protons H (8), H (6) and H (5) showed doublet, double doublet, and doublet multiplicity, respectively, in all compounds. The chemical shifts for H (8) are between $\delta 6.91$ and $\delta 7.39$ ppm and the coupling constant is 2.4 Hz, since this proton is in -meta position related to H (6). The peak for H (6) was shown at chemical shifts between $\delta 7.09$ and $\delta 7.24$ ppm with coupling constants of 8.9 and 2.4 Hz since this proton has the H (5) in -ortho position and the H (8) in -meta position. The proton H (5) showed chemical shifts between $\delta 8.06$ and $\delta 8.23$ ppm and coupling constant 8.9 Hz, expected due to the H (6) in -ortho position [312]. The proton H (2) was identified, in all compounds, as singlet at chemical shifts between $\delta 8.44$ and $\delta 8.84$ ppm.

The benzenic ring protons showed as multiplets, for all compounds.

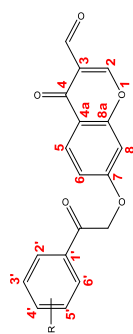
The protons from the CH_3 and CH_2 groups were identified as singlets, for all compounds, at chemical shifts between $\delta 2.45$ and $\delta 5.82$ ppm, integrating for 3 H and 2 H, respectively, thus confirming the identity of these groups.

The proton from the aldehyde group showed singlet multiplicity at chemical shifts between $\delta 10.11$ and $\delta 10.37$ ppm, characteristic zone for this group, in all compounds.

Table 31 highlights the ^{13}C and DEPT NMR data (underlined values) of the EMAC10169 series, indicating the chemical shifts (δ) in ppm. From the ^{13}C and DEPT spectra it was possible to identify some signals.

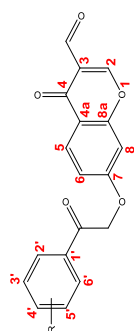
The carbons from the CH_3 and CH_2 , present in the ^{13}C and DEPT NMR spectrum, were identified with chemical shifts between $\delta 21.84$ and $\delta 71.30$ ppm, for all compounds.

For the compound EMAC10169d the carbons of the benzene ring were identified as doublets. C (1') and C (4') are present in the ^{13}C NMR spectra with chemical shifts $\delta 131.40$ and $\delta 165.90$ ppm and coupling constants of 2.8 and 252.6 Hz, respectively. C (2') and C (6'), and C (3') and C (5') are present in the ^{13}C and DEPT NMR spectrum with chemical shifts $\delta 131.51$ and $\delta 116.41$ ppm and coupling constants of 9.6 and 18.7 Hz, respectively. All these data agree with the literature for fluorinated compounds [312].

Table 29. ¹H NMR data from EMAC10169a-d (solvents: CDCl₃ – a, DMSO – b, c, d).

Compound	C(4')XCH ₃	CH ₂	H(6)	H(6)	H(5)	C(2'), H(3'), H(5'), H(6')	H(2)	CHO
EMAC10169a	δ	2.45	5.42	6.91	7.10	8.21	n.d.	10.36
	I	3	2	1	1	1	1	1
	M	s	s	d	dd	d	s	s
	J	-	-	2.4	8.9, 2.4	8.9	-	-
EMAC10169b	δ	3.90	5.39	6.91	7.10	8.20	n.d.	10.36
	I	3	2	1	1	1	1	1
	M	s	s	d	dd	d	s	s
	J	-	-	2.4	8.9, 2.4	8.9	-	-
EMAC10169c	δ	-	5.81	7.39	7.24	8.06	n.d.	10.11
	I	-	2	1	1	1	1	1
	M	-	s	d	dd	d	s	s
	J	-	-	2.4	8.9, 2.4	8.9	-	-
EMAC10169d	δ	-	5.82	7.38	7.24	8.06	n.d.	10.12
	I	-	2	1	1	1	1	1
	M	-	s	d	dd	d	s	s
	J	-	-	2.4	8.9, 2.4	8.9	-	-

n.d. – non defined

Table 30. ¹H NMR data from EMAC 10169g, k, and m (solvent: CDCl₃).

Compound	C(3') OCH ₃	CH ₂	H(8)	H(6)	H(5)	C(2'), H(3'), H(4'), H(5'), H(6')	H(2)	CHO
EMAC10169g	δ	5.47	6.94	7.13	8.23	n.d.	8.46	10.37
	I	2	1	1	1	-	1	1
	M	s	d	dd	d	-	s	s
	J	-	2.4	8.9, 2.4	8.9	-	-	-
EMAC10169k	δ	5.39	6.92	7.09	8.22	n.d.	8.45	10.36
	I	2	1	1	1	-	1	1
	M	s	d	dd	d	-	s	s
	J	-	2.4	8.9, 2.4	8.9	-	-	-
EMAC10169m	δ	5.43	6.91	7.10	8.22	n.d.	8.45	10.37
	I	2	1	1	1	-	1	1
	M	s	d	dd	d	-	s	s
	J	-	2.4	8.9, 2.4	8.9	-	-	-

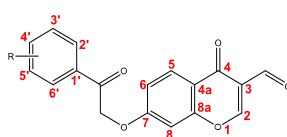
n.d. – non defined

The carbon of the aldehyde group, present in the ^{13}C and DEPT NMR spectra, was identified with chemical shifts between $\delta 188.71$ and $\delta 189.02$ ppm, for all compounds.

The carbon of the ketone group was identified with chemical shifts between $\delta 191.14$ and $\delta 193.24$ ppm, for all compounds.

For carbons to which it was not possible to assign a signal it is necessary to obtain two-dimensional NMR spectra. However, the number of signals present agrees with the number of carbon atoms in the molecule and the set of analyzes performed confirms the identity of the compounds.

Table 31. ^{13}C and DEPT NMR data from the EMAC10169 series (solvent: CDCl_3 – a, g, k, m; DMSO – b, c, d).



Compound	EMAC 10169a	EMAC 10169b	EMAC 10169c	EMAC 10169d	EMAC 10169g	EMAC 10169k	EMAC 10169m
$\text{C}(\text{X}')\text{YCH}_3$	<u>21.84</u>	<u>55.63</u>	-	-	-	-	<u>55.57</u>
$\underline{\text{C}}\text{H}_2$	<u>70.65</u>	<u>70.58</u>	<u>71.30</u>	<u>71.25</u>	<u>70.79</u>	<u>70.72</u>	<u>70.73</u>
$\text{C}(3')$	<u>n.d.</u>	<u>n.d.</u>	<u>n.d.</u>	<u>116.41</u>	<u>n.d.</u>	<u>n.d.</u>	n.d.
$\text{C}(5')$	<u>n.d.</u>	<u>n.d.</u>	<u>n.d.</u>	(d, $J = 18.7$ Hz)	<u>n.d.</u>	<u>n.d.</u>	<u>n.d.</u>
$\text{C}(1')$	n.d.	n.d.	n.d.	131.40 (d, $J = 2.8$ Hz)	n.d.	n.d.	n.d.
$\text{C}(2'), \text{C}(6')$	<u>n.d.</u>	<u>n.d.</u>	<u>n.d.</u>	<u>131.51</u> (d, $J = 9.6$ Hz)	<u>n.d.</u>	<u>n.d.</u>	<u>n.d.</u>
$\text{C}(4')$	n.d.	n.d.	n.d.	165.90 (d, $J = 252.6$ Hz)	n.d.	n.d.	<u>n.d.</u>
$\text{C}(8), \text{C}(6),$ $\text{C}(5), \text{C}(2)$	<u>n.d.</u>	<u>n.d.</u>	<u>n.d.</u>	<u>n.d.</u>	<u>n.d.</u>	<u>n.d.</u>	<u>n.d.</u>
$\text{C}(4), \text{C}(4a),$ $\text{C}(7), \text{C}(8a)$	n.d.	n.d.	n.d.	n.d.	n.d.	n.d.	n.d.
$\underline{\text{C}}\text{HO}$	<u>188.78</u>	<u>188.78</u>	<u>189.01</u>	<u>189.02</u>	<u>188.77</u>	<u>188.71</u>	<u>188.77</u>
$\underline{\text{C}}\text{O}$	192.24	191.14	193.24	192.56	192.28	192.76	192.47

n.d. – non defined

Table 32 reports the mass spectrometry data for EMAC10163, EMAC10164 and EMAC10169 series.

Table 32. Mass spectrometry data.

Compound	Molecular Formula	Mass	Theoretical Mass [M+H ⁺]	Experimental Mass [M+H ⁺]	Accuracy (ppm)
EMAC10163a	C ₂₃ H ₂₂ O ₆	394.42	395.1495	395.1487	-2.0
EMAC10163b	C ₂₃ H ₂₂ O ₇	410.42	411.1444	411.1436	-1.9
EMAC10163c	C ₂₂ H ₁₉ BrO ₆	459.29	459.0443	459.0435	-1.7
EMAC10163d	C ₂₂ H ₁₉ FO ₆	398.39	399.1244	399.1235	-2.2
EMAC10163e	C ₂₂ H ₁₉ NO ₈	425.39	426.1189	426.1181	-1.9
EMAC10163f	C ₂₂ H ₁₉ NO ₈	425.39	426.1189	426.1182	-1.6
EMAC10163g	C ₂₈ H ₂₄ O ₆	456.49	457.1652	457.1643	-2.0
EMAC10163h	C ₂₂ H ₁₈ F ₂ O ₆	416.38	417.1150	417.1142	-1.9
EMAC10163j	C ₂₂ H ₂₀ O ₆	380.40	381.1338	381.1330	-2.1
EMAC10163k	C ₂₂ H ₁₉ ClO ₆	414.84	415.0949	415.0940	-2.2
EMAC10163m	C ₂₃ H ₂₂ O ₇	410.42	411.1444	411.1436	-1.9
EMAC10164a	C ₂₂ H ₁₈ O ₅	362.38	363.1233	363.1226	-1.9
EMAC10164b	C ₂₂ H ₁₈ O ₆	378.38	379.1182	379.1174	-2.1
EMAC10164c	C ₂₁ H ₁₅ BrO ₅	427.25	427.0181	427.0173	-1.9
EMAC10164d	C ₂₁ H ₁₅ FO ₅	366.34	367.0982	367.0974	-2.2
EMAC10164g	C ₂₇ H ₂₀ O ₅	424.13	425.1389	425.1382	-1.6
EMAC10164h	C ₂₁ H ₁₄ F ₂ O ₅	384.33	385.0888	385.0880	-2.1
EMAC10164j	C ₂₁ H ₁₆ O ₅	348.35	349.1076	349.1069	-2.0
EMAC10164k	C ₂₁ H ₁₅ ClO ₅	382.80	383.0687	383.0679	-2.1
EMAC10164m	C ₂₂ H ₁₈ O ₆	378.38	379.1182	379.1174	-2.1
EMAC10169a	C ₁₉ H ₁₄ O ₅	322.32	323.0920	323.0912	-2.5
EMAC10169b	C ₁₉ H ₁₄ O ₆	338.32	339.0868	339.0860	-2.4
EMAC10169c	C ₁₈ H ₁₁ BrO ₅	387.19	386.9868	386.9861	-1.8
EMAC10169d	C ₁₈ H ₁₁ FO ₅	326.28	327.0669	327.0661	-2.4
EMAC10169g	C ₂₄ H ₁₆ O ₅	384.10	385.1076	385.1068	-2.1
EMAC10169k	C ₁₈ H ₁₁ ClO ₅	342.03	343.0374	343.0366	-2.3
EMAC10169m	C ₁₉ H ₁₄ O ₆	338.32	339.0868	339.0860	-2.4

3.4. Carbonic anhydrases inhibition

3.4.2. 2H-chromen compounds (EMAC10163 series)

The inhibition activity of human CAs I, II, IX and XII for the EMAC10163 series was measured and is reported on Table 33.

Accordingly, all the active compounds show less potency than the reference, AAZ. Nevertheless, regarding the selectivity some compounds must be highlighted. EMAC10163a – e and EMAC10163h are selective towards CAs IX and XII. EMAC10163f, g, j, k, and m are selective towards CA XII. The compound with better inhibition activity and selectivity towards CAs IX and XII, in this series, is EMAC10163b ($K_i = 0.53 \mu\text{M}$ and $0.47 \mu\text{M}$, respectively), with a methoxy group on the C4 of the benzene ring. The position change of this group in compound EMAC10163m within the benzene ring (precisely to C3) decreases the inhibition potency of the compound towards CA IX and XII ($K_i = >100 \mu\text{M}$ and $4.86 \mu\text{M}$, respectively). The second best compound within this series is EMAC10163a with a methyl group on the C4 of the benzene ring. Significantly, in contrast with what can be observed for non-specific inhibitors such as AAZ, none of the investigated compounds exhibit activity towards CA I and CA II isoforms.

Table 33. Inhibition data of hCA I, II, IX and XII for the EMAC10163 series and AAZ (used as reference).

Compound	R	K_i (μM) [*]			
		hCA I	hCA II	hCA IX	hCA XII
EMAC10163a	4'-CH ₃	> 100	> 100	2.98	2.52
EMAC10163b	4'-OCH ₃	> 100	> 100	0.53	0.47
EMAC10163c	4'-Br	> 100	> 100	4.16	5.43
EMAC10163d	4'-F	> 100	> 100	2.39	6.04
EMAC10163e	4'-NO ₂	> 100	> 100	4.64	7.84
EMAC10163f	3'-NO ₂	> 100	> 100	> 100	7.82
EMAC10163g	4'-Phenyl	> 100	> 100	> 100	8.88
EMAC10163h	2', 4'-F	> 100	> 100	4.51	5.56
EMAC10163j	-	> 100	> 100	> 100	5.25
EMAC10163k	4'-Cl	> 100	> 100	> 100	2.41
EMAC10163m	3'-OCH ₃	> 100	> 100	> 100	4.86
AAZ	-	0.250	0.0125	0.026	0.0057

* Mean from 3 different assays, by a stopped flow technique (errors were in the range of $\pm 5-10$ % of the reported values).

3.4.3. 7H-furo-chromen compounds (EMAC10164series)

Table 34 lists the results from the inhibition activity of *h*CAs I, II, IX and XII for the EMAC10164 series.

Accordingly, all the active compounds show higher values when compared with the reference, AAZ. Nevertheless, concerning the selectivity, some compounds must be emphasized. EMAC10164d, h, and j, k, and m are selective towards CAs IX and XII. EMAC10164g, with a phenyl group in C4 of the benzene ring, is inactive only in CA I. EMAC10164a, b, and c are selective to CA XII. The compound with better inhibitory activity and selectivity towards CAs IX and XII, in this series, is EMAC10164d, with a fluorine in the C4 of the benzene ring. None of the tested compounds was active toward the CA I and CA II isoforms with the exception of compound EMAC10164g. However, this latter compound could also be considered as CA IX and CA XII selective as its K_i concentrations towards CA II isozyme are 34 and 29 folds higher than the K_i concentrations towards CA IX and CA XII, respectively.

Table 34. Inhibition data of *h*CA I, II, IX and XII for the EMAC10164 series and AAZ (used as reference).

Compound	R	K_i (μ M)*			
		<i>h</i> CA I	<i>h</i> CA II	<i>h</i> CA IX	<i>h</i> CA XII
EMAC10164 a	4'-CH ₃	> 100	> 100	> 100	4.09
EMAC10164b	4'-OCH ₃	> 100	> 100	> 100	4.59
EMAC10164c	4'-Br	> 100	> 100	> 100	4.44
EMAC10164d	4'-F	> 100	> 100	0.46	0.80
EMAC10164g	4'-Phenyl	> 100	24.3	0.71	0.82
EMAC10164h	2', 4'-F	> 100	> 100	4.27	6.37
EMAC10164j	-	> 100	> 100	3.18	3.38
EMAC10164k	4'-Cl	> 100	> 100	3.22	7.86
EMAC10164m	3'-OCH ₃	> 100	> 100	4.16	3.66
AAZ	-I	0.250	0.0125	0.026	0.0057

* Mean from 3 different assays, by a stopped flow technique (errors were in the range of \pm 5-10 % of the reported values).

3.4.4. 4H-chromene compounds (EMAC10169 series)

The results from the inhibition activity of human CAs I, II, IX and XII for the EMAC10169 series are listed on Table 35.

Accordingly, all the active compounds show higher values when compared with the reference, AAZ. However, as for the previous compounds, concerning the selectivity, some of them must be highlighted. The compounds EMAC10169a, g, k, and m are selective towards CAs IX and XII. The compounds with better inhibitory activity, in this series, are EMAC10169k, with chlorine in the C4 of the benzene ring, and EMAC10169m, with a methoxy in the C3 of the benzene ring. The position of the methoxy group within the benzene ring is important, since EMAC10169b, with the methoxy group in the C4, turns the compound inactive. The introduction of a phenyl group in the C4 of the benzene ring showed the worse result within the active compounds, but the selectivity was maintained. As well as in the series EMAC10163 also in this series none of the investigated compounds was active toward the CA I and CA II isoforms.

Table 35. Inhibition data of *hCA* I, II, IX and XII for the EMAC10169 series and AAZ (used as reference).

Compound	R	Ki (μM) [*]			
		<i>hCA</i> I	<i>hCA</i> II	<i>hCA</i> IX	<i>hCA</i> XII
EMAC10169a	4'-CH ₃	> 100	> 100	0.44	0.33
EMAC10169b	4'-OCH ₃	> 100	> 100	> 100	> 100
EMAC10169c	4'-Br	> 100	> 100	> 100	> 100
EMAC10169d	4'-F	> 100	> 100	> 100	> 100
EMAC10169g	4'-Phenyl	> 100	> 100	0.86	0.69
EMAC10169k	4'-Cl	> 100	> 100	0.42	0.28
EMAC10169m	3'-OCH ₃	> 100	> 100	0.31	0.24
AAZ	-	0.250	0.0125	0.026	0.0057

* Mean from 3 different assays, by a stopped flow technique (errors were in the range of \pm 5-10 % of the reported values).

3.5. Theoretical prediction of drug-like properties

As described in section 2.6, to estimate the drug-likeness of the compounds, we carried out *in silico* ADMET prediction [313]. In particular, here we report a selection of the predicted properties, the most significant investigated, using the QikProp software [314], for the series EMAC10163, 10164 and 10169.

The analysis of the predicted properties revealed the good drug-likeness of the compounds. However, the enormous quantity of data collected does not allow to insert all the properties values calculated.

For each series of compounds two tables are reported. One containing the structural properties under Lipinski's rule of five (RO5) and other physicochemical properties, and another with other properties that could affect the pharmacokinetics and the toxicity of the compounds.

As it is shown in all the tables, most of the predicted properties are within the ranges specified with only few exceptions.

Table 36. Predicted properties for the series EMAC10163.

Compound	#stars	mol_MW	donorHB	accptHB	QPlogPo/w	#rotor	PSA	QPlogS
	0 – 5	130 – 725	0 – 6	2 – 20	-2 – 6.5	0 – 15	7 – 200.0	-6.5 – 0.5
EMAC 10163a	1	394.42	0	7	3.3	6	106.7	-5.0
EMAC 10163b	0	410.42	0	8	3.0	7	115.0	-5.0
EMAC 10163c	0	459.29	0	7	3.5	6	106.7	-6.4
EMAC 10163d	0	398.39	0	7	3.2	6	106.7	-5.1
EMAC 10163e	1	425.39	0	8	2.2	7	151.7	-5.2
EMAC 10163f	2	425.39	0	8	2.2	7	151.6	-5.2
EMAC 10163g	2	456.49	0	7	4.6	7	106.7	-6.7
EMAC 10163h	0	416.38	0	7	3.3	6	106.6	-5.5
EMAC 10163j	0	380.40	0	7	2.9	6	106.7	-4.8
EMAC 10163k	0	414.84	0	7	3.4	6	106.7	-5.5
EMAC 10163m	1	410.42	0	8	3.0	7	114.9	-5.0

Table 37. Predicted properties for the series EMAC10164.

Compound	#stars	mol_MW	donorHB	accptHB	QPlogPo/w	#rotor	PSA	QPlogS
	0 – 5	130 – 725	0 – 6	2 – 20	-2 – 6.5	0 – 15	7 – 200.0	-6.5 – 0.5
EMAC 10164a	0	362.38	1	5	9.8	2	93.0	-5.7
EMAC 10164b	0	378.38	1	6	10.3	3	101.3	-5.8
EMAC 10164c	0	427.25	1	5	9.8	2	93.0	-7.0
EMAC 10164d	0	366.34	1	5	9.8	2	93.0	-5.8
EMAC 10164g	1	424.45	1	5	11.0	3	93.0	-7.4
EMAC 10164h	0	384.34	1	5	9.7	2	93.0	-6.2
EMAC 10164j	0	348.35	1	5	10.0	2	93.0	-5.4
EMAC 10164k	0	382.80	1	5	9.8	2	93.0	-6.1
EMAC 10164m	0	378.38	1	6	10.3	3	101.3	-5.8

Table 38. Predicted properties for the series EMAC10169.

Compound	#stars	mol_MW	donorHB	accptHB	QPlogPo/w	#rotor	PSA	QPlogS
	0 – 5	130 – 725	0 – 6	2 – 20	-2 – 6.5	0 – 15	7 – 200.0	-6.5 – 0.5
EMAC 10169a	0	322.32	0	7	4.0	5	106.9	-3.5
EMAC 10169b	0	338.32	0	8	3.8	6	115.2	-3.5
EMAC 10169c	0	387.19	0	7	4.3	5	106.9	-4.9
EMAC 10169d	0	326.28	0	7	4.0	5	106.9	-3.6
EMAC 10169g	1	384.39	0	7	5.4	6	106.9	-5.2
EMAC 10169k	0	342.74	0	7	4.1	5	106.9	-4.0
EMAC 10169m	0	338.32	0	8	3.7	6	115.2	-3.5

Regarding the pharmacokinetics properties calculated considering 95% of drugs, the recommended ranges are listed on Table 39, and the predicted values for the three series are comprised in the tables that follow.

Table 39. Ranges of pharmacokinetics properties calculated considering 95% of drugs.

Property	Recommended range
QPPCaco	< 25 poor >500 great
QPPMDCK	< 25 poor >500 great
PercentHumanOralAbsorption (%OA)	> 80 % is high < 25 % is poor
QPIlogHERG	>-5
CNS	- 2 (inactive) to +2 (active)
QplogBB	-3.0 – 1.2
QplogKhsa	-1.5 – 1.5

Table 40. Predicted pharmacokinetics properties for the series EMAC10163.

Compound	QPPCaco	QPPMDCK	%OA	KPIlogHERG	CNS	QPIlogBB	QPIlogKhsa
EMAC 10163a	314.0	141.4	90.8	-6.0	-2	-1.5	0.1
EMAC 10163b	314.2	141.6	89.2	-6.0	-2	-1.6	-0.1
EMAC 10163c	314.2	374.2	92.2	-6.1	-2	-1.3	0.1
EMAC 10163d	314.5	254.4	90.2	-6.0	-2	-1.4	0.0
EMAC 10163e	37.3	14.2	67.9	-6.1	-2	-2.6	-0.1
EMAC 10163f	37.7	14.3	68.0	-6.0	-2	-2.6	-0.1
EMAC 10163g	313.5	141.2	100.0	-7.3	-2	-1.7	0.6
EMAC 10163h	316.8	341.9	91.0	-5.9	-2	-1.3	0.0
EMAC 10163j	314.0	141.5	88.8	-6.1	-2	-1.5	-0.0
EMAC 10163k	314.4	348.8	91.8	-6.0	-2	-1.3	0.1
EMAC 10163m	314.7	141.8	89.2	-6.0	-2	-1.6	-0.1

Table 41. Predicted pharmacokinetics properties for the series EMAC10164.

Compound	QPPCaco	QPPMDCK	%OA	KPlogHERG	CNS	QPlogBB	QPlogKhsa
EMAC 10164a	101.1	52.8	86.5	-3.8	-2	-1.0	0.5
EMAC 10164b	101.0	52.8	85.2	-3.8	-2	-1.1	0.3
EMAC 10164c	101.0	139.6	88.0	-3.9	-1	-0.9	0.4
EMAC 10164d	101.0	94.8	86.0	-3.8	-1	-0.9	0.4
EMAC 10164g	101.0	52.8	81.2	-5.1	-2	-1.2	0.9
EMAC 10164h	101.2	130.4	86.8	-3.7	-1	-0.8	0.4
EMAC 10164j	101.0	52.8	84.7	-3.9	-2	-1.0	0.3
EMAC 10164k	101.1	130.1	87.6	-3.8	-1	-0.9	0.4
EMAC 10164m	101.1	52.8	85.2	-3.8	-2	-1.1	0.3

Table 42. Predicted pharmacokinetics properties for the series EMAC10169.

Compound	QPPCaco	QPPMDCK	%OA	KPlogHERG	CNS	QPlogBB	QPlogKhsa
EMAC 10169a	238.8	105.2	78.9	-5.8	-2	-1.4	-0.6
EMAC 10169b	238.7	105.2	77.3	-5.8	-2	-1.5	-0.8
EMAC 10169c	238.9	278.2	81.2	-6.2	-2	-1.3	-0.5
EMAC 10169d	239.0	189.0	78.4	-5.8	-2	-1.3	-0.7
EMAC 10169g	238.7	105.2	86.8	-7.1	-2	-1.6	-0.1
EMAC 10169k	238.9	259.2	79.9	-5.8	-2	-1.2	-0.6
EMAC 10169m	239.2	105.4	77.3	-5.8	-2	-1.5	-0.8

All compounds showed from 0 to 2 stars, which indicates that most of them did not exceed the ranges allowed for the following properties: MW, dipole, IP, EA, SASA, FOSA, FISA, PISA, WPSA, PSA, volume, #rotor, donorHB, accptHB, glob, QPpolrz, QPlogPC16, QPlogPoct, QPlogPw, QPlogPo/w, logS, QPLogKhsa, QPlogBB, and #metabol.

In this respect for the g derivatives the biphenyl substitution influences slightly the solubility. The other properties out of range are borderline values.

Additionally, we reported in Table 40, Table 41, and Table 42 few more ADME properties such as: QPPCaco, QPPMDCK, %OA, and QPlogHERG, that contribute to depict a more complete picture.

In fact, tissue distribution is an important element of a drug pharmacokinetic profile united with knowledge of the *in vitro* activity.

The Caco-2 cell monolayer resembles the human intestinal barrier also considering their characteristic in terms of morphology, the monolayer is used routinely to predict drug permeability in the intestine and the fraction of dose absorbed. QSAR models have been developed to predict bioactive compound's passive permeability of gut blood-barrier using data collected experimentally studying these cells, these data do not consider the Pgp efflux [315].

While QSAR models based on data of compounds able to cross the membrane of MDCK (Madin-Darby Canine Kidney) cells can help to understand the ability of the compounds to reach the CNS [316, 317].

In general, all the synthesized compounds have a high predicted oral absorption, and a good gut absorption, except for the nitro- derivatives. The permeability values are lower for the predicted MDCK cells crossing, which indicates a predicted difficulty by these compounds to reach the central nervous system (CNS). This is also shown by the value of -2 of almost all compounds for CNS property and the values of QPlogBB.

The only worrying property is the predicted IC₅₀ for human Ether-à-go-go-Related Gene (HERG) K⁺ Channel Blockage in EMAC10163 and EMAC10168 series, and EMAC10164g compound. The HERG potassium channel plays an important role in cardiac action potential. Many drugs have been withdrawn from the market due to serious HERG-related cardiotoxicity [318]. In certain cases, the value is borderline, in others, requires more attention and should be further experimentally investigated.

Finally, predicted binding to human serum albumin (QPlogKhsa) are within -0,1 – 0.8 ranges, while the reported drugs range is between -1.5 – 1.5. Therefore, we can be confident that, considering these data, all the synthesized compounds may not extensively bind the plasmatic proteins. This should be favorable for the duration and distribution process.

To conclude, the study of the physical-chemical and pharmacokinetic properties is encouraging, emphasizing that these data should be confirmed *in vitro*. Nevertheless, from

the data obtained and eventually by means of some optimization rounds, we are confident that in due course some pharmacokinetic problems can be solved.

Furthermore, other strategies like proper formulations or nanotechnology applications could ultimately help to overcome their limitation to address the tumor localization.

3.6. Molecular docking

Before docking the best compounds of the synthesized series, cross docking experiments were carried out, in order to validate the protocol. In Table 11, section 2.7 are reported the RMSD values between experimental binding mode and best three docking poses of each ligand of selected best protocol. The validation considered twelve ligands for the IX and twenty-three for the XII isoform. Most of the ligands were correctly docked (RMSD < 2.5 Å). However, it was observed that the protocol failed with some ligands co-crystallized in IX isoform i.e pdb code 6G98 and 6G9U. In these complexes the ligand shows a benzosulphonamide moiety in orto position substituted with a bulky group. At the same time these ligands are provided of a p-benzoic moiety. Hence, the docking program selected, as preferred pose, the orientation with the benzoic group chelating the Zn²⁺. Furthermore, the side chain of Gln90 residue, is slightly rotated compared to the crystal chosen (5FL4). The protocol failed also in reproducing the experimental binding mode of 6TL5. In this case the docking pose orientation was correct, but the sulphonamide moiety was slightly shifted and not able to correctly chelate the Zn²⁺. Within the tested compounds, the two compounds that showed the highest potency towards *hCA* IX and XII isoforms of each series were selected and their mechanism of action was investigated in more detail by docking experiments.

Concerning the XII, the ligands whose binding was not fully reproduced are the ones co-crystallized in pdb 4QJW and 4KP8 . In both cases, the benzosulphonamide moiety position is correctly predicted, while the external portion substituents is flipped. However, the electro density map of both crystal is not well defined, revealing that this portion is not fixed. In fact, being exposed to the solvent it can easily rotate. Therefore, the docking suggested binding mode is plausible.

Overall, the validation of the docking protocol was extensive and positive. Hence, can be applied to predict the binding mode of the new synthesized compounds.

Within the tested compounds, the two compounds that showed the highest potency towards *hCA* IX and XII isoforms of each series were selected and their binding mode was investigated in more detail by docking experiments to have more information that could be exploited for future compounds optimization.

3.6.1. CA IX docking

Docking experiments of the two compounds of each series were performed to hCA IX considering 5FL4 [303] CA IX conformation.

Considering the docking experiments of EMAC10163a and EMAC10163b, represented in Figure 73, we obtained two different proposed docking for each compound. One of the proposed binding modes is characterized by the chromene ring orientated toward the zinc. On the contrary, in the second proposed mode, the substituted benzene ring is pointing toward the zinc.

In Figure 74 are represented the docking experiments of EMAC10164d and EMAC10164g. For these compounds the proposed docking were always with the chromene ring orientated to the zinc.

Regarding the EMAC10169 series the selected compounds were EMAC10169k and EMAC10169m, which docking experiments are represented in Figure 75. Similarly to the compounds of EMAC10164 series, the only proposed bindings for these compounds were with the chromene ring orientated to the zinc.

The docking experiments that consider the IX isoform, highlighted that the rigidity of the last two series helps to orientate the compounds in the binding pocket with the chromene portion toward the Zn^{2+} . This lead also to a general better activity of the last two series. The influence of the substituents in the phenyl ring is not clear among the different series. Compared to the previous synthesized compounds the introduction of methyl in position C8 and C9 instead of the propyl moiety (in EMAC10157 and EMAC10160 series, respectively) lead to similar activity [238, 239], while the introduction of a second methyl group in the series EMAC10151 and EMAC10152 series was detrimental for the activity.

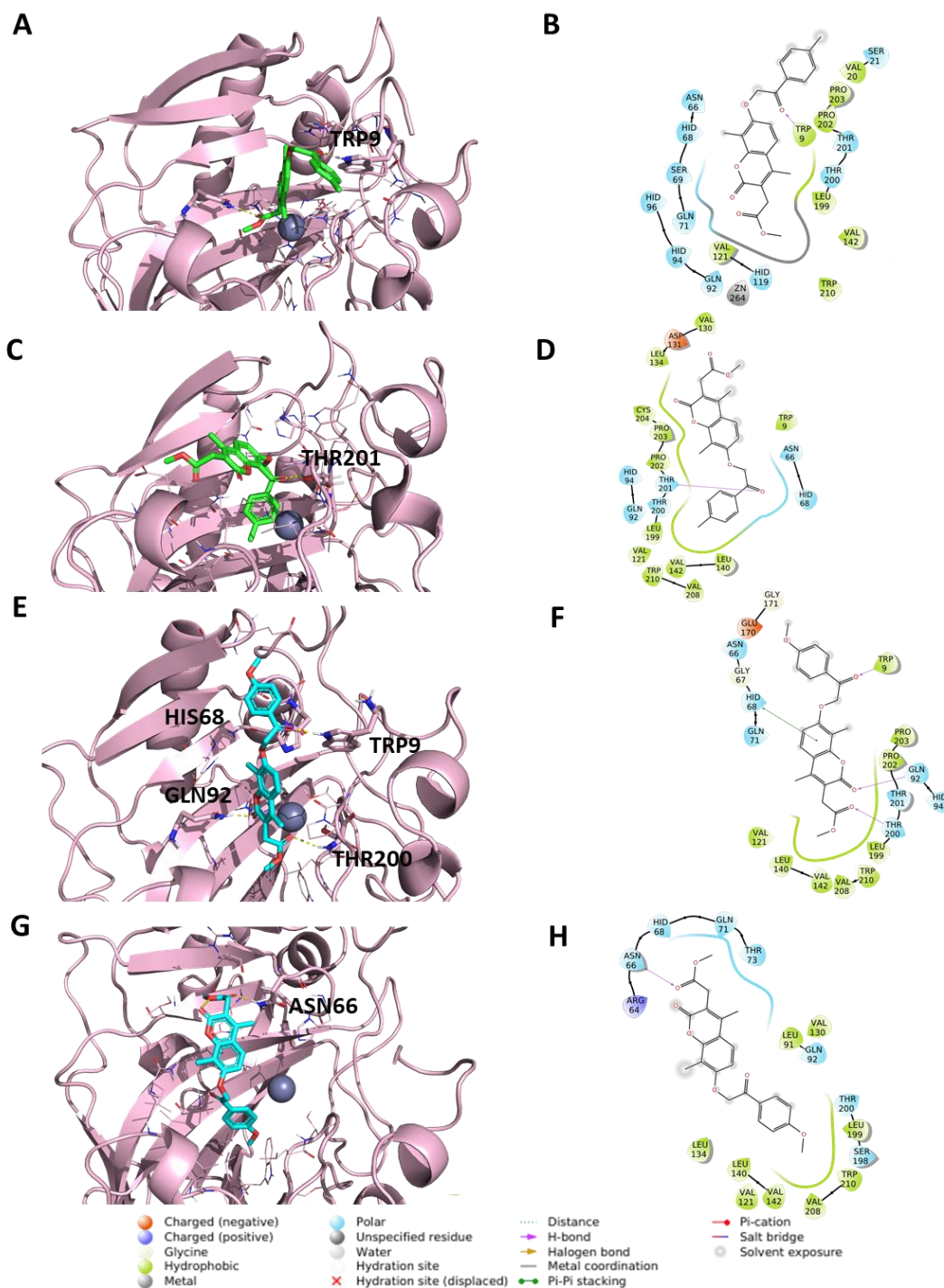


Figure 73. Representation of the putative binding mode of the most potent compounds from EMAC10163 series obtained by docking experiments to *hCA IX*. (A) 3D depiction of EMAC10163a and its respective interactions with CA IX residues; (B) 2D depiction of interactions; (C) 3D depiction of EMAC10163a and its respective interactions with CA IX residues considering a different orientation of the compound; (D) 2D depiction of interactions; (E) 3D depiction of EMAC10163b and its respective interactions with CA IX residues; (F) 2D depiction of interactions; (G) 3D depiction of EMAC10163b and its respective interactions with CA IX residues considering a different orientation of the compound; (H) 2D depiction of interactions.

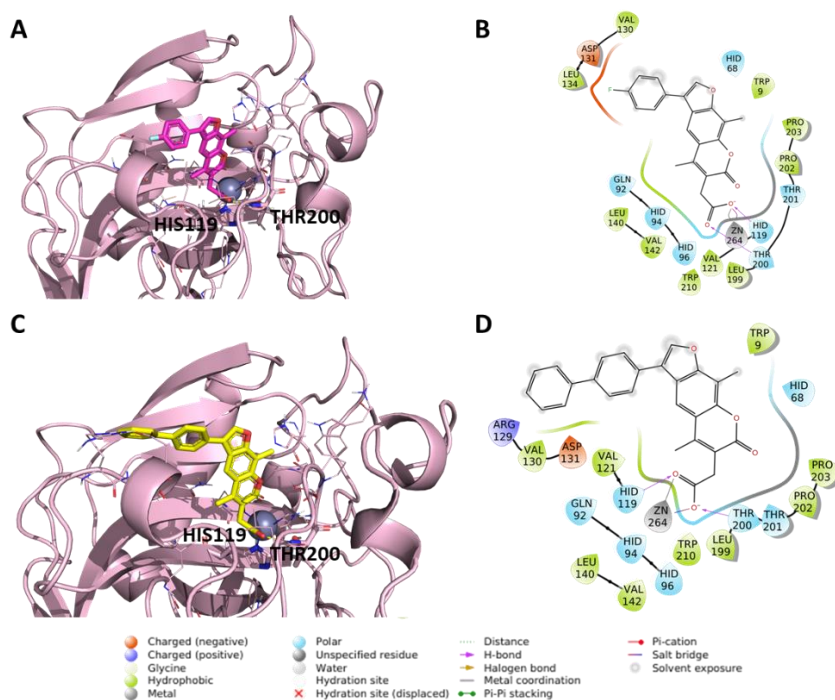


Figure 74. Representation of the putative binding mode of the most potent compounds from EMC10164 series obtained by docking experiments to *hCA IX*. (A) 3D depiction of EMC10164d and its respective interactions with CA IX residues; (B) 2D depiction of interactions; (C) 3D depiction of EMC10164g and its respective interactions with CA IX residues; (D) 2D depiction of interactions.

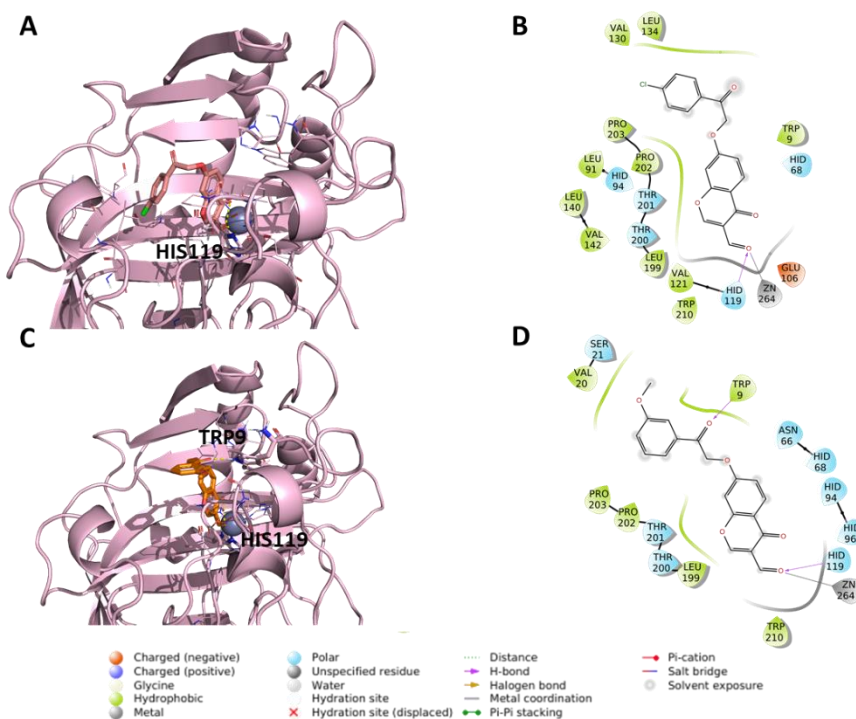


Figure 75. Representation of the putative binding mode of the most potent compounds from EMC10169 series obtained by docking experiments to *hCA IX*. (A) 3D depiction of EMC10164k and its respective interactions with CA IX residues; (B) 2D depiction of interactions; (C) 3D depiction of EMC10164m and its respective interactions with CA IX residues; (D) 2D depiction of interactions.

Considering the interesting *hCA* esterase mediated inhibition mechanism (Figure 76) reported for coumarin derivatives [153, 238-240], the compounds from EMAC10163 and EMAC10164 series were submitted to docking experiments also in their open forms.

Hence, the configurations *E* and *Z* of the four compounds were subjected to docking experiments to predict the putative binding mode of the hydrolyzed forms.

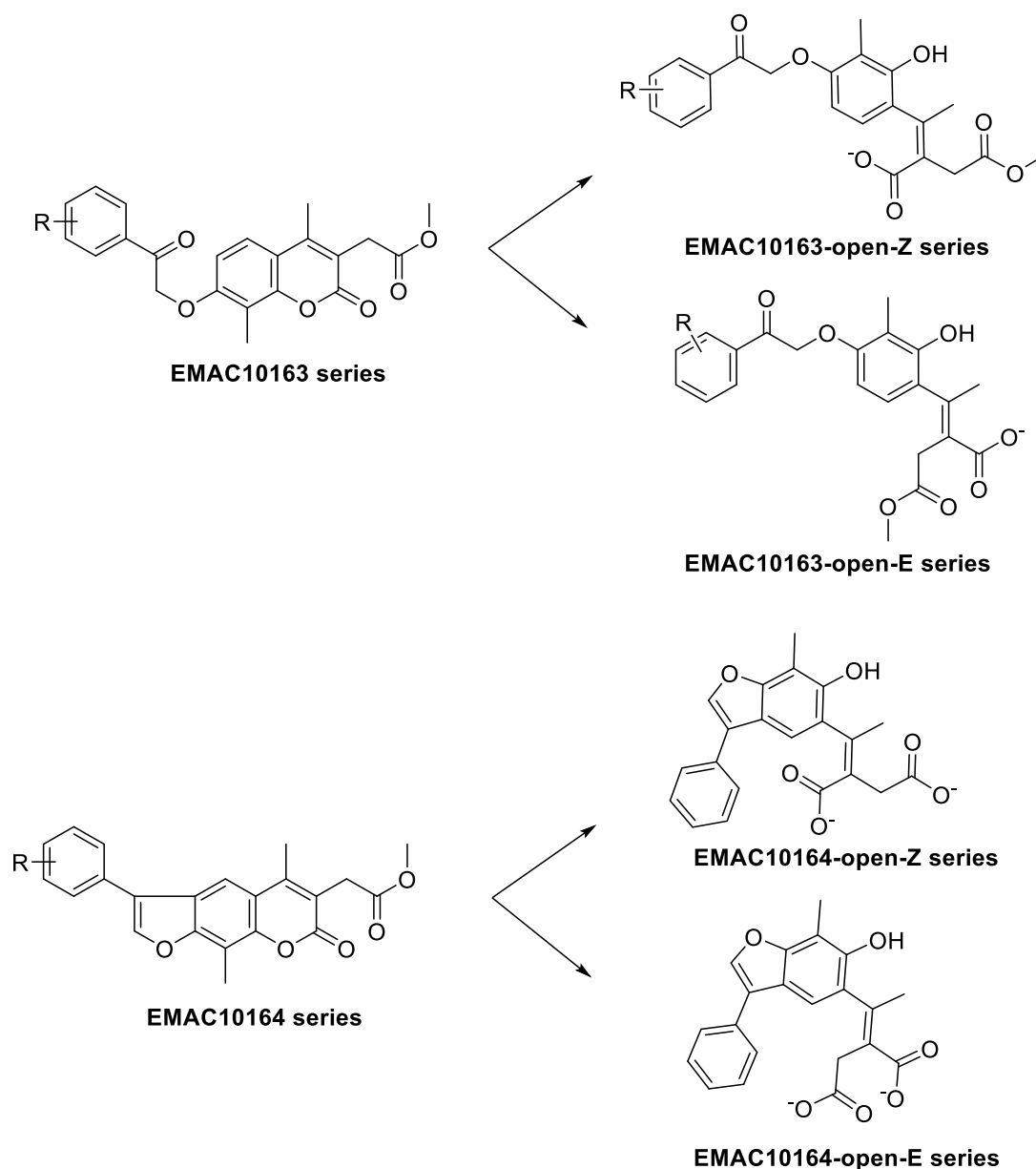


Figure 76. Formation of the open EMAC10163 and EMAC10164 series by the CA-mediated hydrolysis of coumarins.

In the open compounds what seems important is the Zn^{2+} chelation and the interactions between the newly formed carboxylate moiety in the catalytic site.

The representation of the docking experiments for the EMAC10163 and EMAC10164 series compounds can be seen in Figure 77 and Figure 78. For each compounds configurations E and Z are considered.

In particular, the complexes are stabilized by some common interaction residues close to the Zn^{2+} such as His119, Thr200 and Thr201.

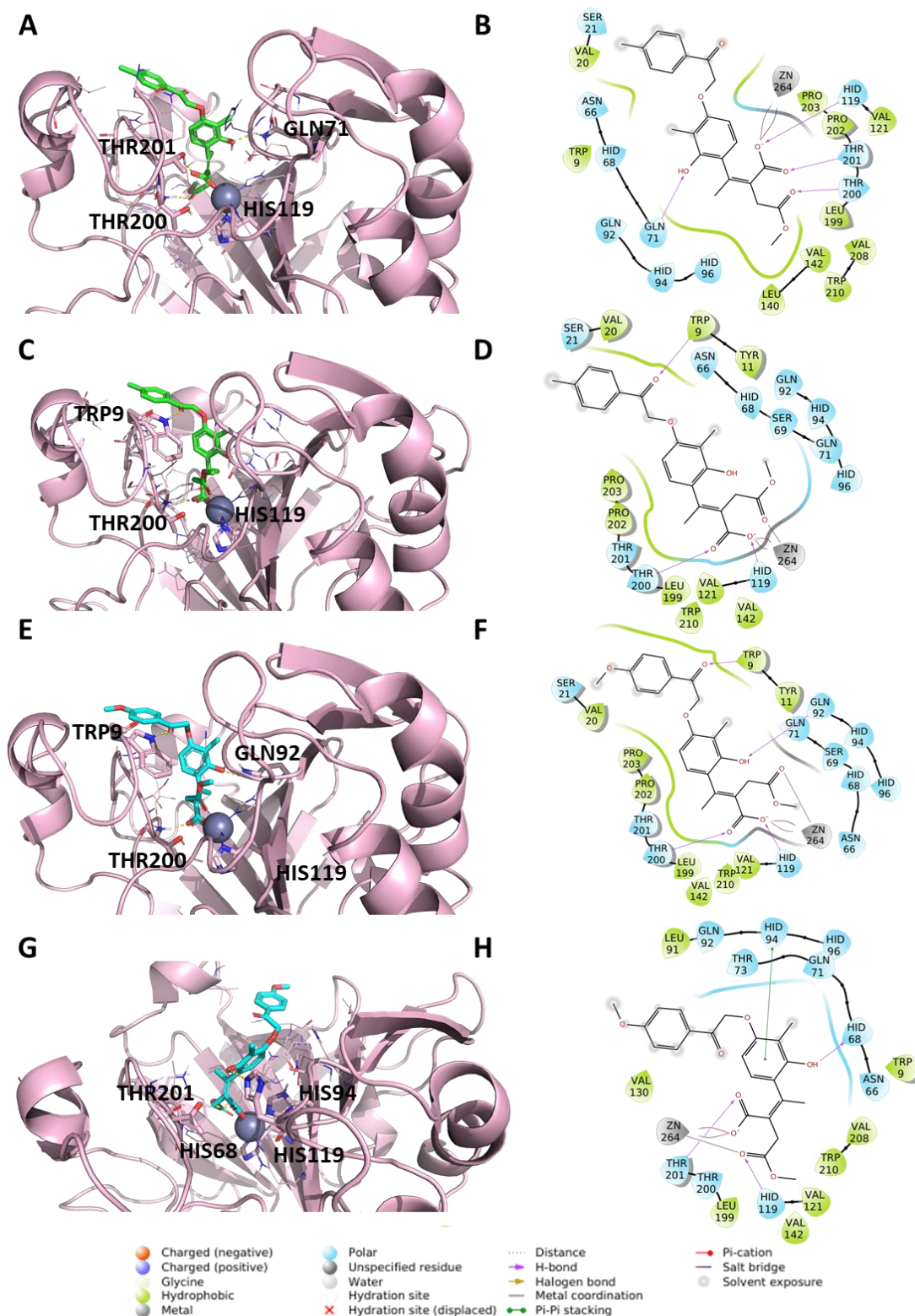


Figure 77. Representation of the putative binding mode of the most potent compounds from EMAC10163-open series obtained by docking experiments to *hCA IX*. (A) 3D depiction of EMAC10163a-open-E and its respective interactions with CA IX residues; (B) 2D depiction of interactions; (C) 3D depiction of EMAC10163a-open-Z and its respective interactions with CA IX residues; (D) 2D depiction of interactions; (E) 3D depiction of EMAC10163b-open-E and its respective interactions with CA IX residues; (F) 2D depiction of interactions; (G) 3D depiction of EMAC10163b-open-Z and its respective interactions with CA IX residues; (H) 2D depiction of interactions.

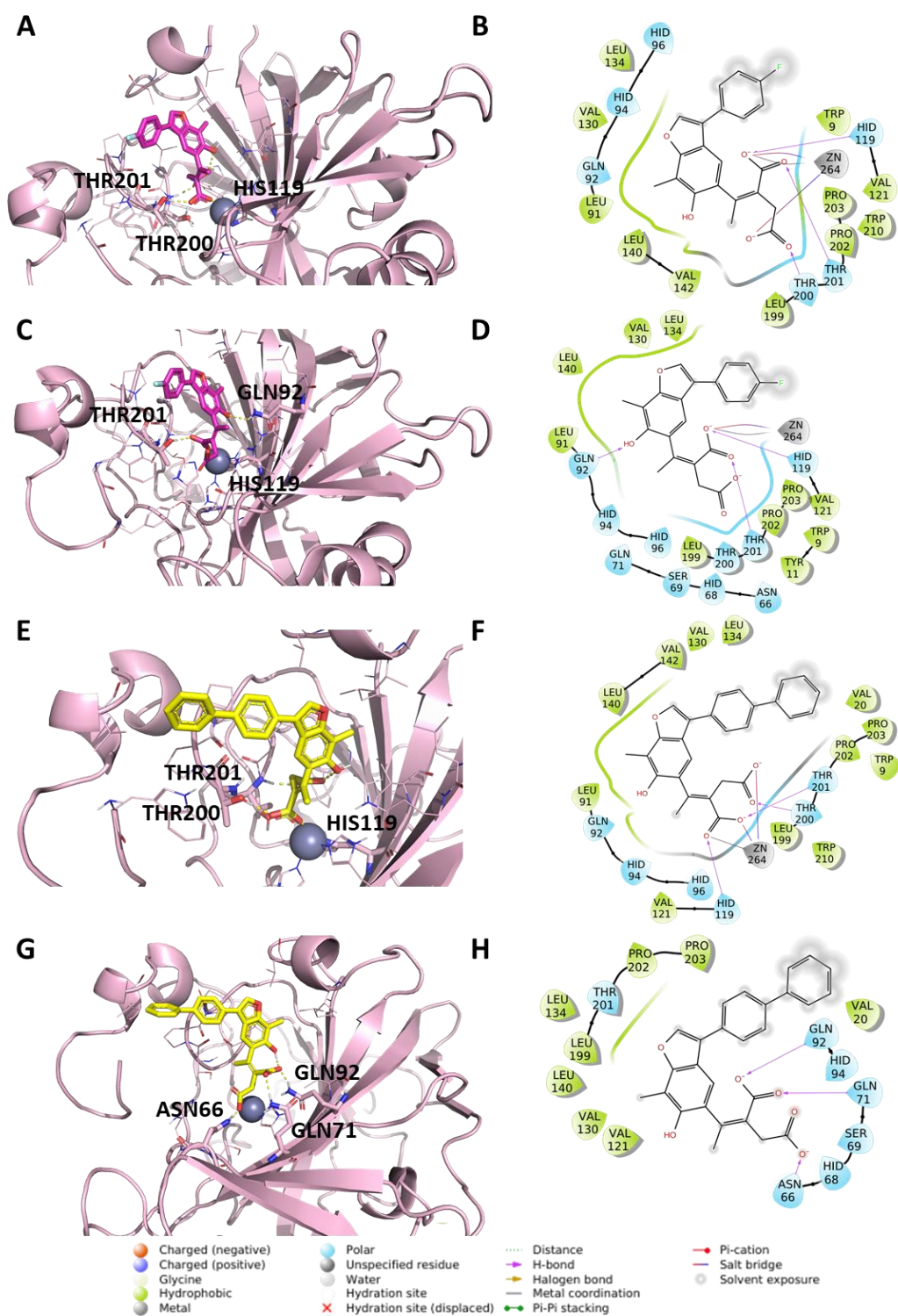


Figure 78. Representation of the putative binding mode of the most potent compounds from EMAC10164-open series obtained by docking experiments to *hCA IX*. (A) 3D depiction of EMAC10164d-open-E and its respective interactions with CA IX residues; (B) 2D depiction of interactions; (C) 3D depiction of EMAC10164d-open-Z and its respective interactions with CA IX residues; (D) 2D depiction of interactions; (E) 3D depiction of EMAC10164g-open-E and its respective interactions with CA IX residues; (F) 2D depiction of interactions; (G) 3D depiction of EMAC10164g-open-Z and its respective interactions with CA IX residues; (H) 2D depiction of interactions.

3.6.2. CA XII docking

Docking experiments of the two best compounds of each series were also performed to hCA XII considering 5MSA [304] CA XII conformation.

EMAC10163a and EMAC10163b docking experiments are represented in Figure 79. Regarding EMAC10163a only one binding pose was obtained with the chromene ring orientated to the zinc. On the contrary, for EMAC10163b two orientations were obtained. One with the chromene ring positioned toward the zinc and another with the substituted benzene ring orientated toward the zinc.

In Figure 80 are represented the docking experiments of EMAC10164d and EMAC10164g. For these compounds the docking predicted binding modes were always with the chromene ring orientated toward the zinc.

Regarding the EMAC10169 series the docking experiments are represented in Figure 81. For these compounds two binding modes were obtained for each. As described before, in one of the binding modes the chromene ring is orientated toward the zinc, and in the other the substituted benzene ring is orientated toward the zinc.

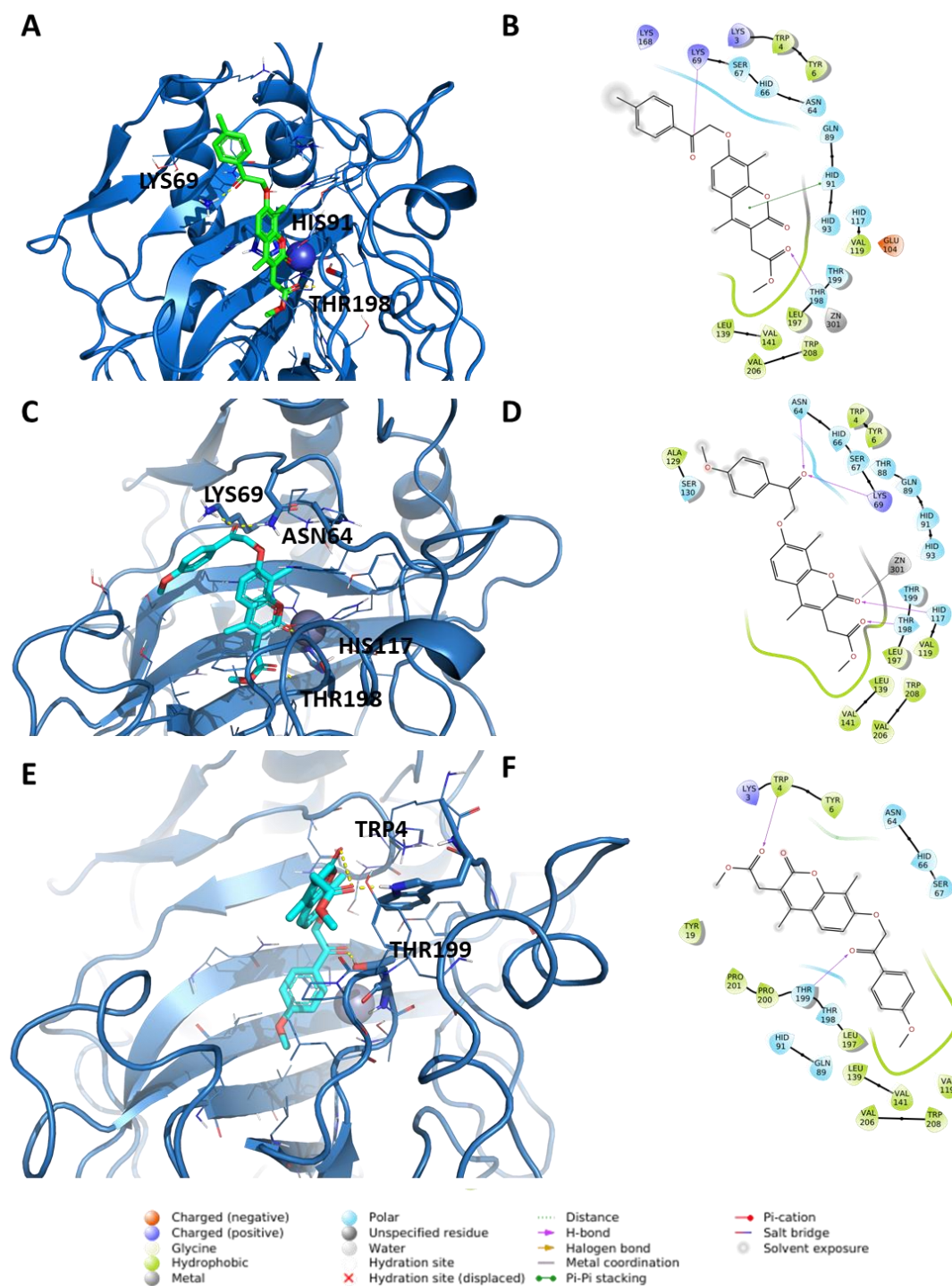


Figure 79. Representation of the putative binding mode of the most potent compounds from EMAC10163 series obtained by docking experiments to *hCA XII*. (A) 3D depiction of EMAC10163a and its respective interactions with CA XII residues; (B) 2D depiction of interactions; (C) 3D depiction of EMAC10163b and its respective interactions with CA XII residues; (D) 2D depiction of interactions; (E) 3D depiction of EMAC10164b and its respective interactions with CA XII residues considering a different orientation of the compound; (F) 2D depiction of interactions.

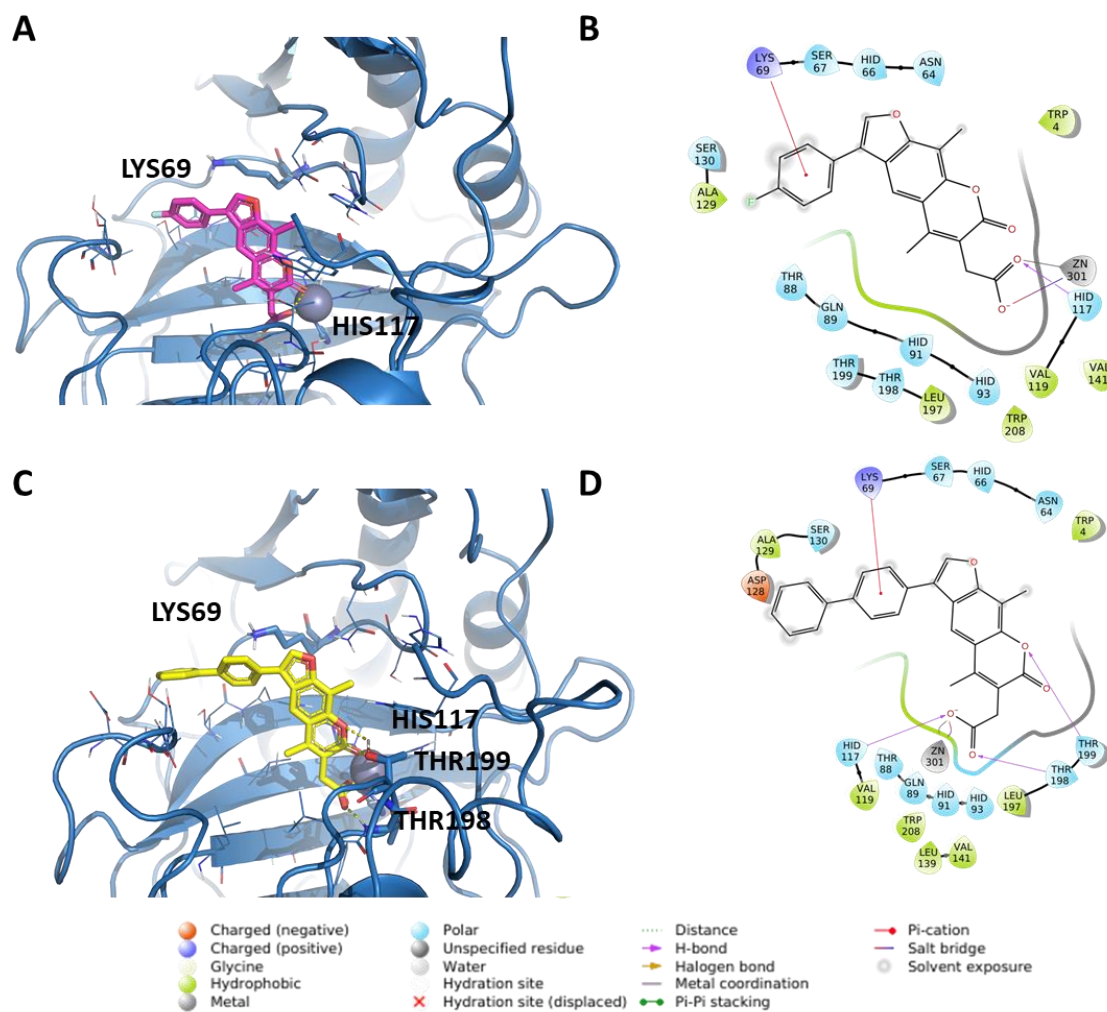


Figure 80. Representation of the putative binding mode of the most potent compounds from EMAC10164 series obtained by docking experiments to *hCA XII*. (A) 3D depiction of EMAC10164d and its respective interactions with CA XII residues; (B) 2D depiction of interactions; (C) 3D depiction of EMAC10164g and its respective interactions with CA XII residues; (D) 2D depiction of interactions.

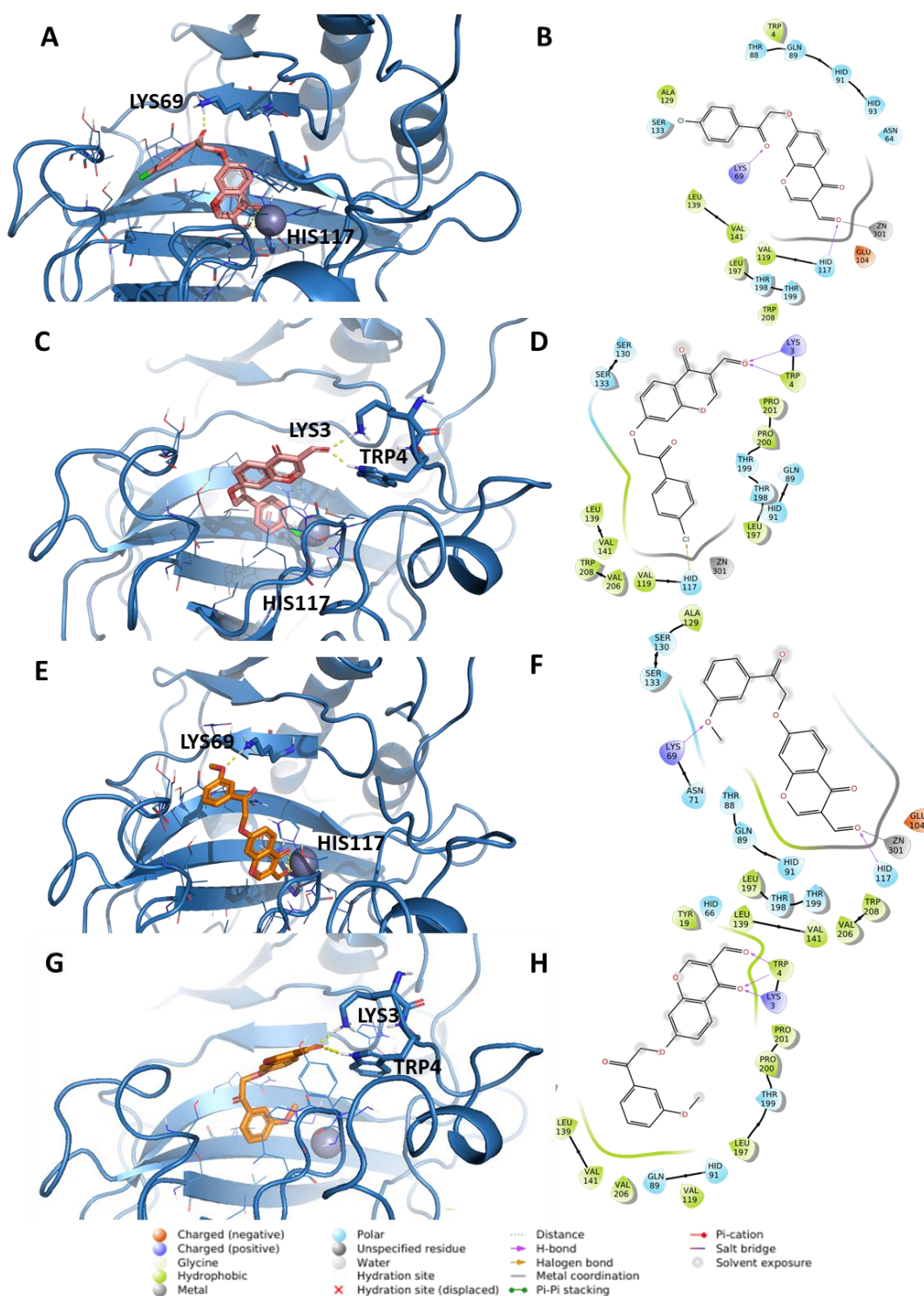


Figure 81. Representation of the putative binding mode of the most potent compounds from EMAC10169 series obtained by docking experiments. (A) 3D depiction of EMAC10169k and its respective interactions with CA XII residues; (B) 2D depiction of interactions; (C) 3D depiction of EMAC10169k and its respective interactions with CA XII residues considering a different orientation of the compound; (D) 2D depiction of interactions; (E) 3D depiction of EMAC10169m and its respective interactions with CA XII residues; (F) 2D depiction of interactions; (G) 3D depiction of EMAC10169m and its respective interactions with CA XII residues considering a different orientation of the compound; (H) 2D depiction of interactions.

As already performed for CA IX, also for CA XII the *hCA* esterase mediated inhibition mechanism was considered, and the docking experiments were submitted to EMAC10163 and EMAC10164 series in their open forms, in both configurations, *trans* and *cis*, to predict the putative binding mode of the hydrolyzed forms.

In these four compounds only the binding modes obtained for the E configuration were reasonable and are represented in Figure 82 and Figure 83. In fact, the proposed binding modes for Z configurations showed the compounds orientated with the substituted benzene ring facing the zinc. This pose is not likely because the chromene ring should be orientated toward the Zn^{2+} in order to be hydrolyzed.

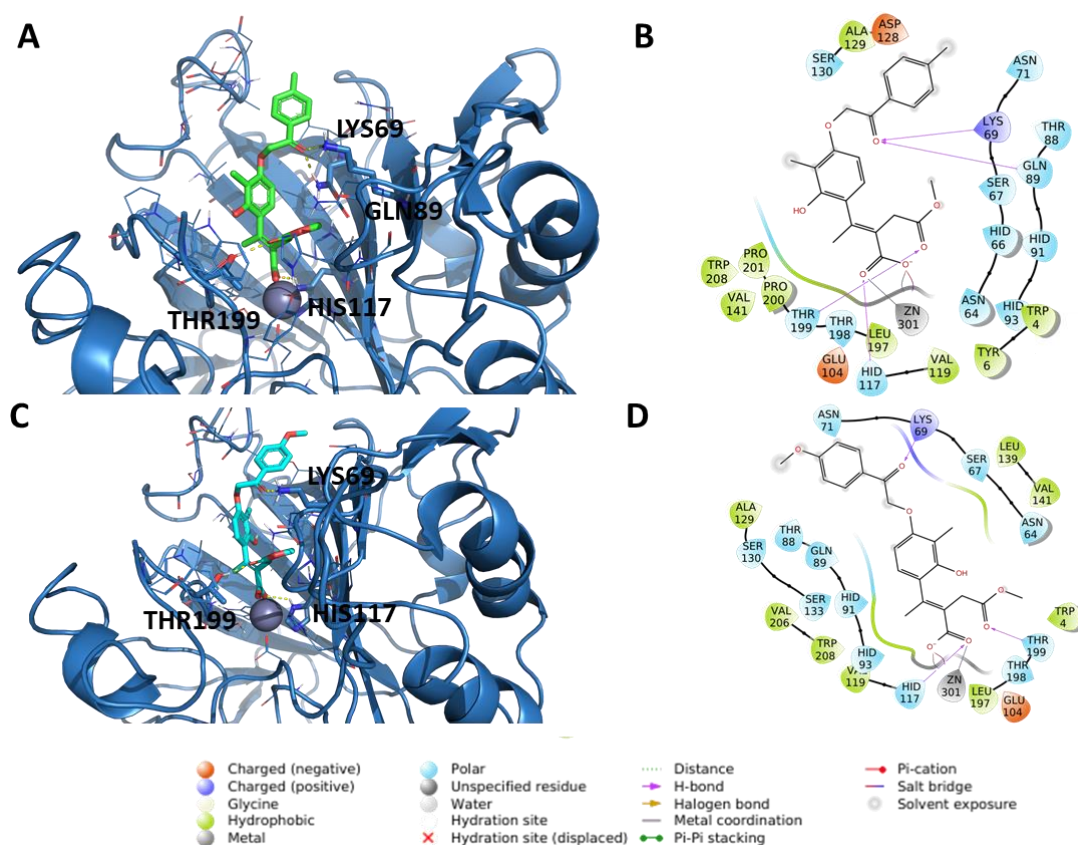


Figure 82. Representation of the putative binding mode of the most potent compounds from EMAC10163-open series obtained by docking experiments to *hCA* XII. (A) 3D depiction of EMAC10163a-open-E and its respective interactions with CA XII residues; (B) 2D depiction of interactions; (C) 3D depiction of EMAC10163b-open-E and its respective interactions with CA XII residues; (D) 2D depiction of interactions.

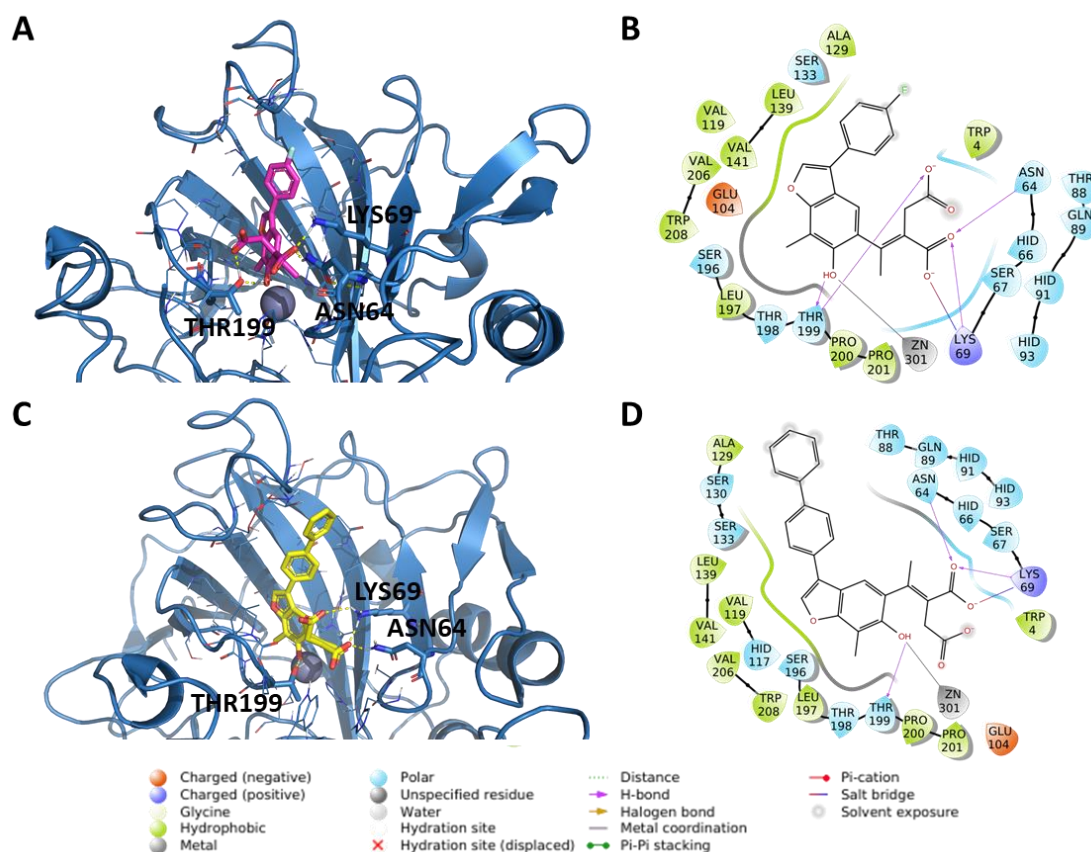


Figure 83. Representation of the putative binding mode of the most potent compounds from EMAC10164-open series obtained by docking experiments to *hCA XII*. (A) 3D depiction of EMAC10164d-open-E and its respective interactions with CA XII residues; (B) 2D depiction of interactions; (C) 3D depiction of EMAC10164g-open-E and its respective interactions with CA XII residues; (D) 2D depiction of interactions.

The docking poses are often characterized by the interaction with common residues such as Lys69, His117, Thr198 or Thr199. Also for the XII isoform the open compounds are stabilized by an array of hydrogen bonds involving the residues in the catalytic cavity.

CHAPTER 4. Conclusions

The experimental results obtained within the scope of this thesis led to the following conclusions:

- **Coumarins and chromone based libraries were successfully synthesized.** Using straightforward synthetic methodologies and cost-effective materials led to overall satisfactory yields. Twenty-seven compounds were synthesized, seventeen of which novel and unreported in literature.
- **A valuable characterization of the libraries was attained.** Structural elucidation was performed by ^1H and ^{13}C NMR and mass spectrometry.
- **The inhibitory activity towards *h*CAs I, II, IX and XII was evaluated.**
- **The majority of the coumarin and chromone-based compounds displayed good drug-likeness requirements.** The predicted properties of the compounds were calculated, and the theoretical parameters were encouraging.
- **Compound EMAC10163b proved to be the most potent and selective compound, within the EMAC10163 series.** EMAC10163b acted as selective inhibitor toward *h*CA IX and XII ($K_i = 0.53\ \mu\text{M}$ and $0.47\ \mu\text{M}$, respectively).
- **Compound EMAC10164d proved to be the most potent and selective compound, within the EMAC10164 series.** EMAC10164d acted as selective inhibitor toward *h*CA IX and XII ($K_i = 0.46\ \mu\text{M}$ and $0.80\ \mu\text{M}$, respectively).
- **Compound EMAC10169m proved to be the most potent and selective compound, within the EMAC10169 series.** EMAC10169m acted as selective inhibitor toward *h*CA IX and XII ($K_i = 0.31\ \mu\text{M}$ and $0.24\ \mu\text{M}$, respectively).
- **Chromone and coumarin are valuable scaffolds for the selective inhibition of the tumor associated CA isoforms IX and XII.** Moreover, both scaffolds allow the synthesis of potential therapeutic agents with a favorable drug-like profile.
- **The rigidity of the EMAC10164 and EMAC10169 series helps to orientate the compounds in the binding pocket with the chromene portion toward the Zn^{2+} .** The docking experiments that consider the IX isoform, highlighted this

characteristic, and showed that the influence of the substituents in the phenyl ring is not clear among the different series.

- **Importance of the Zn²⁺ chelation and the interactions between the newly formed carboxylate moiety in the catalytic site in the open compounds, regarding the IX isoform.** Accordingly, we must assume that also the esterase activity was selective between the different isozymes.
- **Interaction with common residues such as Lys69, His117, Thr198 or Thr199, considering the XII isoform.**
- **Stabilization of the open compounds by an array of hydrogen bonds involving the residues in the catalytic cavity in the XII isoform.**

Overall, the results obtained under the current Thesis endorsed coumarin and chromone as valid scaffolds for the development of selective carbonic anhydrases IX and XII inhibitors. More importantly, the findings of this project encourage the development of future projects, mainly regarding lead optimization and the detailed pharmacological characterization of the most promising coumarin and chromone analogs. The evaluation of these compounds and derivatives in other cancer-associated targets is also viewed as a consistent step towards a multi-target profiling of these interesting scaffolds.

CHAPTER 5. Other Projects

5.1. Studies on synthetic route optimization

This section describes the results that contributed for the following two communications in poster:

Lisa Sequeira, Tiago Silva, and Fernanda Borges. Development of COMT inhibitors and iron chelators: studies on synthetic route optimization. *MuTaLig COST Action CA15135, Annual Meeting 2018*. 18-19 October 2018, Valletta, Malta.

Lisa Sequeira, Tiago Silva, Elias Maccioni, Fernanda Borges. Development of Dual COMT Inhibitors and Iron Chelators. *26th Young Research Fellows Meeting*. 20-22 February 2019, Paris, France.

5.1.1. *An overview on Parkinson's disease*

Parkinson's disease (PD) is globally widespread and is the second most common neurodegenerative disease after Alzheimer's disease, [319] with a prevalence of about 1-2% in the elderly population [320]. Due to the increasing of the life expectancy, it is safe to conclude that this number will continue to follow an upwards trend [321], causing an even bigger social and economic burden on the general population and healthcare systems. Diagnosis of PD is based on symptoms and signs observation which can include prodromal features, that can occur for a long period of time (e.g. sleep dysfunction, olfactory loss, autonomic dysfunction), classical PD motor symptoms (e.g. bradykinesia, rigidity, tremor, postural instability), typically the disease is diagnosed in this stage, and psychological or cognitive symptoms (e.g. mild cognitive impairment or dementia, depression, anxiety) in an advanced stage of PD [321-323]. Pathologically, the disease is characterized by the death of dopaminergic neurons in the substantia nigra [322]. Loss of dopaminergic neurons results in dopamine (DA) deficiency, triggering the motor symptoms associated with PD [322, 323]. Most cases are apparently sporadic and old age remains the most significant risk factor [319, 321].

5.1.2. *Parkinson's disease therapy*

Presently, the therapies for PD allow symptomatic relief and are based in the enhancement of DA levels [320-322]. Levodopa, a DA precursor, is still considered the best effective PD

treatment, regarding life quality enhancement [320, 321, 324]. However, levodopa has a short half-life in vivo, being extensively metabolized, after oral administration, by enzymes such as catechol-O-methyltransferase (COMT) which requires co-administration of drugs to inhibit the enzymes responsible for levodopa inactivation [320, 321, 325]. In mammals, the COMT enzyme is present in a soluble cytosolic form (S-COMT) that occurs mainly in peripheral tissues, and a membrane-bound form (MB-COMT) present predominantly in the brain [324]. Hence, COMT inhibitors increases plasma half-life of levodopa, allowing the orally administered precursor to cross the blood-brain barrier (BBB) into the brain, where it is locally converted to DA. Nitrocatechol-based derivatives are the currently marketed COMT inhibitors (tolcapone, entacapone and opicapone - Figure 84) [326]. Despite its potency and BBB permeability, tolcapone is associated with fatal hepatotoxicity via mitochondrial impairment and is administered only in specific clinical cases under strict liver function monitoring [320, 321, 327]. Entacapone is a safer and widely used peripheral COMT inhibitor, but its low bioavailability decreases its clinical efficacy and requires repeated dosing [328]. Opicapone, a long-acting peripheral COMT inhibitor [325, 328], displays improved safety over tolcapone and higher bioavailability compared to entacapone, but the inhibition of peripheral COMT has been associated with hepatic and intestinal side effects and tolcapone remains the only available centrally-active COMT inhibitor [325]. Therefore, the search for safe and centrally active COMT inhibitors is still extremely important.

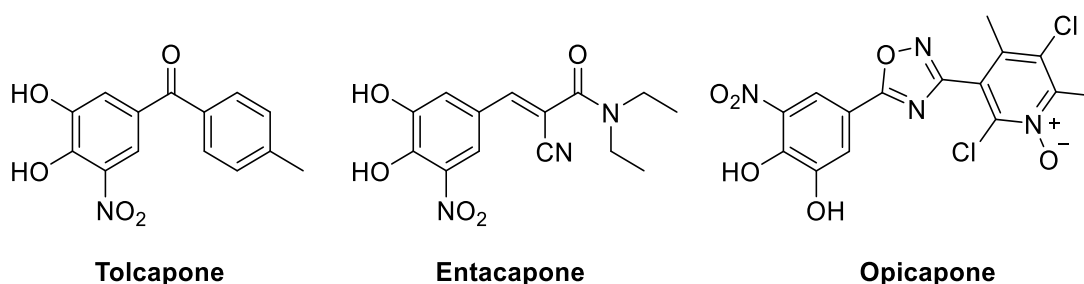


Figure 84. Chemical structures of nitrocatechol-based COMT inhibitors: tolcapone, entacapone and opicapone.

Albeit the nitrocatechol pharmacophore yields potent tight-binding COMT inhibitors, it raises toxicological concerns, particularly with increased lipophilicity [324]. Non-nitrocatechol COMT inhibitors may thus provide a safer alternative. Encouraging preliminary results have been reported, unveiling noteworthy bioactivity for heterocycle catechol mimics (HetCAMs) [324, 329-331]. Additionally, 3-hydroxy-4-pyridinones also acted as chelators of redox-active metals [332]. Given the central role of brain iron accumulation in dopamine-deficiency neurodegenerative diseases, the combination of a

dopaminergic therapy (COMT inhibition) with iron chelation in a single bioactive molecule might be a valid therapeutic strategy to develop drug candidates for these diseases. The aim of this project is to develop HetCAM libraries as smart dual acting COMT inhibitors and iron chelators, designed to meet the structural and pharmacokinetic requirements to interact with COMT and accumulated iron within the brain, while mitigating the toxicological risks of currently available nitrocatechols.

5.1.3. Project's synthetic strategy

Two main groups of HetCAMs have been purposed to develop from a naturally-occurring, cheap and commercially available starting material: kojic acid (compound 1, Figure 85). The main sites of derivatization are the position C2 and the heteroatom. Briefly, hydroxypyridinones will be easily obtained from kojic acid by microwave-assisted heating with the appropriate amines under mild acidic conditions. This strategy will yield a variety of differently substituted nitrogen heterocycles. The chemical versatility of the C2 position is also interesting from a synthetic point of view. By oxidation of the 2-hydroxymethyl moiety (e.g., Jones reagent/acetone) the corresponding carboxylic acid can be obtained, which can be eliminated by heat-induced decarboxylation, leading to C2-unsubstituted derivatives, or further derivatized to the corresponding esters, amines, and thioesters. This synthetic strategy can thus provide two groups of HetCAMs: N-substituted (compound 6) and NH- or O-containing HetCAMs substituted at the C2 position (compounds 8 and 10).

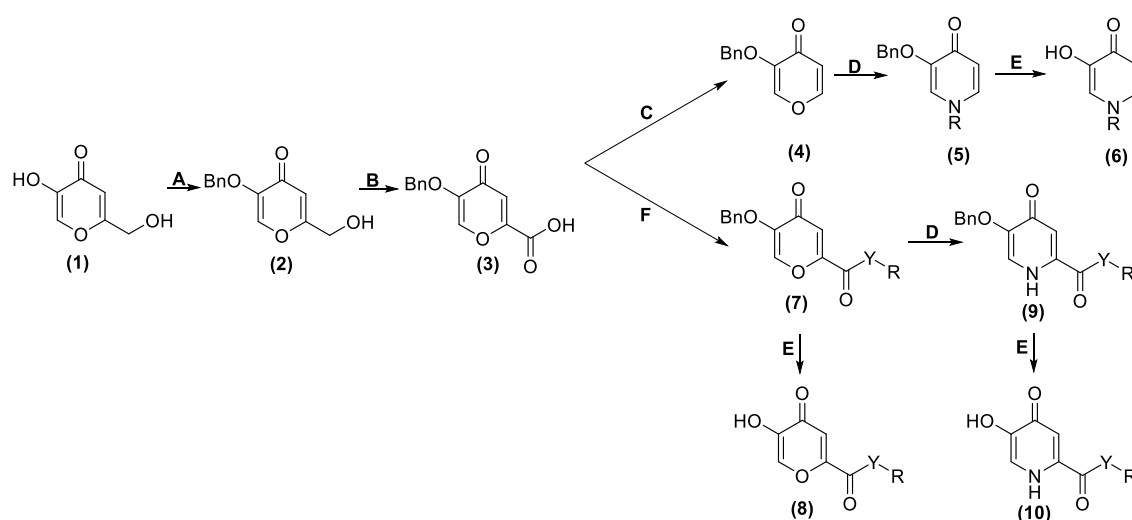


Figure 85. Schematic representation of the synthetic pathway used for the obtention of the HetCAMs libraries. Reaction conditions: (A) methanol, NaOH 1M, benzyl chloride, 100 °C, 7 – 8 h; (B) acetone, Jones reagent 2.5 M, 0 °C, overnight; (C) diphenyl ether, 250 °C, 8 – 10 min; (D) ethanol, 3,4-dimethoxyaniline or 4-chloroaniline, HCl 0.38 M, 100 °C, 1.5 h; (E) anhydrous dichloromethane, BBr₃, -80 °C, 2 h; (F) DMF, POCl₃, room temperature, 24 h.

5.1.4. Synthesis of 5-(benzyloxy)-2-(hydroxymethyl)-4H-pyran-4-one (compound 2)

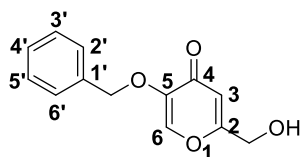


Figure 86. Structure of compound 2.

To a solution of kojic acid (0.5 g, 3.54 mmol) in methanol (5 mL) was added NaOH 10 M (0.360 mL) and the mixture was heated to reflux (100 °C). Benzyl bromide (0.410 mL, 3.56 mmol) was then added dropwise over 1 h and the mixture was stirred under reflux for 7 hours. The reaction mixture was cooled to room temperature, dissolved in the minimum quantity of methanol, and added (dropwise) to cold water. The product was collected by filtration, washed with cold water, recrystallized in ethyl acetate, and collected as a white solid (structure of the desired compound on Figure 86).

Yield: 59.0 %

^1H NMR (400 MHz, CDCl_3): δ = 4.45 (s, 2H, CH_2), 5.07 (s, 2H, CH_2), 6.51 (s, 1H, H(Ar)), 7.31 – 7.41 (m, 5H, H(Ar')), 7.52 (s, 1H, H(Ar)).

^{13}C NMR (101 MHz, CDCl_3): δ = 61.01 (CH_2), 72.00 (CH_2), 112.52 (C(Ar)), 127.84 (2 x C(Ar')), 128.46 (C(Ar)), 128.73 (2 x C(Ar')), 135.71 (C(Ar)), 141.64 (C(Ar)), 147.07 (C(Ar)), 166.39 (C2), 174.93 (C4).

Melting point: [132 – 133] °C.

Molecular weight: 232.24 g/mol.

Rf (DCM/MeOH 9.5:0.5): 0.33.

5.1.5. Synthesis of 5-(benzyloxy)-4-oxo-4H-pyran-2-carboxylicacid (compound 3)

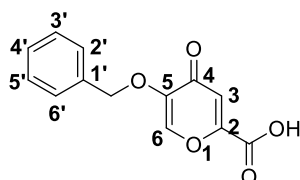


Figure 87. Structure of compound 3.

To a solution of compound 2 (1 g, 4.06 mmol) in acetone (20 mL) was added Jones's reagent 2.5 M (5 mL) at 0 °C. The reaction was stirred overnight. The liquid was drained and concentrated. The concentrated residue was poured into water. The resulting white

solid was collected by filtration, washed with water, and dried to obtain the desired compound (structure on Figure 87).

Yield: 72.7 %

^1H NMR (400 MHz, DMSO): δ = 4.99 (s, 2H, CH_2), 6.94 (s, 1H, H(Ar)), 7.37 – 7.45 (m, 5H, 5 x H(Ar')), 8.37 (s, 1H, H(Ar)).

^{13}C NMR (101 MHz, DMSO): δ = 71.15 (CH_2), 117.65 (C(Ar)), 128.70 (2 x C(Ar)), 128.79 (C(Ar)), 128.96 (2 x C(Ar)), 136.30 (C(Ar)), 142.00 (C(Ar)), 148.71 (C(Ar)), 153.00 (C(Ar)), 161.26 (COOH), 173.51 (C4).

Melting point: [196 – 197] °C.

Molecular weight: 246.22 g/mol.

Rf (DCM/MeOH 9.5:0.5): 0.02.

5.1.6. Synthesis of 3-(benzyloxy)-4H-pyran-4-one (compound 4)

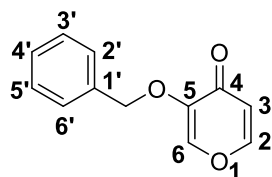


Figure 88. Structure of compound 4.

Compound 3 (0.4 g, 1.63 mmol) was dissolved in diphenyl ether (2.5 ml) and heated to 250°C in an open flask for 9 min. The mixture was cooled to room temperature and the residue was purified by silica gel chromatography (dichloromethane/methanol 99:1 to 90:10) and recrystallized (DCM/ petroleum ether) to obtain the desired compound (structure on Figure 88) as a yellowish solid.

Yield: 12.4 %

Due to the lower yield of the reaction, a bibliographic research was made to discover different reaction conditions for decarboxylate compound 3. A microwave-assisted Cu-catalyzed decarboxylation of aromatic carboxylic acids was found in the literature [333]. Considering this procedure, the reaction was optimized. In this reaction a catalyst is generated in situ from copper(I) oxide and 1,10-phenanthroline. 1-Methyl-2-pyrrolidinone (NMP) and quinoline are used as solvents. Several conditions were tried, with different quantities of reagent, time, and workup, as detailed on Table 43.

Table 43. Detailed reaction conditions for optimization purposes.

Reaction	Compound 3 (mg)	Cu ₂ O (mg)	1,10-phenanthroline (mg)	NMP (mL)	Quinoline (mL)	Workup	Yield (%)
1	247.2	8.4	18.4	1.5	0.5	acidification, extraction, chromatographic column, recrystallization	18.8
2	246.3	7.5	18.2	1.5	0.5	chromatographic column, recrystallization	9.30
3	246.4	8.0	18.2	1.5	0.5	acidification, extraction, chromatographic column, recrystallization	18.7
4	429.9	14.5	36.0	3.0	1.0	acidification, extraction, chromatographic column (different eluent), recrystallization	54.0
5	739.2	21.9	54.4	1.5	0.5	acidification, extraction, recrystallization	57.3
6	734.9	22.0	54.3	1.5	0.5	acidification, extraction, recrystallization	58.2

After the optimization we arrived at the optimal procedure as follows: an oven-dried 10 mL microwave vial was charged with compound 3 (0.7349 g, 2.98 mmol), Cu₂O (22.0 mg, 0.15 mmol) and 1,10-phenanthroline (54.3 mg, 0.30 mmol). After the reaction mixture was made inert, NMP (1.5 mL) and quinoline (0.5 mL) were added via syringe. The resulting mixture was submitted to microwave irradiation at 190 °C for 35 min and subsequently air-jet cooled to room temperature. The mixture was then acidified with HCl (5 M, 30 mL) and extracted repeatedly with diethyl ether (10 x 5 mL). The combined organic layers were washed with 50 mL of HCl 1 M and 50 mL of brine, dried over Na₂SO₄ and filtered. The residue was purified by recrystallization (DCM/ petroleum ether) to provide the desired compound as a light-yellow solid.

Yield: 58.2 %

¹H NMR (400 MHz, CDCl₃): δ = 5.08 (s, 2H, CH₂), 6.42 (d, *J* = 5.6 Hz, 1H, H₃), 7.30 – 7.41 (*m*, 5 H, H(Ar')), 7.55 (d, *J* = 0.8 Hz, 1H, H₆), 7.66 (*dd*, *J* = 5.6, 0.8 Hz, 1H, H₂).

^{13}C NMR (101 MHz, CDCl_3): $\delta = 71.93$ (CH_2), 116.81 ($\text{C}(\text{Ar})$), 127.84 ($2 \times \text{C}(\text{Ar})$), 128.43 ($\text{C}(\text{Ar})$), 128.70 ($2 \times \text{C}(\text{Ar})$), 135.73 ($\text{C}(\text{Ar})$), 142.38 ($\text{C}(\text{Ar})$), 147.95 ($\text{C}(\text{Ar})$), 154.25 ($\text{C}(\text{Ar})$), 174.18 ($\text{C}(4)$).

Melting point: $[84 - 85]^\circ\text{C}$.

Molecular weight: 202.21 g/mol.

R_f (DCM/MeOH 9.5:0.5): 0.61.

5.1.7. Synthesis of 3-(benzyloxy)-4H-pyran-4-one (compound 5)

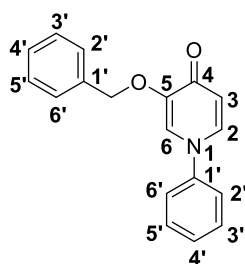


Figure 89. Structure of compound 5.

Compound 4 (0.2011 g, 0.98 mmol) and aniline (710 μL , 5.99 mmol) were dissolved in EtOH: HCl 0.38M (1:1 V/V, 2 mL) and heated to 100°C for 1 hour and 30 minutes in a sealed flask. Upon completion the solvents were removed under reduced pressure and the residue was stirred with HCl 1M (20 mL) for 4 h at room temperature. The solution was extracted 3 times with 10 mL of DCM and the organic layer was washed with HCl 1M (2 x 10 mL), water (2 x 10 mL) and brine (10 mL). The organic layer was dried over anhydrous sodium sulfate, filtered, and concentrated under reduced pressure. The crude product was purified over chromatographic column using AcOEt/Methanol 90:10 (V/V) as eluent, and the fractions containing the product were collected and concentrated. The desired compound (structure on Figure 89) was isolated as a light brown oil.

Yield: 89.1 %.

^1H NMR (400 MHz, CDCl_3): $\delta = 5.07$ (s, 2H, CH_2), 6.44 (d, $J = 7.2$ Hz, 1H, H₃), $7.07 - 7.15$ (m, 2 H, H(Ar)), $7.16 - 7.26$ (m, 4 H, H(Ar)), $7.27 - 7.42$ (m, 6 H, H(Ar)).

^{13}C NMR (101 MHz, CDCl_3): $\delta = 71.69$ (CH_2), 117.32 ($\text{C}(\text{Ar})$), 122.63 ($2 \times \text{C}(\text{Ar})$), 125.52 ($\text{C}(\text{Ar})$), 127.89 ($2 \times \text{C}(\text{Ar})$), 128.11 ($\text{C}(\text{Ar})$), 128.36 ($\text{C}(\text{Ar})$), 128.55 ($2 \times \text{C}(\text{Ar})$), 130.16 ($2 \times \text{C}(\text{Ar})$), 136.42 ($\text{C}(\text{Ar})$), 136.47 ($\text{C}(\text{Ar})$), 143.18 ($\text{C}(\text{Ar})$), 148.64 ($\text{C}(\text{Ar})$), 173.13 ($\text{C}(4)$).

Melting point: $[215 - 217]^\circ\text{C}$.

Molecular weight: 277.32 g/mol.

R_f (DCM/MeOH 9.5:0.5): 0.38.

5.1.8. Final remarks

A synthetic pathway was optimized to obtain N-substituted HetCAMs, particularly the decarboxylation step which yield rose from 10 to 60 %. With this synthetic revision, several new N-substituted HetCAMs can be synthesized as well as NH- or O-containing HetCAMs substituted at the C2 position. All compounds were characterized by ¹H, ¹³C and DEPT NMR. The work herein present comprises the first steps on the development of dual acting COMT inhibitors and iron chelators.

5.2. Investigation on potential anti-HIV multi-target agents

This section describes a general introduction about HIV infection that contributed for the following publication:

Rita Meleddu, Angela Corona, Simona Distinto, Filippo Cotiglia, Serenella Deplano, **Lisa Sequeira**, Daniela Secci, Alessia Onali, Erica Sanna, Francesca Esposito, Italo Cirone, Francesco Ortuso, Stefano Alcaro, Enzo Tramontano, Péter Mátyus and Elias Maccioni. Exploring New Scaffolds for the Dual Inhibition of HIV-1 RT Polymerase and Ribonuclease Associated Functions. *Molecules*, 2021. **26** (13).

5.2.1. *HIV – an overview*

Human immunodeficiency virus (HIV) was identified as the cause of the acquired immunodeficiency syndrome (AIDS) in 1983, and further accepted by the scientific and medical community in 1984 [334, 335]. Since then, several research groups pursued the solid establishment of a linkage between agent and disease. The blood test for HIV was developed and become available in blood-transfusion centers producing the undoubted evidence of the association between HIV infection and AIDS. This test also helped in the cloning and molecular characterization of the virus genetic material, which proved that the new virus belong to the subfamily of lentivirus [334]. In 2020 there were around 36.8 million people living with HIV worldwide [336], reason why this disease continues to be a burden in economies, health systems and patients [335, 337]. In less than 30 years an impressive drug discovery rush was seen and led to the identification of several HIV-targeted antiviral agents [338, 339].

5.2.2. *HIV targets and their inhibitors*

HIV is a single-stranded RNA retrovirus. The virus particle contains two identical RNA strands along with enzymes such as integrase, reverse transcriptase, and protease in the capsid core. The nucleocapsid protein stabilizes the RNA of the virus and the mature virion particle is conical in shape. It is surrounded by a lipid envelope embedded with transmembrane proteins. The drugs to control the infection in the patients use several proteins in HIV as targets [340].

Along the years, with the HIV treatment improvement, a better life quality of HIV-infected patients was accomplished. The future is even more promising as an increased understanding of the immunopathogenesis of HIV and global public health initiatives are

driving novel treatment approaches with objectives of prevent, control and, ultimately, eradicate HIV. Nowadays there is a wide array of drugs acting against HIV taking into account each patient case [341].

5.2.2.1. Nucleoside and nucleotide reverse transcriptase inhibitors (NRTIs)

The first NRTI introduced was azidothymidine [342], in 1987 [341]. These drugs inhibit the enzyme reverse transcriptase to prevent the transcription of viral RNA to proviral DNA by getting incorporated into the replicating DNAs and terminate the elongation prematurely. The nucleoside reverse transcriptase inhibitors include the compounds on Figure 90. Tenofovir is the only nucleotide reverse transcriptase inhibitor [340].

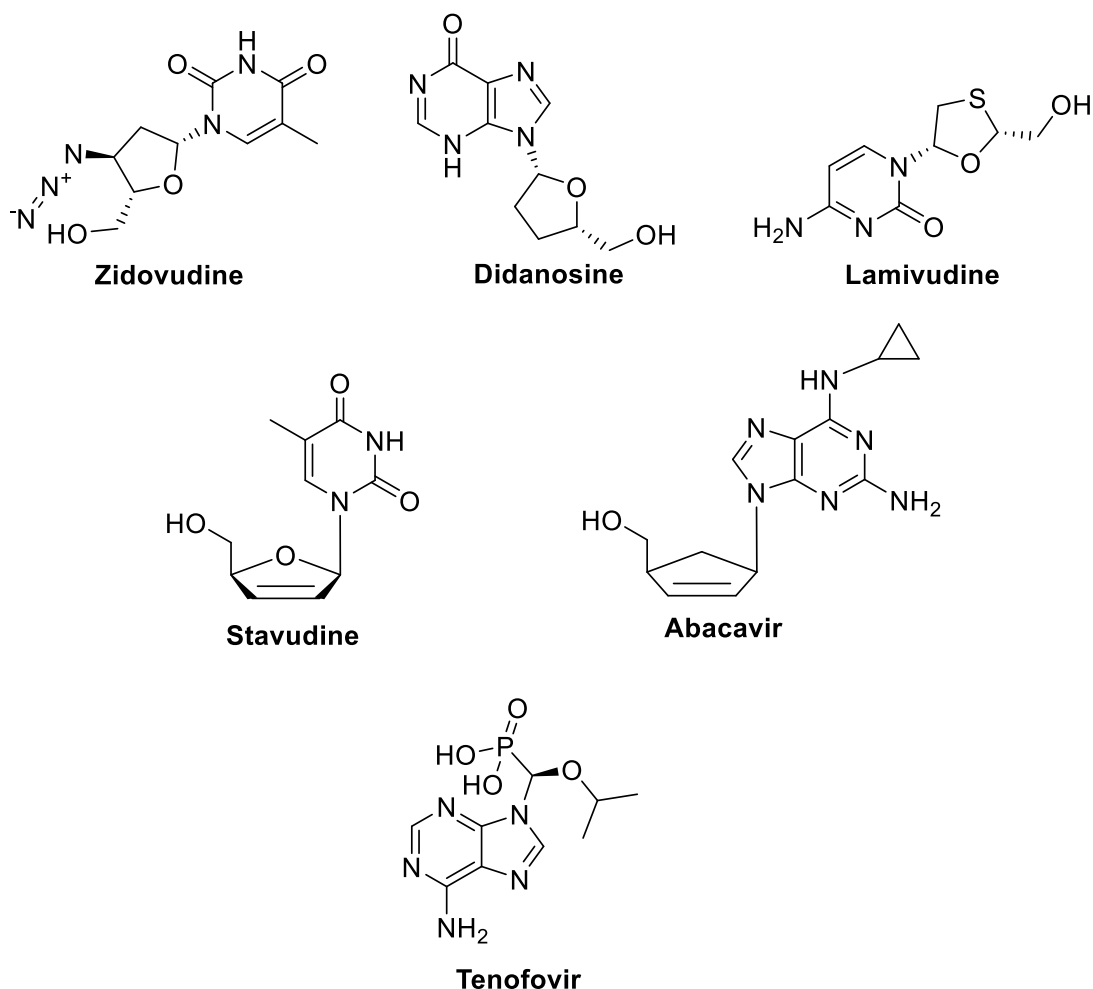


Figure 90. Structure of nucleoside reverse transcriptase inhibitors and the nucleotide reverse transcriptase inhibitor.

5.2.2.2. Non-nucleoside reverse transcriptase inhibitors (NNRTIs)

It is 25 years since NNRTIs were identified as a new class of antiretroviral drugs for the treatment of HIV-1 infection [339, 341]. This type of inhibitors binds to p66 subunit of the reverse transcriptase and induces conformational changes that inhibit the catalytic activities of this enzyme [339, 340]. The approved NNRTIs are represented on Figure 91.

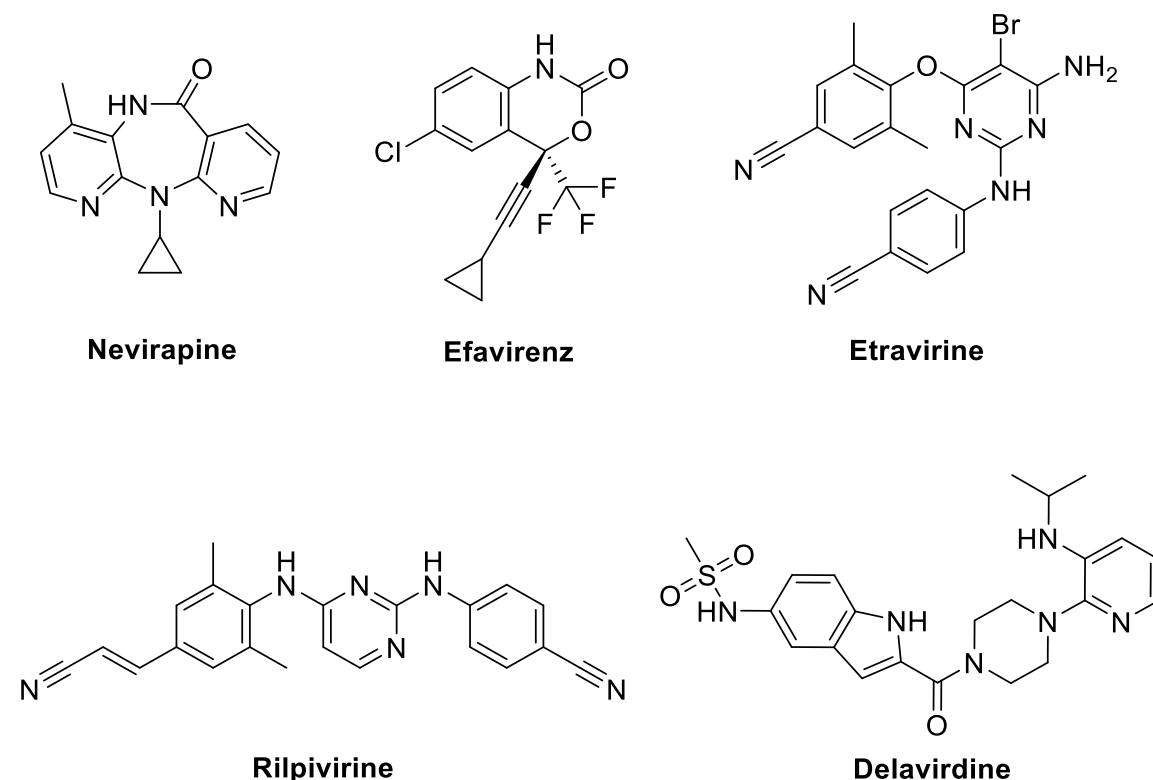


Figure 91. Structure of the approved NNRTIs.

5.2.2.3. Protease inhibitors (PIs)

In 1995 the first PI was approved [341]. These inhibitors competitively inhibit the enzyme aspartyl protease in a virus with cleavage at the N-terminal side of proline residues. These inhibit the cleavage of large polyprotein into structural proteins and enzymes [340]. The main action of PIs is to prevent subsequent waves of infection [343, 344]. Figure 92 shows the approved PIs [340].

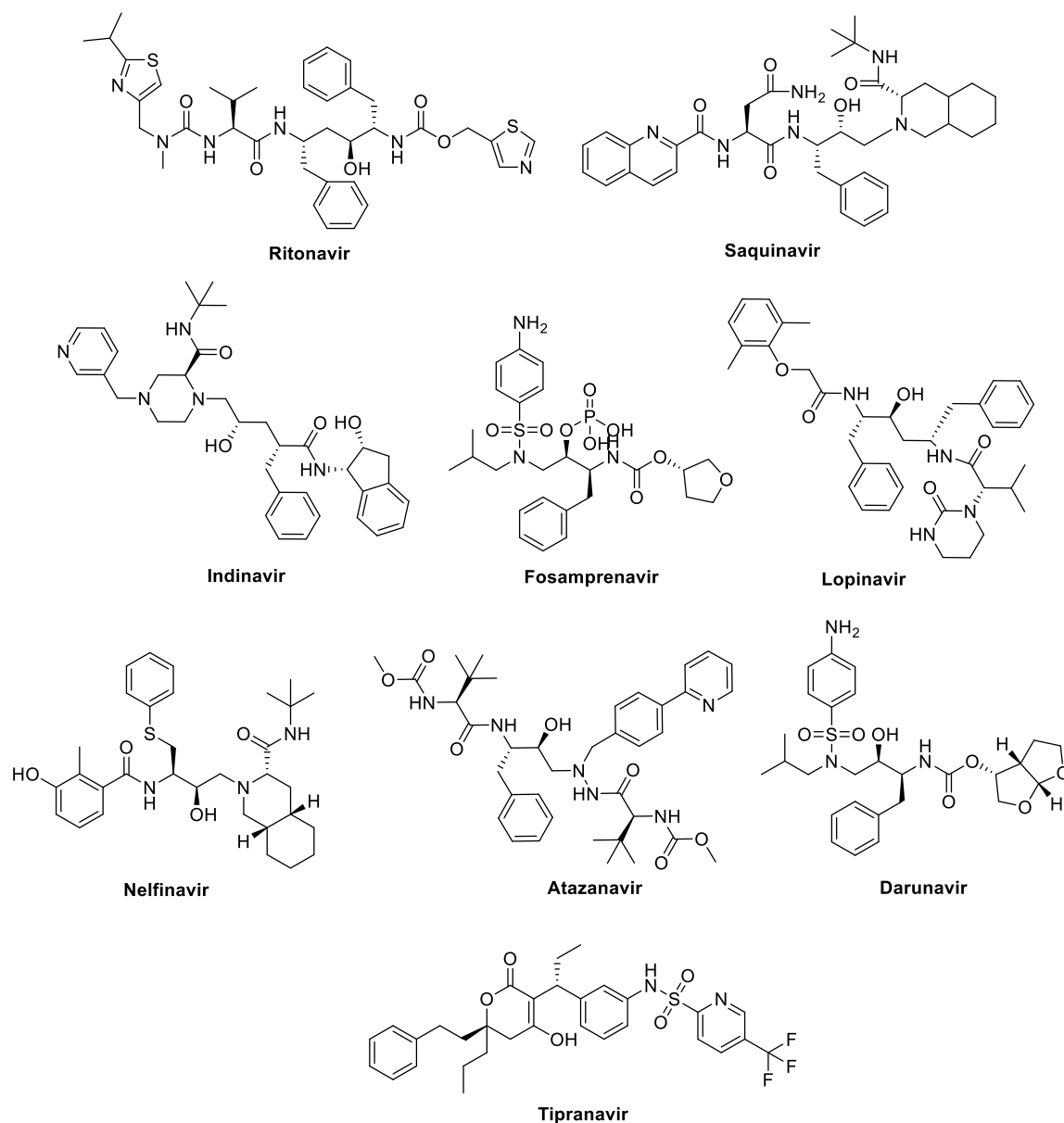


Figure 92. Structure of approved PIs.

5.2.2.4. Integrase inhibitors (INIs)

In 2008, the first INI, raltegravir, was approved [341]. INIs are potent and well-tolerated drugs that inhibit the integration of viral DNA into the human DNA via catalytic activity of integrase enzyme inhibition [345]. These agents are active in the virus which has become resistant to other antiretrovirals [340]. The drugs available as INIs are represented on Figure 93.

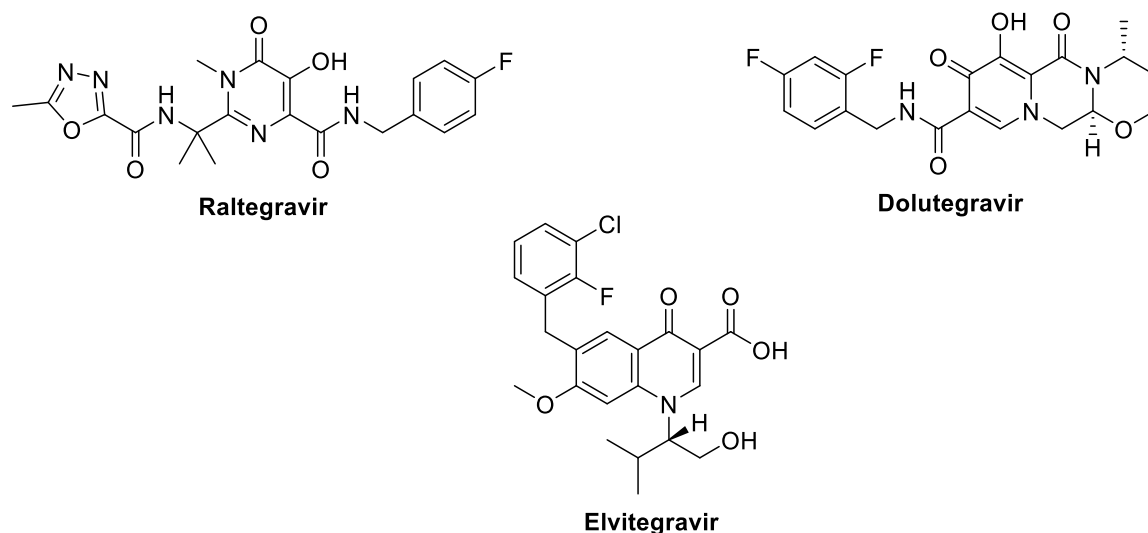


Figure 93. Structure of the marketed INIs.

5.2.2.5. Entry inhibitors (EIs)

Enfuvirtide was the first approved EI, in 2003 [341]. These type of inhibitors have different mechanisms of action [340]. Enfuvirtide binds to a region of transmembrane glycoprotein gp41 and disrupts the conformational changes associated with membrane fusion, hence blocking virus entry and inhibiting viral replication [346]. Maraviroc (Figure 94) blocks the binding of glycoprotein gp120 to CCR5 chemokine receptors which is an important step in the entry of the virus into the host cell [347]. Ibalizumab is a monoclonal antibody that binds the glycoprotein CD4 and inhibits HIV from entering in the host cells [348].

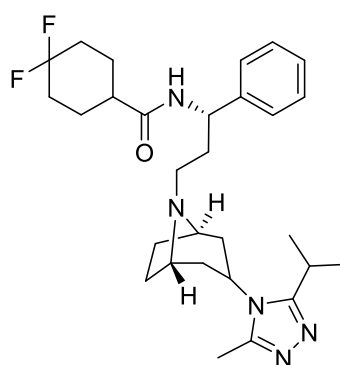


Figure 94. Structure of the marketed EI, maraviroc.

5.2.3. Therapy in the management of HIV

Nowadays, the general recommendation for all patients with HIV, who have detectable viremia, is to start antiretroviral therapy as soon as possible [338]. The most effective approach in the treatment of infected patients comprises a combination of two or more drugs with different mechanisms of action, accordingly with the presence of viral coinfections and therapy response to the different agents [338, 340, 349]. Although very efficient in the management of the infection, the existing therapeutic strategies are not capable of eradicating the virus from the patient and exhibit several disadvantages. Particularly, drug resistance and poly-drug-related toxicities [340, 350].

5.2.4. New approaches for HIV treatment

The complexity of diseases such as AIDS showed that the traditional one-target drugs are inadequate to achieve the best therapeutic effect. In fact, along the years we have learned that multi-target molecules may possess in principle a safer profile when compared with single-target ones [351]. In particular, a multi-target approach on the case of HIV could be a way to surpass the drawbacks of the current therapies. A multi-target strategy could reduce both the daily number of pills and the additive toxicity of different agents and overcome the drug resistance development [335, 352].

CHAPTER 6. Bibliography

-
- [1] P. Um, Cancer, Definition, in: S.K. Highlander, F. Rodriguez-Valera, B.A. White (Eds.) *Encyclopedia of Metagenomics: Environmental Metagenomics*, Springer US, Boston, MA, 2015, pp. 65.
- [2] D. Hanahan, Robert A. Weinberg, Hallmarks of Cancer: The Next Generation, *Cell*, 144 (2011) 646-674.
- [3] C.G. Drake, E. Jaffee, D.M. Pardoll, Mechanisms of Immune Evasion by Tumors, in: *Advances in Immunology*, Academic Press, 2006, pp. 51-81.
- [4] C.I. Diakos, K.A. Charles, D.C. McMillan, S.J. Clarke, Cancer-related inflammation and treatment effectiveness, *The Lancet Oncology*, 15 (2014) 493-503.
- [5] D. Hanahan, Rethinking the war on cancer, *The Lancet*, 383 (2014) 558-563.
- [6] R.L. Siegel, K.D. Miller, A. Jemal, Cancer statistics, 2020, *CA: A Cancer Journal for Clinicians*, 70 (2020) 7-30.
- [7] D.C. Whiteman, L.F. Wilson, The fractions of cancer attributable to modifiable factors: A global review, *Cancer Epidemiology*, 44 (2016) 203-221.
- [8] O. World Health, WHO report on cancer: setting priorities, investing wisely and providing care for all, World Health Organization, Geneva, 2020.
- [9] C.P. Wild, C. Espina, L. Bauld, B. Bonanni, H. Brenner, K. Brown, J. Dillner, D. Forman, E. Kampman, M. Nilbert, K. Steindorf, H. Storm, P. Vineis, M. Baumann, J. Schüz, Cancer Prevention Europe, *Molecular Oncology*, 13 (2019) 528-534.
- [10] R.L. Siegel, K.D. Miller, A. Jemal, Cancer statistics, 2018, *CA: A Cancer Journal for Clinicians*, 68 (2018) 7-30.
- [11] S. Pilleron, E. Soto-Perez-de-Celis, J. Vignat, J. Ferlay, I. Soerjomataram, F. Bray, D. Sarfati, Estimated global cancer incidence in the oldest adults in 2018 and projections to 2050, *International Journal of Cancer*, 148 (2021) 601-608.
- [12] S.H. Hassanpour, M. Dehghani, Review of cancer from perspective of molecular, *Journal of Cancer Research and Practice*, 4 (2017) 127-129.
- [13] N. Bhakta, L.M. Force, C. Allemani, R. Atun, F. Bray, M.P. Coleman, E. Steliarova-Foucher, A.L. Frazier, L.L. Robison, C. Rodriguez-Galindo, C. Fitzmaurice, Childhood cancer burden: a review of global estimates, *The Lancet Oncology*, 20 (2019) e42-e53.
- [14] X. Ma, H. Yu, Global burden of cancer, *Yale Journal of Biology and Medicine*, 79 (2006) 85-94.

- [15] C. Global Burden of Disease Cancer, The Global Burden of Cancer 2013, *JAMA Oncology*, 1 (2015) 505-527.
- [16] C. de Martel, D. Georges, F. Bray, J. Ferlay, G.M. Clifford, Global burden of cancer attributable to infections in 2018: a worldwide incidence analysis, *The Lancet Global Health*, 8 (2020) 180-190.
- [17] G.W. Dy, J.L. Gore, M.H. Forouzanfar, M. Naghavi, C. Fitzmaurice, Global Burden of Urologic Cancers, 1990–2013, *European Urology*, 71 (2017) 437-446.
- [18] P. Anand, A.B. Kunnumakara, C. Sundaram, K.B. Harikumar, S.T. Tharakan, O.S. Lai, B. Sung, B.B. Aggarwal, Cancer is a Preventable Disease that Requires Major Lifestyle Changes, *Pharmaceutical Research*, 25 (2008) 2097-2116.
- [19] C. Willett Walter, Balancing Life-Style and Genomics Research for Disease Prevention, *Science*, 296 (2002) 695-698.
- [20] H. Hanson, S. Hodgson, Cancer genetics and reproduction, *Best Practice & Research Clinical Obstetrics & Gynaecology*, 24 (2010) 3-18.
- [21] P. Lichtenstein, N.V. Holm, P.K. Verkasalo, A. Iliadou, J. Kaprio, M. Koskenvuo, E. Pukkala, A. Skytthe, K. Hemminki, Environmental and Heritable Factors in the Causation of Cancer — Analyses of Cohorts of Twins from Sweden, Denmark, and Finland, *New England Journal of Medicine*, 343 (2000) 78-85.
- [22] C. Turnbull, S. Hodgson, Genetic predisposition to cancer, *Clinical Medicine (London)*, 5 (2005) 491-498.
- [23] S. Koutros, K.L. Decker, D. Baris, L.A. Pardo, A. Johnson, G.M.M. Hosain, N. Rothman, M.R. Karagas, M.R. Schwenn, D.T. Silverman, Bladder cancer risk associated with family history of cancer, *International Journal of Cancer*, 148 (2021) 2915-2923.
- [24] H.S. Evans, C.M. Lewis, D. Robinson, C.M.J. Bell, H. Møller, S.V. Hodgson, Cancer risks in women with 2 breast or ovarian cancers: Clues to genetic cancer susceptibility, *International Journal of Cancer*, 94 (2001) 758-759.
- [25] M. Soegaard, K. Frederiksen, A. Jensen, E. HØGdall, C. HØGdall, J.A.N. Blaakaer, S.J. Ramus, S.A. Gayther, S.K. Kjaer, Risk of ovarian cancer in women with first-degree relatives with cancer, *Acta Obstetrica et Gynecologica Scandinavica*, 88 (2009) 449-456.
- [26] K. Nones, J. Johnson, F. Newell, A.M. Patch, H. Thorne, S.H. Kazakoff, X.M. de Luca, M.T. Parsons, K. Ferguson, L.E. Reid, A.E. McCart Reed, S. Srihari, V. Lakis, A.L. Davidson, P. Mukhopadhyay, O. Holmes, Q. Xu, S. Wood, C. Leonard, J. Beesley, J.M. Harris, D. Barnes, A. Degasperi, M.A. Ragan, A.B. Spurdle, K.K. Khanna, S.R. Lakhani,

J.V. Pearson, S. Nik-Zainal, G. Chenevix-Trench, N. Waddell, P.T. Simpson, Whole-genome sequencing reveals clinically relevant insights into the aetiology of familial breast cancers, *Annals of Oncology*, 30 (2019) 1071-1079.

[27] L.B. Alexandrov, M. Zhivagui, Mutational Signatures and the Etiology of Human Cancers, in: P. Boffetta, P. Hainaut (Eds.) *Encyclopedia of Cancer (Third Edition)*, Academic Press, Oxford, 2019, pp. 499-510.

[28] S.H. Abidi, F. Bilwani, K. Ghias, F. Abbas, Viral etiology of prostate cancer: Genetic alterations and immune response. A literature review, *International Journal of Surgery*, 52 (2018) 136-140.

[29] B.T. Hill, Etiology of Cancer, in: A.D. Singh, B.E. Damato (Eds.) *Clinical Ophthalmic Oncology: Basic Principles*, Springer International Publishing, Cham, 2019, pp. 11-17.

[30] M.A. Shaikh, S. Hussain, R. Gilhotra, S.K. Singh, S. Rawat, Y. Singh, S. Satija, M. Mehta, K. Dua, G. Gupta, Chapter 1 - Introduction to cancer cell biology, in: K. Dua, M. Mehta, T. de Jesus Andreoli Pinto, L.G. Pont, K.A. Williams, M.J. Rathbone (Eds.) *Advanced Drug Delivery Systems in the Management of Cancer*, Academic Press, 2021, pp. 1-7.

[31] H. Kuper, P. Boffetta, H.O. Adami, Tobacco use and cancer causation: association by tumour type, *Journal of Internal Medicine*, 252 (2002) 206-224.

[32] P. Gomez-Rubio, E.L. de Maturana, Molecular Epidemiology and Cancer Risk, in: P. Boffetta, P. Hainaut (Eds.) *Encyclopedia of Cancer (Third Edition)*, Academic Press, Oxford, 2019, pp. 487-493.

[33] E. Theodoratou, M. Timofeeva, X. Li, X. Meng, J.P.A. Ioannidis, Nature, Nurture, and Cancer Risks: Genetic and Nutritional Contributions to Cancer, *Annual Review of Nutrition*, 37 (2017) 293-320.

[34] C. Tiffon, The Impact of Nutrition and Environmental Epigenetics on Human Health and Disease, *International Journal of Molecular Sciences*, 19 (2018) 3425-3443.

[35] H. Mirghani, E.M. Sturgis, A. Aupérin, J. Monsonego, P. Blanchard, Is there an increased risk of cancer among spouses of patients with an HPV-related cancer: A systematic review, *Oral Oncology*, 67 (2017) 138-145.

[36] E.L. Bolf, B.L. Sprague, F.E. Carr, A Linkage Between Thyroid and Breast Cancer: A Common Etiology?, *Cancer Epidemiology Biomarkers Prevention*, 28 (2019) 643.

[37] F.L. Horsfall, Jr., A Unifying Concept Of The Genesis Of Cancer, *Medical Clinics of North America*, 50 (1966) 869-874.

- [38] K.D. Crew, A.I. Neugut, Epidemiology of gastric cancer, *World Journal of Gastroenterology*, 12 (2006) 354-362.
- [39] L. Roos, T.D. Spector, C.G. Bell, Using epigenomic studies in monozygotic twins to improve our understanding of cancer, *Epigenomics*, 6 (2014) 299-309.
- [40] A.S. Hamilton, T.M. Mack, Puberty and Genetic Susceptibility to Breast Cancer in a Case–Control Study in Twins, *New England Journal of Medicine*, 348 (2003) 2313-2322.
- [41] D. Hanahan, R.A. Weinberg, The Hallmarks of Cancer, *Cell*, 100 (2000) 57-70.
- [42] N. Darwiche, Epigenetic mechanisms and the hallmarks of cancer: an intimate affair, *American Journal of Cancer Research*, 10 (2020) 1954-1978.
- [43] M.W. Pickup, J.K. Mouw, V.M. Weaver, The extracellular matrix modulates the hallmarks of cancer, *EMBO reports*, 15 (2014) 1243-1253.
- [44] D. Paul, The systemic hallmarks of cancer, *Journal of Cancer Metastasis and Treatment*, 6 (2020).
- [45] D. Hanahan, R.A. Weinberg, Chapter 2 : Hallmarks of Cancer : An Organizing Principle for Cancer Medicine, (2015).
- [46] D.R. Welch, D.R. Hurst, Defining the Hallmarks of Metastasis, *Cancer Research*, 79 (2019) 3011-3027.
- [47] M.B. Nierengarten, Aggressive surgical approach for stage II pancreatic cancer, *Cancer*, 127 (2021) 2826-2827.
- [48] A. Wellstein, General Principles in the Pharmacotherapy of Cancer, in: L.L. Brunton, R. Hilal-Dandan, B.C. Knollmann (Eds.) *Goodman & Gilman's: The Pharmacological Basis of Therapeutics*, 13e., McGraw-Hill Education, New York, NY, 2017.
- [49] L.G. Pont, K. Dua, R.L. Cutler, H. Benson, M. Hagi, V.G. Cardenas, C.C.H. Smit, A. Ao, K.A. Williams, Chapter 2 - Current practice in cancer pharmacotherapy, in: K. Dua, M. Mehta, T. de Jesus Andreoli Pinto, L.G. Pont, K.A. Williams, M.J. Rathbone (Eds.) *Advanced Drug Delivery Systems in the Management of Cancer*, Academic Press, 2021, pp. 9-15.
- [50] Y.H. Kim, M. Mishima, Maintenance chemotherapy for non-small-cell lung cancer, *Cancer Treatment Reviews*, 37 (2011) 505-510.
- [51] M. Alexander, S.Y. Kim, H. Cheng, Update 2020: Management of Non-Small Cell Lung Cancer, *Lung*, 198 (2020) 897-907.

- [52] F. Cardoso, S. Kyriakides, S. Ohno, F. Penault-Llorca, P. Poortmans, I.T. Rubio, S. Zackrisson, E. Senkus, Early breast cancer: ESMO Clinical Practice Guidelines for diagnosis, treatment and follow-up, *Annals of Oncology*, 30 (2019) 1194-1220.
- [53] C. Parker, E. Castro, K. Fizazi, A. Heidenreich, P. Ost, G. Procopio, B. Tombal, S. Gillessen, Prostate cancer: ESMO Clinical Practice Guidelines for diagnosis, treatment and follow-up, *Annals of Oncology*, 31 (2020) 1119-1134.
- [54] G. Argilés, J. Taberero, R. Labianca, D. Hochhauser, R. Salazar, T. Iveson, P. Laurent-Puig, P. Quirke, T. Yoshino, J. Taieb, E. Martinelli, D. Arnold, Localised colon cancer: ESMO Clinical Practice Guidelines for diagnosis, treatment and follow-up, *Annals of Oncology*, 31 (2020) 1291-1305.
- [55] I. Urbino, C. Secreto, M. Olivi, V. Apolito, S. D'Ardia, C. Frairia, V. Giai, S. Aydin, R. Freilone, C. Dellacasa, L. Giaccone, D. Ferrero, E. Audisio, A. Busca, M. Cerrano, Evolving Therapeutic Approaches for Older Patients with Acute Myeloid Leukemia in 2021, *Cancers*, 13 (2021) 5075-5113.
- [56] C. Isaacs, A. Wellstein, A.T. Riegel, Hormones and Related Agents in the Therapy of Cancer, in: L.L. Brunton, R. Hilal-Dandan, B.C. Knollmann (Eds.) *Goodman & Gilman's: The Pharmacological Basis of Therapeutics*, 13e, McGraw-Hill Education, New York, NY, 2017.
- [57] L. Zhong, Y. Li, L. Xiong, W. Wang, M. Wu, T. Yuan, W. Yang, C. Tian, Z. Miao, T. Wang, S. Yang, Small molecules in targeted cancer therapy: advances, challenges, and future perspectives, *Signal Transduction and Targeted Therapy*, 6 (2021) 201.
- [58] K. Bixel, J.L. Hays, Olaparib in the management of ovarian cancer, *Pharmacogenomics and Personalized Medicine*, 8 (2015) 127-135.
- [59] T. Mehrling, Chemotherapy is getting 'smarter', *Future Oncology*, 11 (2015) 549-552.
- [60] P.E. Hughes, S. Caenepeel, L.C. Wu, Targeted Therapy and Checkpoint Immunotherapy Combinations for the Treatment of Cancer, *Trends in Immunology*, 37 (2016) 462-476.
- [61] P. Prasher, M. Sharma, K. Dua, Chapter 4 - Emerging need of advanced drug delivery systems in cancer, in: K. Dua, M. Mehta, T. de Jesus Andreoli Pinto, L.G. Pont, K.A. Williams, M.J. Rathbone (Eds.) *Advanced Drug Delivery Systems in the Management of Cancer*, Academic Press, 2021, pp. 27-36.

[62] S. Saini, Chapter 5 - Target drug delivery in cancer, in: K. Dua, M. Mehta, T. de Jesus Andreoli Pinto, L.G. Pont, K.A. Williams, M.J. Rathbone (Eds.) *Advanced Drug Delivery Systems in the Management of Cancer*, Academic Press, 2021, pp. 37-45.

[63] N. Verma, K. Thapa, K. Dua, Chapter 6 - Material and strategies used in oncology drug delivery, in: K. Dua, M. Mehta, T. de Jesus Andreoli Pinto, L.G. Pont, K.A. Williams, M.J. Rathbone (Eds.) *Advanced Drug Delivery Systems in the Management of Cancer*, Academic Press, 2021, pp. 47-62.

[64] B. Mishra, J. Singh, Chapter 7 - Hydrogel-based drug delivery systems for cancer therapy, in: K. Dua, M. Mehta, T. de Jesus Andreoli Pinto, L.G. Pont, K.A. Williams, M.J. Rathbone (Eds.) *Advanced Drug Delivery Systems in the Management of Cancer*, Academic Press, 2021, pp. 63-74.

[65] V. Schirmacher, From chemotherapy to biological therapy: A review of novel concepts to reduce the side effects of systemic cancer treatment (Review), *International Journal of Oncology*, 54 (2019) 407-419.

[66] U. Bender, Y.S. Rho, I. Barrera, S. Aghajanyan, J. Acoba, P. Kavan, Adjuvant Therapy for Stages II and III Colon Cancer: Risk Stratification, Treatment Duration, and Future Directions, *Current Oncology*, 26 (2019) 43-52.

[67] C.J. Herting, I. Karpovsky, G.B. Lesinski, The tumor microenvironment in pancreatic ductal adenocarcinoma: current perspectives and future directions, *Cancer and Metastasis Reviews*, (2021) 675-689.

[68] C.R. Quijia, M. Chorilli, Piperine for treating breast cancer: A review of molecular mechanisms, combination with anticancer drugs, and nanosystems, *Phytotherapy Research*, (2021) 147-163.

[69] J. Lindberg, J. Nilvebrant, P.-Å. Nygren, F. Lehmann, Progress and Future Directions with Peptide-Drug Conjugates for Targeted Cancer Therapy, *Molecules*, 26 (2021) 6042-6056.

[70] T.H. Maren, Carbonic anhydrase: chemistry, physiology, and inhibition, *Physiological Reviews*, 47 (1967) 595-781.

[71] S. Singh, C.L. Lomelino, M.Y. Mboge, S.C. Frost, R. McKenna, Cancer Drug Development of Carbonic Anhydrase Inhibitors beyond the Active Site, *Molecules*, 23 (2018) 1045-1066.

[72] C. Supuran, Carbonic Anhydrases An Overview, *Current pharmaceutical design*, 14 (2008) 603-614.

- [73] C.T. Supuran, Carbonic anhydrases, *Bioorganic & Medicinal Chemistry*, 21 (2013) 1377-1378.
- [74] A. Nocentini, C.T. Supuran, C. Capasso, An overview on the recently discovered iotacarboxylic anhydrases, *Journal of Enzyme Inhibition and Medicinal Chemistry*, 36 (2021) 1988-1995.
- [75] C.T. Supuran, C. Capasso, An Overview of the Bacterial Carbonic Anhydrases, *Metabolites*, 7 (2017) 56-74.
- [76] A. Angeli, M. Pinteala, S.S. Maier, S. Del Prete, C. Capasso, B.C. Simionescu, C.T. Supuran, Inhibition of α -, β -, γ -, δ -, ζ - and η -class carbonic anhydrases from bacteria, fungi, algae, diatoms and protozoans with famotidine, *Journal of Enzyme Inhibition and Medicinal Chemistry*, 34 (2019) 644-650.
- [77] A. Angeli, S. Del Prete, F.A.S. Alasmary, L.S. Alqahtani, Z. AlOthman, W.A. Donald, C. Capasso, C.T. Supuran, The first activation studies of the η -carbonic anhydrase from the malaria parasite *Plasmodium falciparum* with amines and amino acids, *Bioorganic Chemistry*, 80 (2018) 94-98.
- [78] C. Schlicker, R.A. Hall, D. Vullo, S. Middelhaufe, M. Gertz, C.T. Supuran, F.A. Mühlischlegel, C. Steegborn, Structure and Inhibition of the CO₂-Sensing Carbonic Anhydrase Can2 from the Pathogenic Fungus *Cryptococcus neoformans*, *Journal of Molecular Biology*, 385 (2009) 1207-1220.
- [79] M. Hilvo, M. Tolvanen, A. Clark, B. Shen, G.N. Shah, A. Waheed, P. Halmi, M. Hänninen, J.M. Hämäläinen, M. Vihinen, W.S. Sly, S. Parkkila, Characterization of CA XV, a new GPI-anchored form of carbonic anhydrase, *Biochememical Journal*, 392 (2005) 83-92.
- [80] O. Ozensoy Guler, C. Capasso, C.T. Supuran, A magnificent enzyme superfamily: carbonic anhydrases, their purification and characterization, *Journal of Enzyme Inhibition and Medicinal Chemistry*, 31 (2016) 689-694.
- [81] S.C. Frost, Physiological Functions of the Alpha Class of Carbonic Anhydrases, in: S.C. Frost, R. McKenna (Eds.) *Carbonic Anhydrase: Mechanism, Regulation, Links to Disease, and Industrial Applications*, Springer Netherlands, Dordrecht, 2014, pp. 9-30.
- [82] N. Pala, R. Cadoni, M. Sechi, Chapter 3 - Carbonic Anhydrase I, in: C.T. Supuran, G. De Simone (Eds.) *Carbonic Anhydrases as Biocatalysts*, Elsevier, Amsterdam, 2015, pp. 31-49.

- [83] K. D'Ambrosio, G. De Simone, C.T. Supuran, Chapter 2 - Human Carbonic Anhydrases: Catalytic Properties, Structural Features, and Tissue Distribution, in: C.T. Supuran, G. De Simone (Eds.) *Carbonic Anhydrases as Biocatalysts*, Elsevier, Amsterdam, 2015, pp. 17-30.
- [84] B.P. Mahon, R. McKenna, Chapter 5 - Carbonic Anhydrase III, in: C.T. Supuran, G. De Simone (Eds.) *Carbonic Anhydrases as Biocatalysts*, Elsevier, Amsterdam, 2015, pp. 91-108.
- [85] A. Waheed, W.S. Sly, Chapter 6 - Carbonic Anhydrase IV, in: C.T. Supuran, G. De Simone (Eds.) *Carbonic Anhydrases as Biocatalysts*, Elsevier, Amsterdam, 2015, pp. 109-124.
- [86] A. Akdemir, Ö. Güzel-Akdemir, Chapter 7 - The Structure, Physiological Role, and Potential Medicinal Applications of Carbonic Anhydrase V, in: C.T. Supuran, G. De Simone (Eds.) *Carbonic Anhydrases as Biocatalysts*, Elsevier, Amsterdam, 2015, pp. 125-138.
- [87] J. Leinonen, S. Parkkila, Chapter 8 - Secreted Carbonic Anhydrase Isoenzyme VI, in: C.T. Supuran, G. De Simone (Eds.) *Carbonic Anhydrases as Biocatalysts*, Elsevier, Amsterdam, 2015, pp. 139-149.
- [88] S.M. Monti, C.T. Supuran, G. De Simone, A. Di Fiore, Chapter 9 - Carbonic Anhydrase VII, in: C.T. Supuran, G. De Simone (Eds.) *Carbonic Anhydrases as Biocatalysts*, Elsevier, Amsterdam, 2015, pp. 151-168.
- [89] E. Ondriskova, M. Debreova, S. Pastorekova, Chapter 10 - Tumor-Associated Carbonic Anhydrases IX and XII, in: C.T. Supuran, G. De Simone (Eds.) *Carbonic Anhydrases as Biocatalysts*, Elsevier, Amsterdam, 2015, pp. 169-205.
- [90] C.T. Supuran, C. Capasso, Chapter 13 - Acatalytic Carbonic Anhydrases (CAs VIII, X, XI), in: C.T. Supuran, G. De Simone (Eds.) *Carbonic Anhydrases as Biocatalysts*, Elsevier, Amsterdam, 2015, pp. 239-245.
- [91] A. Aspatwar, M.E.E. Tolvanen, H. Barker, S. Parkkila, Chapter 11 - Carbonic Anhydrase XIII, in: C.T. Supuran, G. De Simone (Eds.) *Carbonic Anhydrases as Biocatalysts*, Elsevier, Amsterdam, 2015, pp. 207-219.
- [92] E.R. Swenson, Respiratory and renal roles of carbonic anhydrase in gas exchange and acid-base regulation, in: W.R. Chegwidden, N.D. Carter, Y.H. Edwards (Eds.) *The Carbonic Anhydrases: New Horizons*, Birkhäuser Basel, Basel, 2000, pp. 281-341.

- [93] A. Nocentini, W.A. Donald, C.T. Supuran, Chapter 8 - Human carbonic anhydrases: tissue distribution, physiological role, and druggability, in: C.T. Supuran, A. Nocentini (Eds.) *Carbonic Anhydrases*, Academic Press, 2019, pp. 151-185.
- [94] S. Lindskog, D.N. Silverman, The catalytic mechanism of mammalian carbonic anhydrases, in: W.R. Chegwidden, N.D. Carter, Y.H. Edwards (Eds.) *The Carbonic Anhydrases: New Horizons*, Birkhäuser Basel, Basel, 2000, pp. 175-195.
- [95] A.J. Esbaugh, B.L. Tufts, The structure and function of carbonic anhydrase isozymes in the respiratory system of vertebrates, *Respiratory Physiology & Neurobiology*, 154 (2006) 185-198.
- [96] C.T. Supuran, A. Scozzafava, A. Casini, Carbonic anhydrase inhibitors, *Medicinal Research Reviews*, 23 (2003) 146-189.
- [97] C.T. Supuran, C. Capasso, The η -class carbonic anhydrases as drug targets for antimalarial agents, *Expert Opinion on Therapeutic Targets*, 19 (2015) 551-563.
- [98] C.T. Supuran, C. Capasso, Antibacterial carbonic anhydrase inhibitors: an update on the recent literature, *Expert Opinion on Therapeutic Patents*, 30 (2020) 963-982.
- [99] Y. Xu, L. Feng, P.D. Jeffrey, Y. Shi, F.M.M. Morel, Structure and metal exchange in the cadmium carbonic anhydrase of marine diatoms, *Nature*, 452 (2008) 56-61.
- [100] M. Ferraroni, S. Del Prete, D. Vullo, C. Capasso, C.T. Supuran, Crystal structure and kinetic studies of a tetrameric type II [beta]-carbonic anhydrase from the pathogenic bacterium *Vibrio cholerae*, *Acta Crystallographica Section D*, 71 (2015) 2449-2456.
- [101] G. De Simone, S.M. Monti, V. Alterio, M. Buonanno, V. De Luca, M. Rossi, V. Carginale, C.T. Supuran, C. Capasso, A. Di Fiore, Crystal structure of the most catalytically effective carbonic anhydrase enzyme known, SazCA from the thermophilic bacterium *Sulfurihydrogenibium azorense*, *Bioorganic & Medicinal Chemistry Letters*, 25 (2015) 2002-2006.
- [102] A. Di Fiore, C. Capasso, V. De Luca, S.M. Monti, V. Carginale, C.T. Supuran, A. Scozzafava, C. Pedone, M. Rossi, G. De Simone, X-ray structure of the first 'extremo-[alpha]-carbonic anhydrase', a dimeric enzyme from the thermophilic bacterium *Sulfurihydrogenibium yellowstonense* YO3AOP1, *Acta Crystallographica Section D*, 69 (2013) 1150-1159.
- [103] C.L. Lomelino, B.P. Mahon, R. McKenna, F. Carta, C.T. Supuran, Kinetic and X-ray crystallographic investigations on carbonic anhydrase isoforms I, II, IX and XII of a thioureido analog of SLC-0111, *Bioorganic & Medicinal Chemistry*, 24 (2016) 976-981.

- [104] K. D'Ambrosio, A. Di Fiore, M. Buonanno, S.M. Monti, G. De Simone, Chapter 7 - η - and θ -carbonic anhydrases, in: C.T. Supuran, A. Nocentini (Eds.) *Carbonic Anhydrases*, Academic Press, 2019, pp. 139-148.
- [105] V. Alterio, E. Langella, F. Viparelli, D. Vullo, G. Ascione, N.A. Dathan, F.M.M. Morel, C.T. Supuran, G. De Simone, S.M. Monti, Structural and inhibition insights into carbonic anhydrase CDCA1 from the marine diatom *Thalassiosira weissflogii*, *Biochimie*, 94 (2012) 1232-1241.
- [106] A. Di Fiore, E. Truppo, C.T. Supuran, V. Alterio, N. Dathan, F. Booterabi, S. Parkkila, S.M. Monti, G.D. Simone, Crystal structure of the C183S/C217S mutant of human CA VII in complex with acetazolamide, *Bioorganic & Medicinal Chemistry Letters*, 20 (2010) 5023-5026.
- [107] D.M. Duda, C. Tu, S.Z. Fisher, H. An, C. Yoshioka, L. Govindasamy, P.J. Laipis, M. Agbandje-McKenna, D.N. Silverman, R. McKenna, Human Carbonic Anhydrase III: Structural and Kinetic Study of Catalysis and Proton Transfer, *Biochemistry*, 44 (2005) 10046-10053.
- [108] V. Alterio, M. Hilvo, A. Di Fiore, C.T. Supuran, P. Pan, S. Parkkila, A. Scaloni, J. Pastorek, S. Pastorekova, C. Pedone, A. Scozzafava, S.M. Monti, G. De Simone, Crystal structure of the catalytic domain of the tumor-associated human carbonic anhydrase IX, *Proceedings of the National Academy of Sciences*, 106 (2009) 16233-16238.
- [109] S. Lindskog, Structure and mechanism of carbonic anhydrase, *Pharmacology & Therapeutics*, 74 (1997) 1-20.
- [110] B. Sjöblom, M. Polentarutti, K. Djinović-Carugo, Structural study of X-ray induced activation of carbonic anhydrase, *Proceedings of the National Academy of Sciences*, 106 (2009) 10609-10613.
- [111] V. Alterio, A. Di Fiore, K. D'Ambrosio, C.T. Supuran, G. De Simone, Multiple Binding Modes of Inhibitors to Carbonic Anhydrases: How to Design Specific Drugs Targeting 15 Different Isoforms?, *Chemical Reviews*, 112 (2012) 4421-4468.
- [112] K.S. Smith, J.G. Ferry, Prokaryotic carbonic anhydrases, *FEMS Microbiology Reviews*, 24 (2000) 335-366.
- [113] D.A. Whittington, A. Waheed, B. Ulmasov, G.N. Shah, J.H. Grubb, W.S. Sly, D.W. Christianson, Crystal structure of the dimeric extracellular domain of human carbonic anhydrase XII, a bitopic membrane protein overexpressed in certain cancer tumor cells, *Proceedings of the National Academy of Sciences*, 98 (2001) 9545-9550.

- [114] E.S. Pilka, G. Kochan, U. Oppermann, W.W. Yue, Crystal structure of the secretory isozyme of mammalian carbonic anhydrases CA VI: Implications for biological assembly and inhibitor development, *Biochemical and Biophysical Research Communications*, 419 (2012) 485-489.
- [115] J.F. Domsic, B.S. Avvaru, C.U. Kim, S.M. Gruner, M. Agbandje-McKenna, D.N. Silverman, R. McKenna, Entrapment of Carbon Dioxide in the Active Site of Carbonic Anhydrase II, *Journal of Biological Chemistry*, 283 (2008) 30766-30771.
- [116] C.T. Supuran, Structure-based drug discovery of carbonic anhydrase inhibitors, *Journal of Enzyme Inhibition and Medicinal Chemistry*, 27 (2012) 759-772.
- [117] T.S. Claudiu, Carbonic Anhydrases as Drug Targets - An Overview, *Current Topics in Medicinal Chemistry*, 7 (2007) 825-833.
- [118] C.T. Supuran, Carbonic Anhydrases as Drug Targets: General Presentation, in: C.T. Supuran, J.-Y. Winum (Eds.) *Drug Design of Zinc-Enzyme Inhibitors*, John Wiley & Sons, Inc., New Jersey, 2009, pp. 13-38.
- [119] G. De Simone, V. Alterio, C.T. Supuran, Exploiting the hydrophobic and hydrophilic binding sites for designing carbonic anhydrase inhibitors, *Expert Opinion on Drug Discovery*, 8 (2013) 793-810.
- [120] D.W. Christianson, C.A. Fierke, Carbonic Anhydrase: Evolution of the Zinc Binding Site by Nature and by Design, *Accounts of Chemical Research*, 29 (1996) 331-339.
- [121] D.N. Silverman, S. Lindskog, The catalytic mechanism of carbonic anhydrase: implications of a rate-limiting protolysis of water, *Accounts of Chemical Research*, 21 (1988) 30-36.
- [122] R.L. Mikulski, D.N. Silverman, Proton transfer in catalysis and the role of proton shuttles in carbonic anhydrase, *Biochimica et Biophysica Acta (BBA) - Proteins and Proteomics*, 1804 (2010) 422-426.
- [123] Claudiu T. Supuran, Structure and function of carbonic anhydrases, *Biochemical Journal*, 473 (2016) 2023-2032.
- [124] C.M. Maupin, N. Castillo, S. Taraphder, C. Tu, R. McKenna, D.N. Silverman, G.A. Voth, Chemical Rescue of Enzymes: Proton Transfer in Mutants of Human Carbonic Anhydrase II, *Journal of the American Chemical Society*, 133 (2011) 6223-6234.
- [125] C.T. Supuran, Carbonic anhydrases: novel therapeutic applications for inhibitors and activators, *Nature Reviews Drug Discovery*, 7 (2008) 168-181.

- [126] C. Temperini, A. Scozzafava, D. Vullo, C.T. Supuran, Carbonic Anhydrase Activators. Activation of Isozymes I, II, IV, VA, VII, and XIV with L- and D-Histidine and Crystallographic Analysis of Their Adducts with Isoform II: Engineering Proton-Transfer Processes within the Active Site of an Enzyme, *Chemistry – A European Journal*, 12 (2006) 7057-7066.
- [127] C.T. Supuran, Carbonic anhydrase activators, *Future Medicinal Chemistry*, 10 (2018) 561-573.
- [128] E. Licsandru, M. Tanc, I. Kocsis, M. Barboiu, C.T. Supuran, A class of carbonic anhydrase I – selective activators, *Journal of Enzyme Inhibition and Medicinal Chemistry*, 32 (2017) 37-46.
- [129] A. Nocentini, D. Cuffaro, L. Ciccone, E. Orlandini, S. Nencetti, E. Nuti, A. Rossello, C.T. Supuran, Activation of carbonic anhydrases from human brain by amino alcohol oxime ethers: towards human carbonic anhydrase VII selective activators, *Journal of Enzyme Inhibition and Medicinal Chemistry*, 36 (2021) 48-57.
- [130] M.-C. Saada, J.-L. Montero, D. Vullo, A. Scozzafava, J.-Y. Winum, C.T. Supuran, Carbonic Anhydrase Activators: Gold Nanoparticles Coated with Derivatized Histamine, Histidine, and Carnosine Show Enhanced Activatory Effects on Several Mammalian Isoforms, *Journal of Medicinal Chemistry*, 54 (2011) 1170-1177.
- [131] D. Vullo, V. De Luca, A. Scozzafava, V. Carginale, M. Rossi, C.T. Supuran, C. Capasso, The first activation study of a bacterial carbonic anhydrase (CA). The thermostable α -CA from *Sulfurihydrogenibium yellowstonense* YO3AOP1 is highly activated by amino acids and amines, *Bioorganic & Medicinal Chemistry Letters*, 22 (2012) 6324-6327.
- [132] C.T. Supuran, Carbonic anhydrase inhibitors and activators for novel therapeutic applications, *Future Medicinal Chemistry*, 3 (2011) 1165-1180.
- [133] A. Thiry, j.-m. dogné, C. Supuran, B. Masereel, Anticonvulsant Sulfonamides/Sulfamates/Sulfamides with Carbonic Anhydrase Inhibitory Activity: Drug Design and Mechanism of Action, *Current pharmaceutical design*, 14 (2008) 661-671.
- [134] C. Supuran, Diuretics: From Classical Carbonic Anhydrase Inhibitors to Novel Applications of the Sulfonamides, *Current pharmaceutical design*, 14 (2008) 641-648.
- [135] E. Masini, F. Carta, A. Scozzafava, C.T. Supuran, Antiglaucoma carbonic anhydrase inhibitors: a patent review, *Expert Opinion on Therapeutic Patents*, 23 (2013) 705-716.

- [136] T.J. Wolfensberger, The role of carbonic anhydrase inhibitors in the management of macular edema, *Documenta Ophthalmologica*, 97 (1999) 387-397.
- [137] M. Aggarwal, B. Kondeti, R. McKenna, Anticonvulsant/antiepileptic carbonic anhydrase inhibitors: a patent review, *Expert Opinion on Therapeutic Patents*, 23 (2013) 717-724.
- [138] A. Scozzafava, C.T. Supuran, F. Carta, Antiobesity carbonic anhydrase inhibitors: a literature and patent review, *Expert Opinion on Therapeutic Patents*, 23 (2013) 725-735.
- [139] C.T. Supuran, Carbonic Anhydrase Inhibition and the Management of Hypoxic Tumors, *Metabolites*, 7 (2017) 48-61.
- [140] C.T. Supuran, Carbonic anhydrase inhibition and the management of neuropathic pain, *Expert Review of Neurotherapeutics*, 16 (2016) 961-968.
- [141] L. Di Cesare Mannelli, L. Micheli, F. Carta, A. Cozzi, C. Ghelardini, C.T. Supuran, Carbonic anhydrase inhibition for the management of cerebral ischemia: in vivo evaluation of sulfonamide and coumarin inhibitors, *Journal of Enzyme Inhibition and Medicinal Chemistry*, 31 (2016) 894-899.
- [142] S. Bua, L. Di Cesare Mannelli, D. Vullo, C. Ghelardini, G. Bartolucci, A. Scozzafava, C.T. Supuran, F. Carta, Design and Synthesis of Novel Nonsteroidal Anti-Inflammatory Drugs and Carbonic Anhydrase Inhibitors Hybrids (NSAIDs–CAIs) for the Treatment of Rheumatoid Arthritis, *Journal of Medicinal Chemistry*, 60 (2017) 1159-1170.
- [143] J.-Y. Winum, J.-L. Montero, A. Scozzafava, C. Supuran, Zinc Binding Functions in the Design of Carbonic Anhydrase Inhibitors, in: C.T. Supuran, J.-Y. Winum (Eds.) *Drug Design of Zinc-Enzyme Inhibitors*, John Wiley & Sons, Inc., New Jersey, 2009, pp. 39-72.
- [144] C.T. Supuran, How many carbonic anhydrase inhibition mechanisms exist?, *Journal of Enzyme Inhibition and Medicinal Chemistry*, 31 (2016) 345-360.
- [145] M.A. Ilies, Metal Complexes of Sulfonamides as Dual Carbonic Anhydrase Inhibitors, in: C.T. Supuran, J.-Y. Winum (Eds.) *Drug Design of Zinc-Enzyme Inhibitors*, John Wiley & Sons, Inc., New Jersey, 2009, pp. 439-472.
- [146] F. Carta, C. Temperini, A. Innocenti, A. Scozzafava, K. Kaila, C.T. Supuran, Polyamines Inhibit Carbonic Anhydrases by Anchoring to the Zinc-Coordinated Water Molecule, *Journal of Medicinal Chemistry*, 53 (2010) 5511-5522.
- [147] A. Innocenti, S. Beyza Öztürk Sarıkaya, İ. Gülçin, C.T. Supuran, Carbonic anhydrase inhibitors. Inhibition of mammalian isoforms I–XIV with a series of natural product polyphenols and phenolic acids, *Bioorganic & Medicinal Chemistry*, 18 (2010) 2159-2164.

- [148] D.P. Martin, S.M. Cohen, Nucleophile recognition as an alternative inhibition mode for benzoic acid based carbonic anhydrase inhibitors, *Chemical Communications*, 48 (2012) 5259-5261.
- [149] K. Tars, D. Vullo, A. Kazaks, J. Leitans, A. Lends, A. Grandane, R. Zalubovskis, A. Scozzafava, C.T. Supuran, Sulfocoumarins (1,2-Benzoxathiine-2,2-dioxides): A Class of Potent and Isoform-Selective Inhibitors of Tumor-Associated Carbonic Anhydrases, *Journal of Medicinal Chemistry*, 56 (2013) 293-300.
- [150] L.E. Riafrecha, O.M. Rodríguez, D. Vullo, C.T. Supuran, P.A. Colinas, Synthesis of C-cinnamoyl glycosides and their inhibitory activity against mammalian carbonic anhydrases, *Bioorganic & Medicinal Chemistry*, 21 (2013) 1489-1494.
- [151] C.T. Supuran, Carbonic anhydrase inhibition with natural products: novel chemotypes and inhibition mechanisms, *Molecular Diversity*, 15 (2011) 305-316.
- [152] A. Maresca, C. Temperini, H. Vu, N.B. Pham, S.-A. Poulsen, A. Scozzafava, R.J. Quinn, C.T. Supuran, Non-Zinc Mediated Inhibition of Carbonic Anhydrases: Coumarins Are a New Class of Suicide Inhibitors, *Journal of the American Chemical Society*, 131 (2009) 3057-3062.
- [153] A. Maresca, C. Temperini, L. Pochet, B. Masereel, A. Scozzafava, C.T. Supuran, Deciphering the Mechanism of Carbonic Anhydrase Inhibition with Coumarins and Thiocoumarins, *Journal of Medicinal Chemistry*, 53 (2010) 335-344.
- [154] K. D'Ambrosio, S. Carradori, S.M. Monti, M. Buonanno, D. Secci, D. Vullo, C.T. Supuran, G. De Simone, Out of the active site binding pocket for carbonic anhydrase inhibitors, *Chemical Communications*, 51 (2015) 302-305.
- [155] D. Ekinçi, İ. Fidan, S. Durdagi, Ş. Kaban, C.T. Supuran, Kinetic and in silico analysis of thiazolidin-based inhibitors of α -carbonic anhydrase isoenzymes, *Journal of Enzyme Inhibition and Medicinal Chemistry*, 28 (2013) 370-374.
- [156] M. Arslan, M. Şentürk, İ. Fidan, O. Talaz, D. Ekinçi, S. Coşgun, C.T. Supuran, Synthesis of 3,4-dihydropyrrolidine-2,5-dione and 3,5-dihydroxybenzoic acid derivatives and evaluation of the carbonic anhydrase I and II inhibition, *Journal of Enzyme Inhibition and Medicinal Chemistry*, 30 (2015) 896-900.
- [157] G. Compain, A. Martin-Mingot, A. Maresca, S. Thibaudeau, C.T. Supuran, Superacid synthesis of halogen containing N-substituted-4-aminobenzene sulfonamides: New selective tumor-associated carbonic anhydrase inhibitors, *Bioorganic & Medicinal Chemistry*, 21 (2013) 1555-1563.

- [158] B. Métayer, A. Mingot, D. Vullo, C.T. Supuran, S. Thibaudeau, New superacid synthesized (fluorinated) tertiary benzenesulfonamides acting as selective hCA IX inhibitors: toward a new mode of carbonic anhydrase inhibition by sulfonamides, *Chemical Communications*, 49 (2013) 6015-6017.
- [159] V. Král, P. Mader, R. Collard, M. Fábry, M. Hořejší, P. Řezáčová, M. Kožíšek, J. Závada, J. Sedláček, L. Rulíšek, J. Brynda, Stabilization of antibody structure upon association to a human carbonic anhydrase IX epitope studied by X-ray crystallography, microcalorimetry, and molecular dynamics simulations, *Proteins: Structure, Function, and Bioinformatics*, 71 (2008) 1275-1287.
- [160] N.K. Tafreshi, M.C. Lloyd, M.M. Bui, R.J. Gillies, D.L. Morse, Carbonic anhydrase IX as an imaging and therapeutic target for tumors and metastases, *Sub-cellular Biochemistry*, 75 (2014) 221-254.
- [161] C.T. Supuran, A. Mugelli, Polypharmacology of carbonic anhydrase inhibitors, *Pharmadvances*, (2019) 14-38.
- [162] B.-B. Gao, A. Clermont, S. Rook, S.J. Fonda, V.J. Srinivasan, M. Wojtkowski, J.G. Fujimoto, R.L. Avery, P.G. Arrigg, S.-E. Bursell, L.P. Aiello, E.P. Feener, Extracellular carbonic anhydrase mediates hemorrhagic retinal and cerebral vascular permeability through prekallikrein activation, *Nature Medicine*, 13 (2007) 181-188.
- [163] F. Mincione, A. Scozzafava, C. Supuran, The development of topically acting carbonic anhydrase inhibitors as anti-glaucoma agents, *Current topics in medicinal chemistry*, 7 (2007) 849-854.
- [164] L. Ciccone, C. Cerri, S. Nencetti, E. Orlandini, Carbonic Anhydrase Inhibitors and Epilepsy: State of the Art and Future Perspectives, *Molecules*, 26 (2021) 6380-6396.
- [165] E.R. Swenson, L.J. Teppema, Prevention of acute mountain sickness by acetazolamide: as yet an unfinished story, *Journal of Applied Physiology*, 102 (2007) 1305-1307.
- [166] U.-J.P. Zimmerman, P. Wang, X. Zhang, S. Bogdanovich, R.E. Forster, Anti-Oxidative Response of Carbonic Anhydrase III in Skeletal Muscle, *IUBMB Life*, 56 (2004) 343-347.
- [167] R. Datta, A. Waheed, G. Bonapace, G.N. Shah, W.S. Sly, Pathogenesis of retinitis pigmentosa associated with apoptosis-inducing mutations in carbonic anhydrase IV, *Proceedings of the National Academy of Sciences*, 106 (2009) 3437-3442.

- [168] I. Bulli, I. Dettori, E. Coppi, F. Cherchi, M. Venturini, L. Di Cesare Mannelli, C. Ghelardini, A. Nocentini, C.T. Supuran, A.M. Pugliese, F. Pedata, Role of Carbonic Anhydrase in Cerebral Ischemia and Carbonic Anhydrase Inhibitors as Putative Protective Agents, *International Journal of Molecular Sciences*, 22 (2021) 5029-5039.
- [169] G. De Simone, A. Di Fiore, C. Supuran, Are Carbonic Anhydrase Inhibitors Suitable for Obtaining Antiobesity Drugs ?, *Current pharmaceutical design*, 14 (2008) 655-660.
- [170] I. Nishimori, T. Minakuchi, S. Onishi, D. Vullo, A. Scozzafava, C.T. Supuran, Carbonic Anhydrase Inhibitors. DNA Cloning, Characterization, and Inhibition Studies of the Human Secretory Isoform VI, a New Target for Sulfonamide and Sulfamate Inhibitors, *Journal of Medicinal Chemistry*, 50 (2007) 381-388.
- [171] G. De Simone, A. Scozzafava, C.T. Supuran, Which Carbonic Anhydrases are Targeted by the Antiepileptic Sulfonamides and Sulfamates?, *Chemical Biology & Drug Design*, 74 (2009) 317-321.
- [172] G. De Simone, C.T. Supuran, Carbonic anhydrase IX: Biochemical and crystallographic characterization of a novel antitumor target, *Biochimica et Biophysica Acta (BBA) - Proteins and Proteomics*, 1804 (2010) 404-409.
- [173] C.T. Supuran, J.-Y. Winum, Carbonic anhydrase IX inhibitors in cancer therapy: an update, *Future Medicinal Chemistry*, 7 (2015) 1407-1414.
- [174] O.O. Guler, D.G. Simone, T.C. Supuran, Drug Design Studies of the Novel Antitumor Targets Carbonic Anhydrase IX and XII, *Current Medicinal Chemistry*, 17 (2010) 1516-1526.
- [175] C. Battke, E. Kremmer, J. Mysliwicz, G. Gondi, C. Dumitru, S. Brandau, S. Lang, D. Vullo, C. Supuran, R. Zeidler, Generation and characterization of the first inhibitory antibody targeting tumour-associated carbonic anhydrase XII, *Cancer Immunology, Immunotherapy*, 60 (2011) 649-658.
- [176] A. Scozzafava, C.T. Supuran, Glaucoma and the Applications of Carbonic Anhydrase Inhibitors, in: S.C. Frost, R. McKenna (Eds.) *Carbonic Anhydrase: Mechanism, Regulation, Links to Disease, and Industrial Applications*, Springer Netherlands, Dordrecht, 2014, pp. 349-359.
- [177] J. Lehtonen, B. Shen, M. Vihinen, A. Casini, A. Scozzafava, C.T. Supuran, A.-K. Parkkila, J. Saarnio, A.J. Kivelä, A. Waheed, W.S. Sly, S. Parkkila, Characterization of CA XIII, a Novel Member of the Carbonic Anhydrase Isozyme Family, *Journal of Biological Chemistry*, 279 (2004) 2719-2727.

- [178] J.M. Ogilvie, K.K. Ohlemiller, G.N. Shah, B. Ulmasov, T.A. Becker, A. Waheed, A.K. Hennig, P.D. Lukasiewicz, W.S. Sly, Carbonic anhydrase XIV deficiency produces a functional defect in the retinal light response, *Proceedings of the National Academy of Sciences*, 104 (2007) 8514-8519.
- [179] P. Brancaccio, G. Lippi, N. Maffulli, Biochemical markers of muscular damage, *Clinical Chemistry and Laboratory Medicine*, 48 (2010) 757-767.
- [180] Y. Tang, H. Xu, X.L. Du, L. Lit, W. Walker, A. Lu, R. Ran, J.P. Gregg, M. Reilly, A. Pancioli, J.C. Khoury, L.R. Sauerbeck, J.A. Carrozzella, J. Spilker, J. Clark, K.R. Wagner, E.C. Jauch, D.J. Chang, P. Verro, J.P. Broderick, F.R. Sharp, Gene Expression in Blood Changes Rapidly in Neutrophils and Monocytes after Ischemic Stroke in Humans: A Microarray Study, *Journal of Cerebral Blood Flow & Metabolism*, 26 (2006) 1089-1102.
- [181] M.Y. Mboge, B.P. Mahon, R. McKenna, S.C. Frost, Carbonic Anhydrases: Role in pH Control and Cancer, *Metabolites*, 8 (2018) 19-50.
- [182] S. Pastorekova, S. Parkkila, J. Závada, Tumor-associated Carbonic Anhydrases and Their Clinical Significance, *Advances in clinical chemistry*, 42 (2006) 167-216.
- [183] C.T. Supuran, V. Alterio, A. Di Fiore, K. D' Ambrosio, F. Carta, S.M. Monti, G. De Simone, Inhibition of carbonic anhydrase IX targets primary tumors, metastases, and cancer stem cells: Three for the price of one, *Medicinal Research Reviews*, 38 (2018) 1799-1836.
- [184] A. Nocentini, C.T. Supuran, Carbonic anhydrase inhibitors as antitumor/antimetastatic agents: a patent review (2008–2018), *Expert Opinion on Therapeutic Patents*, 28 (2018) 729-740.
- [185] H.M. Becker, Carbonic anhydrase IX and acid transport in cancer, *British Journal of Cancer*, 122 (2020) 157-167.
- [186] S. Pastorekova, R.J. Gillies, The role of carbonic anhydrase IX in cancer development: links to hypoxia, acidosis, and beyond, *Cancer and Metastasis Reviews*, 38 (2019) 65-77.
- [187] J. Pastorek, S. Pastoreková, I. Callebaut, J.P. Mornon, V. Zelník, R. Opavsky, M. Zat'ovicová, S.Y. Liao, D. Portetelle, E.J. Stanbridge, Cloning and characterization of MN, a human tumor-associated protein with a domain homologous to carbonic anhydrase and a putative helix-loop-helix DNA binding segment, *Oncogene*, 9 (1994) 2877-2888.
- [188] J.T. Andring, M. Fouch, S. Akocak, A. Angeli, C.T. Supuran, M.A. Ilies, R. McKenna, Structural Basis of Nanomolar Inhibition of Tumor-Associated Carbonic Anhydrase IX: X-

Ray Crystallographic and Inhibition Study of Lipophilic Inhibitors with Acetazolamide Backbone, *Journal of Medicinal Chemistry*, 63 (2020) 13064-13075.

[189] A.P. Aldera, D. Govender, Carbonic anhydrase IX: a regulator of pH and participant in carcinogenesis, *Journal of Clinical Pathology*, 74 (2021) 350-354.

[190] T. Wingo, C. Tu, P.J. Laipis, D.N. Silverman, The Catalytic Properties of Human Carbonic Anhydrase IX, *Biochemical and Biophysical Research Communications*, 288 (2001) 666-669.

[191] A. Di Fiore, C.T. Supuran, A. Scaloni, G. De Simone, Post-translational modifications in tumor-associated carbonic anhydrases, *Amino Acids*, (2021).

[192] Ö. Türeci, U. Sahin, E. Vollmar, S. Siemer, E. Göttert, G. Seitz, A.-K. Parkkila, G.N. Shah, J.H. Grubb, M. Pfreundschuh, W.S. Sly, Human carbonic anhydrase XII: cDNA cloning, expression, and chromosomal localization of a carbonic anhydrase gene that is overexpressed in some renal cell cancers, *Proceedings of the National Academy of Sciences*, 95 (1998) 7608-7613.

[193] S. Parkkila, A.-K. Parkkila, J. Saarnio, J. Kivelä, T.J. Karttunen, K. Kaunisto, A. Waheed, W.S. Sly, Ö. Türeci, I. Virtanen, H. Rajaniemi, Expression of the Membrane-associated Carbonic Anhydrase Isozyme XII in the Human Kidney and Renal Tumors, *Journal of Histochemistry & Cytochemistry*, 48 (2000) 1601-1608.

[194] A. McIntyre, S. Patiar, S. Wigfield, J.-I. Li, I. Ledaki, H. Turley, R. Leek, C. Snell, K. Gatter, W.S. Sly, R.D. Vaughan-Jones, P. Swietach, A.L. Harris, Carbonic Anhydrase IX Promotes Tumor Growth and Necrosis In Vivo and Inhibition Enhances Anti-VEGF Therapy, *Clinical Cancer Research*, 18 (2012) 3100-3111.

[195] A. Waheed, W.S. Sly, Carbonic anhydrase XII functions in health and disease, *Gene*, 623 (2017) 33-40.

[196] S. Daunys, V. Petrikaitė, The roles of carbonic anhydrases IX and XII in cancer cell adhesion, migration, invasion and metastasis, *Biology of the Cell*, 112 (2020) 383-397.

[197] J. Chiche, K. Ilc, M.C. Brahimi-Horn, J. Pouyssegur, Membrane-bound carbonic anhydrases are key pH regulators controlling tumor growth and cell migration, *Advances in Enzyme Regulation*, 50 (2010) 20-33.

[198] H.M. Becker, J.W. Deitmer, Proton Transport in Cancer Cells: The Role of Carbonic Anhydrases, *International Journal of Molecular Sciences*, 22 (2021) 3171-3188.

- [199] S. Kumar, S. Rulhania, S. Jaswal, V. Monga, Recent advances in the medicinal chemistry of carbonic anhydrase inhibitors, *European Journal of Medicinal Chemistry*, 209 (2021) 112923-112964.
- [200] C.B. Mishra, M. Tiwari, C.T. Supuran, Progress in the development of human carbonic anhydrase inhibitors and their pharmacological applications: Where are we today?, *Medicinal Research Reviews*, 40 (2020) 2485-2565.
- [201] C. Temperini, A. Cecchi, A. Scozzafava, C.T. Supuran, Carbonic anhydrase inhibitors. Sulfonamide diuretics revisited—old leads for new applications?, *Organic & Biomolecular Chemistry*, 6 (2008) 2499-2506.
- [202] R. Kassamali, D.A. Sica, Acetazolamide: A Forgotten Diuretic Agent, *Cardiology in Review*, 19 (2011) 276-278.
- [203] S. Bua, A. Nocentini, C.T. Supuran, Chapter 14 - Carbonic anhydrase inhibitors as diuretics, in: C.T. Supuran, A. Nocentini (Eds.) *Carbonic Anhydrases*, Academic Press, 2019, pp. 287-309.
- [204] A.P. Cherecheanu, G. Garhofer, D. Schmidl, R. Werkmeister, L. Schmetterer, Ocular perfusion pressure and ocular blood flow in glaucoma, *Current Opinion in Pharmacology*, 13 (2013) 36-42.
- [205] C.T. Supuran, A.S.A. Altamimi, F. Carta, Carbonic anhydrase inhibition and the management of glaucoma: a literature and patent review 2013-2019, *Expert Opinion on Therapeutic Patents*, 29 (2019) 781-792.
- [206] C.T. Supuran, A. Scozzafava, Carbonic anhydrase inhibitors and their therapeutic potential, *Expert Opinion on Therapeutic Patents*, 10 (2000) 575-600.
- [207] E. Masini, S. Sgambellone, L. Lucarini, Carbonic anhydrase inhibitors as ophthalmologic drugs for the treatment of glaucoma, in: C.T. Supuran, A. Nocentini (Eds.) *Carbonic Anhydrases*, Academic Press, 2019, pp. 269-285.
- [208] C. Holroyd, C. Cooper, E. Dennison, Epidemiology of osteoporosis, *Best Practice & Research Clinical Endocrinology & Metabolism*, 22 (2008) 671-685.
- [209] R. Riihonen, C.T. Supuran, S. Parkkila, S. Pastorekova, H.K. Väänänen, T. Laitala-Leinonen, Membrane-bound carbonic anhydrases in osteoclasts, *Bone*, 40 (2007) 1021-1031.
- [210] A.D. Kenny, Role of Carbonic Anhydrase in Bone: Plasma Acetazolamide Concentrations Associated with Inhibition of Bone Loss, *Pharmacology*, 31 (1985) 97-107.

[211] E. Berrino, F. Carta, Chapter 15 - Carbonic anhydrase inhibitors for the treatment of epilepsy and obesity, in: C.T. Supuran, A. Nocentini (Eds.) Carbonic Anhydrases, Academic Press, 2019, pp. 311-329.

[212] A. Thiry, J.-M. Dogne, T.C. Supuran, B. Masereel, Carbonic Anhydrase Inhibitors as Anticonvulsant Agents, *Current Topics in Medicinal Chemistry*, 7 (2007) 855-864.

[213] C. Temperini, A. Innocenti, A. Mastrolorenzo, A. Scozzafava, C.T. Supuran, Carbonic anhydrase inhibitors. Interaction of the antiepileptic drug sulthiame with twelve mammalian isoforms: Kinetic and X-ray crystallographic studies, *Bioorganic & Medicinal Chemistry Letters*, 17 (2007) 4866-4872.

[214] F. Picard, Y. Deshaies, J. Lalonde, P. Samson, D. Richard, Topiramate Reduces Energy and Fat Gains in Lean (Fa/?) and Obese (fa/fa) Zucker Rats, *Obesity Research*, 8 (2000) 656-663.

[215] C.T. Supuran, Carbonic anhydrase inhibitors in the treatment and prophylaxis of obesity, *Expert Opinion on Therapeutic Patents*, 13 (2003) 1545-1550.

[216] C.T. Supuran, Carbonic anhydrase inhibitors as emerging drugs for the treatment of obesity, *Expert Opinion on Emerging Drugs*, 17 (2012) 11-15.

[217] K.M. Gadde, D.M. Franciscy, H.R. Wagner II, K.R.R. Krishnan, Zonisamide for Weight Loss in Obese Adults A Randomized Controlled Trial, *JAMA*, 289 (2003) 1820-1825.

[218] D.J. Lonneman, Jr., J.A. Rey, B.D. McKee, Phentermine/Topiramate extended-release capsules (qsymia) for weight loss, *P & T*, 38 (2013) 446-452.

[219] A. Angeli, M. Ferraroni, A. Nocentini, S. Selleri, P. Gratteri, C.T. Supuran, F. Carta, Polypharmacology of epacadostat: a potent and selective inhibitor of the tumor associated carbonic anhydrases IX and XII, *Chemical Communications*, 55 (2019) 5720-5723.

[220] P.C. McDonald, J.-Y. Winum, C.T. Supuran, S. Dedhar, Recent Developments in Targeting Carbonic Anhydrase IX for Cancer Therapeutics, *Oncotarget*, 3 (2012) 84 - 97.

[221] A. Thiry, J.-M. Dogné, B. Masereel, C.T. Supuran, Targeting tumor-associated carbonic anhydrase IX in cancer therapy, *Trends in Pharmacological Sciences*, 27 (2006) 566-573.

[222] A. Angeli, F. Carta, A. Nocentini, J.-Y. Winum, R. Zalubovskis, A. Akdemir, V. Onnis, W.M. Eldehna, C. Capasso, G.D. Simone, S.M. Monti, S. Carradori, W.A. Donald, S. Dedhar, C.T. Supuran, Carbonic Anhydrase Inhibitors Targeting Metabolism and Tumor Microenvironment, *Metabolites*, 10 (2020) 412-433.

- [223] S.K. Sharma, S. Kumar, K. Chand, A. Kathuria, A. Gupta, R. Jain, An Update on Natural Occurrence and Biological Activity of Chromones, *Current Medicinal Chemistry*, 18 (2011) 3825-3852.
- [224] T. Al-Warhi, A. Sabt, E.B. Elkaeed, W.M. Eldehna, Recent advancements of coumarin-based anticancer agents: An up-to-date review, *Bioorganic Chemistry*, 103 (2020) 104163-104178.
- [225] F. Annunziata, C. Pinna, S. Dallavalle, L. Tamborini, A. Pinto, An Overview of Coumarin as a Versatile and Readily Accessible Scaffold with Broad-Ranging Biological Activities, *International Journal of Molecular Sciences*, 21 (2020) 4618-4699.
- [226] E.M. Riveiro, N. De Kimpe, A. Moglioni, R. Vazquez, F. Monczor, C. Shayo, C. Davio, Coumarins: Old Compounds with Novel Promising Therapeutic Perspectives, *Current Medicinal Chemistry*, 17 (2010) 1325-1338.
- [227] D. Wardrop, D. Keeling, The story of the discovery of heparin and warfarin, *British Journal of Haematology*, 141 (2008) 757-763.
- [228] D. Dawood, R. Batran, T. Farghaly, M. Khedr, M. Abdalla, New Coumarin Derivatives as Potent Selective COX-2 Inhibitors: Synthesis, Anti-Inflammatory, QSAR, and Molecular Modeling Studies, *Archiv der Pharmazie*, 348 (2015) 878-888.
- [229] L. Souza, M. Rennó, J. Figueroa-Villar, Coumarins as cholinesterase inhibitors: A review, *Chemico-Biological Interactions*, 254 (2016) 11-23.
- [230] U. Salar, K. Khan, A. Jabeen, A. Faheem, F. Naqvi, S. Ahmed, E. Iqbal, F. Ali, Kanwal, S. Perveen, ROS Inhibitory Activity and Cytotoxicity Evaluation of Benzoyl, Acetyl, Alkyl Ester, and Sulfonate Ester Substituted Coumarin Derivatives, *Medicinal Chemistry*, 15 (2019) 1099-1111.
- [231] N. Au, A.E. Rettie, Pharmacogenomics of 4-Hydroxycoumarin Anticoagulants, *Drug Metabolism Reviews*, 40 (2008) 355-375.
- [232] N.A. Gormley, G. Orphanides, A. Meyer, P.M. Cullis, A. Maxwell, The Interaction of Coumarin Antibiotics with Fragments of the DNA Gyrase B Protein, *Biochemistry*, 35 (1996) 5083-5092.
- [233] M. Shaikh, D. Subhedar, F. Khan, J. Sangshetti, B. Shingate, 1,2,3-Triazole incorporated coumarin derivatives as potential antifungal and antioxidant agents, *Chinese Chemical Letters*, 27 (2015) 295-301.
- [234] M. Campagna, C. Rivas, Antiviral activity of resveratrol, *Biochemical Society Transactions*, 38 (2010) 50-53.

[235] S. Goud N, P. Kumar, R. Bharath, Recent Developments of Target Based Coumarin Derivatives as Potential Anticancer Agents, *Mini-Reviews in Medicinal Chemistry*, 20 (2020) 1754-1766.

[236] E. Küpeli Akkol, Y. Genç, B. Karpuz, E. Sobarzo-Sánchez, R. Capasso, Coumarins and Coumarin-Related Compounds in Pharmacotherapy of Cancer, *Cancers*, 12 (2020) 1959-1984.

[237] A. Carneiro, M.J. Matos, E. Uriarte, L. Santana, Trending Topics on Coumarin and Its Derivatives in 2020, *Molecules*, 26 (2021) 501-516.

[238] C. Melis, S. Distinto, G. Bianco, R. Meleddu, F. Cottiglia, B. Fois, D. Taverna, R. Angius, S. Alcaro, F. Ortuso, M. Gaspari, A. Angeli, S. Del Prete, C. Capasso, C.T. Supuran, E. Maccioni, Targeting Tumor Associated Carbonic Anhydrases IX and XII: Highly Isozyme Selective Coumarin and Psoralen Inhibitors, *ACS Medicinal Chemistry Letters*, 9 (2018) 725-729.

[239] R. Meleddu, S. Deplano, E. Maccioni, F. Ortuso, F. Cottiglia, D. Secci, A. Onali, E. Sanna, A. Angeli, R. Angius, S. Alcaro, C. Supuran, S. Distinto, Selective inhibition of carbonic anhydrase IX and XII by coumarin and psoralen derivatives, *Journal of Enzyme Inhibition and Medicinal Chemistry*, 36 (2021) 685-692.

[240] B. Fois, S. Distinto, R. Meleddu, S. Deplano, E. Maccioni, C. Floris, A. Rosa, M. Nieddu, P. Caboni, C. Sissi, A. Angeli, C.T. Supuran, F. Cottiglia, Coumarins from *Magydaris pastinacea* as inhibitors of the tumour-associated carbonic anhydrases IX and XII: isolation, biological studies and in silico evaluation, *Journal of Enzyme Inhibition and Medicinal Chemistry*, 35 (2020) 539-548.

[241] T. Liu, Y. Lin, X. Wen, R.N. Jorissen, M.K. Gilson, BindingDB: a web-accessible database of experimentally determined protein-ligand binding affinities, *Nucleic Acids Research*, 35 (2007) D198-D201.

[242] N. Chandak, M. Ceruso, C.T. Supuran, P.K. Sharma, Novel sulfonamide bearing coumarin scaffolds as selective inhibitors of tumor associated carbonic anhydrase isoforms IX and XII, *Bioorganic & Medicinal Chemistry*, 24 (2016) 2882-2886.

[243] M. Ferraroni, F. Carta, A. Scozzafava, C.T. Supuran, Thioxocoumarins Show an Alternative Carbonic Anhydrase Inhibition Mechanism Compared to Coumarins, *Journal of Medicinal Chemistry*, 59 (2016) 462-473.

[244] A. Bonardi, M. Falsini, D. Catarzi, F. Varano, L. Mannelli, B. Tenci, C. Ghelardini, A. Angeli, C. Supuran, V. Colotta, Structural investigations on coumarins leading to chromeno[4,3-c]pyrazol-4-ones and pyrano[4,3-c]pyrazol-4-ones: New scaffolds for the

design of the tumor-associated carbonic anhydrase isoforms IX and XII, *European Journal of Medicinal Chemistry*, 146 (2018) 47-59.

[245] N. Touisni, A. Maresca, P.C. McDonald, Y. Lou, A. Scozzafava, S. Dedhar, J.-Y. Winum, C.T. Supuran, Glycosyl Coumarin Carbonic Anhydrase IX and XII Inhibitors Strongly Attenuate the Growth of Primary Breast Tumors, *Journal of Medicinal Chemistry*, 54 (2011) 8271-8277.

[246] A. Nocentini, F. Carta, M. Ceruso, G. Bartolucci, C.T. Supuran, Click-tailed coumarins with potent and selective inhibitory action against the tumor-associated carbonic anhydrases IX and XII, *Bioorganic & Medicinal Chemistry*, 23 (2015) 6955-6966.

[247] L. De Luca, F. Mancuso, S. Ferro, M.R. Buemi, A. Angeli, S. Del Prete, C. Capasso, C.T. Supuran, R. Gitto, Inhibitory effects and structural insights for a novel series of coumarin-based compounds that selectively target human CA IX and CA XII carbonic anhydrases, *European Journal of Medicinal Chemistry*, 143 (2018) 276-282.

[248] M. Bozdag, M. Ferraroni, F. Carta, D. Vullo, L. Lucarini, E. Orlandini, A. Rossello, E. Nuti, A. Scozzafava, E. Masini, C.T. Supuran, Structural Insights on Carbonic Anhydrase Inhibitory Action, Isoform Selectivity, and Potency of Sulfonamides and Coumarins Incorporating Arylsulfonylureido Groups, *Journal of Medicinal Chemistry*, 57 (2014) 9152-9167.

[249] C. Temperini, A. Innocenti, A. Scozzafava, C.T. Supuran, Carbonic anhydrase inhibitors. Interaction of the antitumor sulfamate EMD 486019 with twelve mammalian carbonic anhydrase isoforms: Kinetic and X-ray crystallographic studies, *Bioorganic & Medicinal Chemistry Letters*, 18 (2008) 4282-4286.

[250] A. Maresca, A. Scozzafava, C.T. Supuran, 7,8-Disubstituted- but not 6,7-disubstituted coumarins selectively inhibit the transmembrane, tumor-associated carbonic anhydrase isoforms IX and XII over the cytosolic ones I and II in the low nanomolar/subnanomolar range, *Bioorganic & Medicinal Chemistry Letters*, 20 (2010) 7255-7258.

[251] E. Berrino, A. Angeli, D.D. Zhdanov, A.P. Kiryukhina, A. Milaneschi, A. De Luca, M. Bozdag, S. Carradori, S. Selleri, G. Bartolucci, T.S. Peat, M. Ferraroni, C.T. Supuran, F. Carta, Azidothymidine "Clicked" into 1,2,3-Triazoles: First Report on Carbonic Anhydrase–Telomerase Dual-Hybrid Inhibitors, *Journal of Medicinal Chemistry*, 63 (2020) 7392-7409.

[252] F. Pacchiano, F. Carta, P.C. McDonald, Y. Lou, D. Vullo, A. Scozzafava, S. Dedhar, C.T. Supuran, Ureido-Substituted Benzenesulfonamides Potently Inhibit Carbonic

Anhydrase IX and Show Antimetastatic Activity in a Model of Breast Cancer Metastasis, *Journal of Medicinal Chemistry*, 54 (2011) 1896-1902.

[253] E. Berrino, L. Milazzo, L. Micheli, D. Vullo, A. Angeli, M. Bozdog, A. Nocentini, M. Menicatti, G. Bartolucci, L. di Cesare Mannelli, C. Ghelardini, C.T. Supuran, F. Carta, Synthesis and Evaluation of Carbonic Anhydrase Inhibitors with Carbon Monoxide Releasing Properties for the Management of Rheumatoid Arthritis, *Journal of Medicinal Chemistry*, 62 (2019) 7233-7249.

[254] B. Zengin Kurt, F. Sonmez, D. Ozturk, A. Akdemir, A. Angeli, C.T. Supuran, Synthesis of coumarin-sulfonamide derivatives and determination of their cytotoxicity, carbonic anhydrase inhibitory and molecular docking studies, *European Journal of Medicinal Chemistry*, 183 (2019) 111702-111716.

[255] R.S. Keri, S. Budagumpi, R.K. Pai, R.G. Balakrishna, Chromones as a privileged scaffold in drug discovery: A review, *European Journal of Medicinal Chemistry*, 78 (2014) 340-374.

[256] J. Reis, A. Gaspar, N. Milhazes, F. Borges, Chromone as a Privileged Scaffold in Drug Discovery: Recent Advances, *Journal of Medicinal Chemistry*, 60 (2017) 7941-7957.

[257] A. Gaspar, M.J. Matos, J. Garrido, E. Uriarte, F. Borges, Chromone: A Valid Scaffold in Medicinal Chemistry, *Chemical Reviews*, 114 (2014) 4960-4992.

[258] V.M. Patil, N. Masand, S. Verma, V. Masand, Chromones: Privileged scaffold in anticancer drug discovery, *Chemical Biology & Drug Design*, 98 (2021) 943-953.

[259] D.S. Ghotekar, P. Mandhane, R. Joshi, S. Bhagat, C. Gill, Synthesis of chromones and pyrazolines as antimicrobial & antifungal agents, *Indian Journal of Heterocyclic Chemistry*, 19 (2010) 341-344.

[260] S.M. Abu-Bakr, M.D. Khidre, M.A. Omar, S.A. Swelam, H.M. Awad, Synthesis of furo[3,2-g]chromones under microwave irradiation and their antitumor activity evaluation, *Journal of Heterocyclic Chemistry*, 57 (2020) 731-743.

[261] M. Kuroda, S. Uchida, K. Watanabe, Y. Mimaki, Chromones from the tubers of *Eranthis cilicica* and their antioxidant activity, *Phytochemistry*, 70 (2009) 288-293.

[262] R. Kaur, N. Taheem, A.K. Sharma, R. Kharb, Important Advances on Antiviral Profile of Chromone Derivatives, *Research Journal of Pharmaceutical, Biological and Chemical Sciences*, 4 (2013) 79-96.

[263] P. Djemgou, D. Gatsing, M. Tchuendem, B. Ngadjui, P. Tane, A. Ahmed, A. Gamal-Eldeen, G. Adoga, T. Hirata, T. Mabry, Antitumor and Immunostimulatory Activity of Two

Chromones and Other Constituents from *Cassia Petersiana*, Natural product communications, 1 (2006) 961-968.

[264] M. Sumiyoshi, Y. Kimura, Enhancing effects of a chromone glycoside, eucryphin, isolated from *Astilbe* rhizomes on burn wound repair and its mechanism, *Phytomedicine : international journal of phytotherapy and phytopharmacology*, 17 (2010) 820-829.

[265] A.A. Abu-Hashem, M.M. Youssef, Synthesis of New Visnagen and Khellin Furochromone Pyrimidine Derivatives and Their Anti-Inflammatory and Analgesic Activity, *Molecules*, 16 (2011) 1956-1972.

[266] M. El Amrani, D. Lai, A. Debbab, A.H. Aly, K. Siems, C. Seidel, M. Schnekenburger, A. Gaigneaux, M. Diederich, D. Feger, W. Lin, P. Proksch, Protein Kinase and HDAC Inhibitors from the Endophytic Fungus *Epicoccum nigrum*, *Journal of Natural Products*, 77 (2014) 49-56.

[267] Y. Jung, S.Y. Shin, Y. Yong, H. Jung, S. Ahn, Y.H. Lee, Y. Lim, Plant-Derived Flavones as Inhibitors of Aurora B Kinase and Their Quantitative Structure–Activity Relationships, *Chemical Biology & Drug Design*, 85 (2015) 574-585.

[268] G. Balboni, C. Congiu, V. Onnis, A. Maresca, A. Scozzafava, J.-Y. Winum, A. Maietti, C.T. Supuran, Flavones and structurally related 4-chromenones inhibit carbonic anhydrases by a different mechanism of action compared to coumarins, *Bioorganic & Medicinal Chemistry Letters*, 22 (2012) 3063-3066.

[269] A. Karioti, M. Ceruso, F. Carta, A.-R. Bilia, C.T. Supuran, New natural product carbonic anhydrase inhibitors incorporating phenol moieties, *Bioorganic & Medicinal Chemistry*, 23 (2015) 7219-7225.

[270] M.I. Fernández-Bachiller, C. Pérez, L. Monjas, J. Rademann, M.I. Rodríguez-Franco, New Tacrine–4-Oxo-4H-chromene Hybrids as Multifunctional Agents for the Treatment of Alzheimer’s Disease, with Cholinergic, Antioxidant, and β -Amyloid-Reducing Properties, *Journal of Medicinal Chemistry*, 55 (2012) 1303-1317.

[271] A. Golonko, T. Pienkowski, R. Swislocka, R. Lazny, M. Roszko, W. Lewandowski, Another look at phenolic compounds in cancer therapy the effect of polyphenols on ubiquitin-proteasome system, *European Journal of Medicinal Chemistry*, 167 (2019) 291-311.

[272] Y. Muftuoglu, G. Mustata Wilson, Pharmacophore Modeling Strategies for the Development of Novel Nonsteroidal Inhibitors of Human Aromatase (CYP19), *Bioorganic & medicinal chemistry letters*, 20 (2010) 3050-3064.

[273] J. Cui, Q. Meng, X. Zhang, Q. Cui, W. Zhou, S. Li, Design and Synthesis of New α -Naphthoflavones as Cytochrome P450 (CYP) 1B1 Inhibitors To Overcome Docetaxel-Resistance Associated with CYP1B1 Overexpression, *Journal of Medicinal Chemistry*, 58 (2015) 3534-3547.

[274] Y.A. Sonawane, M.A. Taylor, J.V. Napoleon, S. Rana, J.I. Contreras, A. Natarajan, Cyclin Dependent Kinase 9 Inhibitors for Cancer Therapy, *Journal of Medicinal Chemistry*, 59 (2016) 8667-8684.

[275] L. Zhao, X. Yuan, J. Wang, Y. Feng, F. Ji, Z. Li, J. Bian, A review on flavones targeting serine/threonine protein kinases for potential anticancer drugs, *Bioorganic & Medicinal Chemistry*, 27 (2019) 677-685.

[276] U. Singh, G. Chashoo, S.U. Khan, P. Mahajan, A. Nargotra, G. Mahajan, A. Singh, A. Sharma, M.J. Mintoo, S.K. Guru, H. Aruri, T. Thatikonda, P. Sahu, P. Chibber, V. Kumar, S.A. Mir, S.S. Bharate, S. Madishetti, U. Nandi, G. Singh, D.M. Mondhe, S. Bhushan, F. Malik, S. Mignani, R.A. Vishwakarma, P.P. Singh, Design of Novel 3-Pyrimidinylazaindole CDK2/9 Inhibitors with Potent In Vitro and In Vivo Antitumor Efficacy in a Triple-Negative Breast Cancer Model, *Journal of Medicinal Chemistry*, 60 (2017) 9470-9489.

[277] J. Liu, P.T. Pham, E.V. Skripnikova, S. Zheng, L.n.J. Lovings, Y. Wang, N. Goyal, S.M. Bellow, L.M. Mensah, A.J. Chatters, M.R. Bratton, T.E. Wiese, M. Zhao, G. Wang, M. Foroozesh, A Ligand-Based Drug Design. Discovery of 4-Trifluoromethyl-7,8-pyrano-coumarin as a Selective Inhibitor of Human Cytochrome P450 1A2, *Journal of Medicinal Chemistry*, 58 (2015) 6481-6493.

[278] X. Chang, W. Kang, Antioxidant and α -glucosidase inhibitory compounds from *Pimpinella candolleana* Wight et Arn, *Medicinal Chemistry Research*, 21 (2012) 4324–4329.

[279] R. Sharma, L. Gatchie, I. Williams, S. Jain, R. Vishwakarma, B. Chaudhuri, S. Bharate, Glycyrrhiza glabra extract and quercetin reverses cisplatin resistance in triple-negative MDA-MB-468 breast cancer cells via inhibition of cytochrome P450 1B1 enzyme, *Bioorganic & Medicinal Chemistry Letters*, 27 (2017) 5400-5403.

[280] M. Kuzikov, E. Costanzi, J. Reinshagen, F. Esposito, L. Vangeel, M. Wolf, B. Ellinger, C. Claussen, G. Geisslinger, A. Corona, D. Iaconis, C. Talarico, C. Manelfi, R. Cannalire, J. Gossen, S. Albani, F. Musiani, K. Herzog, A. Zaliani, Identification of inhibitors of SARS-CoV-2 3CL-Pro enzymatic activity using a small molecule in-vitro repurposing screen, *ACS Pharmacology & Translational Science* 4 (2021) 1096-1110.

- [281] M. Poratti, G. Marzaro, Third-generation CDK inhibitors: A review on the synthesis and binding modes of Palbociclib, Ribociclib and Abemaciclib, *European Journal of Medicinal Chemistry*, 172 (2019) 143-153.
- [282] J.B. Baell, Feeling Nature's PAINS: Natural Products, Natural Product Drugs, and Pan Assay Interference Compounds (PAINS), *Journal of Natural Products*, 79 (2016) 616-628.
- [283] J. Reis, F. Cagide, M.E. Valencia, J. Teixeira, D. Bagetta, C. Pérez, E. Uriarte, P.J. Oliveira, F. Ortuso, S. Alcaro, M.I. Rodríguez-Franco, F. Borges, Multi-target-directed ligands for Alzheimer's disease: Discovery of chromone-based monoamine oxidase/cholinesterase inhibitors, *European Journal of Medicinal Chemistry*, 158 (2018) 781-800.
- [284] M. Bryan, K. Biswas, T. Peterkin, R. Rzasa, L. Arik, S. Lehto, H. Sun, F.-Y. Hsieh, C. Xu, R. Fremeau, J. Allen, Chromenones as potent bradykinin B1 antagonists, *Bioorganic & medicinal chemistry letters*, 22 (2011) 619-622.
- [285] F.M. Awadallah, T.A. El-Waei, M.M. Hanna, S.E. Abbas, M. Ceruso, B.E. Oz, O.O. Guler, C.T. Supuran, Synthesis, carbonic anhydrase inhibition and cytotoxic activity of novel chromone-based sulfonamide derivatives, *European Journal of Medicinal Chemistry*, 96 (2015) 425-435.
- [286] L. Puccetti, G. Fasolis, D. Vullo, Z. Chohan, A. Scozzafava, C. Supuran, Carbonic anhydrase inhibitors. Inhibition of cytosolic/tumor-associated carbonic anhydrase isozymes I, II, IX, and XII with Schiff's bases incorporating chromone and aromatic sulfonamide moieties, and their zinc complexes, *Bioorganic & medicinal chemistry letters*, 15 (2005) 3096-3101.
- [287] R.G. Khalifah, The Carbon Dioxide Hydration Activity of Carbonic Anhydrase: I. Stop-Flow Kinetic Studies On The Native Human Isoenzymes B And C, *Journal of Biological Chemistry*, 246 (1971) 2561-2573.
- [288] S. Bilginer, B. Gonder, H.I. Gul, R. Kaya, I. Gulcin, B. Anil, C.T. Supuran, Novel sulphonamides incorporating triazene moieties show powerful carbonic anhydrase I and II inhibitory properties, *Journal of enzyme inhibition and medicinal chemistry*, 35 (2020) 325-329.
- [289] H.E.P. Sánchez, I. Kondov, J.M. García, K.V. Klenin, W. Wenzel, A Pipeline Pilot based SOAP implementation of FlexScreen for High-Throughput Virtual Screening, in: *IWSG-Life*, 2011.

[290] C.A. Lipinski, F. Lombardo, B.W. Dominy, P.J. Feeney, Experimental and computational approaches to estimate solubility and permeability in drug discovery and development settings, *Advanced Drug Delivery Reviews*, 23 (1997) 3-25.

[291] C.A. Lipinski, Drug-like properties and the causes of poor solubility and poor permeability, *Journal of Pharmacological and Toxicological Methods*, 44 (2000) 235-249.

[292] D.F. Veber, S.R. Johnson, H.-Y. Cheng, B.R. Smith, K.W. Ward, K.D. Kopple, Molecular Properties That Influence the Oral Bioavailability of Drug Candidates, *Journal of Medicinal Chemistry*, 45 (2002) 2615-2623.

[293] L. Jorgensen William, The Many Roles of Computation in Drug Discovery, *Science*, 303 (2004) 1813-1818.

[294] W.L. Jorgensen, E.M. Duffy, Prediction of drug solubility from structure, *Advanced Drug Delivery Reviews*, 54 (2002) 355-366.

[295] L. Ioakimidis, L. Thoukydidis, A. Mirza, S. Naeem, J. Reynisson, Benchmarking the Reliability of QikProp. Correlation between Experimental and Predicted Values, *QSAR & Combinatorial Science*, 27 (2008) 445-456.

[296] W.L. Jorgensen, E.M. Duffy, Prediction of drug solubility from Monte Carlo simulations, *Bioorganic & Medicinal Chemistry Letters*, 10 (2000) 1155-1158.

[297] G.M. Boratyn, A.A. Schäffer, R. Agarwala, S.F. Altschul, D.J. Lipman, T.L. Madden, Domain enhanced lookup time accelerated BLAST, *Biology Direct*, 7 (2012) 12-26.

[298] R. Meleddu, S. Distinto, F. Cottiglia, R. Angius, M. Gaspari, D. Taverna, C. Melis, A. Angeli, G. Bianco, S. Deplano, B. Fois, S. Del Prete, C. Capasso, S. Alcaro, F. Ortuso, M. Yanez, C.T. Supuran, E. Maccioni, Tuning the Dual Inhibition of Carbonic Anhydrase and Cyclooxygenase by Dihydrothiazole Benzensulfonamides, *ACS Medicinal Chemistry Letters*, 9 (2018) 1045-1050.

[299] F. Mohamadi, N.G.J. Richards, W.C. Guida, R. Liskamp, M. Lipton, C. Caufield, G. Chang, T. Hendrickson, W.C. Still, MacroModel—an integrated software system for modeling organic and bioorganic molecules using molecular mechanics, *Journal of Computational Chemistry*, 11 (1990) 440-467.

[300] T.A. Halgren, Merck molecular force field. II. MMFF94 van der Waals and electrostatic parameters for intermolecular interactions, *Journal of Computational Chemistry*, 17 (1996) 520-552.

[301] P.A. Kollman, I. Massova, C. Reyes, B. Kuhn, S. Huo, L. Chong, M. Lee, T. Lee, Y. Duan, W. Wang, O. Donini, P. Cieplak, J. Srinivasan, D.A. Case, T.E. Cheatham,

Calculating Structures and Free Energies of Complex Molecules: Combining Molecular Mechanics and Continuum Models, *Accounts of Chemical Research*, 33 (2000) 889-897.

[302] H.M. Berman, J. Westbrook, Z. Feng, G. Gilliland, T.N. Bhat, H. Weissig, I.N. Shindyalov, P.E. Bourne, The Protein Data Bank, *Nucleic Acids Research*, 28 (2000) 235-242.

[303] J. Leitans, A. Kazaks, A. Balode, J. Ivanova, R. Zalubovskis, C.T. Supuran, K. Tars, Efficient Expression and Crystallization System of Cancer-Associated Carbonic Anhydrase Isoform IX, *Journal of Medicinal Chemistry*, 58 (2015) 9004-9009.

[304] A. Smirnov, A. Zubrienė, E. Manakova, S. Gražulis, D. Matulis, Crystal structure correlations with the intrinsic thermodynamics of human carbonic anhydrase inhibitor binding, *PeerJ*, 6 (2018) 4412-4412.

[305] J.Y. Chung, J.-M. Hah, A.E. Cho, Correlation between Performance of QM/MM Docking and Simple Classification of Binding Sites, *Journal of Chemical Information and Modeling*, 49 (2009) 2382-2387.

[306] Z. Wang, Pechmann Reaction, in: Z. Wang (Ed.) *Comprehensive Organic Name Reactions and Reagents*, John Wiley & Sons, Inc., 2010, pp. 2151-2156.

[307] R.J. Ouellette, J.D. Rawn, 16 - Ethers and Epoxides, in: R.J. Ouellette, J.D. Rawn (Eds.) *Organic Chemistry Study Guide*, Elsevier, Boston, 2015, pp. 277-297.

[308] R.K. Parashar, Stabilized Carbanions, Enamines and Ylides, in: R.K. Parashar (Ed.) *Reaction Mechanisms in Organic Synthesis*, John Wiley & Sons, Inc., 2008, pp. 112-147.

[309] I. Salim, Z. Jabarah, S. Jk, Rawa, R. Majeed, Chemical biology of cyclization reactions by using POCL₃, *Eurasian Journal of Biosciences*, (2020) 973-976.

[310] T.E. Ali, M.A. Ibrahim, Z.M. El-Gendy, E.M. El-Amin, 4,6-Diacetylresorcinol in Heterocyclic Synthesis, Part I: Synthesis and Biological Evaluation of Some New Linearly and Angularly Substituted Pyrano[3,2-g] Chromenes via Vilsmeier–Haack Formylation of 4,6-Diacetylresorcinol, Its Schiff Bases, and Hydrazones, *Synthetic Communications*, 43 (2013) 3329-3341.

[311] K.C. Rajanna, F. Solomon, M.M. Ali, P.K. Saiprakash, Kinetics and mechanism of Vilsmeier-Haack synthesis of 3-formyl chromones derived from o-hydroxy aryl alkyl ketones: A structure reactivity study, *Tetrahedron*, 52 (1996) 3669-3682.

[312] M. Badertscher, P. Bühlmann, E. Pretsch, *Structure Determination of Organic Compounds*, Springer-Verlag, New York, 2001.

- [313] D. Lagorce, C. Reynes, A.-C. Camproux, M.A. Miteva, O. Sperandio, B.O. Villoutreix, In silico ADME/Tox predictions, in: *ADMET for Medicinal Chemists*, John Wiley & Sons, Inc., 2011, pp. 29-124.
- [314] N. Walker, D. Stuart, An empirical method for correcting diffractometer data for absorption effects, *Acta Crystallographica, Section A*, 39 (1983) 158-166.
- [315] Y. Sambuy, I. Angelis, G. Ranaldi, M.L. Scarino, A. Stammati, F. Zucco, The Caco-2 cell line as a model of the intestinal barrier: influence of cell and culture-related factors on Caco-2 cell functional characteristics, *Cell Biology and Toxicology*, 21 (2005) 1-26.
- [316] E. Dolgih, M.P. Jacobson, Predicting efflux ratios and blood-brain barrier penetration from chemical structure: combining passive permeability with active efflux by P-glycoprotein, *ACS Chemical Neuroscience*, 4 (2013) 361-367.
- [317] J.D. Irvine, L. Takahashi, K. Lockhart, J. Cheong, J.W. Tolan, H.E. Selick, J.R. Grove, MDCK (Madin-Darby Canine Kidney) Cells: A Tool for Membrane Permeability Screening, *Journal of Pharmaceutical Sciences*, 88 (1999) 28-33.
- [318] R. Gualdani, M.M. Cavalluzzi, F. Tadini-Buoninsegni, M. Convertino, P. Gailly, A. Stary-Weinzinger, G. Lentini, Molecular Insights into hERG Potassium Channel Blockade by Lubeluzole, *Cellular Physiology and Biochemistry*, 45 (2018) 2233-2245.
- [319] L.M.L. de Lau, M.M.B. Breteler, Epidemiology of Parkinson's disease, *The Lancet Neurology*, 5 (2006) 525-535.
- [320] D. Gonçalves, G. Alves, A. Fortuna, P. Soares-da-Silva, A. Falcão, Pharmacokinetics of opicapone, a third-generation COMT inhibitor, after single and multiple oral administration: A comparative study in the rat, *Toxicology and Applied Pharmacology*, 323 (2017) 9-15.
- [321] A.J. Lees, J. Hardy, T. Revesz, Parkinson's disease, *The Lancet*, 373 (2009) 2055-2066.
- [322] M.J. Armstrong, M.S. Okun, Diagnosis and Treatment of Parkinson Disease: A Review, *JAMA*, 323 (2020) 548-560.
- [323] B.R. Bloem, M.S. Okun, C. Klein, Parkinson's disease, *The Lancet*, 397 (2021) 2284-2303.
- [324] L.E. Kiss, P. Soares-da-Silva, Medicinal Chemistry of Catechol O-Methyltransferase (COMT) Inhibitors and Their Therapeutic Utility, *Journal of Medicinal Chemistry*, 57 (2014) 8692-8717.

- [325] T. Silva, T. Mohamed, A. Shakeri, P.P.N. Rao, L. Martínez-González, D.I. Pérez, A. Martínez, M.J. Valente, J. Garrido, E. Uriarte, P. Serrão, P. Soares-da-Silva, F. Remião, F. Borges, Development of Blood–Brain Barrier Permeable Nitrocatechol-Based Catechol O-Methyltransferase Inhibitors with Reduced Potential for Hepatotoxicity, *Journal of Medicinal Chemistry*, 59 (2016) 7584-7597.
- [326] T.B. Silva, F. Borges, M.P. Serrão, P. Soares-da-Silva, Liver says no: the ongoing search for safe catechol O-methyltransferase inhibitors to replace tolcapone, *Drug Discovery Today*, 25 (2020) 1846-1854.
- [327] F. Assal, L. Spahr, A. Hadengue, L. Rubbici-Brandt, P.R. Burkhard, Tolcapone and fulminant hepatitis, *The Lancet*, 352 (1998) 958.
- [328] A. Castro Caldas, T. Teodoro, J.J. Ferreira, The launch of opicapone for Parkinson's disease: negatives versus positives, *Expert Opinion on Drug Safety*, 17 (2018) 331-337.
- [329] R.G. Robinson, S.M. Smith, S.E. Wolkenberg, M. Kandebo, L. Yao, C.R. Gibson, S.T. Harrison, S. Polsky-Fisher, J.C. Barrow, P.J. Manley, J.J. Mulhearn, K.K. Nanda, J.W. Schubert, B.W. Trotter, Z. Zhao, J.M. Sanders, R.F. Smith, D. McLoughlin, S. Sharma, D.L. Hall, T.L. Walker, J.L. Kershner, N. Bhandari, P.H. Hutson, N.A. Sachs, Characterization of non-nitrocatechol pan and isoform specific catechol-O-methyltransferase inhibitors and substrates, *ACS Chemical Neuroscience*, 3 (2012) 129-140.
- [330] S.T. Harrison, M.S. Poslusney, J.J. Mulhearn, Z. Zhao, N.R. Kett, J.W. Schubert, J.Y. Melamed, T.J. Allison, S.B. Patel, J.M. Sanders, S. Sharma, R.F. Smith, D.L. Hall, R.G. Robinson, N.A. Sachs, P.H. Hutson, S.E. Wolkenberg, J.C. Barrow, Synthesis and Evaluation of Heterocyclic Catechol Mimics as Inhibitors of Catechol-O-methyltransferase (COMT), *ACS Medicinal Chemistry Letters*, 6 (2015) 318-323.
- [331] Z. Zhao, S.T. Harrison, J.W. Schubert, J.M. Sanders, S. Polsky-Fisher, N.R. Zhang, D. McLoughlin, C.R. Gibson, R.G. Robinson, N.A. Sachs, M. Kandebo, L. Yao, S.M. Smith, P.H. Hutson, S.E. Wolkenberg, J.C. Barrow, Synthesis and optimization of N-heterocyclic pyridinones as catechol-O-methyltransferase (COMT) inhibitors, *Bioorganic & Medicinal Chemistry Letters*, 26 (2016) 2952-2956.
- [332] R. Sheng, L. Tang, L. Jiang, L. Hong, Y. Shi, N. Zhou, Y. Hu, Novel 1-Phenyl-3-hydroxy-4-pyridinone Derivatives as Multifunctional Agents for the Therapy of Alzheimer's Disease, *ACS Chemical Neuroscience*, 7 (2016) 69-81.

[333] L.J. Goossen, F. Manjolinho, B.A. Khan, N. Rodríguez, Microwave-Assisted Cu-Catalyzed Protodecarboxylation of Aromatic Carboxylic Acids, *The Journal of Organic Chemistry*, 74 (2009) 2620-2623.

[334] R.C. Gallo, L. Montagnier, The Discovery of HIV as the Cause of AIDS, *New England Journal of Medicine*, 349 (2003) 2283-2285.

[335] S. de Castro, M.-J. Camarasa, Polypharmacology in HIV inhibition: can a drug with simultaneous action against two relevant targets be an alternative to combination therapy?, *European Journal of Medicinal Chemistry*, 150 (2018) 206-227.

[336] D. Jahagirdar, M.K. Walters, A. Novotney, E.D. Brewer, T.D. Frank, A. Carter, M.H. Biehl, H. Abbastabar, E.S. Abhilash, E. Abu-Gharbieh, L.J. Abu-Raddad, V. Adekanmbi, D.A. Adeyinka, Q.E.S. Adnani, S. Afzal, S. Aghababaei, B.O. Ahinkorah, S. Ahmad, K. Ahmadi, S. Ahmadi, E. Ahmadpour, M.B. Ahmed, T. Ahmed Rashid, Y. Ahmed Salih, A. Aklilu, T. Akram, C.J. Akunna, H. Al Hamad, F. Alahdab, F.M. Alanezi, E.A. Aleksandrova, K.A. Alene, L. Ali, V. Alipour, S. Almustanyir, N. Alvis-Guzman, E.K. Ameyaw, H. Amu, C.L. Andrei, T. Andrei, D. Anvari, J. Arabloo, O. Aremu, J. Arulappan, D.D. Atnafu, B.P. Ayala Quintanilla, M.A. Ayza, S. Azari, D.B. B, M. Banach, T.W. Bärnighausen, F. Barra, A. Barrow, S. Basu, S. Bazargan-Hejazi, H.G. Belay, T.M. Berheto, W.M. Bezabhe, Y.M. Bezabih, A.S. Bhagavathula, N. Bhardwaj, P. Bhardwaj, K. Bhattacharyya, S. Bibi, A. Bijani, C. Bisignano, O.A. Bolarinwa, A. Bloor, A.A. Boltaev, N.I. Briko, D. Buonsenso, K. Burkart, Z.A. Butt, C. Cao, J. Charan, S. Chatterjee, S.K. Chattu, V.K. Chattu, S.G. Choudhari, D.-T. Chu, R.A.S. Couto, R.G. Cowden, B.A. Dachew, O. Dadras, A.B. Dagneu, S.M.A. Dahlawi, X. Dai, L. Dandona, R. Dandona, J. das Neves, L. Degenhardt, F.M. Demeke, A.A. Desta, K. Deuba, D. Dhamnetiya, G.P. Dhungana, M. Dianatinasab, D. Diaz, S. Djalalinia, L.P. Doan, F. Dorostkar, H.A. Edinur, A. Effiong, S. Eftekhazadeh, M. El Sayed Zaki, R. Elayedath, M. Elhadi, S.I. El-Jaafary, Z. El-Khatib, A. Elsharkawy, A. Endalamaw, A.Y. Endries, S. Eskandarieh, I.J. Ezeonwumelu, S. Ezzikouri, M. Farahmand, E.J.A. Faraon, A.O. Fasanmi, S. Ferrero, L. Ferro Desideri, I. Filip, F. Fischer, M.O. Folayan, M. Foroutan, T. Fukumoto, M.M. Gad, M.A. Gadanya, A.M. Gaidhane, T. Garg, R.T. Gayesa, E.A. Gebreyohannes, H.A. Gesesew, A. Getachew Obsa, K. Ghadiri, A. Ghashghaee, S.A. Gilani, T.G. Ginindza, I.-R. Glavan, E.V. Glushkova, M. Golechha, H.C. Gugnani, B. Gupta, S. Gupta, V.B. Gupta, V.K. Gupta, S. Hamidi, S. Handanagic, S. Haque, H. Harapan, A. Hargono, A.I. Hasaballah, A. Hashi, S. Hassan, S. Hassanipour, K. Hayat, I. Heredia-Pi, K. Hezam, R. Holla, P. Hoogar, M.E. Hoque, M. Hosseini, M. Hosseinzadeh, M. Hsairi, R. Hussain, S.E. Ibitoye, B. Idrisov, K.S. Ikuta, O.S. Ilesanmi, I.M. Ilic, M.D. Ilic, S.S.N. Irvani, M.M. Islam, N.E. Ismail, R. Itumalla, I.O. Iyamu, R. Jabbarinejad, V. Jain, R. Jayawardena, R.P. Jha, N. Joseph, A. Kabir, Z. Kabir, R. Kalhor,

F. Kaliyadan, A. Kamath, T. Kanchan, H. Kandel, G. Kassahun, P.D.M.C. Katoto, G.A. Kayode, E.M. Kebede, H.K. Kebede, H. Khajuria, N. Khalid, E.A. Khan, G. Khan, K. Khatab, M.S. Kim, Y.J. Kim, A. Kisa, S. Kisa, S. Kochhar, V.A. Korshunov, P.A. Koul, S.L. Koulmane Laxminarayana, A. Koyanagi, K. Krishan, B. Kuate Defo, G.A. Kumar, M. Kumar, N. Kumar, A. Kwarteng, D.K. Lal, I. Landires, S. Lasrado, Z.S. Lassi, J.V. Lazarus, J.J.-H. Lee, Y.Y. Lee, K.E. LeGrand, C. Lin, X. Liu, E.R. Maddison, H. Magdy Abd El Razek, P.W. Mahasha, A. Majeed, A. Makki, A.A. Malik, W.A. Manamo, M.A. Mansournia, F.R. Martins-Melo, S.Z. Masoumi, Z.A. Memish, R.G. Menezes, E.W. Mengesha, H.E. Merie, A.G. Mersha, T. Mestrovic, P. Meylaks, N. Mheidly, T.R. Miller, A. Mirica, B. Moazen, Y. Mohammad, M. Mohammadi, A. Mohammed, S. Mohammed, S. Mohammed, M. Moitra, A.H. Mokdad, M. Molokhia, M.A. Moni, G. Moradi, Y. Moradi, C. Mpundu-Kaambwa, S. Mubarik, S.B. Munro, L. Mwanri, J.B. Nachega, A.J. Nagarajan, A.I. Narayana, M. Naveed, B.P. Nayak, S.O. Nduaguba, S. Neupane Kandel, G. Nguefack-Tsague, T.H. Nguyen, M.R. Nixon, C.A. Nnaji, J.J. Noubiap, V. Nuñez-Samudio, T.E. Nyirenda, O.B. Oghenetega, A.T. Olagunju, B.O. Olakunde, O.F. Owopetu, M. P A, J.R. Padubidri, S. Pakhale, T. Parekh, F. Pashazadeh Kan, S. Pawar, V.C.F. Pepito, E.K. Peprah, M. Pinheiro, K.N. Pokhrel, R.V. Polibin, R.C.G. Pollok, M.J. Postma, Z. Quazi Syed, A. Radfar, R.A. Radhakrishnan, F. Rahim, V. Rahimi-Movaghar, S. Rahimzadeh, M. Rahman, A.M. Rahmani, P. Ram, C.L. Ranabhat, P. Ranasinghe, C.R. Rao, S.J. Rao, P. Rathi, D.L. Rawaf, S. Rawaf, L.D. Regassa, I.u. Rehman, A.M.N. Renzaho, N. Rezaei, O. Reza Hosseini, M.s. Rezai, A. Rezapour, R.K. Ripon, V. Rodrigues, D.O. Roshchin, G.M. Rwegerera, U. Saeed, S. Saeedi Moghaddam, R. Sagar, K.M. Saif-Ur-Rahman, M.R. Salem, M. Samaei, A.M. Samy, M.M. Santric-Milicevic, S. Saroshe, B. Sathian, M. Satpathy, M. Sawhney, A.E. Schutte, A. Seylani, M.A. Shaikh, M.F. Shaka, H. Shamshad, M. Shamsizadeh, M. Shannawaz, A. Shetty, J.I. Shin, K.M. Shivakumar, J.A. Singh, V.Y. Skryabin, A.A. Skryabina, R. Somayaji, S. Soshnikov, E.E. Spurlock, D.J. Stein, M.a.B. Sufiyan, H. Tadbiri, B.T. Tadesse, E.G. Tadesse, A.T. Tamiru, E.E. Tarkang, N. Taveira, Y. Tekalegn, F.H. Tesfay, G.A. Tessema, R. Thapar, M.R. Tovani-Palone, E. Traini, B.X. Tran, A.C. Tsai, B.S. Tusa, S. Ullah, C.D. Umeokonkwo, B. Unnikrishnan, S. Valadan Tahbaz, J.H. Villafañe, S.K. Vladimirov, B. Vo, A. Vongpradith, G.T. Vu, Y. Waheed, R.G. Wamai, G. Wang, Y. Wang, P. Ward, R. Westerman, A.S. Winkler, L. Yadav, S.H. Yahyazadeh Jabbari, T.S. Yazie, S. Yi, V. Yigit, B.W. Yirdaw, N. Yonemoto, C. Yu, I. Yunusa, M.S. Zastrozhin, A. Zastrozhina, Z.-J. Zhang, A. Zumla, J.A. Salomon, J.W. Eaton, M. Naghavi, L. Dwyer-Lindgren, H. Wang, S.S. Lim, S.I. Hay, C.J.L. Murray, H.H. Kyu, Global, regional, and national sex-specific burden and control of the HIV epidemic, 1990–2019, for 204 countries and territories: the Global Burden of Diseases Study 2019, *The Lancet HIV*, 8 (2021) e633-e651.

[337] A. Pandey, A.P. Galvani, The global burden of HIV and prospects for control, *The Lancet HIV*, 6 (2019) e809-e811.

[338] M.S. Saag, R.T. Gandhi, J.F. Hoy, R.J. Landovitz, M.A. Thompson, P.E. Sax, D.M. Smith, C.A. Benson, S.P. Buchbinder, C. del Rio, J.J. Eron, Jr., G. Fätkenheuer, H.F. Günthard, J.-M. Molina, D.M. Jacobsen, P.A. Volberding, Antiretroviral Drugs for Treatment and Prevention of HIV Infection in Adults: 2020 Recommendations of the International Antiviral Society–USA Panel, *JAMA*, 324 (2020) 1651-1669.

[339] M.-P. de Béthune, Non-nucleoside reverse transcriptase inhibitors (NNRTIs), their discovery, development, and use in the treatment of HIV-1 infection: A review of the last 20 years (1989–2009), *Antiviral Research*, 85 (2010) 75-90.

[340] H. Lal, T. Kumar, S. Dutta, K. Ram, A Concise Review of Existing Therapies and Recent Advances in the Management of HIV Infection, *International Journal of Pharmaceutical Sciences Review and Research*, 64 (2020) 153-158.

[341] A. Tseng, J. Seet, E.J. Phillips, The evolution of three decades of antiretroviral therapy: challenges, triumphs and the promise of the future, *British Journal of Clinical Pharmacology*, 79 (2015) 182-194.

[342] M.A. Fischl, D.D. Richman, M.H. Grieco, M.S. Gottlieb, P.A. Volberding, O.L. Laskin, J.M. Leedom, J.E. Groopman, D. Mildvan, R.T. Schooley, G.G. Jackson, D.T. Durack, D. King, The Efficacy of Azidothymidine (AZT) in the Treatment of Patients with AIDS and AIDS-Related Complex, *New England Journal of Medicine*, 317 (1987) 185-191.

[343] C. Flexner, HIV-Protease Inhibitors, *New England Journal of Medicine*, 338 (1998) 1281-1293.

[344] Z. Lv, Y. Chu, Y. Wang, HIV protease inhibitors: a review of molecular selectivity and toxicity, *HIV AIDS (Auckl)*, 7 (2015) 95-104.

[345] K.M. Brooks, E.M. Sherman, E.F. Egelund, A. Brotherton, S. Durham, M.E. Badowski, D.B. Cluck, Integrase Inhibitors: After 10 Years of Experience, Is the Best Yet to Come?, *Pharmacotherapy: The Journal of Human Pharmacology and Drug Therapy*, 39 (2019) 576-598.

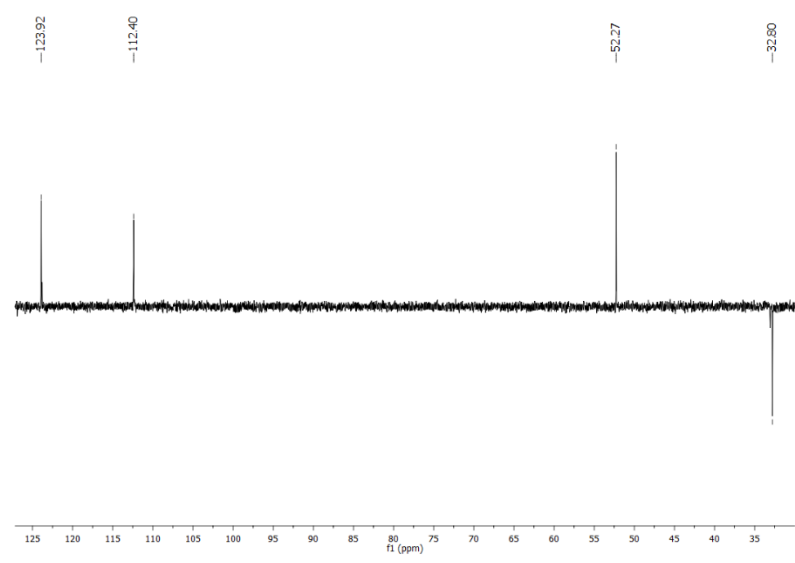
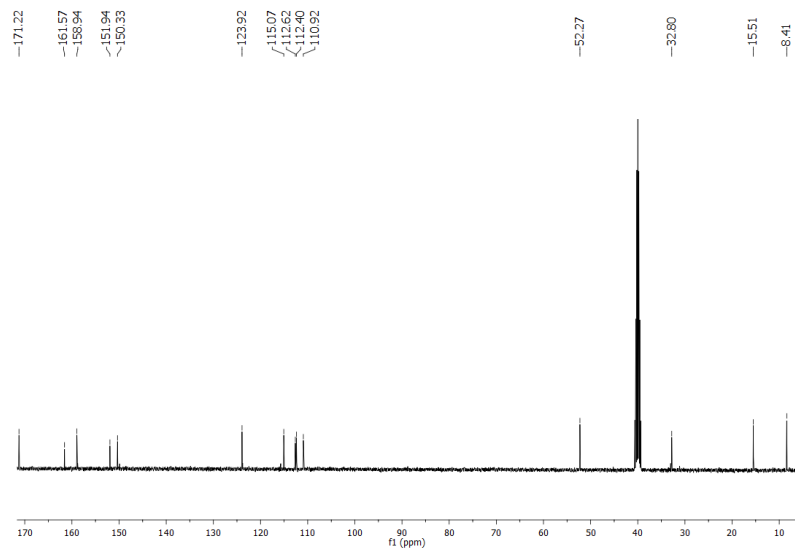
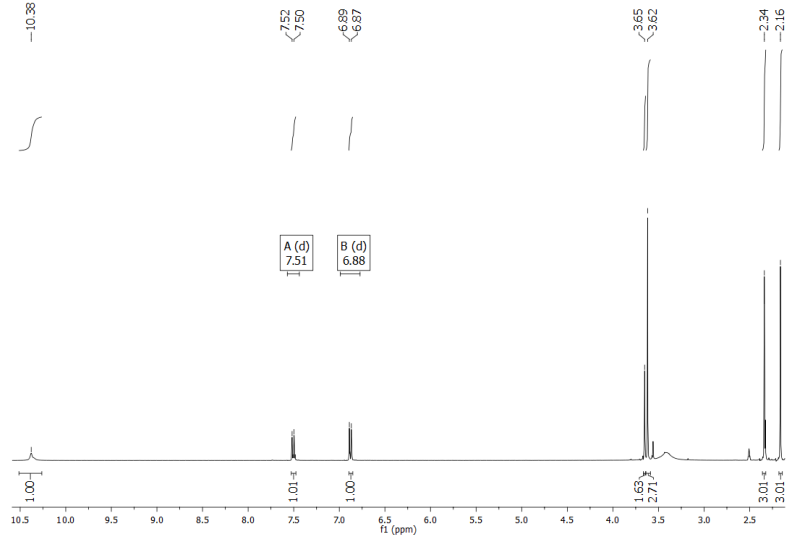
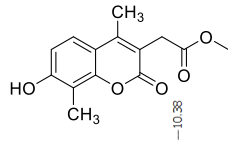
[346] J. LaBonte, J. Lebbos, P. Kirkpatrick, Enfuvirtide, *Nature Reviews Drug Discovery*, 2 (2003) 345-346.

[347] N.J. Carter, G.M. Keating, Maraviroc, *Drugs*, 67 (2007) 2277-2288.

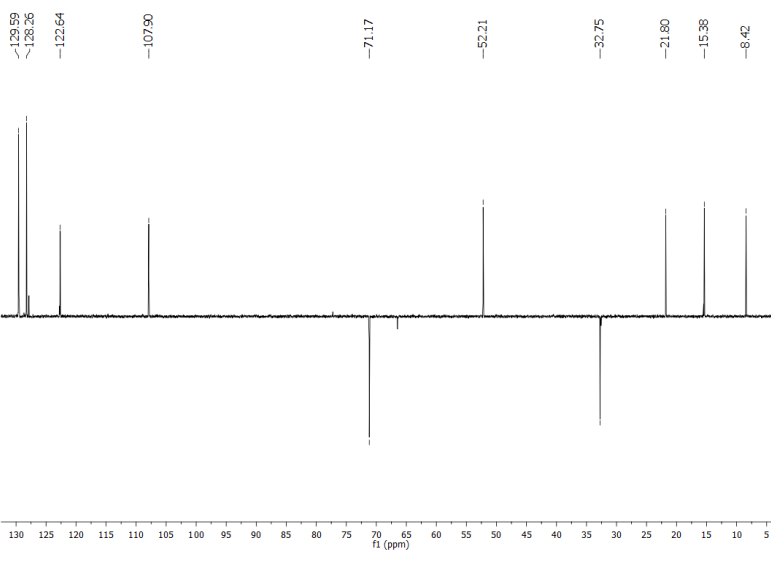
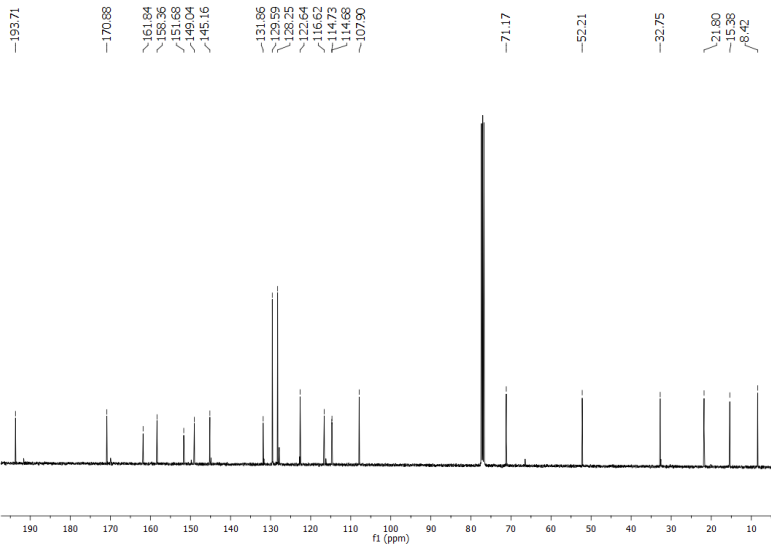
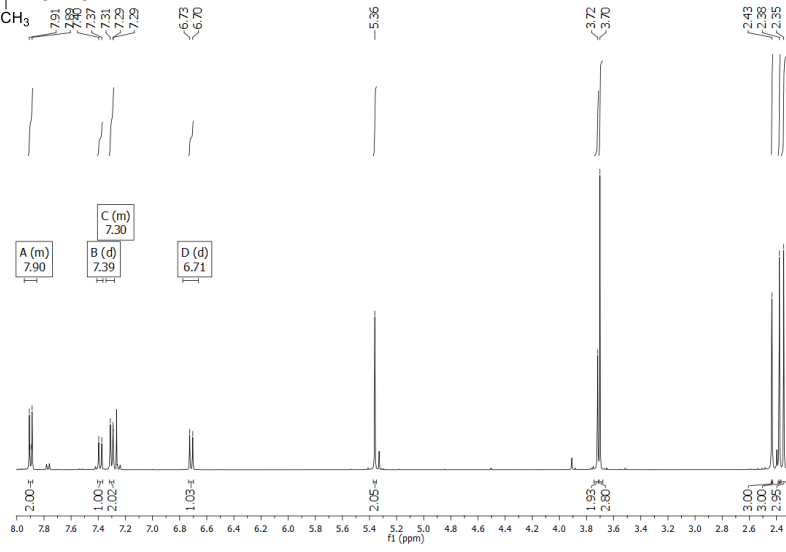
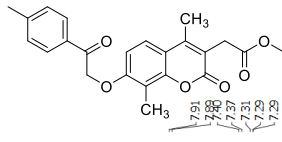
-
- [348] M.V. Beccari, B.T. Mogle, E.F. Sidman, K.A. Mastro, E. Asiago-Reddy, W.D. Kufel, Ibalizumab, a Novel Monoclonal Antibody for the Management of Multidrug-Resistant HIV-1 Infection, *Antimicrobial Agents and Chemotherapy*, 63 (2019) e110-119.
- [349] B. Rossetti, F. Montagnani, A. De Luca, Current and emerging two-drug approaches for HIV-1 therapy in ART-naïve and ART-experienced, virologically suppressed patients, *Expert Opinion on Pharmacotherapy*, 19 (2018) 713-738.
- [350] A.M. Margolis, H. Heverling, P.A. Pham, A. Stolbach, A review of the toxicity of HIV medications, *Journal of Medical Toxicology*, 10 (2014) 26-39.
- [351] R.R. Ramsay, M.R. Popovic-Nikolic, K. Nikolic, E. Uliassi, M.L. Bolognesi, A perspective on multi-target drug discovery and design for complex diseases, *Clinical and Translational Medicine*, 7 (2018) 3.
- [352] G.N. Nikolenko, S. Palmer, F. Maldarelli, J.W. Mellors, J.M. Coffin, V.K. Pathak, Mechanism for nucleoside analog-mediated abrogation of HIV-1 replication: balance between RNase H activity and nucleotide excision, *Proceedings of the National Academy of Sciences of the USA*, 102 (2005) 2093-2098.

Appendix

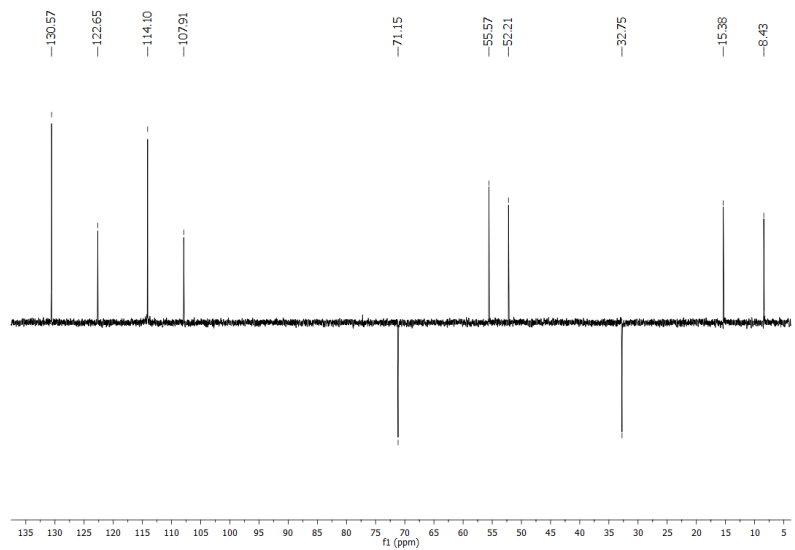
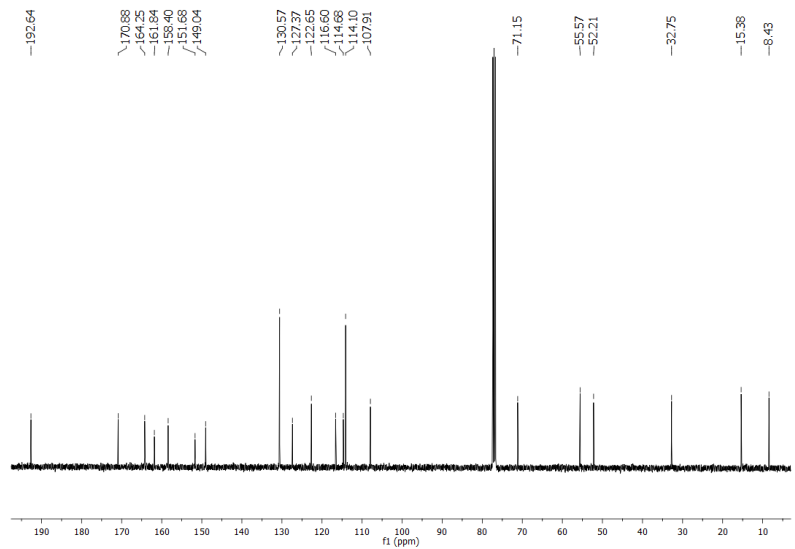
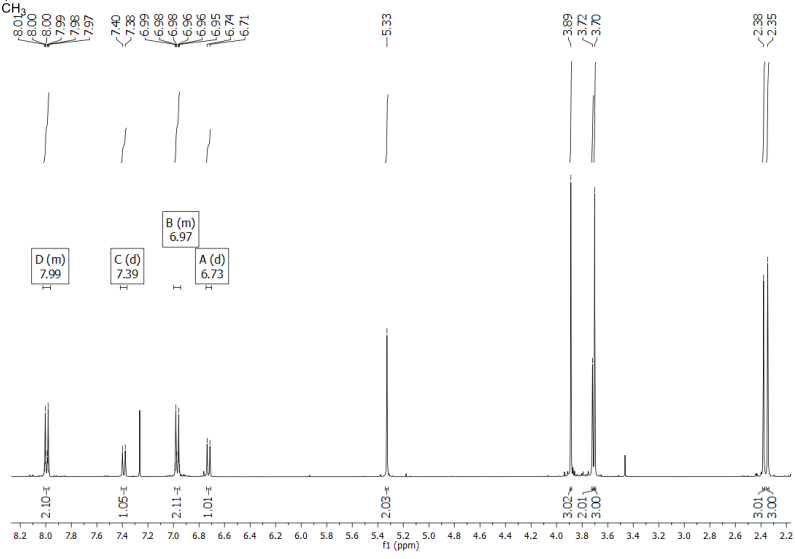
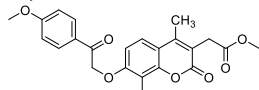
¹H, ¹³C and DEPT NMR spectra of EMAC10163



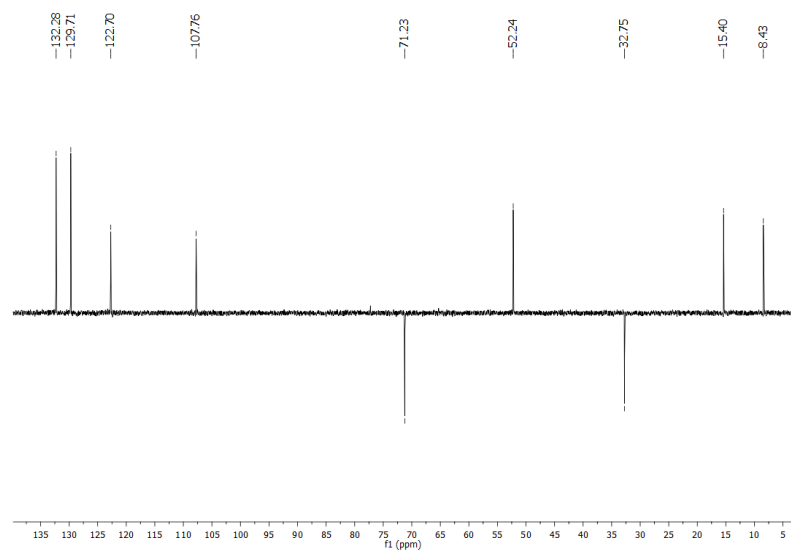
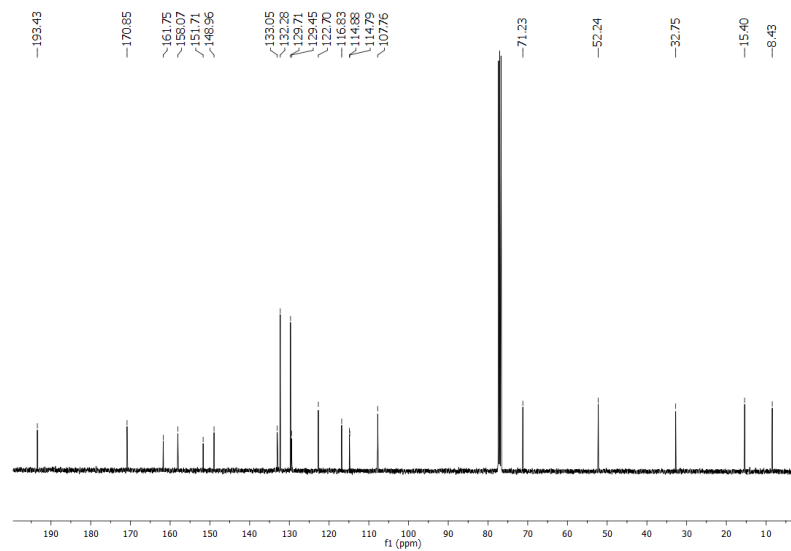
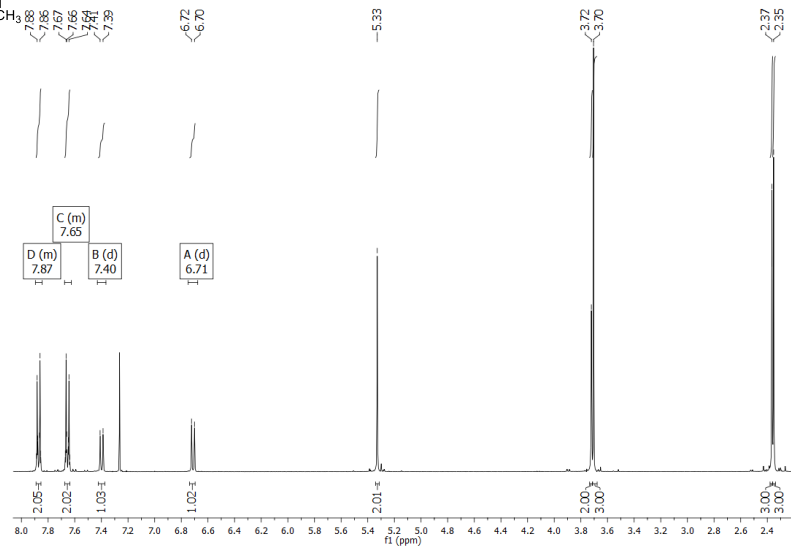
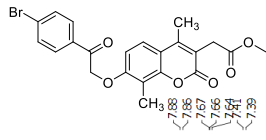
^1H , ^{13}C and DEPT NMR spectra of EMAC10163a



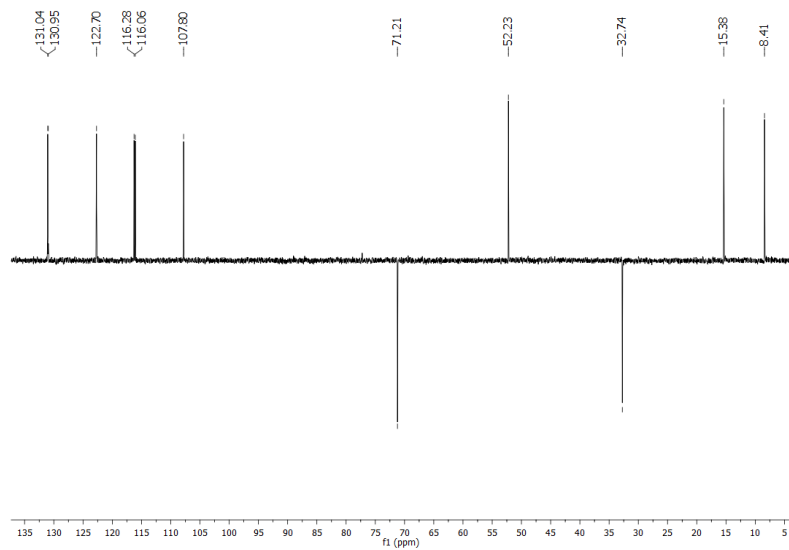
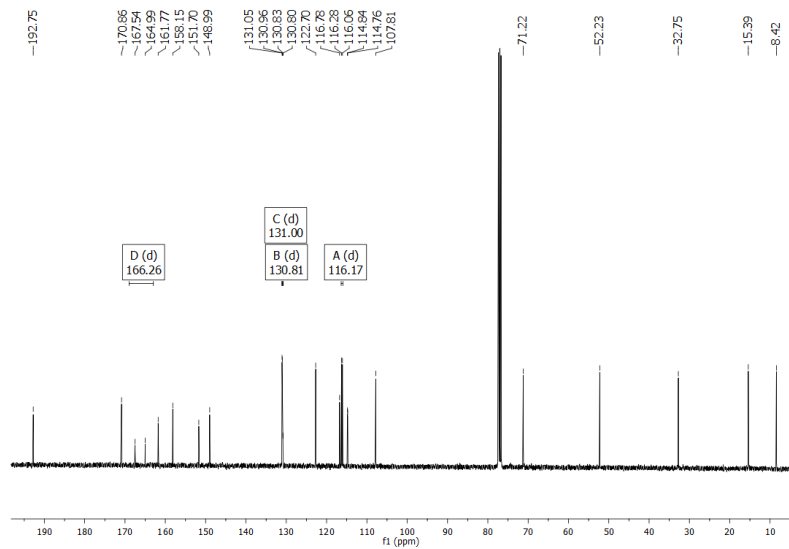
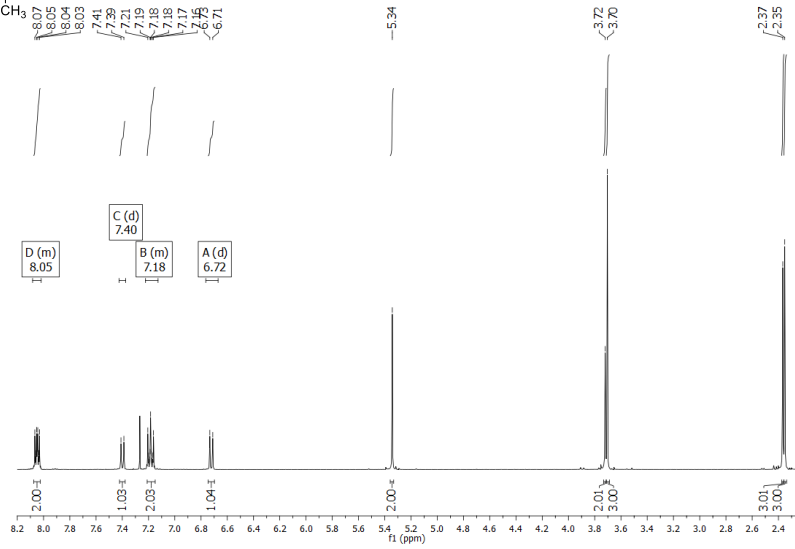
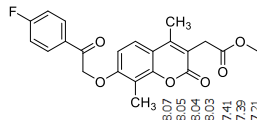
¹H, ¹³C and DEPT NMR spectra of EMAC10163b



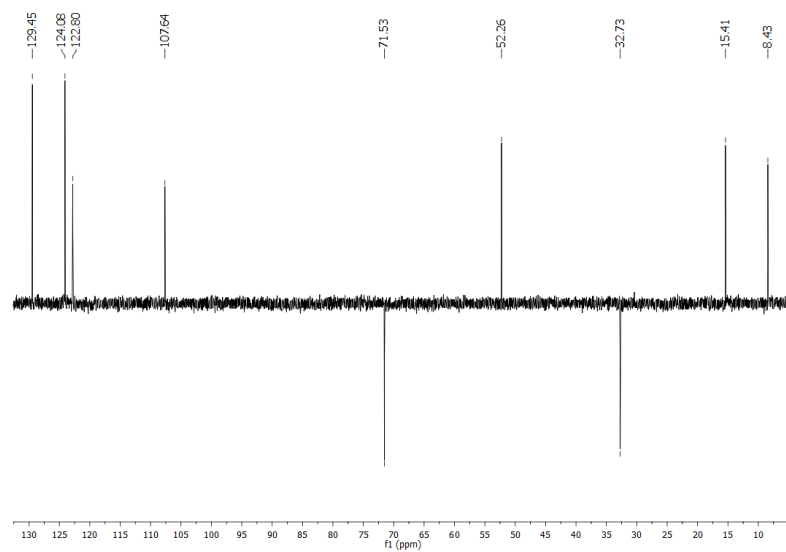
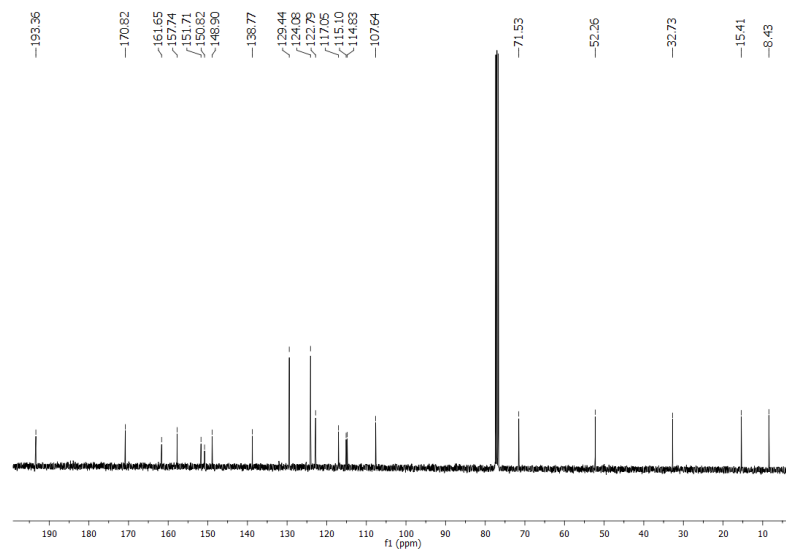
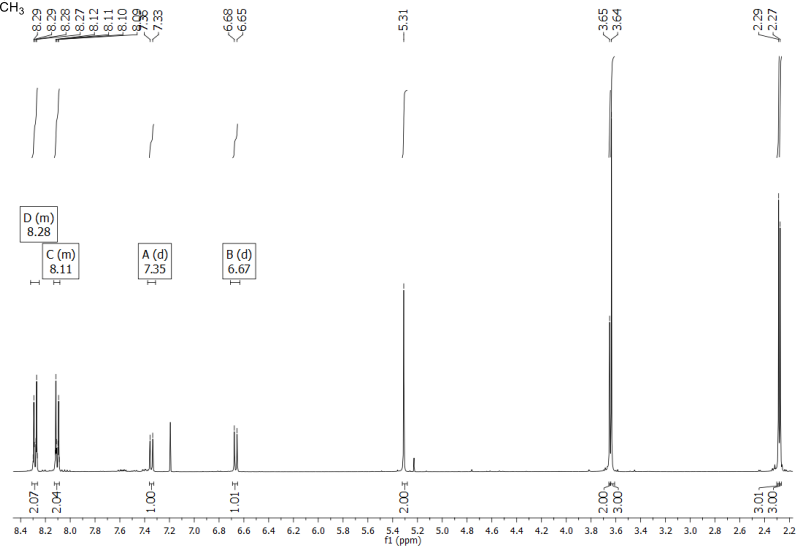
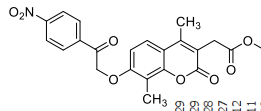
^1H , ^{13}C and DEPT NMR spectra of EMAC10163c



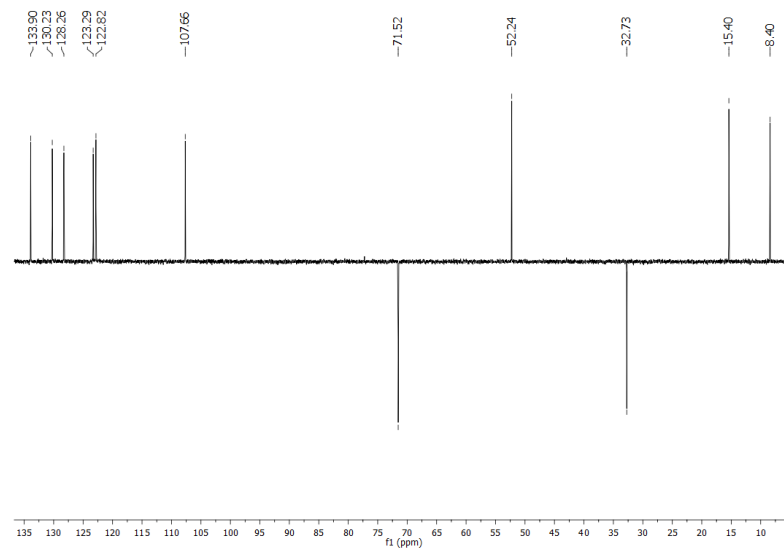
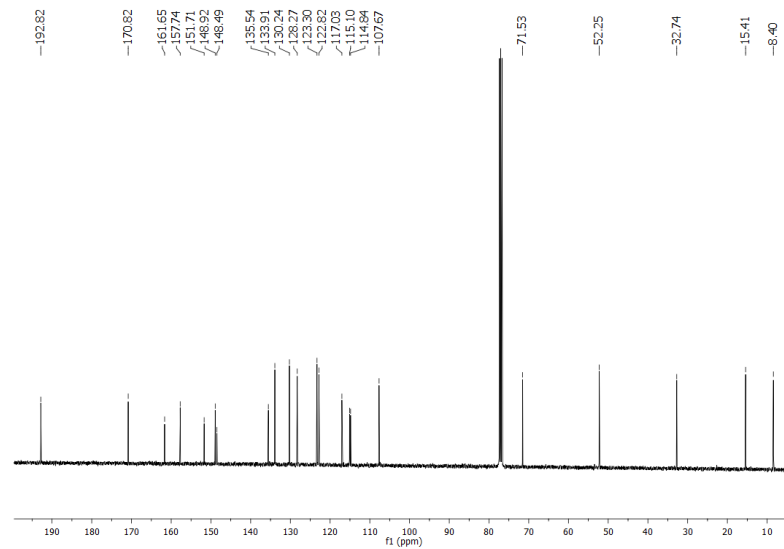
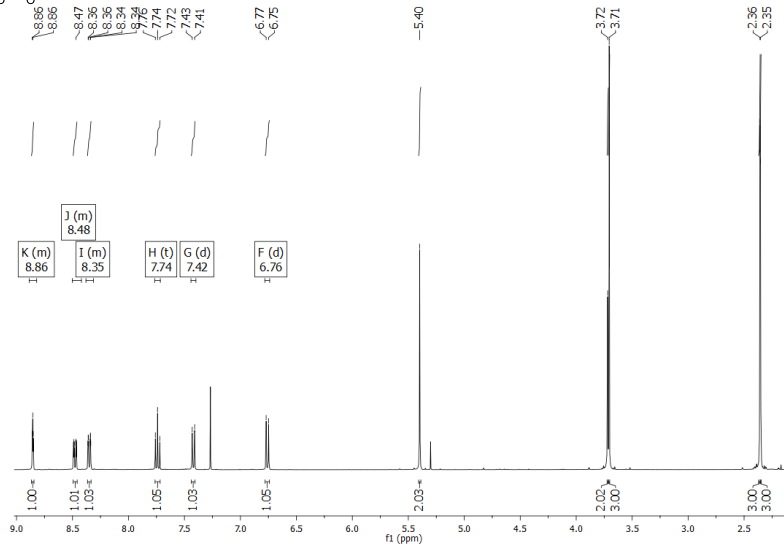
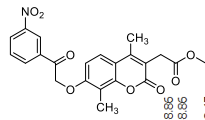
^1H , ^{13}C and DEPT NMR spectra of EMAC10163d



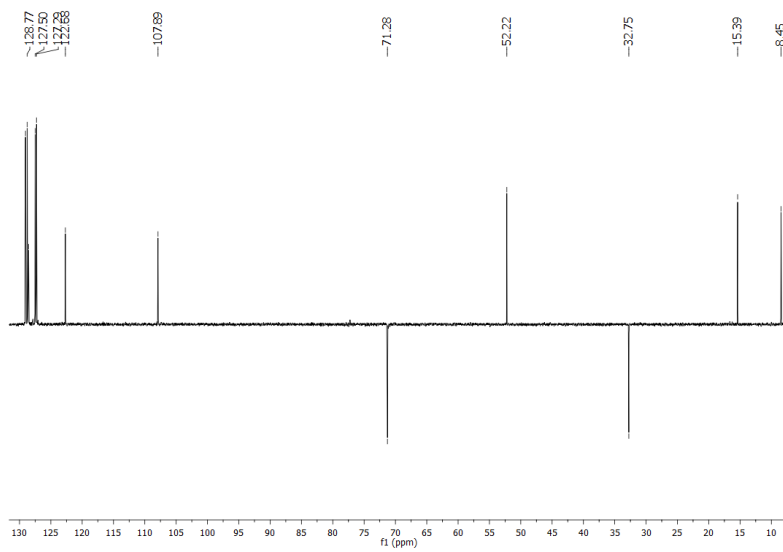
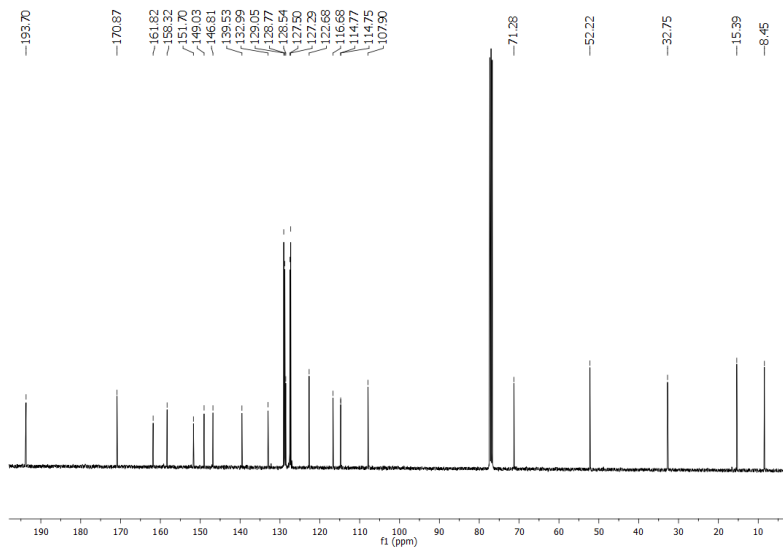
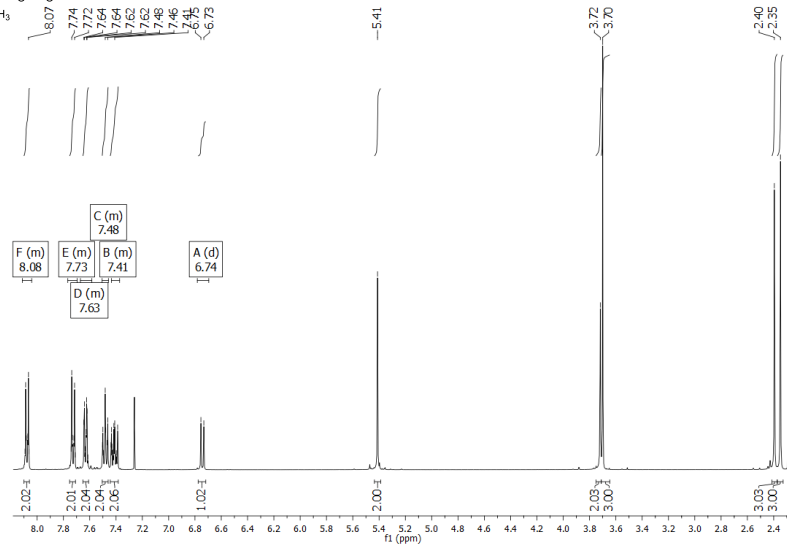
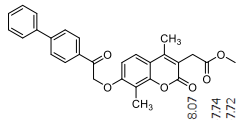
^1H , ^{13}C and DEPT NMR spectra of EMAC10163e



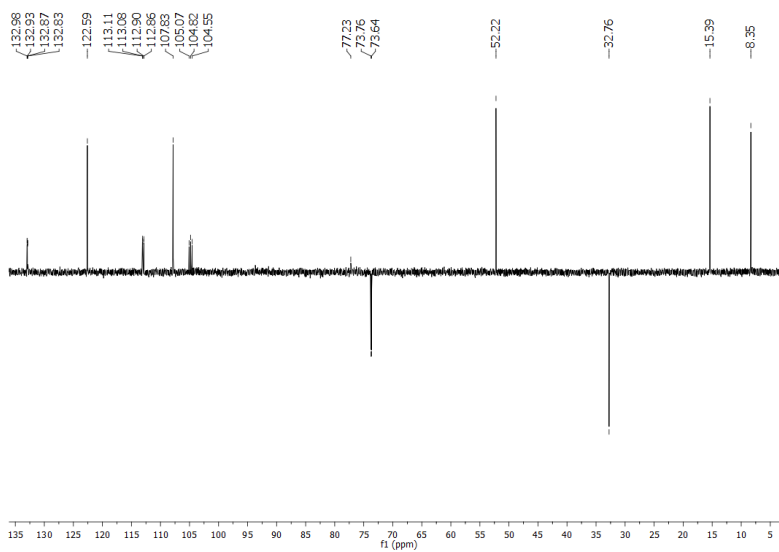
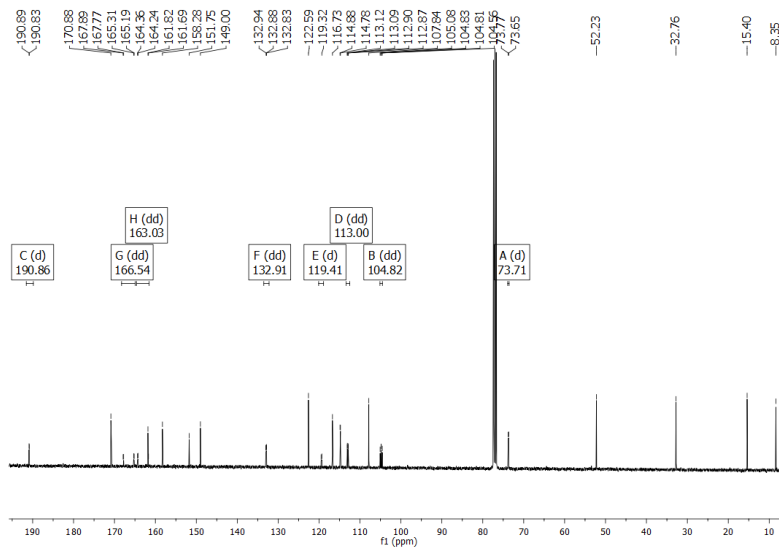
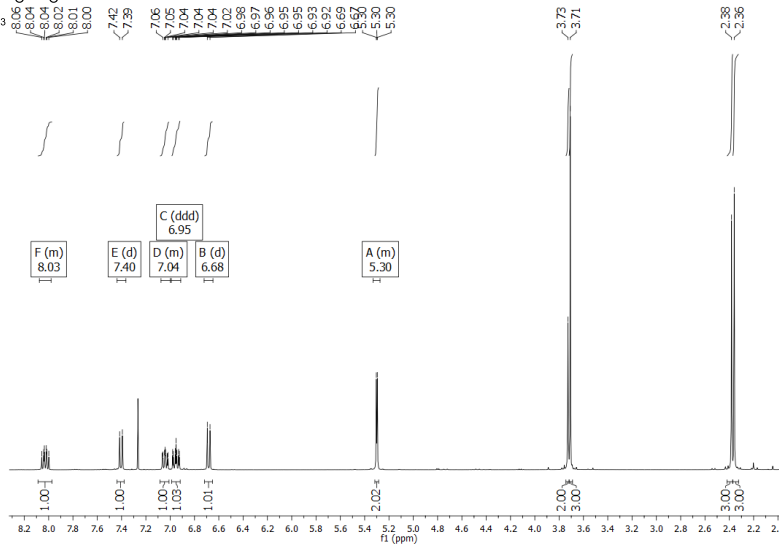
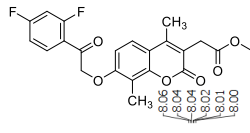
^1H , ^{13}C and DEPT NMR spectra of EMAC10163f



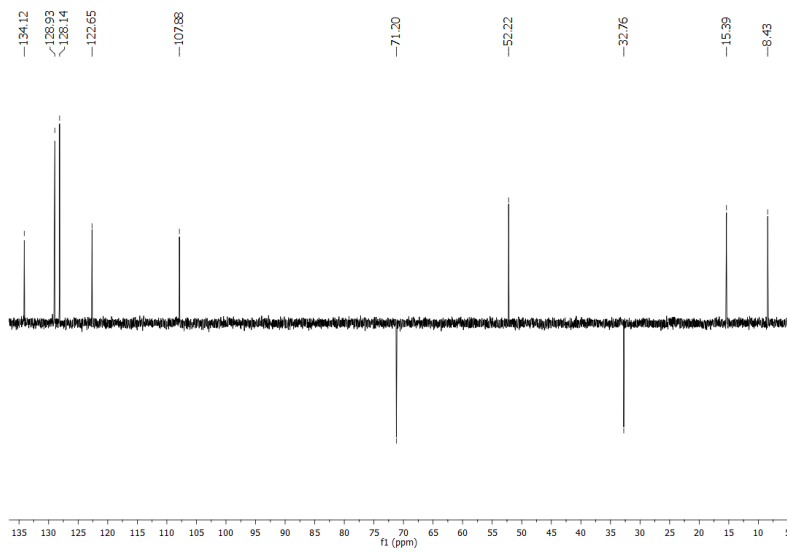
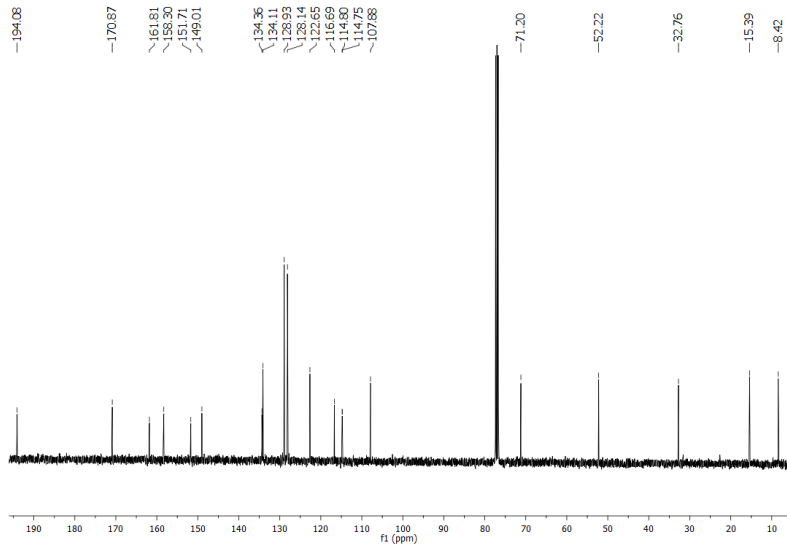
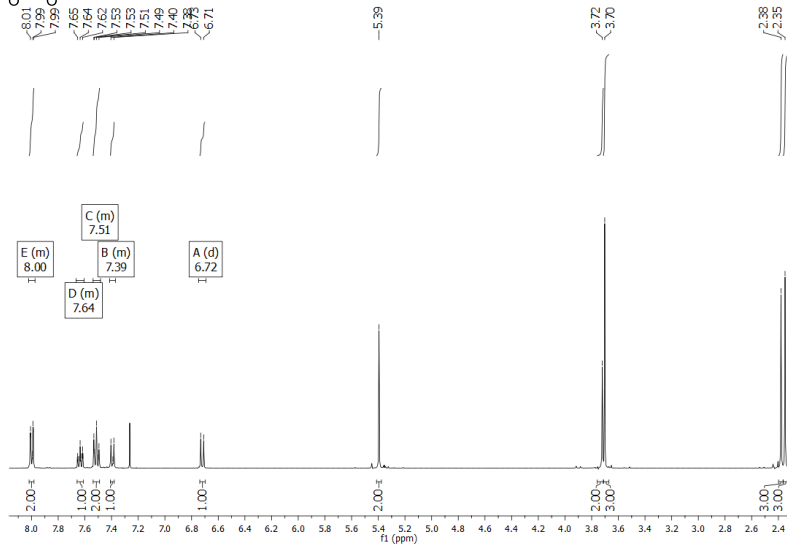
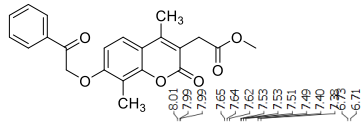
¹H, ¹³C and DEPT NMR spectra of EMAC10163g



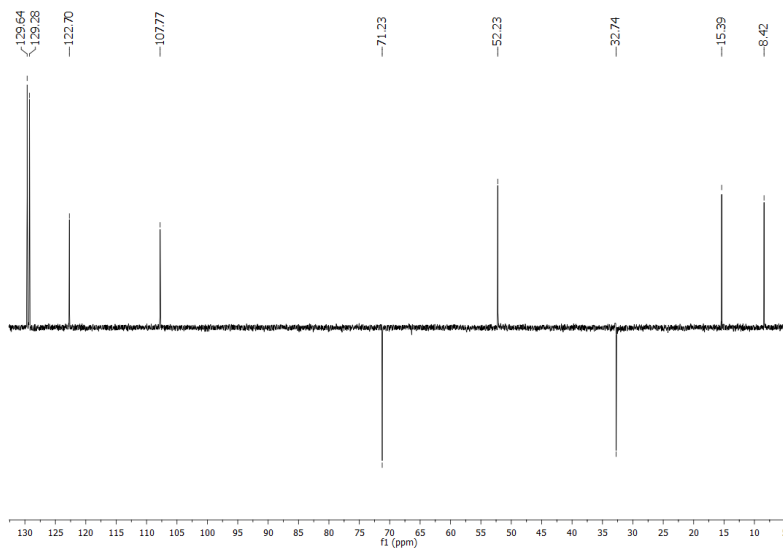
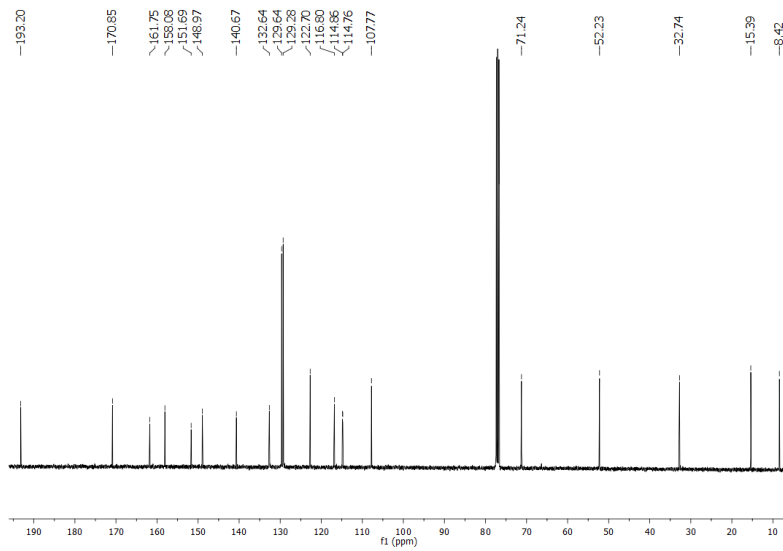
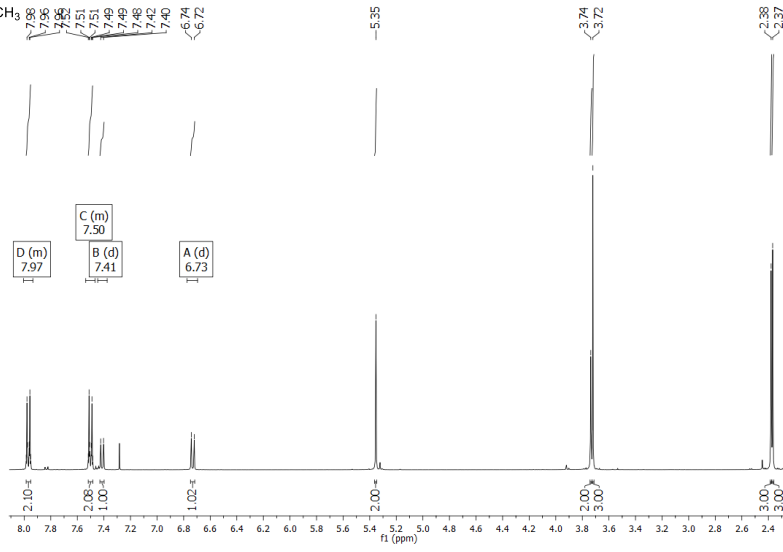
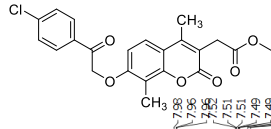
^1H , ^{13}C and DEPT NMR spectra of EMAC10163h



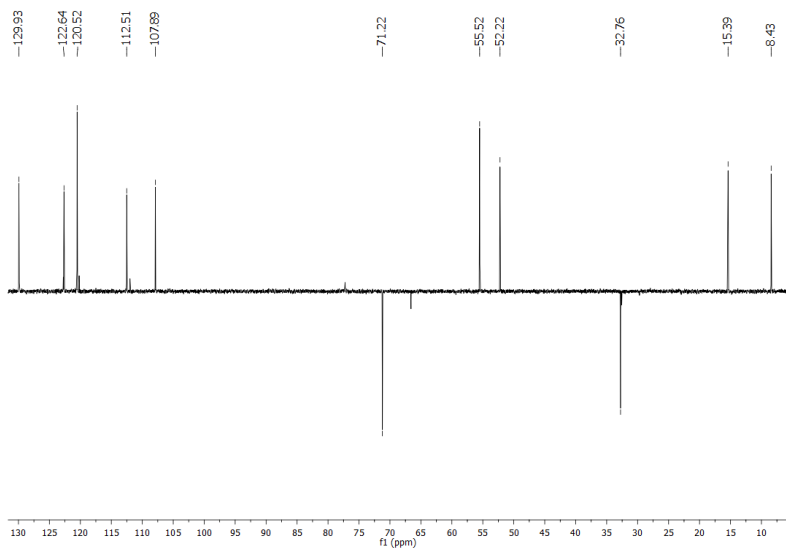
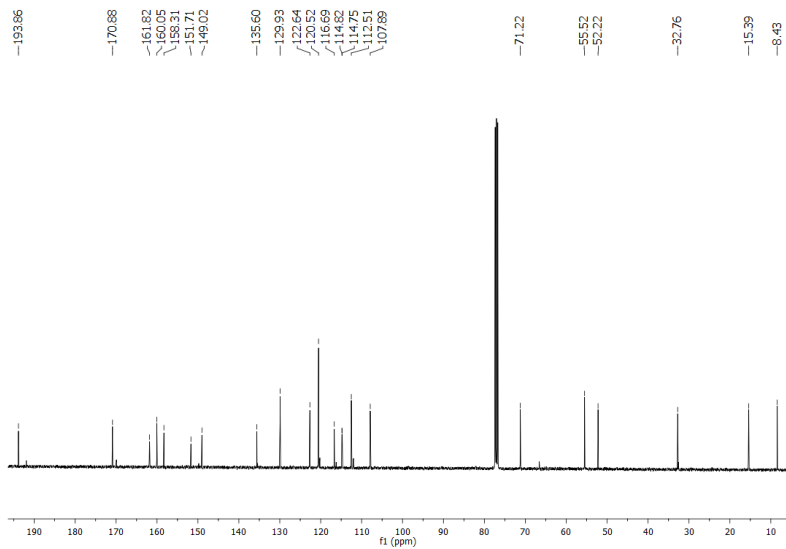
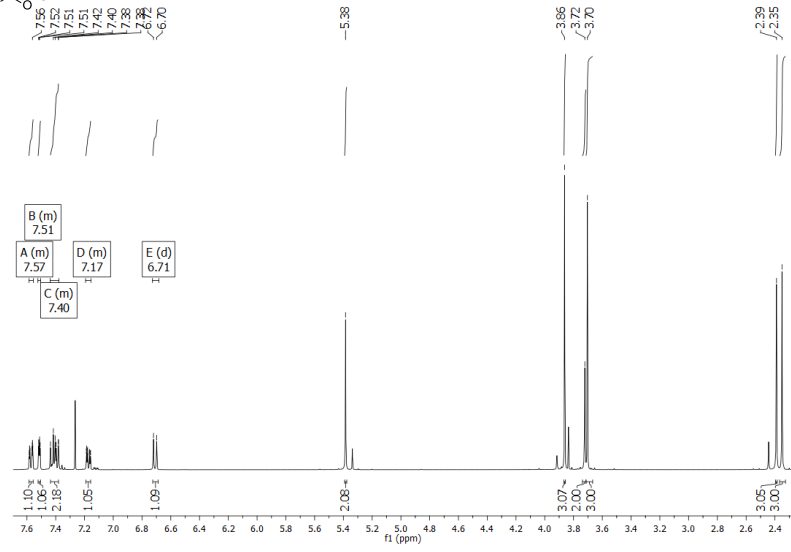
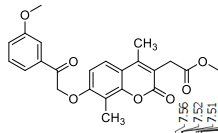
¹H, ¹³C and DEPT NMR spectra of EMAC10163j



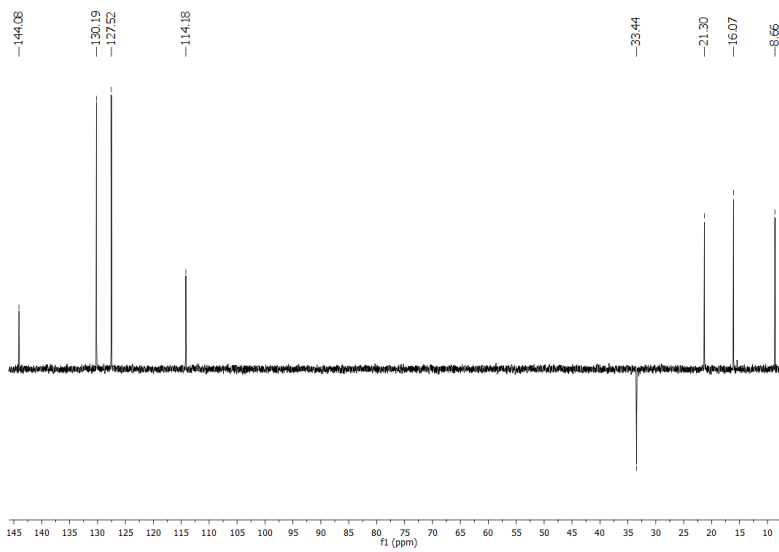
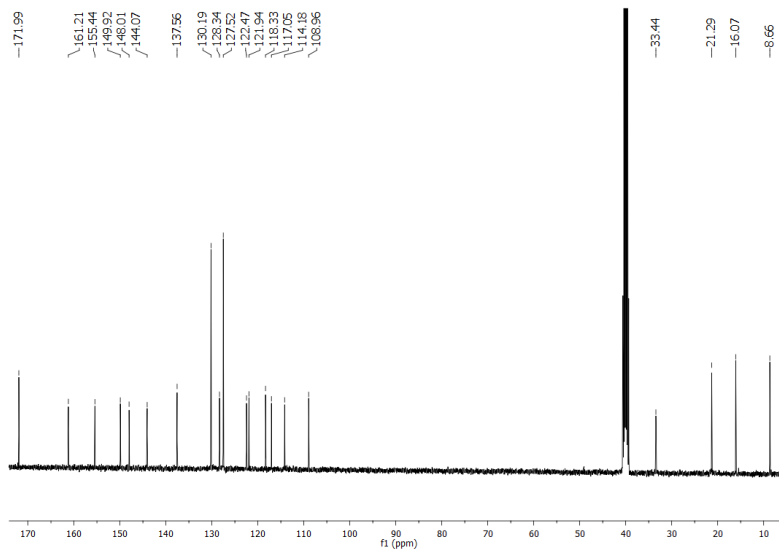
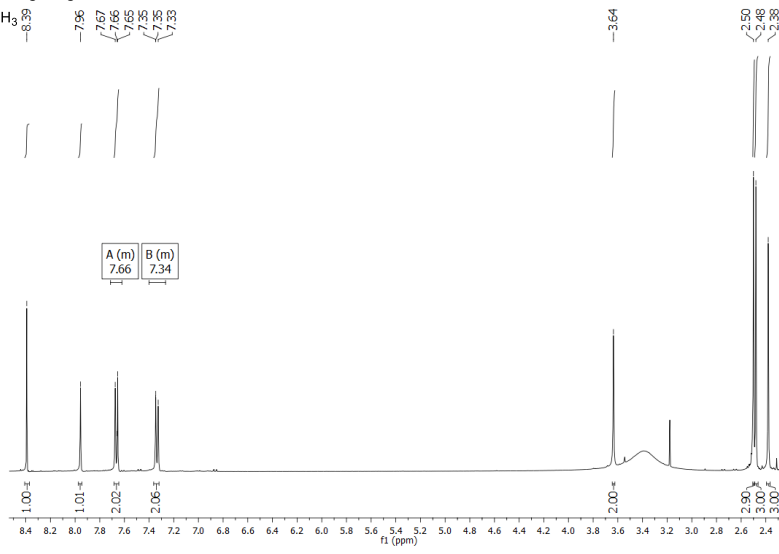
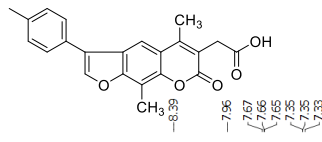
¹H, ¹³C and DEPT NMR spectra of EMAC10163k



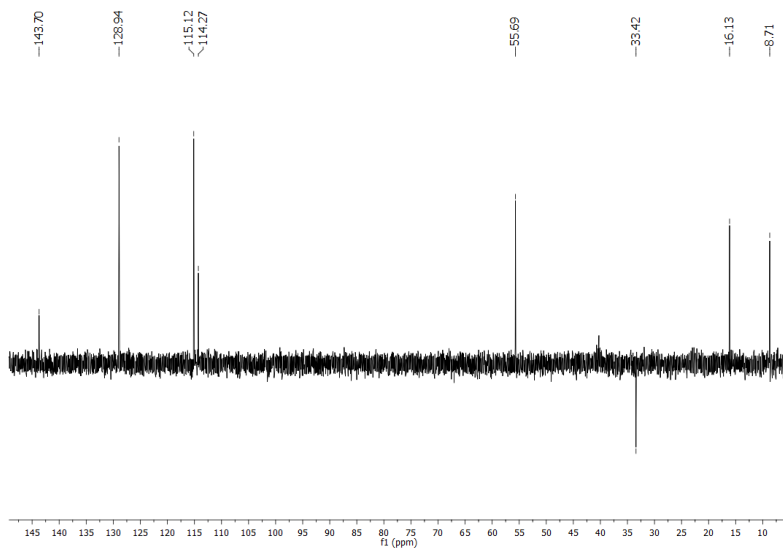
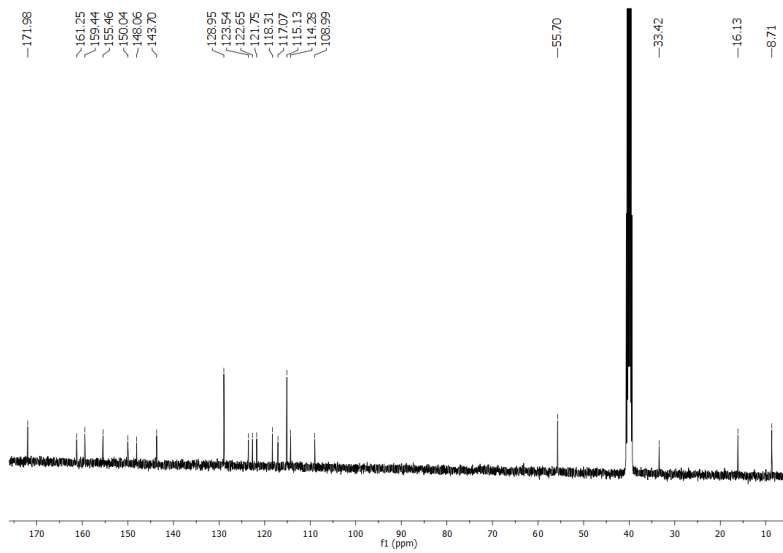
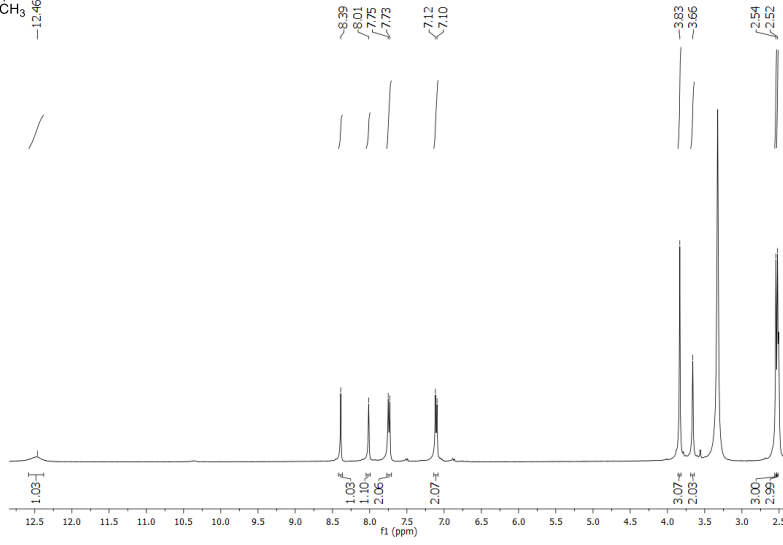
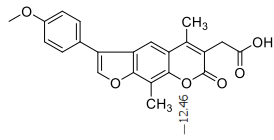
^1H , ^{13}C and DEPT NMR spectra of EMAC10163m



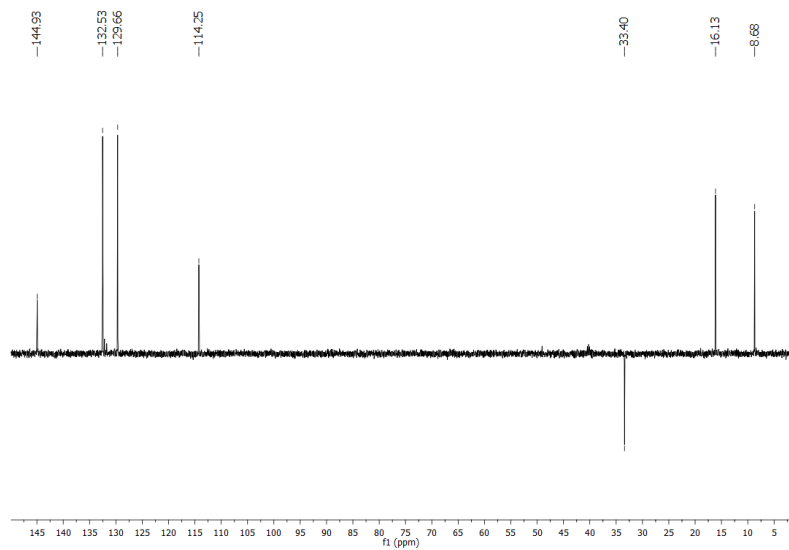
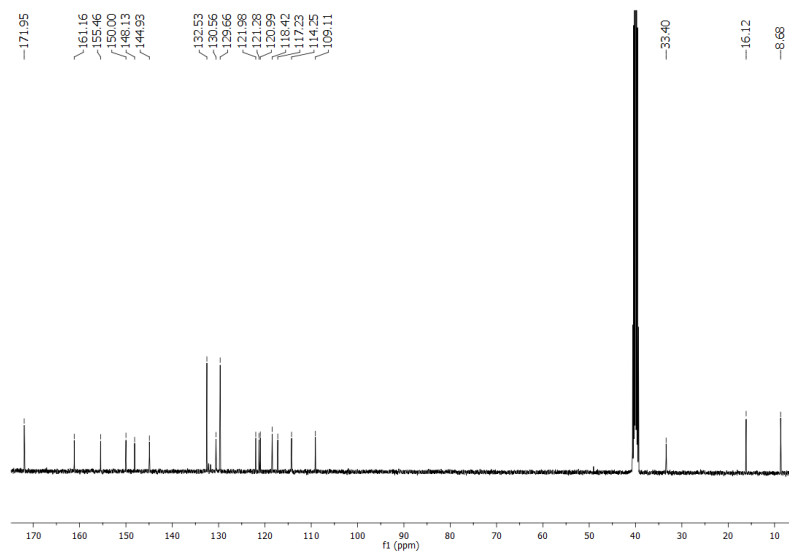
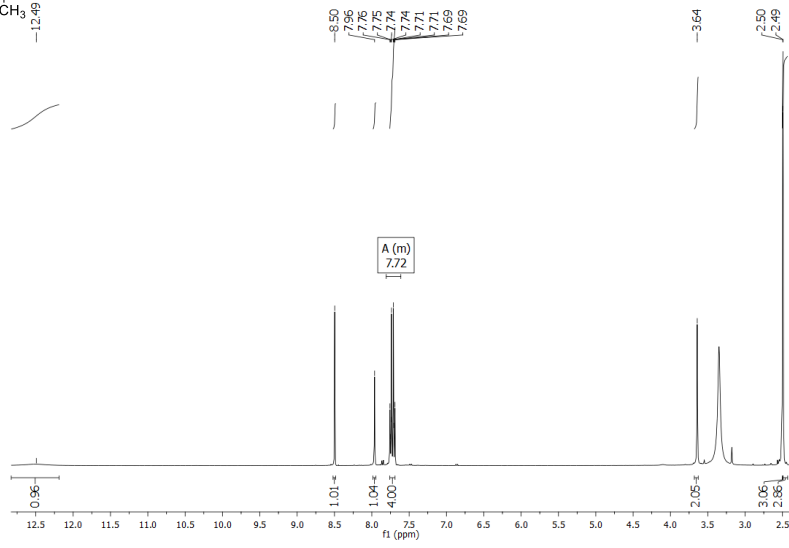
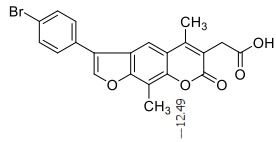
¹H, ¹³C and DEPT NMR spectra of EMAC10164a



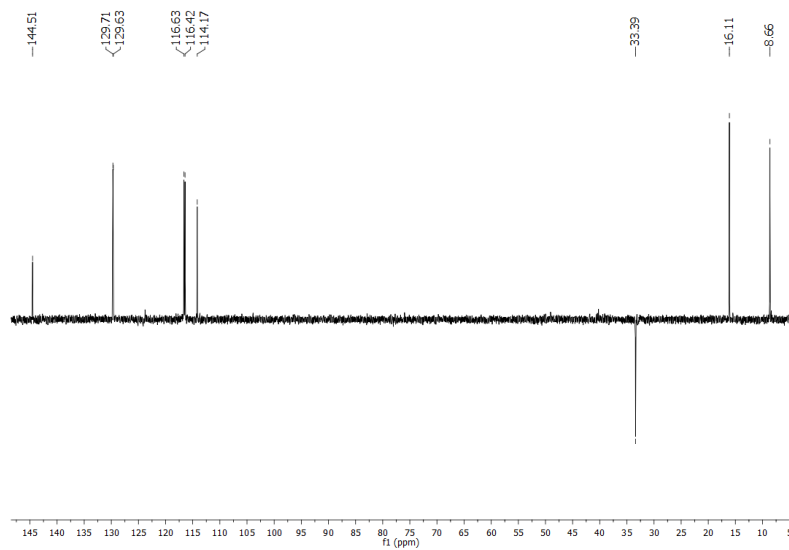
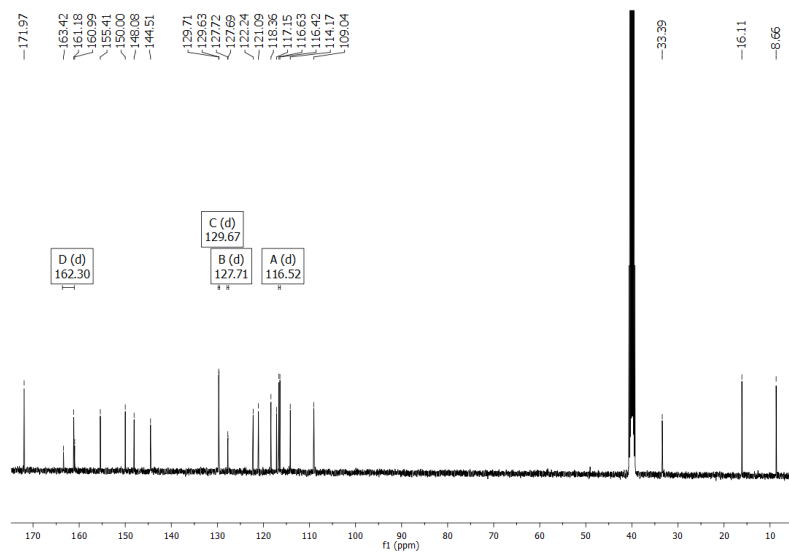
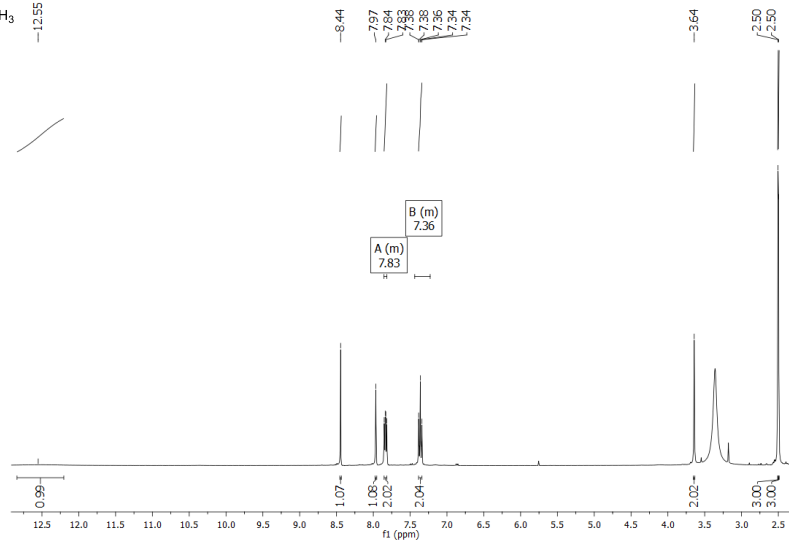
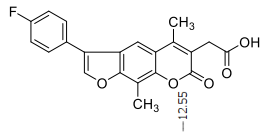
¹H, ¹³C and DEPT NMR spectra of EMAC10164b



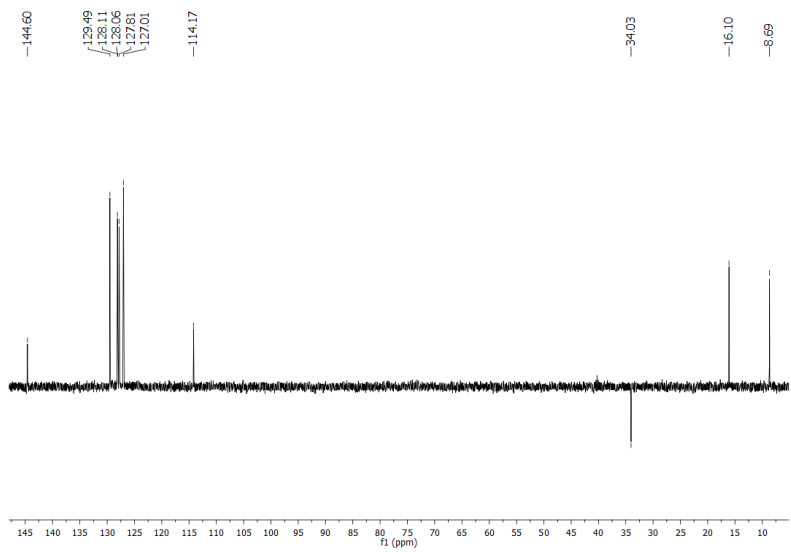
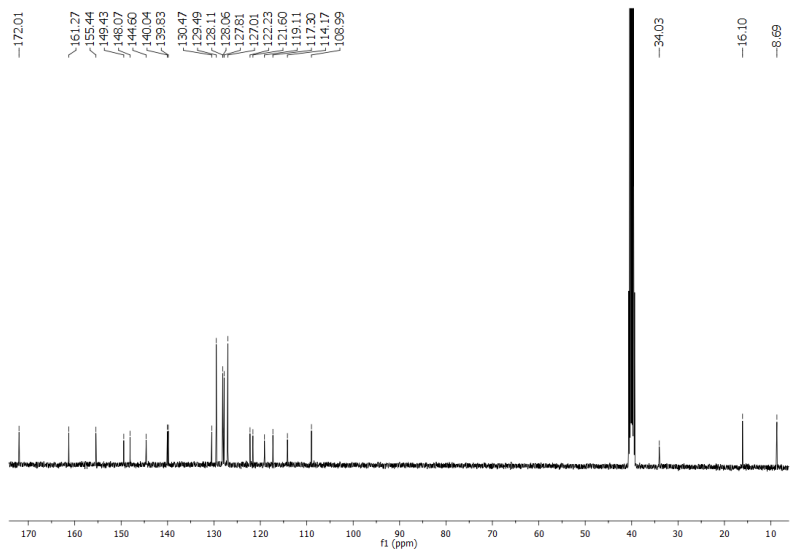
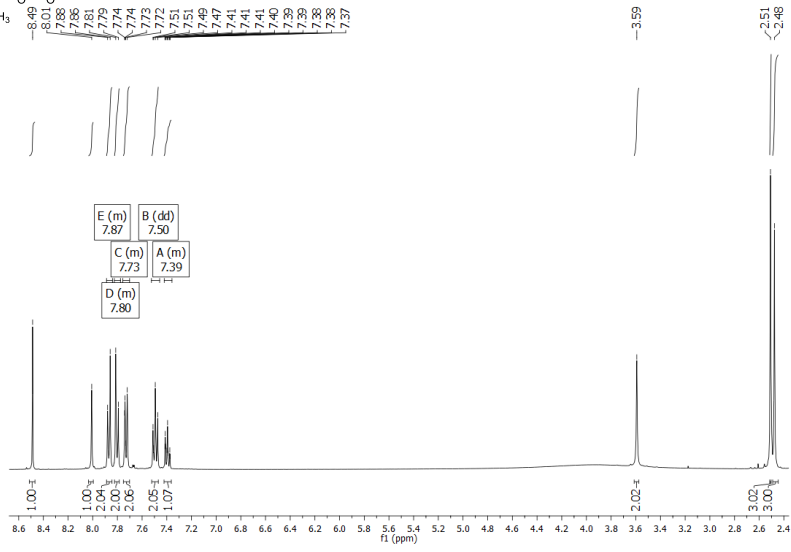
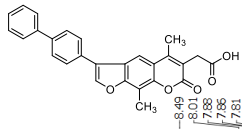
¹H, ¹³C and DEPT NMR spectra of EMAC10164c



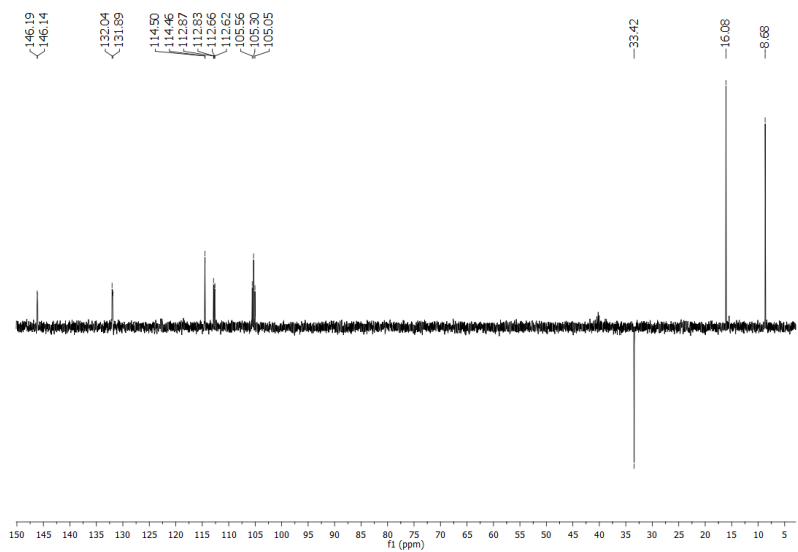
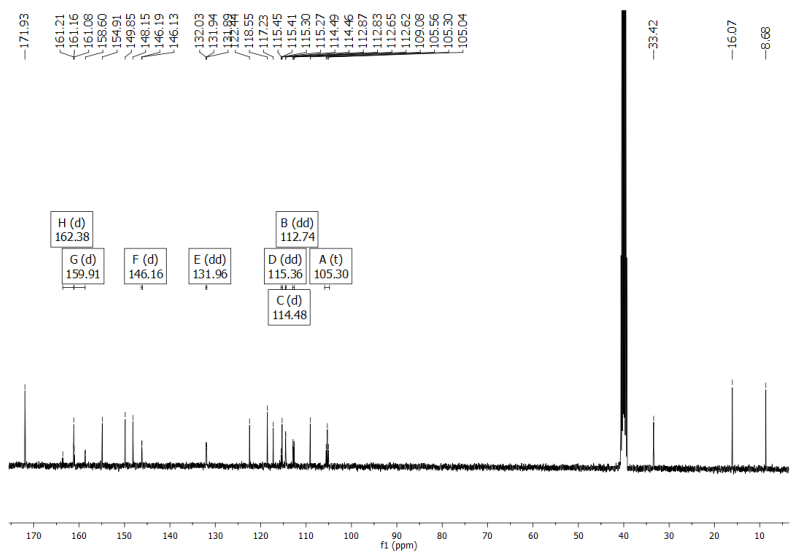
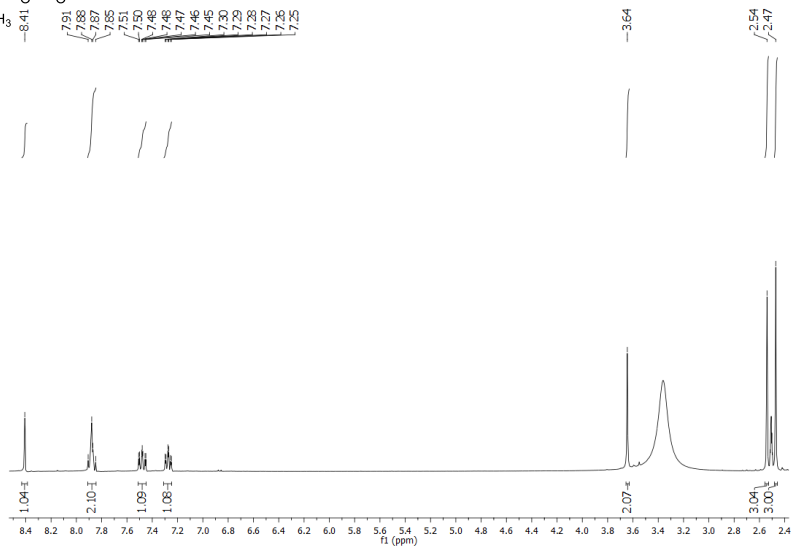
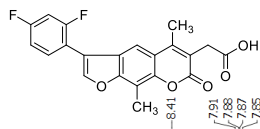
^1H , ^{13}C and DEPT NMR spectra of EMAC10164d



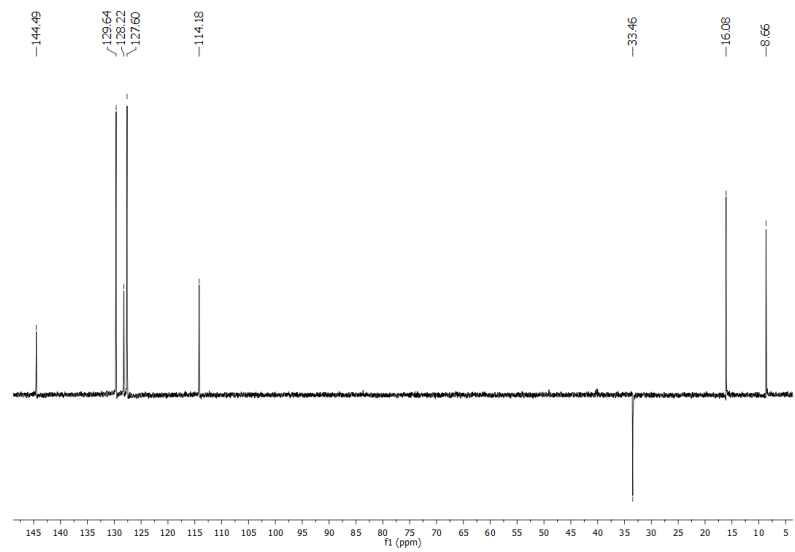
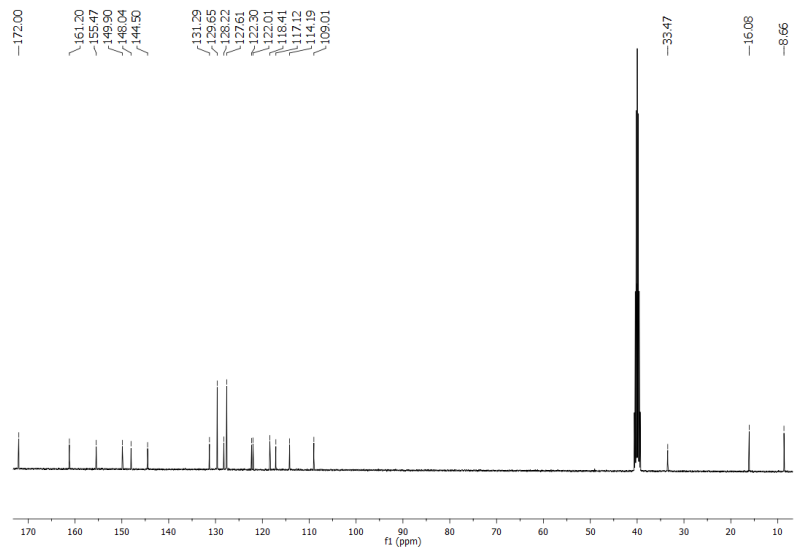
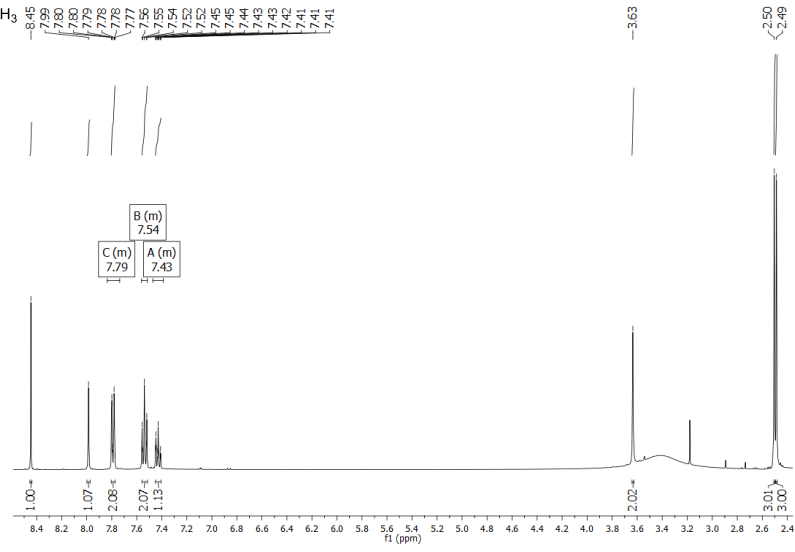
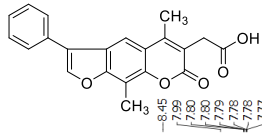
^1H , ^{13}C and DEPT NMR spectra of EMAC10164g



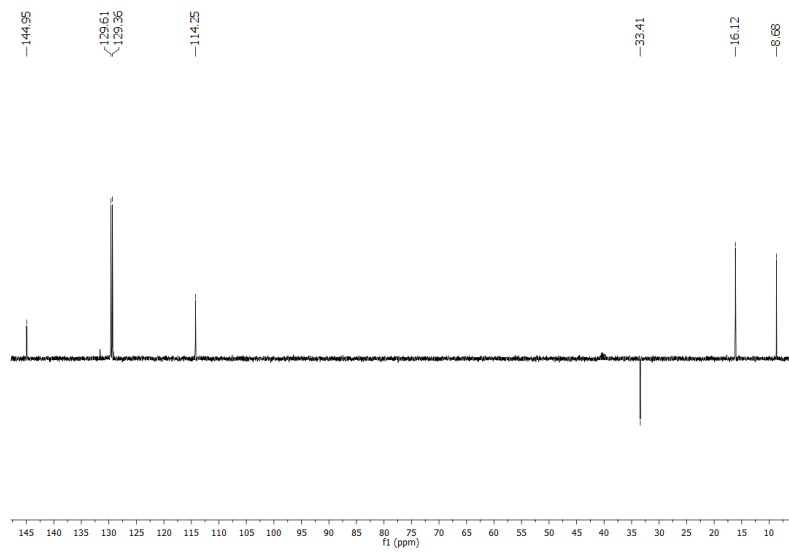
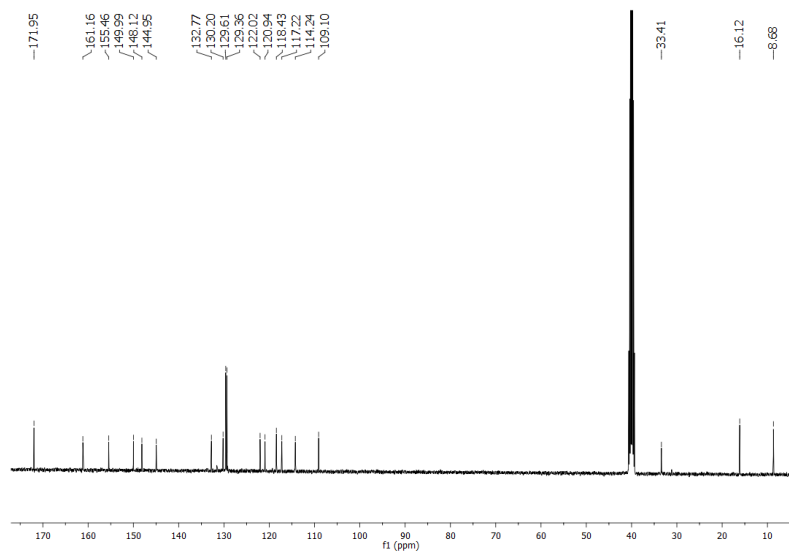
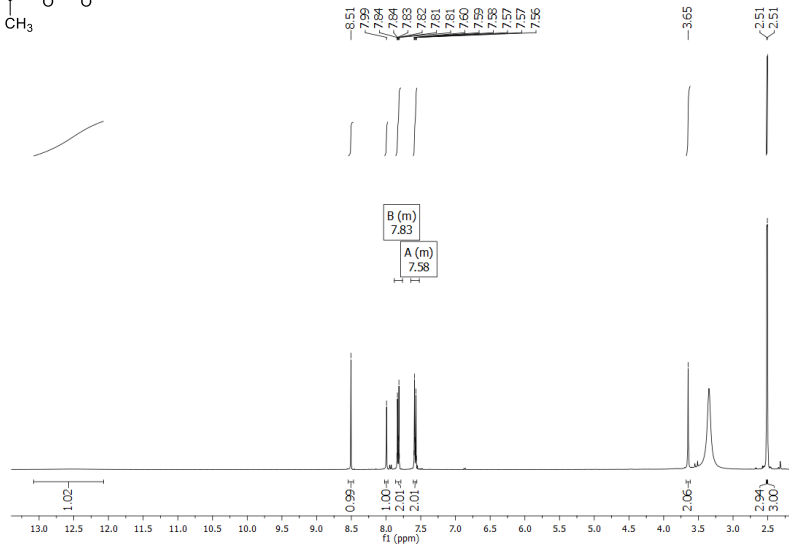
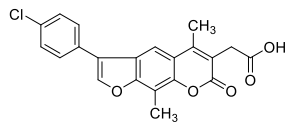
¹H, ¹³C and DEPT NMR spectra of EMAC10164h



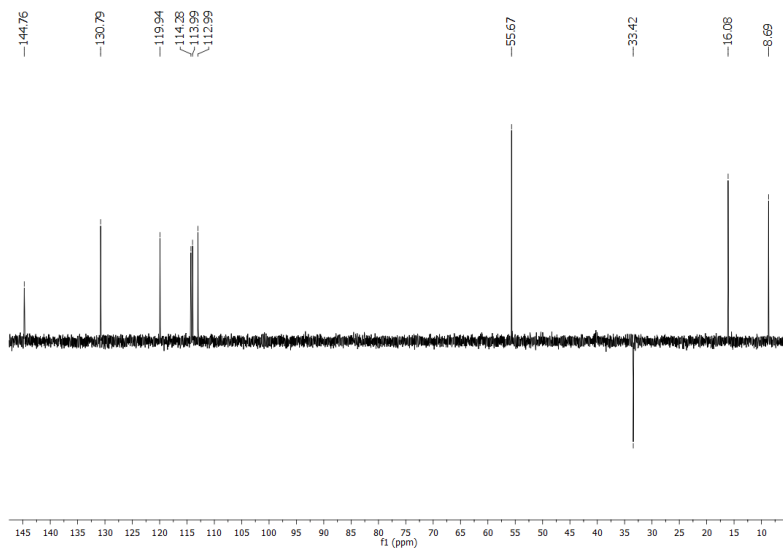
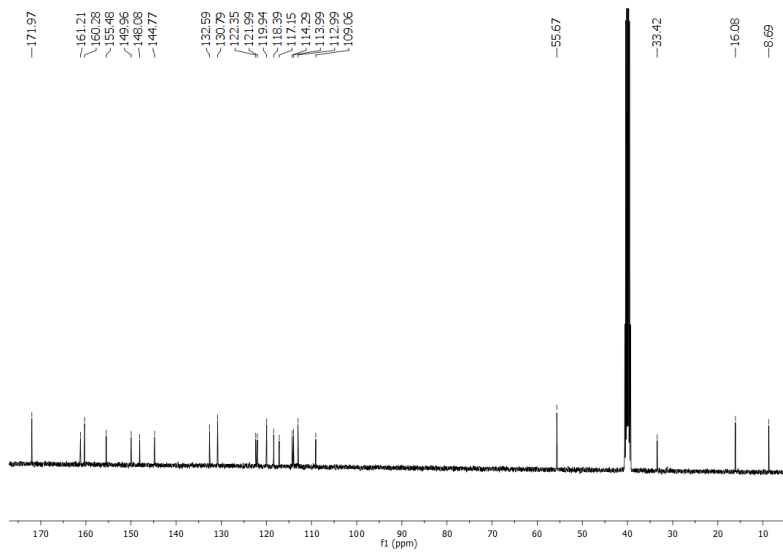
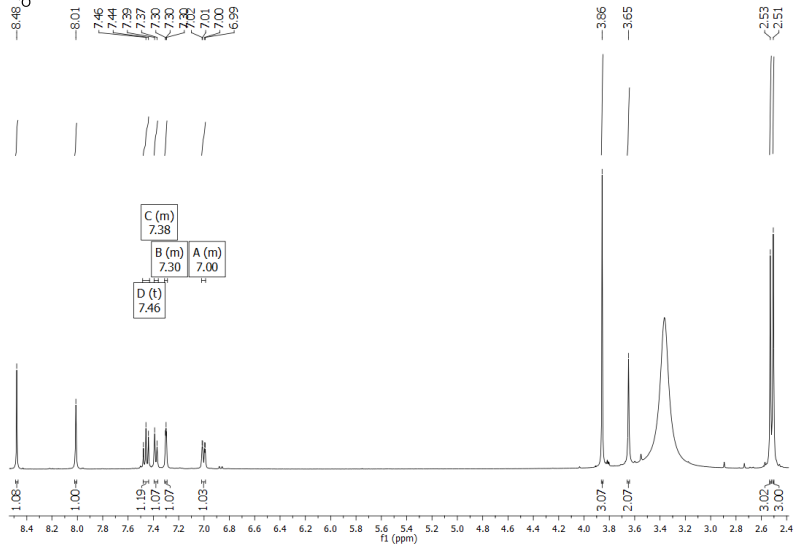
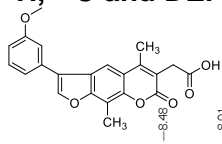
^1H , ^{13}C and DEPT NMR spectra of EMAC10164j



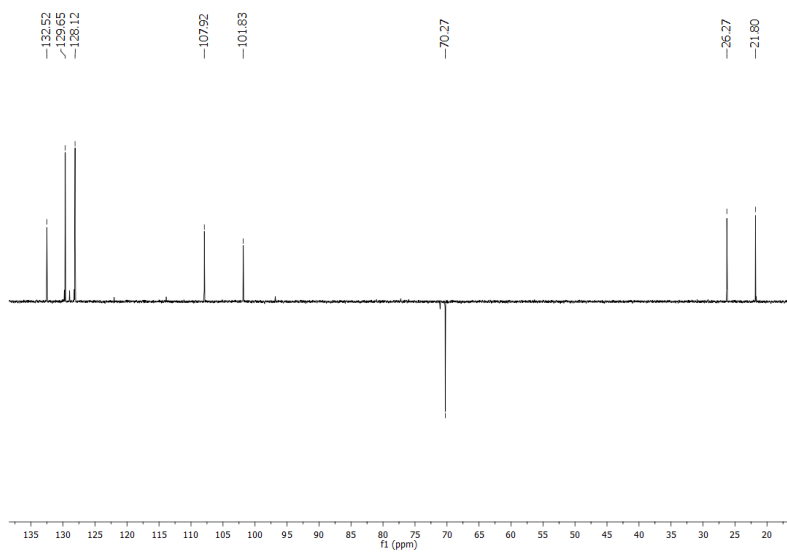
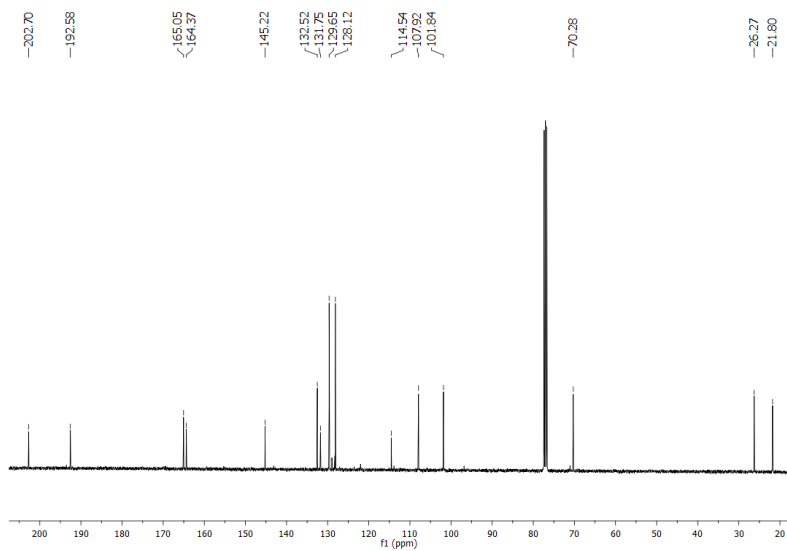
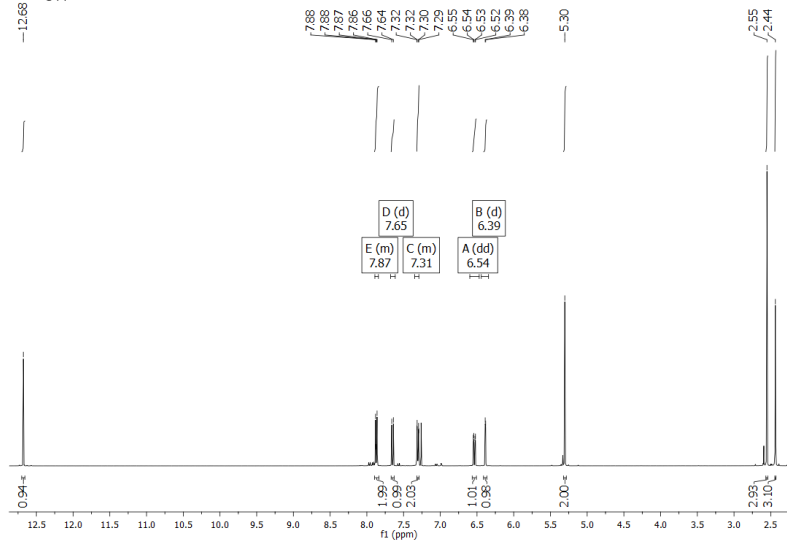
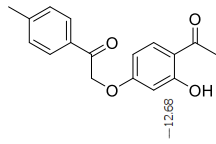
¹H, ¹³C and DEPT NMR spectra of EMAC10164k



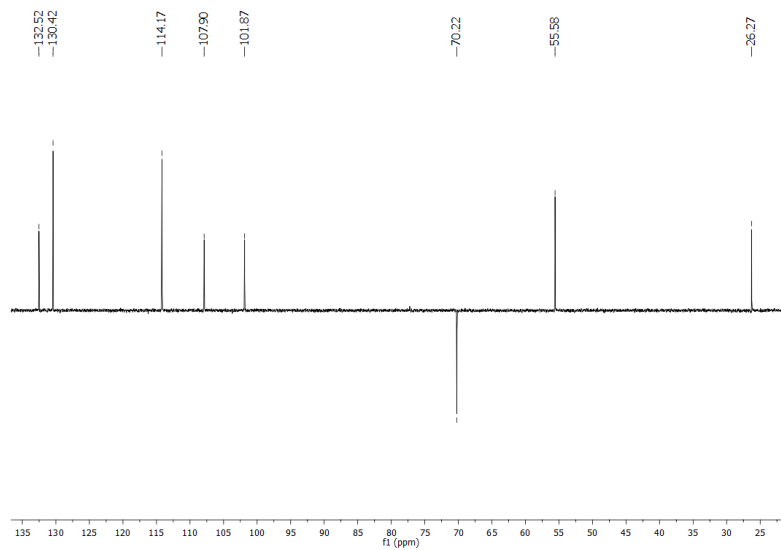
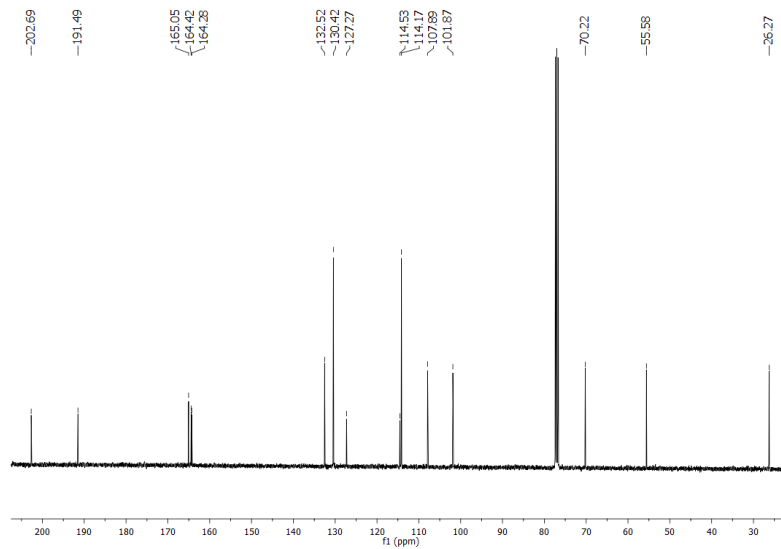
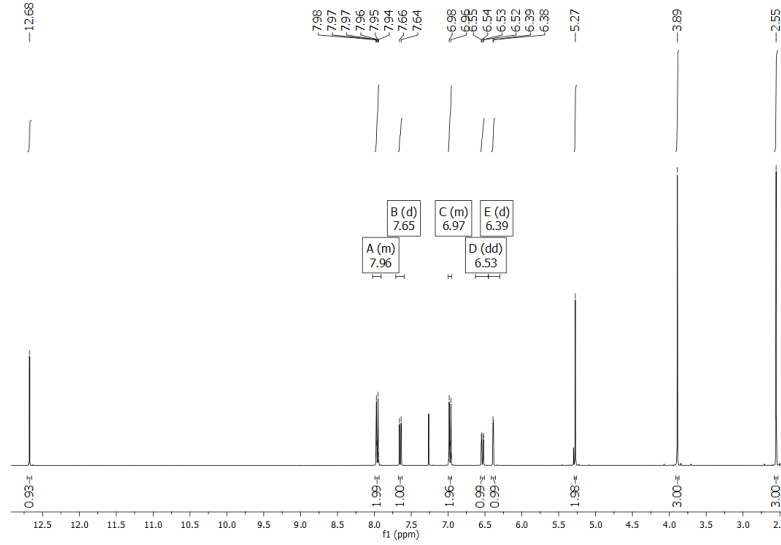
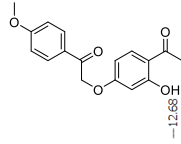
^1H , ^{13}C and DEPT NMR spectra of EMAC10164m



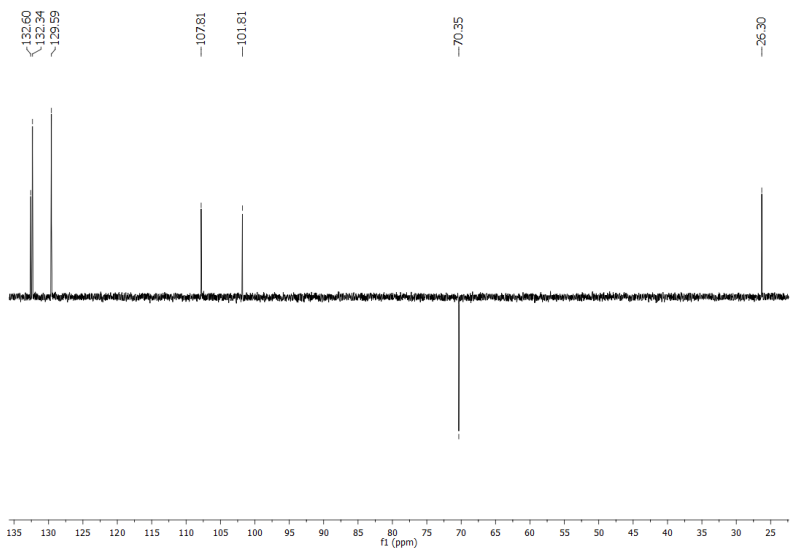
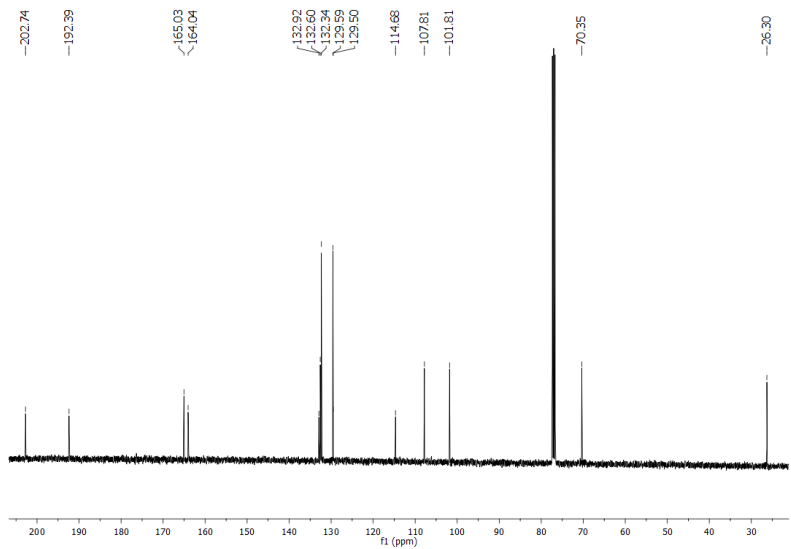
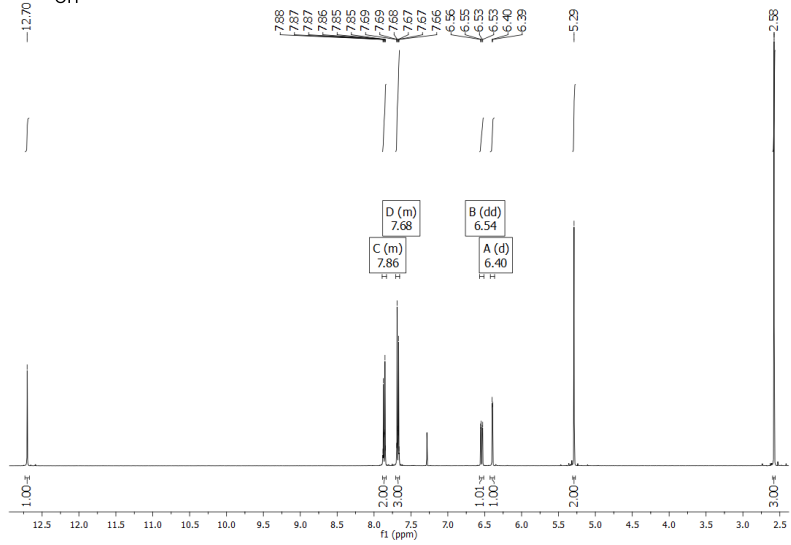
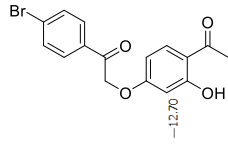
^1H , ^{13}C and DEPT NMR spectra of EMAC10168a



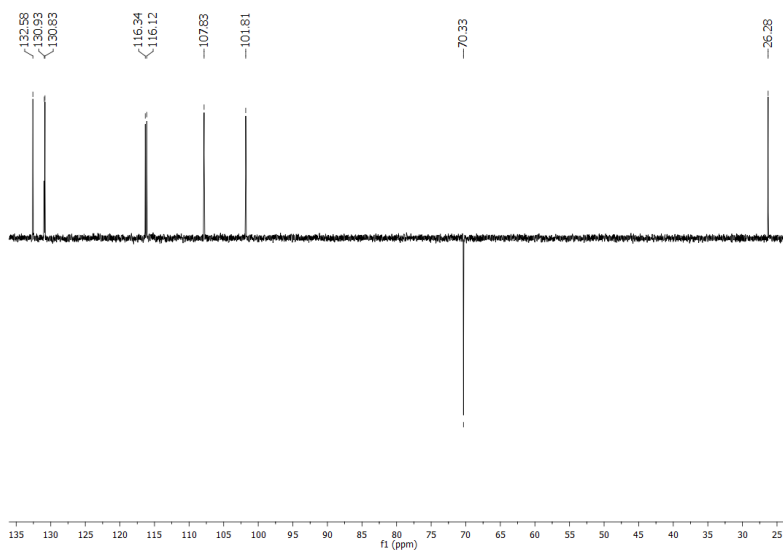
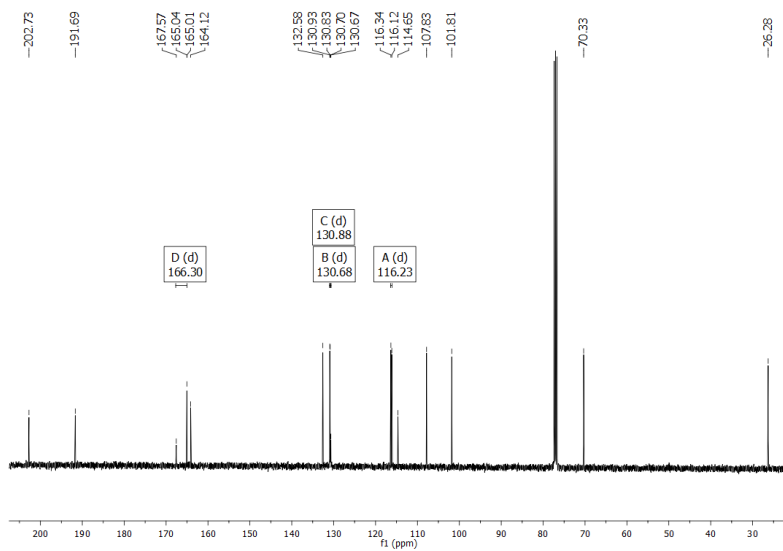
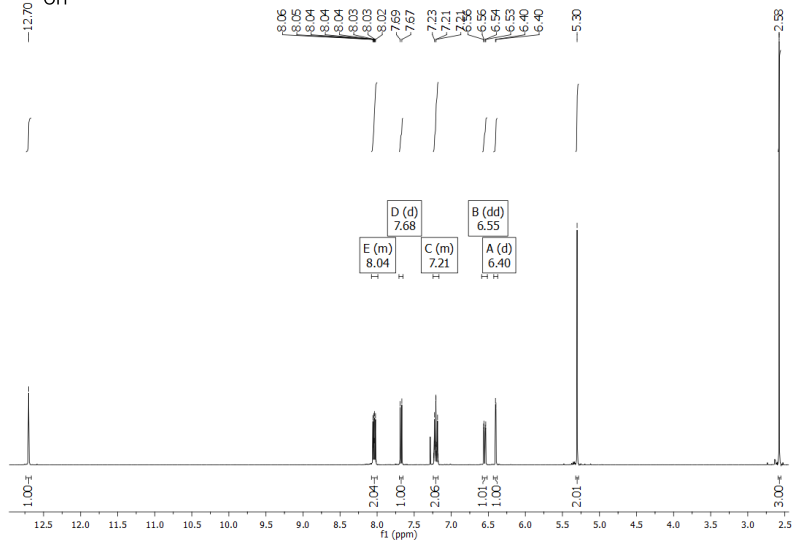
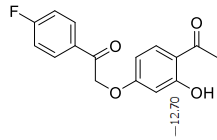
¹H, ¹³C and DEPT NMR spectra of EMAC10168b



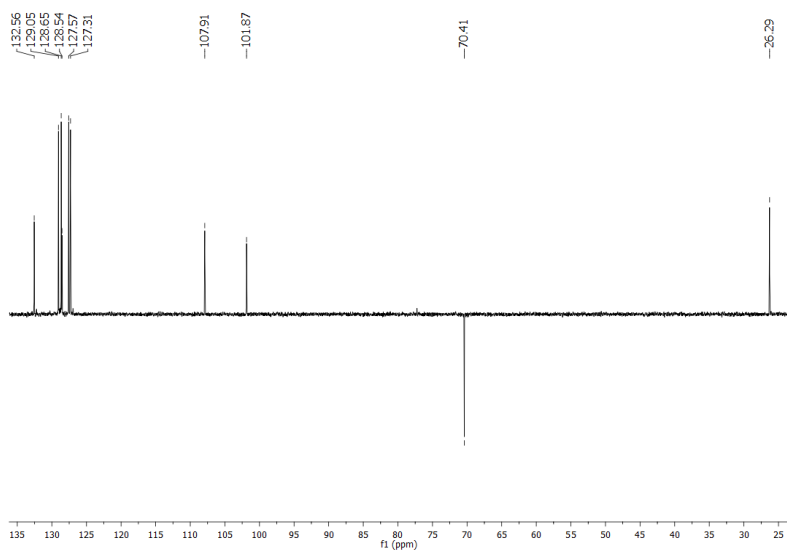
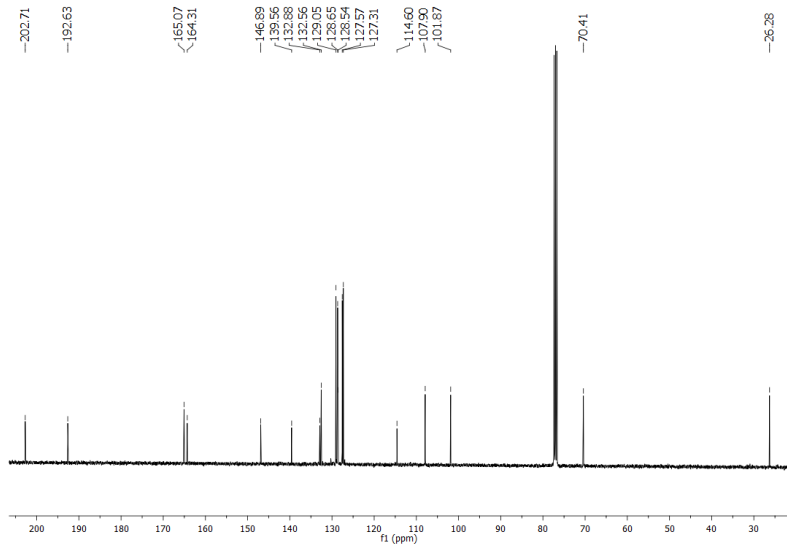
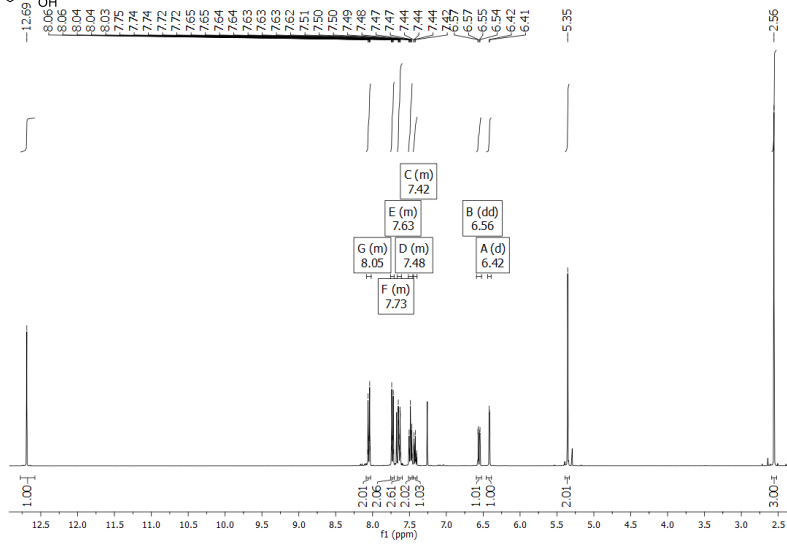
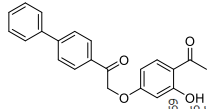
^1H , ^{13}C and DEPT NMR spectra of EMAC10168c



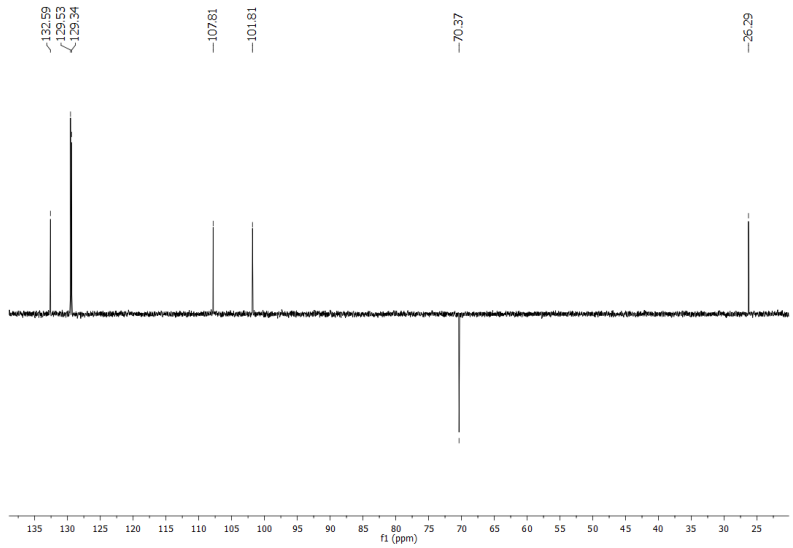
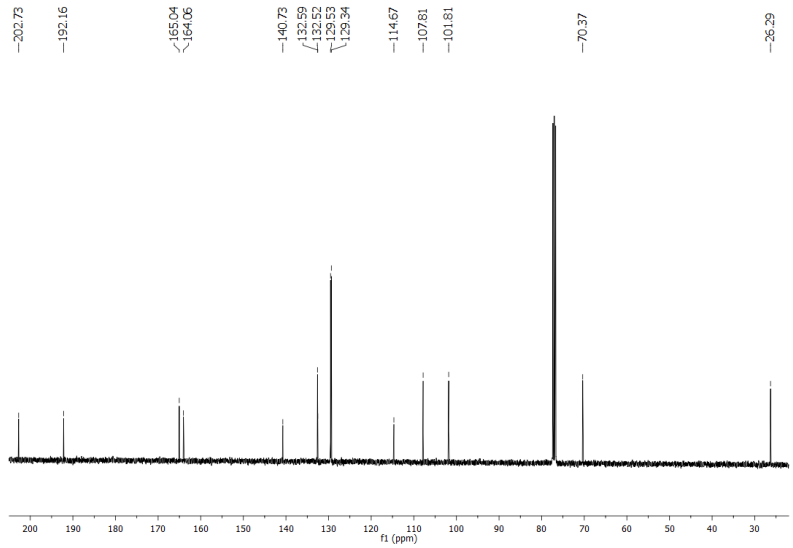
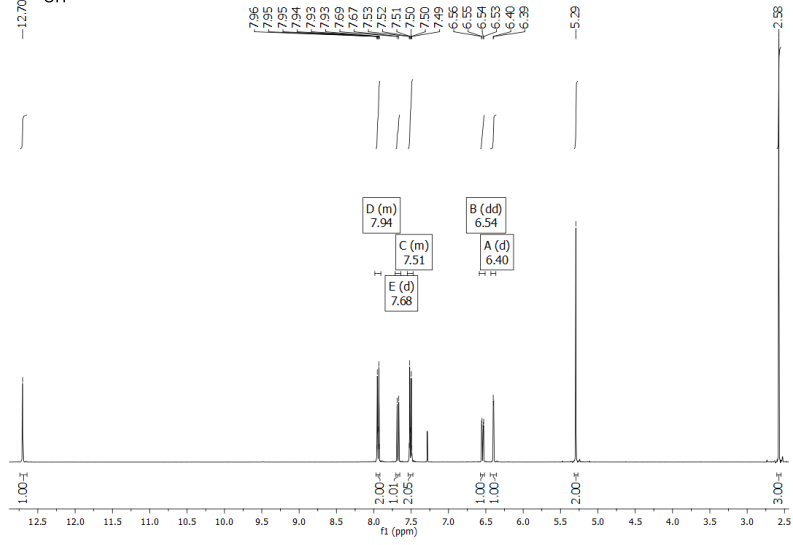
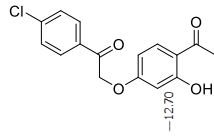
¹H, ¹³C and DEPT NMR spectra of EMAC10168d



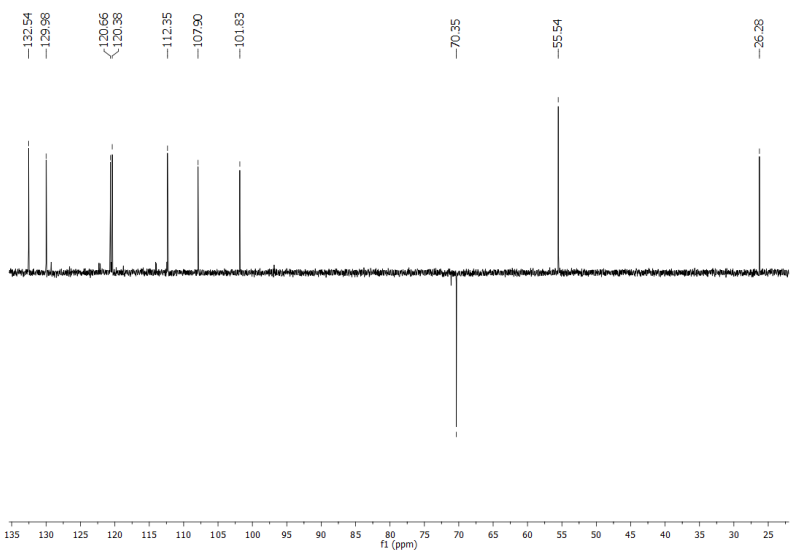
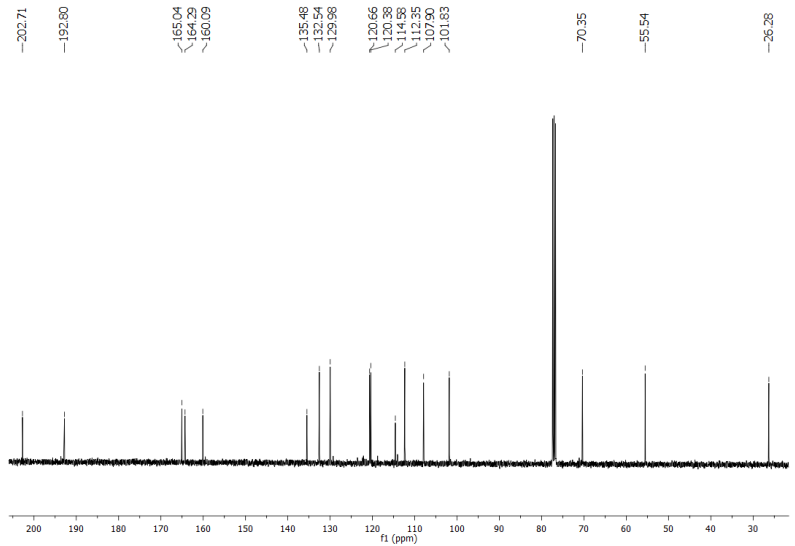
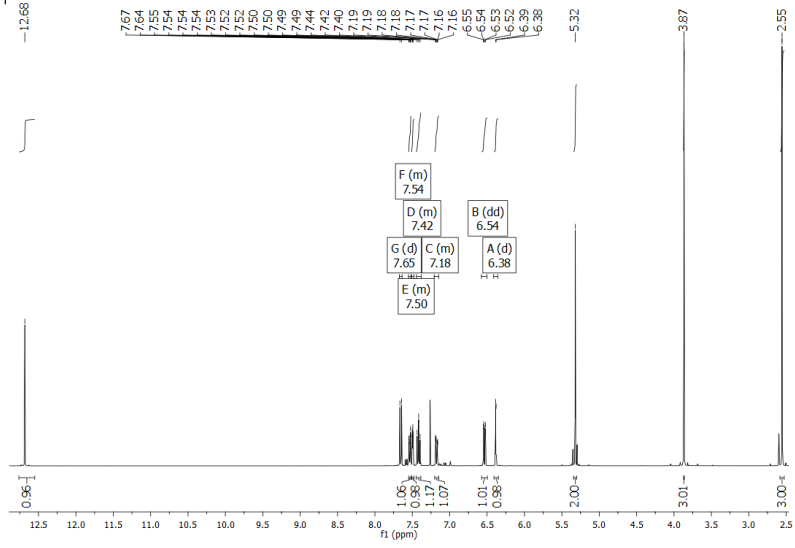
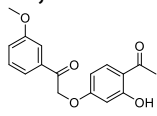
^1H , ^{13}C and DEPT NMR spectra of EMAC10168g



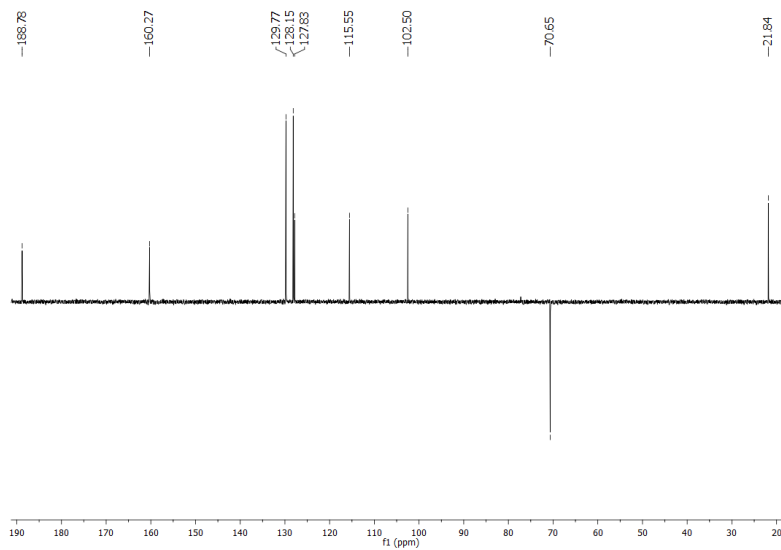
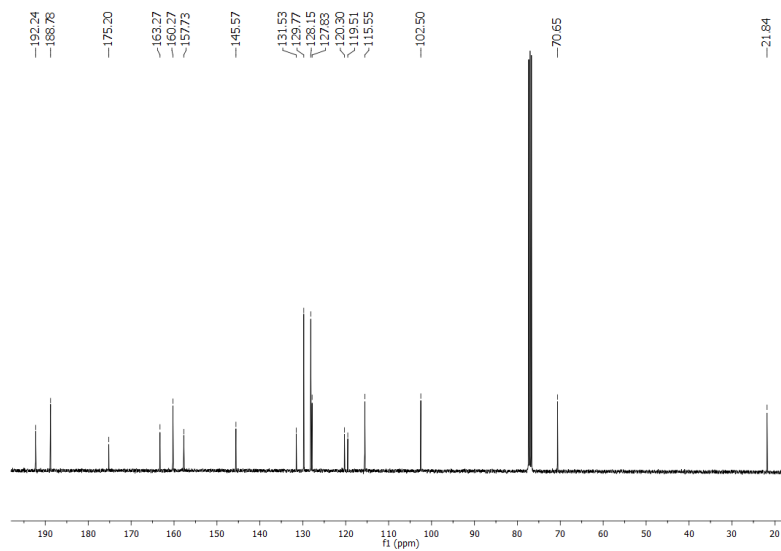
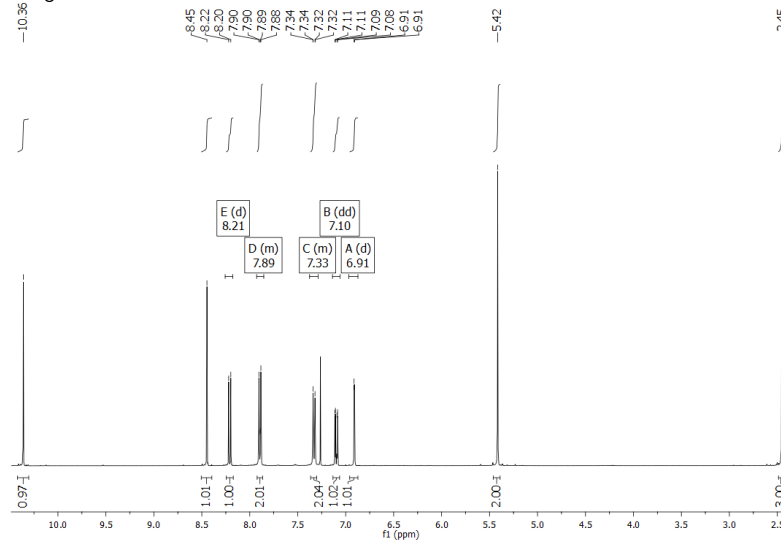
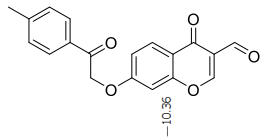
¹H, ¹³C and DEPT NMR spectra of EMAC10168k



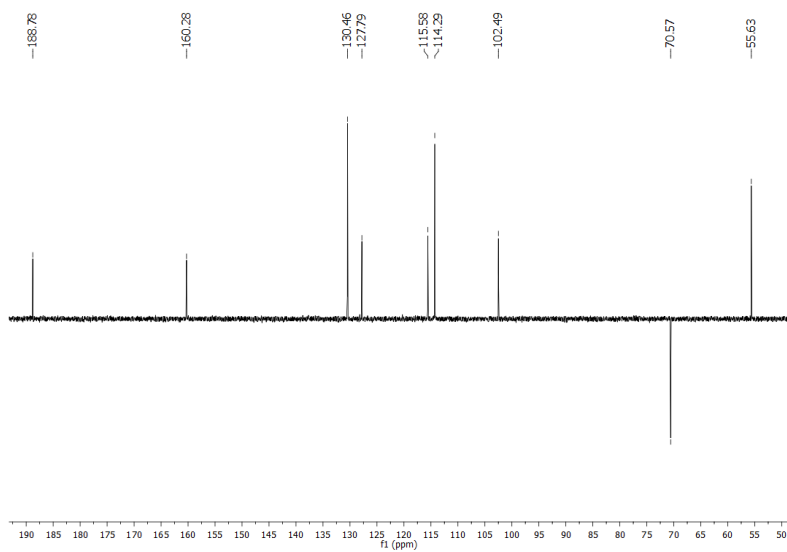
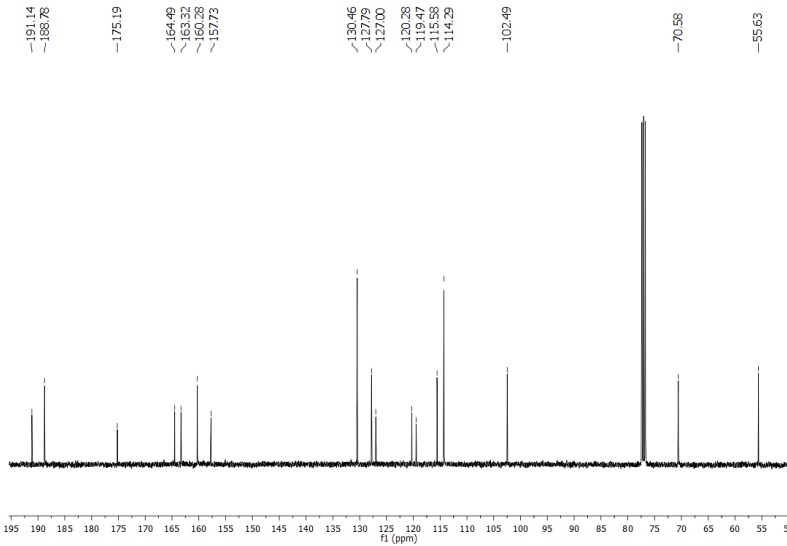
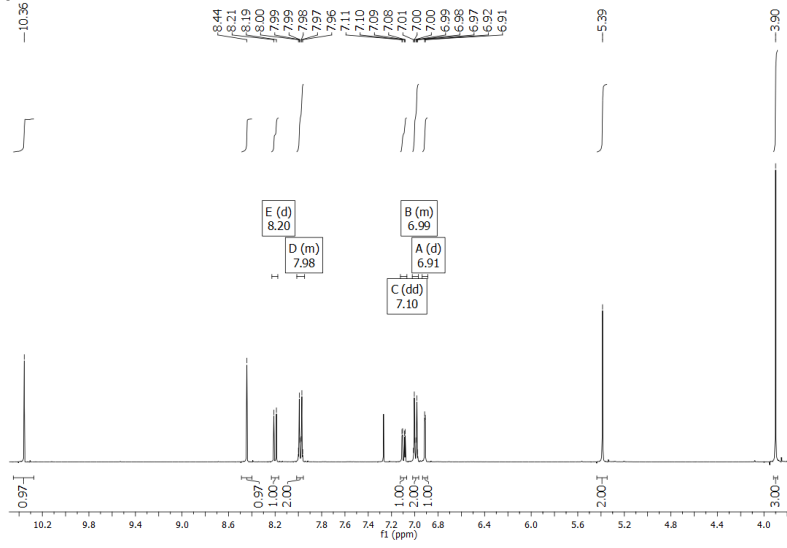
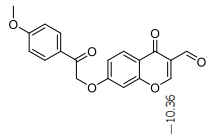
¹H, ¹³C and DEPT NMR spectra of EMAC10168m



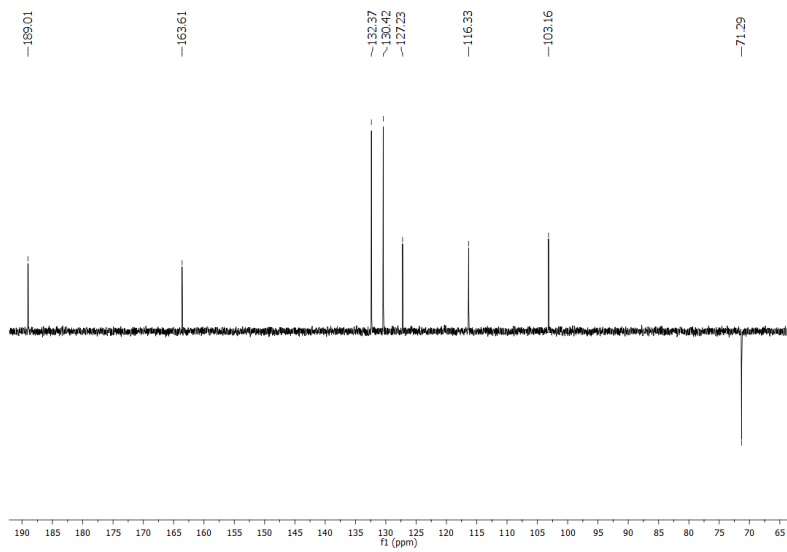
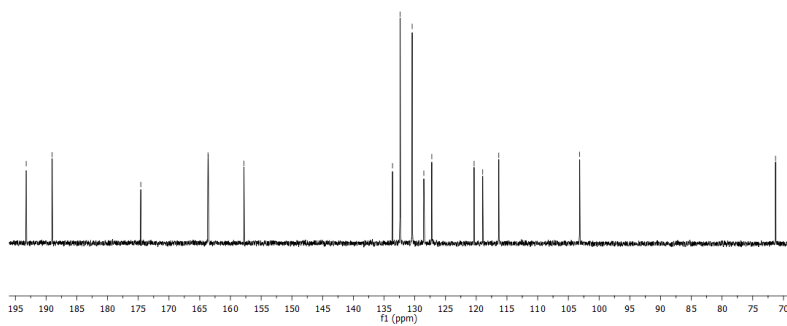
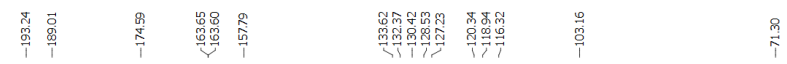
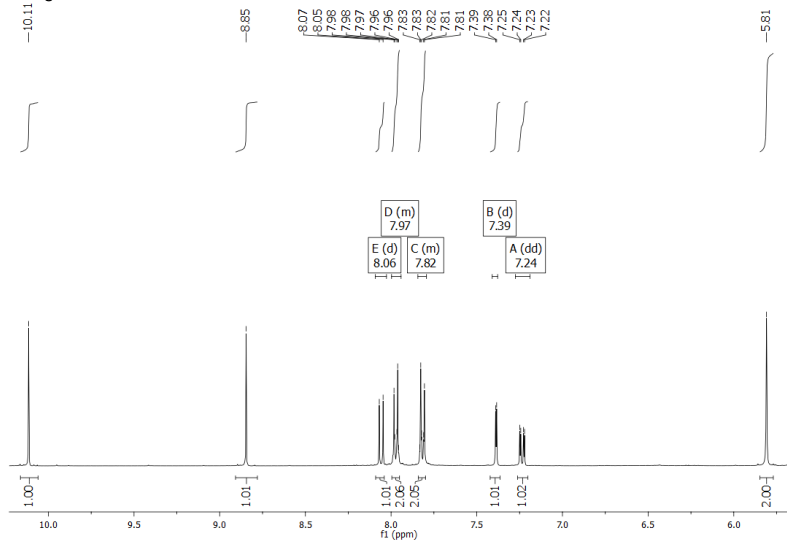
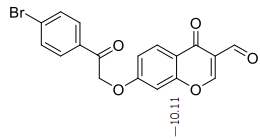
¹H, ¹³C and DEPT NMR spectra of EMAC10169a



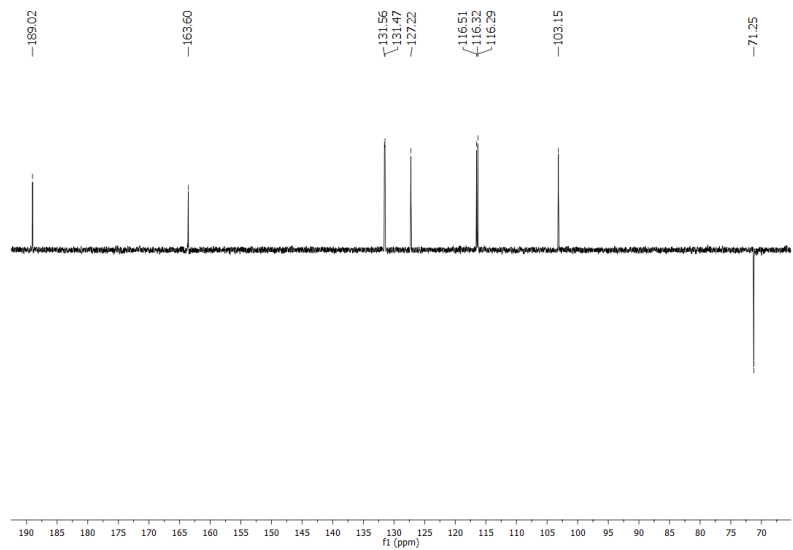
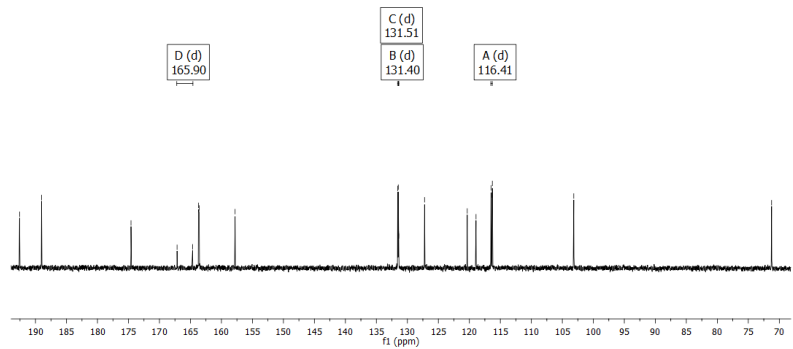
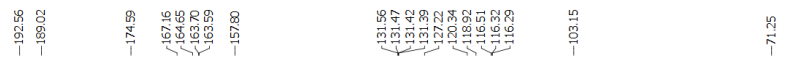
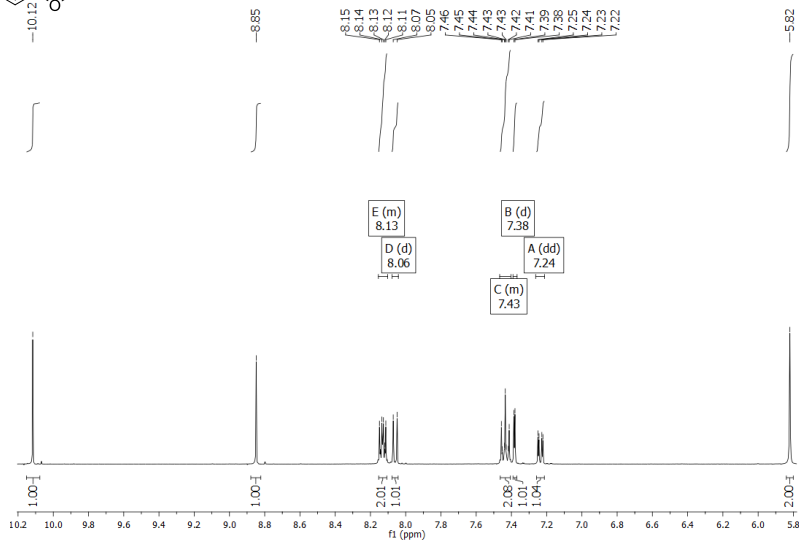
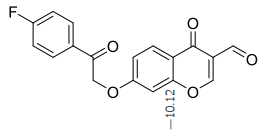
¹H, ¹³C and DEPT NMR spectra of EMAC10169b



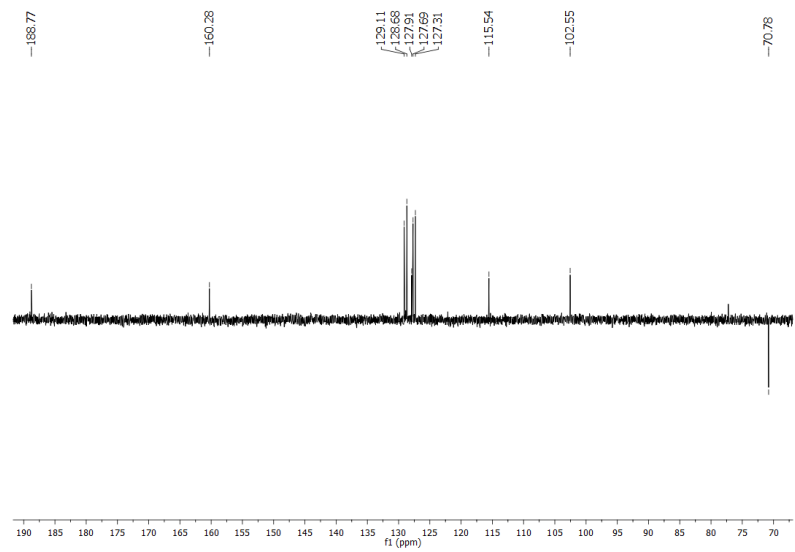
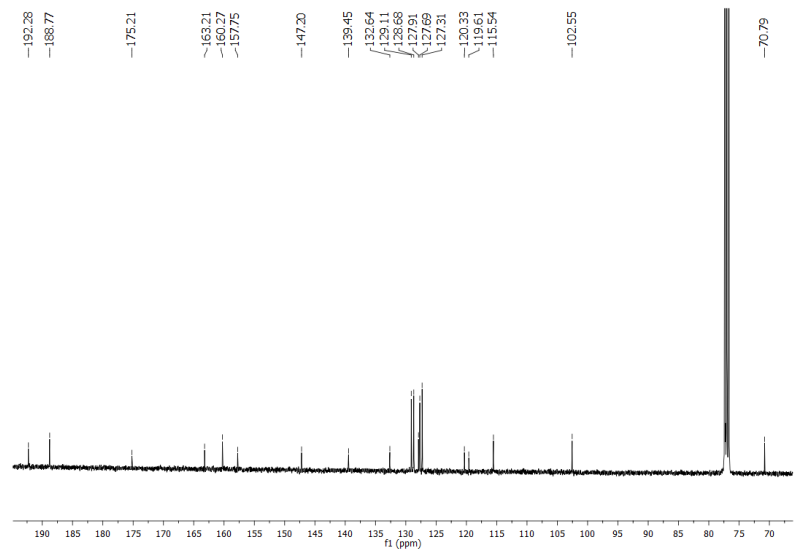
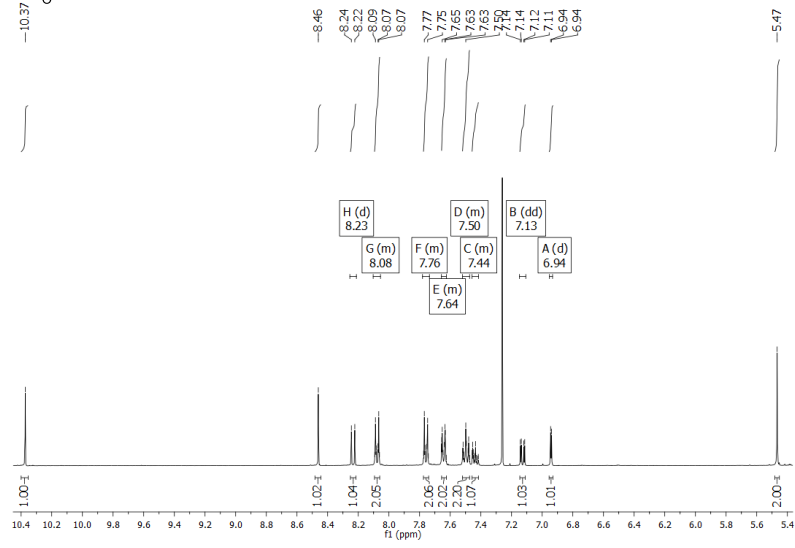
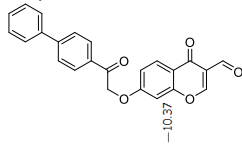
^1H , ^{13}C and DEPT NMR spectra of EMAC10169c



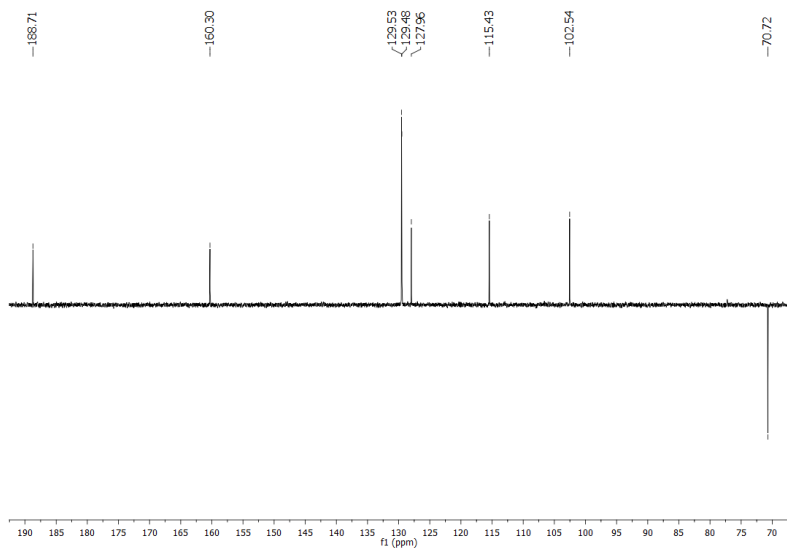
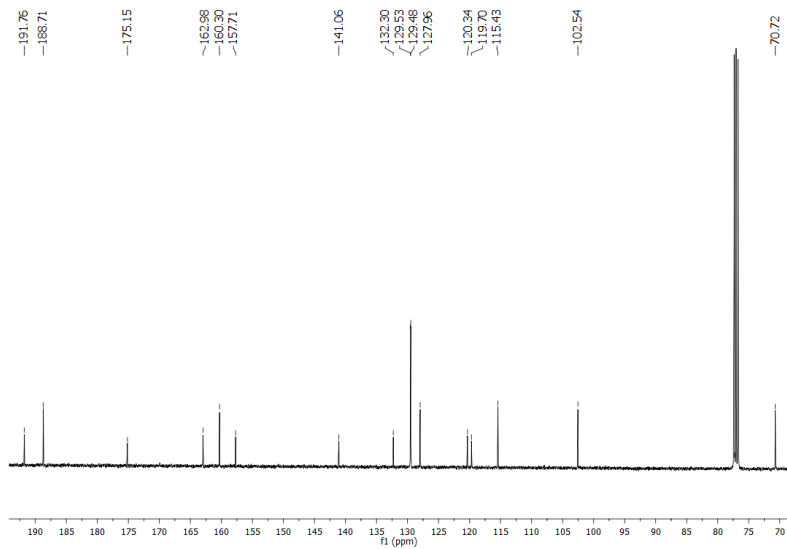
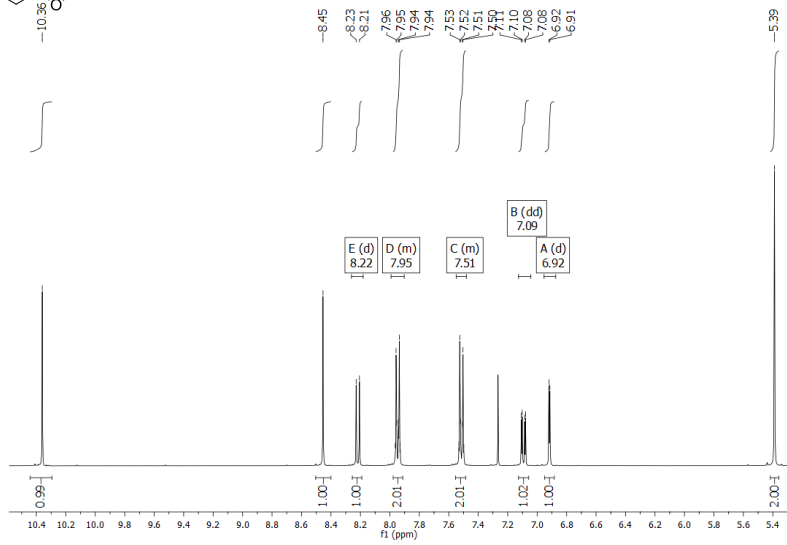
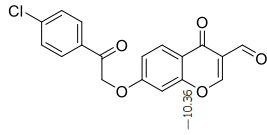
¹H, ¹³C and DEPT NMR spectra of EMAC10169d



¹H, ¹³C and DEPT NMR spectra of EMAC10169g



¹H, ¹³C and DEPT NMR spectra of EMAC10169k



^1H , ^{13}C and DEPT NMR spectra of EMAC10169m

